DOCTOR OF PHILOSOPHY

Structural and mechanistic studies of catalysts

Bennett, Elliot Leon

Award date:
2013

Awarding institution:
Bangor University

Structural and Mechanistic Studies of Catalysts

A Thesis presented in partial fulfilment
for the

Degree of
PhD

in the

School of Chemistry

by

Elliot Leon Bennett

Prifysgol Bangor • Bangor University

Acknowledgements

Foremost I would like to thank Paddy, Greg, Stewart, Sophie and my family. I would also like to thank Dan (and other members of the Murphy group), Gwynfor, Dennis, Mike, Sam, Nick, Jeff, Glyn, Tracey, Siobhan, Caroline and all the technicians and staff at the Bangor University Chemistry Department. Thanks to KESS (Knowledge Economy Skills Scholarships), STFC (Science and Technology Facilities Council) / ISIS – World Centre for Neutrons and Muons (at the Rutherford Appleton Laboratory), Dr AnnMarie C. O'Donoghue (Durham University Chemistry Department) and the EPSRC National Mass Spectrometry Service Centre (Swansea).

Abstract

Synthesis and characterisation of tetracyclic guanidinium phase transfer catalysts **I** and **II** from ethyl (*R*)-3-hydroxybutyrate was undertaken as well as the determination of their pKa's to provide insight into the mechanism of their use in phase transfer catalysis. Their proficiency at catalysing the Michael addition of 2-hydroxy-1,4-napthaquinone **III** to trans-β-nitrostyrene **IV** was studied. Catalyst **II** showing improved reaction times and e.e.'s over **I**. The synthesis of tetracyclic guanidinium salt **V** was also attempted unsuccessfully,

Synthesis of copper (I) hydride (CuH.X, X = H_2O and pyridine) from three different routes (Würtz Reaction [1], $NaBH_4$ reduction [2] $LiAlH_4$ reduction in pyridine [3]) and their subsequent investigation by inelastic neutron scattering (INS) techniques (neutron diffraction/spectroscopy) and X-Ray diffraction (XRD) provided insight into the structure of the copper hydride core and also the nature of the stabilising surface shell (H_2O and pyridine respectively). Direct synthesis of Stryker's reagent $[HCu\{P(C_6H_5)_3\}]_6$ from copper (II) acetate ($Cu(OAc)_2$) and also its deuterium analogues $[DCu\{P(C_6H_5)_3\}]_6$ and $[HCu\{P(C_6D_5)_3\}]_6$ were achieved and the location of their hydride ligands using INS (SANDALS - neutron diffraction) was determined.

Synthesis of organometallic *bis*-(η^3-π-allyl)M (M = Ni **VI** & Pd **VII**) cross-coupling catalysts from the Grignard reaction of metal halides and preparation of active Ni-terpyridyl complexes (general formula $LNiI_2$, L = TPY) **VIII - XI** from the reaction of $Ni(COD)_2$ and I_2 with the starting material TPY's was achieved and vibrational INS spectra (TOSCA - neutron spectroscopy) was used to investigate the low energy vibrations which are linked to catalytic activity. Similar studies were performed on the commercially available Pd stabilised NHC PEPPSI pre-catalysts (IPr **XII** and IMes **XIII**)).

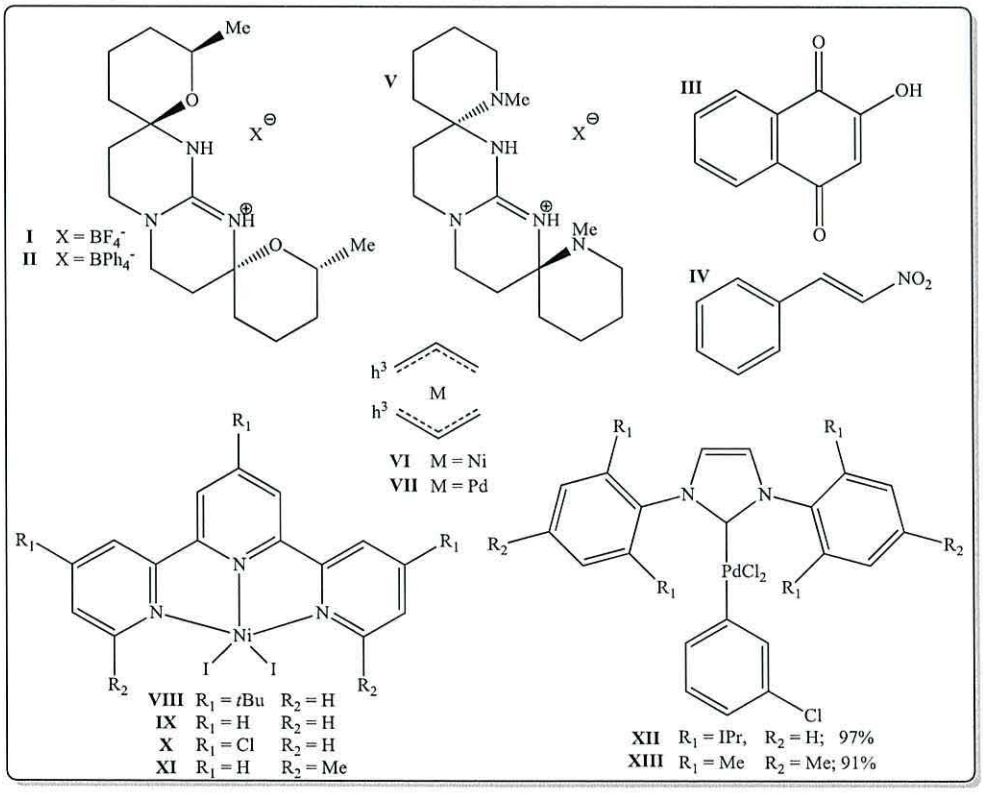

Abbreviations

AMTP	Acetylmethylenetriphenylphosphorane
BHE	Beta-Hydride Elimination
COD	Cyclo-octadiene
DCM	Dichloromethane
DEPT	Distortionless Enhancement by Polarization Transfer
DFT	Density Functional Theory
DIBAL-H	Diisobutylaluminium Hydride (DIBAH / DIBAL)
DMAP	4-Dimethylaminopyridine
DMF	Dimethylformamide
DMSO	Dimethyl Sulfoxide
DPAA	Diphenylacetic Acid
e.e.	Enantiomeric Excess
ENS	Elastic Neutron Scattering
EPB	Extracted Proton Beam
e.r.	Enantiomeric Ratio
EROS	Encyclopaedia of Reagents for Organic Synthesis
ESI	Electrospray Ionisation
FTIR/IR	Fourier Transform / Infra-red Spectroscopy
FWHM	Full Width at Half Maximum
HPLC	High-Performance Liquid Chromatography
IMes	1,3-Bis(mesityl)-4,5-Dihydroimidazolium
INS	Inelastic Neutron Scattering
IPr	Diisopropyl Phenylimidazolium
MS	Mass Spectrometry
NHC	*N*-heterocyclic Carbenes
NMP	*N*-Methyl-2-pyrrolidone
NMR	Nuclear Magnetic Resonance
OA	Oxidative Addition
PEPPSI	Pyridine-Enhanced Precatalyst Preparation Stabilisation and Initiation
Petrol	Petroleum Ether bp. 40 - 60°C
PMA	Phosphomolybdic Acid
PTC	Phase Transfer Catalyst
QGCT	Quartz Glass Capillary Tube
RE	Reductive Elimination

RFQ	Radio Frequency Quadrupole
Rochelle's Salt	Potassium Sodium Tartrate
RT	Room Temperature
TBS	*tert*-Butyldimethylsilane (Protecting Group)
TEM	Transmission Electron Microscopy
THF	Tetrahydrofuran
TLC	Thin Layer Chromatography
TM	Transition Metal
TOS	Tosyl (Protecting Group)
TPPO	Triphenylphosphine Oxide
TPY	Terpyridine
UV-Vis	Ultraviolet-Visible Spectroscopy
XPS	X-Ray Photoelectron Spectroscopy
XRD	X-Ray Diffraction

Publications

Published

i. M.A. Beckett, **E.L. Bennett**, P.N. Horton, M.B. Hursthouse; Tetraphenyl boroxinate(1-) salts of monoborate cations: Synthesis and single-crystal X-ray structures of [Ph2B{OCH2CH2N(Me)(CH2)n}2][Ph4B3O3] (n =4, 5), *Journal of Organometallic Chemistry*, 2010, 695, 1080–1083, (BSc Project)

ii. **E.L. Bennett**, G.P. Black, P. Browne, A. Hizi, M. Jaffar, J.P. Leyland, C. Martin, I. Oz-Gleenberg, P.J. Murphy, T.D. Roberts, A.J. Thornhill, S.A. Vale; Synthesis and biological activity of analogues of batzelladine F, *Tetrahedron*, 2013, 69, 3061–3066, (MChem Project).

In Submission

iii. G.A. Chass, D.C. Fang, E.A.B. Kantchev, **E.L. Bennett**, P.J. Murphy, S.F. Parker, F. Kargl, G.N. Greaves; Coorperative Terahertz Dynamics Drive Catalytic Selectivity - Revealed by Inelastic Neutrons and Quantum Theory, *Nature Materials* (PhD).

In Preparation

iv. S.F. Parker, E. Barney, A. Hannon, S. Imberti, **E.L. Bennett**, G.A. Chass, P.J. Murphy, T. Wilson, K. Refson; CuH: A (Nearly) 200 yr Old Problem, (PhD).

v. S.F. Parker, S. Imberti, P.J. Murphy, **E.L. Bennett**; Characterisation of the Hydrides in Stryker's Reagent: $[HCu\{P(C_6H_5)_3\}]_6$, (PhD).

vi. M.T. Allingham, **E.L. Bennett**, D.H. Davies, P.M. Harper, A. Howard-Jones, P.J. Murphy, D.A. Thomas; Synthesis, Applications and Mechanistic Investigations of C_2-Symmetric Guanidine Bases, (PhD).

Contribution Report -

The author wishes to clarify his contributions to the above publications:

Performed all synthetic work for papers i, iii, iv and v. Joint synthetic work for papers ii and vi. Joint performance of practical neutron spectroscopy for papers iii, iv and v. Contributions to the manuscript preparation of papers i, ii, vi.

Preamble

Advances in science have enabled us to observe and investigate our impact on the environment, with climate change (and other environmental issues) being a growing concern internationally. Industrial ecology is the study of materials and energy flow through industrial systems, reduction of energy usage (such as heat, electricity and materials etc) is of the utmost importance. The use of catalysts to increase the rate of a particular chemical reaction and to promote formation of desired products whilst reducing energy costs and waste materials is vital both financially and environmentally.[1]

The vast array of materials produced worldwide would be completely inconceivable without catalysts, they are of critical importance in organic synthesis (eg. production of medicinal compounds, pesticides and food additives) as well as being used in over 90% of all chemical products. Catalytic processes are responsible for ≈ 75% (by value) of all chemical and petroleum based products and are said to generate $900B in products annually.[2] Products created by the formation of particular bonds that utilise catalysts to lower the activation energy required for successful reaction, have opened the way to compounds and materials previously thought inaccessible. Catalysis now spans a wide array of subject areas with heterogeneous, homogeneous and biological catalysts[3] becoming increasingly important as the only rational means of economically producing useful compounds in an energy saving and environmentally benign way.

Efficient catalysts must be capable of being scaled up, effectively synthesised and exhibit high selectivity. The relatively new principle of "Green Chemistry" should be applied to all large scale chemical processes with the 3 R's kept in mind (reduction, recycling and re-use).[4]

Chemists are now being challenged with producing perfect chemical reactions that produce only the desired products with 100% selectivity and 100% yield, without any unwanted waste.[5] To achieve this goal, scientists must be educated in a wide spectrum of scientific disciplines as the solutions must overcome multiple and varied problems, with over-specialisation having the potential to limit one's ability to achieve said goal.

The rational design and optimisation of catalysts would offer a superior and more efficient alternative to current trial and error methods, using vast quantities of materials and solvents, which are often to no avail (not to mention the time and effort of the scientists themselves). A combination of computational calculation, advanced synthesis and application of powerful characterisation techniques (such as neutron scattering) can lead us, in small steps, to improved and greener chemistry.

This study uses these disciplines (computational studies, synthesis and characterisation) in different ways and applies them to various catalytic systems. Improvement of multi-step organic syntheses with the aim of increasing catalytic efficiency has been performed on organic guanidine containing catalysts. The use of neutron scattering techniques combined with synthesis of relatively large quantities of "active" and unstable organometallic catalysts has been performed with the aim of understanding the molecular vibrations related to increased catalytic performance. The study of copper(I) hydride containing catalysts and reagents, both on stoichiometric compounds and on those containing bulk properties (eg. CuH_x, $x = 0.4 - 0.9$), has also been probed using the powerful technique of neutron scattering combined with large scale synthesis.

Contents

CHAPTER 4: SYNTHESIS AND NEUTRON CHARACTERISATION OF ORGANOMETALLIC CATALYSTS

Methodologies -

CHAPTER 1:

CHAPTER 3:

CHAPTER 4:

Chapter 1: Synthesis and Mechanistic Studies of C_2-Symmetric Guanidine Catalysts

1.1. Introduction

1.1.1. Synthetic and Mechanistic Studies of a C_2-Symmetric Guanidine Bases

Guanidines are very strong bases, for example guanidine itself (Figure 1.) has a pK_a of 13.6, which is nearly as strong as NaOH. Guanidine **1** was first synthesised in 1861 from the natural product guanine, isolated from Peruvian guano (sea bird excrement).[6] When protonated the guanidinium cation **2** can undergo delocalisation to distribute the positive charge across all three nitrogens (Figure 2.) and it is this delocalisation which lends itself to the strong basic nature of the guanidine function.[7]

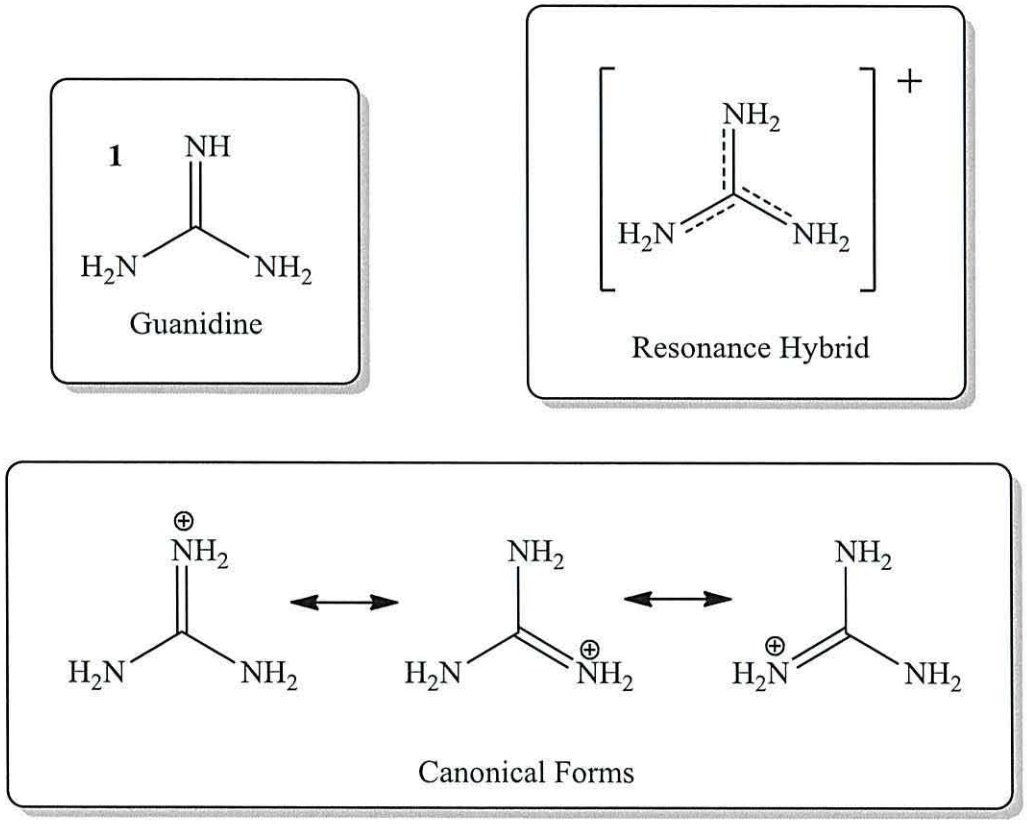

Figure 1. Guanidine representations.

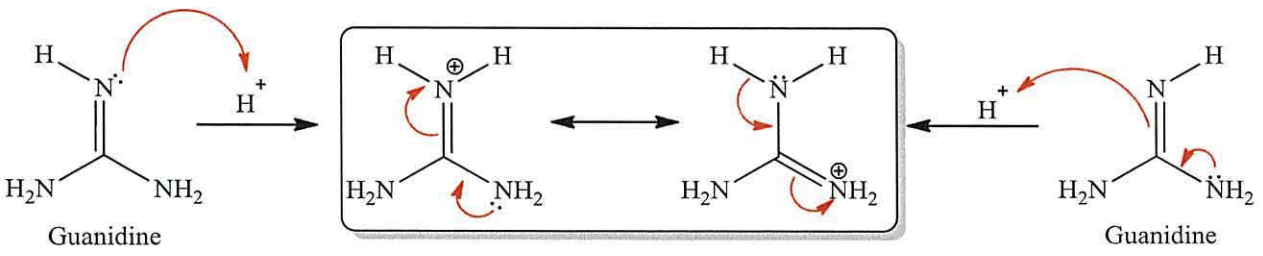

Figure 2. Protonation mechanisms of guanidine.

Guanidine has various uses, such as in the manufacture of plastics and explosives, and the guanidinium function is ubiquitous in nature, for example it is found in the side chain on the essential α-amino acid arginine (Figure 3.).[8]

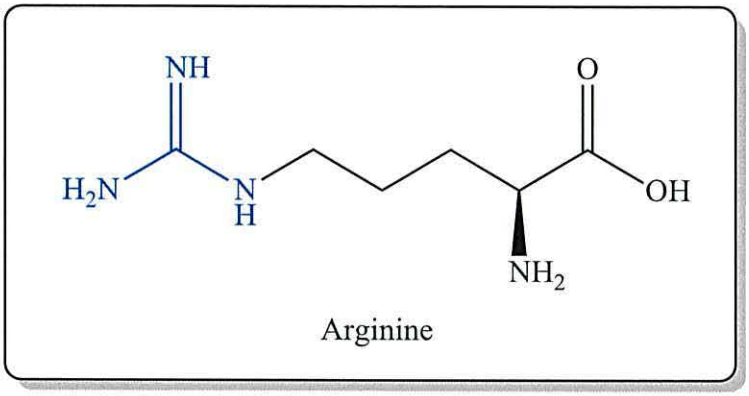

Figure 3. Molecular structure of Arginine, one of the 20 amino acids with DNA and RNA codons.

With a high pK_a of 12.5, the guanidinium group gives arginine basic chemical properties and once protonated allows for formation of multiple hydrogen bonds. There are many uses of guanidine in chemistry, medicine, biology and it is even being considered as an alternative fuel,[9] as a mole of guanidine and 2 moles of water can react (in the presence of a catalyst) to form 3 moles of ammonia and 1 mole of carbon dioxide (Equation 1.). The guanidine can be used in its crystalline form and the ammonia can be broken down into nitrogen and hydrogen and used in fuel cells, or could be used directly in a combustion engine.

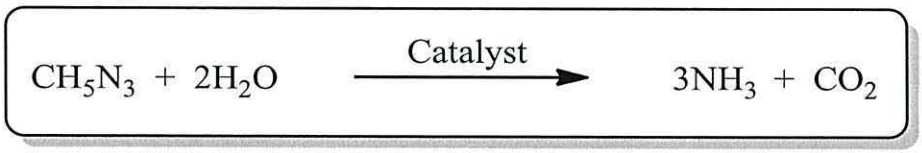

Equation 1. Reaction of guanidine and water in the presence of a catalyst, as an alternative fuel source.

The guanidine containing compound Saxitoxin[10] (STX), which is a naturally occurring neurotoxin produced in cyanobacteria and dinoflagellates was rumoured to be given to spy plane pilots as a means of suicide in the event of capture and impossible escape.

As part of a synthetic project directed towards the synthesis of marine natural products, Murphy *et al* reported that the addition of guanidine to the vinyl ketone **2** gave the tetracyclic guanidinium salts **3** and **4** which possess *meso*- and C_2-symmetry respectively (Scheme 1.).[11]

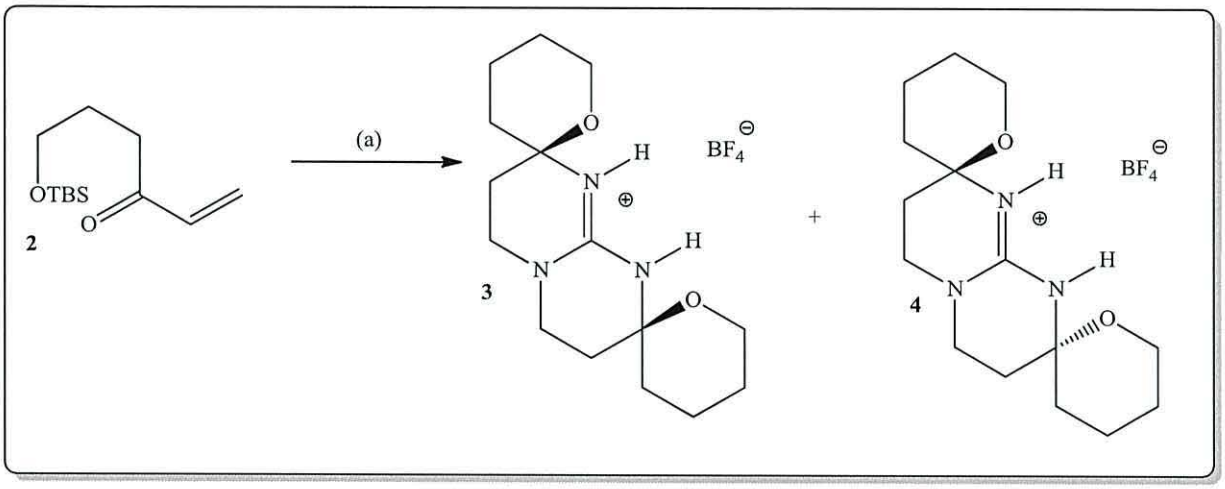

Scheme 1. (a) (i) guanidine / DMF ; (ii) MeOH / HCl / 0°C; (iii) sat. HBF_4 (aq) / 80% overall.

As a result of this new understanding of C_2-symmetric guanidine catalysis, significant effort went into the synthesis of novel guanidine compounds of this type. From consideration of the X-ray data for compounds **3** and **4** Murphy *et al* came to the conclusion that if substituents were placed on the pyran rings, they would act as conformational "locks" for the system and drive any equilibrium between **3** and **4** to favour an overall *trans* arrangement, thus offering a potential route to enantiomerically pure C_2-symmetric guanidine bases.[11] To test this hypothesis ethyl (*R*)-3-hydroxybutyrate **5** was converted in 5 steps to ketone **6** which was reacted with guanidine and after cyclisation and deprotection resulted in the C_2-symmetric guanidine **7** as a single enantiomer in 44% yield (Scheme 2.).

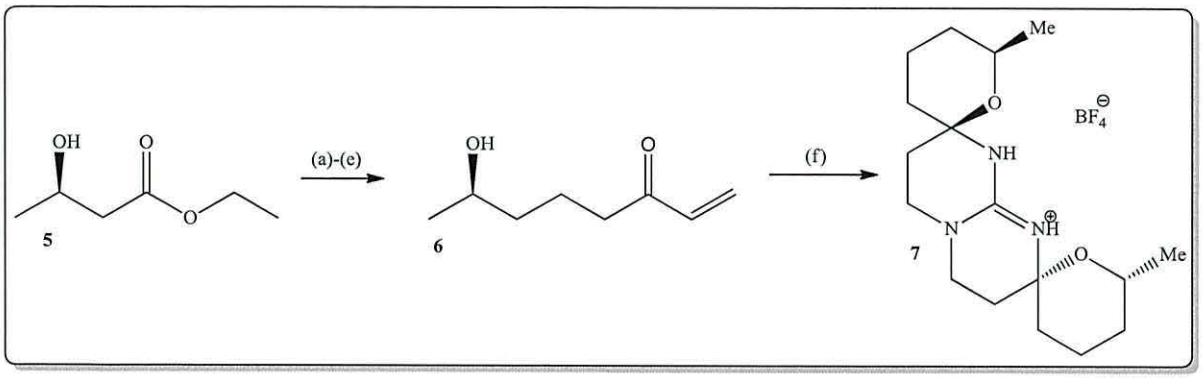

Scheme 2. (a) TBDMSCl / Imid / DMF; 99%; (b) DIBAH / hexane / -78°C; 82%; (c) TosCl / Py; 80%; (d) NaI / acetone; 85%; (e) (i) $CH_3COCHPPh_3$ / *n*-BuLi, (ii) H_2O quench, (iii) excess (aq) formaldehyde; 69%; (f) (i) guanidine / DMF / 0°C / 16h, (ii) HCl / MeOH / 3h, (iii) $NaBF_4$ / DCM; 44%.[12]

Similarly **8** was converted to the enone **9** and addition of guanidine to this gave the very hygroscopic guanidine **10** which could be protected by silylation leading to **11** and **12** in good overall yields (Scheme 3.).

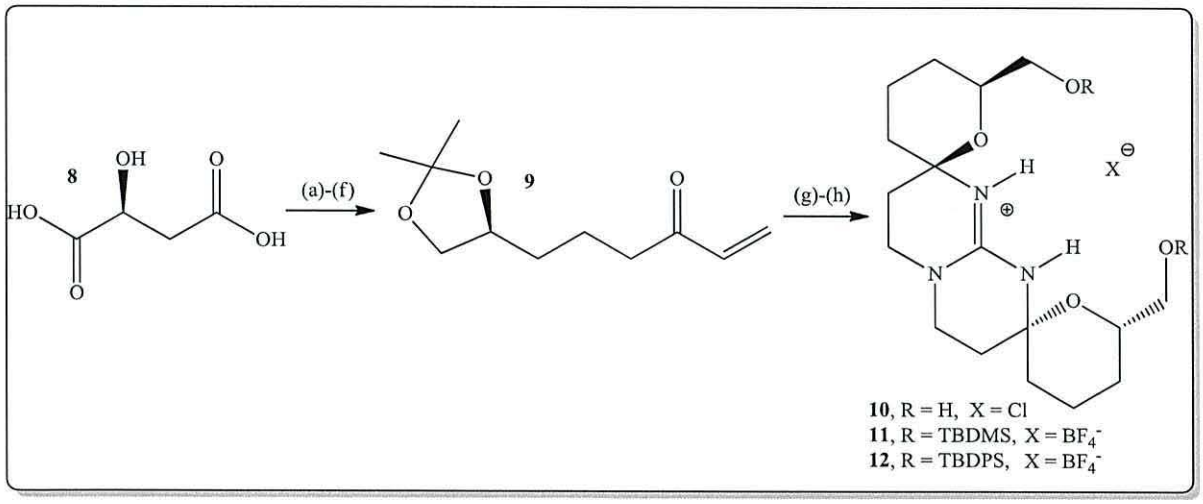

Scheme 3. (a) MeOH / HCl; 70%; (b) BH_3:SMe_2 / $NaBH_4$; 92%; (c) $(MeO)_2CMe_2$, TosOH; (d) $LiAlH_4$ (60%, two steps); (e) PPh_3I_2 / Imid; 91%; (f) (i) $CH_3COCHPPh_3$ / *n*-BuLi, (ii) (aq) CH_2O; 72%; (g) (i) guanidine / DMF, (ii) HCl / MeOH; **10** 45%; (h) as (g) then (i) 3 x R_3SiCl / Imid / DMF, (ii) ion exchange (**11**; 29%, **12**; 36%).[13]

With these catalysts in hand several studies were performed to determine if they were of use in asymmetric transformations. Mendoza *et al* reported that C_2-symmetric guanidinium salts would catalyse the Michael addition of pyrrolidine **13** to the unsaturated lactones **14a** & **14b**, to give the adducts **15a** & **15b** with an 8.4 fold increase in reaction rate (Scheme 4.).[14]

The tetraphenyl borate (BPh_4^-) anion showed better catalytic activity the chloride salt and was attributed to its well-known lower co-ordination ability.[15/16]

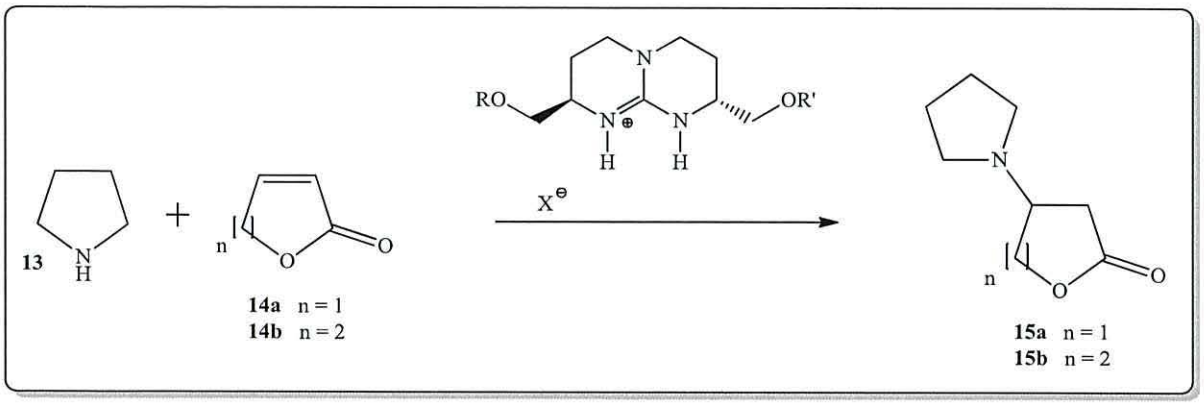

Scheme 4. Michael addition of pyrrolidine **13** to unsaturated lactones **14a** & **14b**.

Application of the catalysts **7**, **11** and **12** prepared by Murphy *et al* to this reaction demonstrated that a 4-fold increase in the rate of reaction was achieved when **7** was used as a catalyst but that exchanging the counter ion to BPh_4^- **16** led to a 16.3-fold increase in rate of reaction (Table 1.),[12] which was in agreement with the findings of de Mendoza.[14]

Table 1. The effects of guanidinium salts on reaction rates.[13]

Base	$t_{1/2}$	Relative rate increase
None	135	-
7	35	4.0
11	12	11
12	108	1.25
16[12]	7	16.3

Application of these guanidine bases as catalysts for the nitro-aldol (Henry reaction)[17] and nitro-Michael reactions[18] was also reported. The guanidinium salt **7** catalysed the reaction of isovaleraldehyde **17** with nitromethane to give (*R*)-**18** in 52% yield and 20% e.e.[19] Guanidinium salt **7** also catalysed the Michael addition of 2-nitropropane to chalcone **19** to give (*S*)-**20** in 70% yield and 23% e.e (Scheme 5.).[20]

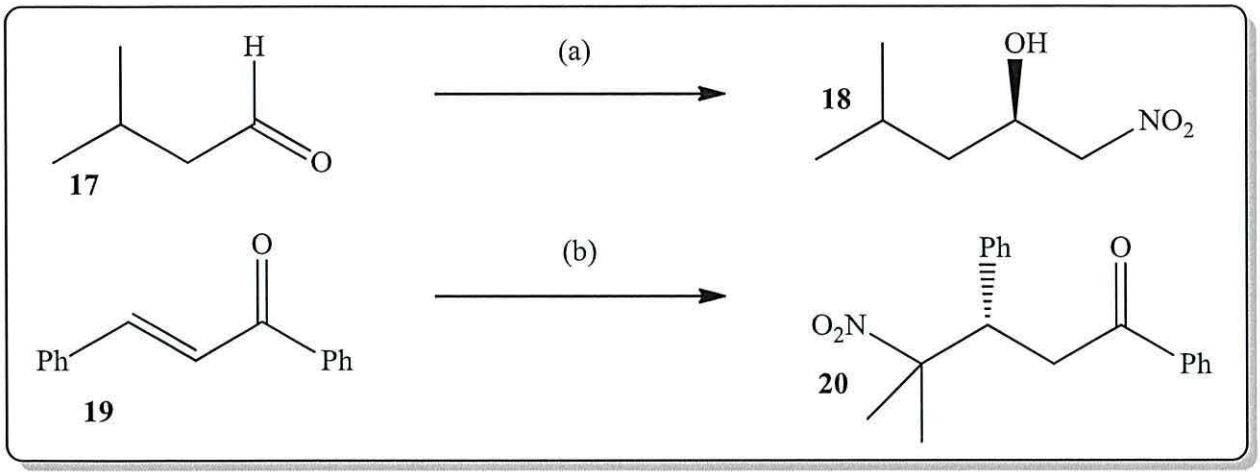

Scheme 5. (a) (i) **7** (0.1 equiv.), NaOMe (0.09 equiv.), MeOH, 30 min then remove solvent; (ii) CCl_4 RT, **17**, $MeNO_2$, 16h; (b) (i) **7** (0.1 equiv.), *t*-BuOK (0.09 equiv.), THF, $(Me)_2CHNO_2$, **19**, RT, 24h.

These reactions were of limited use but applications in phase transfer catalysis proved more effective. Phase transfer catalysis (PTC) is a form of bi-phasic catalysis that has proven to be an extremely useful tool for organic synthesis. Asymmetric PTC utilises well characterised chiral, non-racemic, catalysts (both natural and non-natural products) to perform various types of bond forming reactions.[21] The reaction conditions are often mild, cost efficient and environmentally benign.[22] In 1971 Starks first introduced the term PTC to explain how tetraalkylammonium or phosphonium salts can promote the reaction of substances in 2 different phases, which was described as the use of small quantities of an agent which transfers one reactant across the interface into the other phase so that reaction can proceed.[23]

An example being the bi-phasic mixture of 1-bromooctane ($C_8H_{17}Br_{(org)}$) with an aqueous solution of sodium cyanide ($NaCN_{(aq)}$), that after 2 weeks at 100°C only hydrolyses NaCN to sodium formate (HCOONa). However when a phase-transfer agent is introduced (such as the previously mentioned organic-soluble quaternary ammonium or phosphate cations, Q^+ in Figure 4.) the transport of ions from the aqueous phase to the organic phase promotes catalysis of cyanide displacement on 1-bromooctane (Figure 4.).

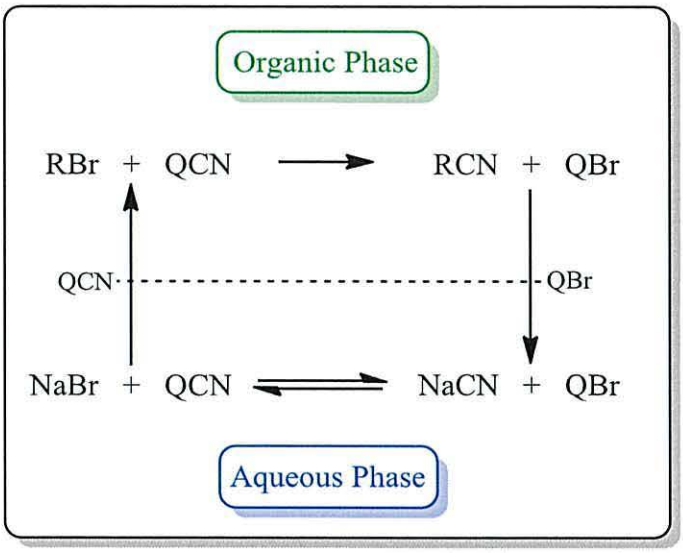

Figure 4. PTC of the cyanide displacement of 1-bromooctane by a quaternary salt.[24]

Application of catalysts **7** & **10-12** to the phase transfer benzylation of the Schiff's base **21** (Scheme 6.) demonstrated (Table 2.) that the guanidinium salt **7** was the best PTC for the transformation with the enantiomer (*R*)-**22** obtained in 86% e.e.[13]

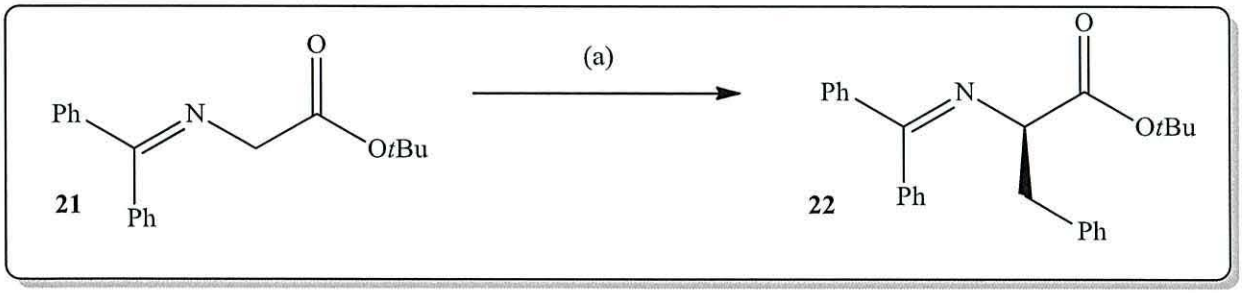

Scheme 6. Guanidinium base (0.1 equiv.), NaOH (2M), BnBr (2 equiv.), CH_2Cl, 16h, 0°C-RT.

Table 2. Results of the PTC investigations from (**Scheme 6.**).[13]

Catalyst	Conv.(%)	e.e.(%)
7	>97	86 (*R*)
10	15	21 (*R*)
11	70	65 (*R*)
12	80	74 (*R*)

These findings were in accord with the data reported by Nagasawa *et al* involving similar pentacyclic guanidinium salts **23** and **24**, who proposed the mechanism shown in Figure 5. The catalyst used remained unchanged during these reactions and could be recovered and recycled after counter-ion exchange.

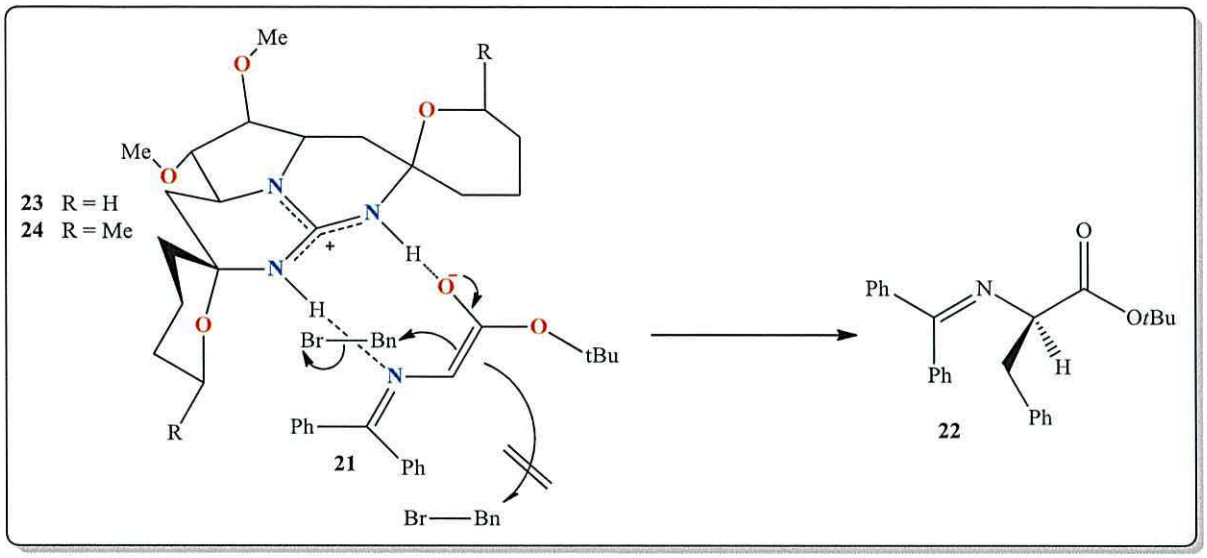

Figure 5. Alkylation mechanism of **21** with benzyl bromide with pentacyclic guanidine catalysts **23** & **24**.

Following this the PTC epoxidation of chalcones **25** & **26** using catalyst **7** was investigated and was shown to give the chacones **27** and **28** in high yield (> 95%) and high e.e.'s (> 90% see Scheme 7.). Again the catalyst can be recovered and recycled.[25]

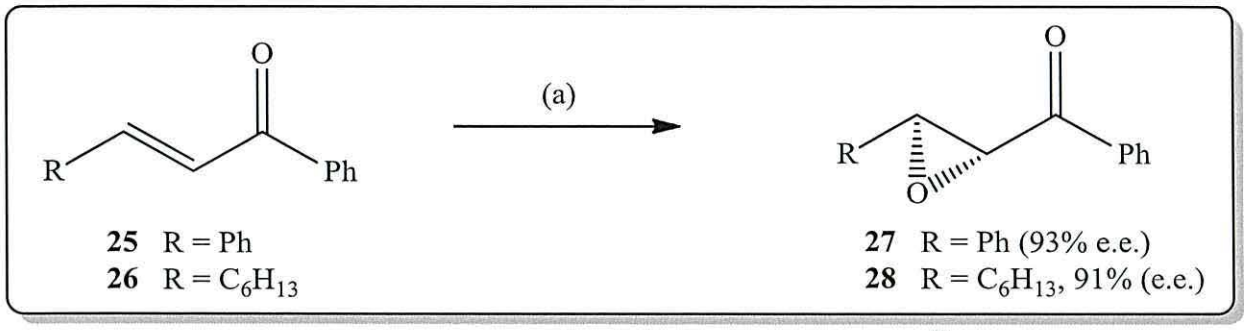

Scheme 7. (a) **7** (0.05 equiv.), NaOCl (aq), Tol, 16h, 0°C-RT.[13]

1.1.2. Aims & Hypothesis

1.1.2.1. Synthesis of the C_2-Symmetric Guanidinium Salt - Murphy's Catalyst 7

The initial stages of the study will focus on the synthesis of the guanidinium salt **7** from the readily available compound ethyl (*R*)-3-hydroxybutyrate **5**. Ion exchange to **7** (from Cl^- to BF_4^-) will be undertaken to hopefully obtain multi-gram quantities of **7** the pK_a of which will be determined. As previously observed,[12] exchanging the catalysts BF_4^- ion for the much bulkier BPh_4^- ion leads to an increase in reaction rate in Michael additions and this will be undertaken. Catalyst **16** will then be tested for its proficiency in the quinone Michael-addition reaction shown in Scheme 8. The results obtained will be directly comparable to those previously obtained using catalyst **7** (Table 3.).[26]

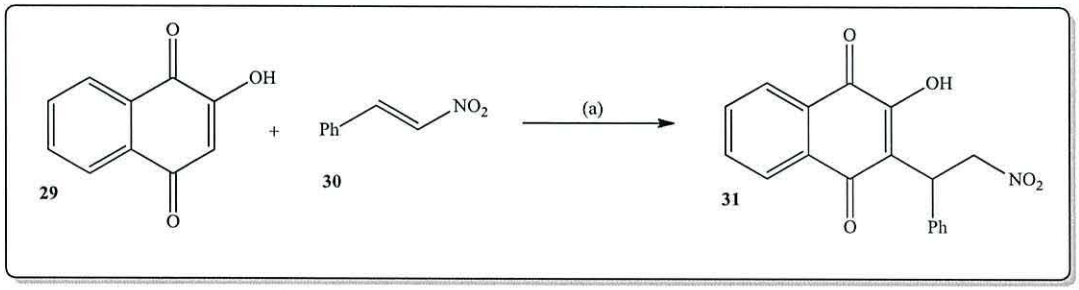

Scheme 8. (a) Catalyst **16** 0.05 eqv / Solvent (THF / EtOH) / 0°C → RT.

Table 3. Quinone Michael Addition results, using Catalyst **7** 0.05 eqv / Solvent / H_2O / 0°C → RT.[26]

Entry	Solvent	$T_{½}$ (h)	Conv.(%)	e.e.(%)
1	DCM	1058 (44 days)	9	8
2	CH_3CN	945 (40 days)	7	6
3	Et_2O	295 (12 days)	45	14
4	EtOH	83 (3 days)	92	2
5	THF	67 (3 days)	100	2

It was determined from these results that the addition of water increases the rate (and in some cases initiates the reaction) and it was observed that racemic or low e.e. products were obtained. It is intended that the current study will employ anhydrous conditions

focusing on the reaction solvents THF and EtOH which have previously given the fastest rates of reaction.

1.1.2.2. Phase Transfer Catalysis (PTC)

Investigations into determining the pK_a of **7** will hopefully give an insight into the mechanism of the PTC process involved in the epoxidation reaction (Scheme 7.) as there are several possibilities for the mechanism. Classically the guanidinium salt **7** could exchange its BF_4^- counter ion for ClO^- at the solvent interface and this species effects the asymmetric epoxidation (Figure 6.).

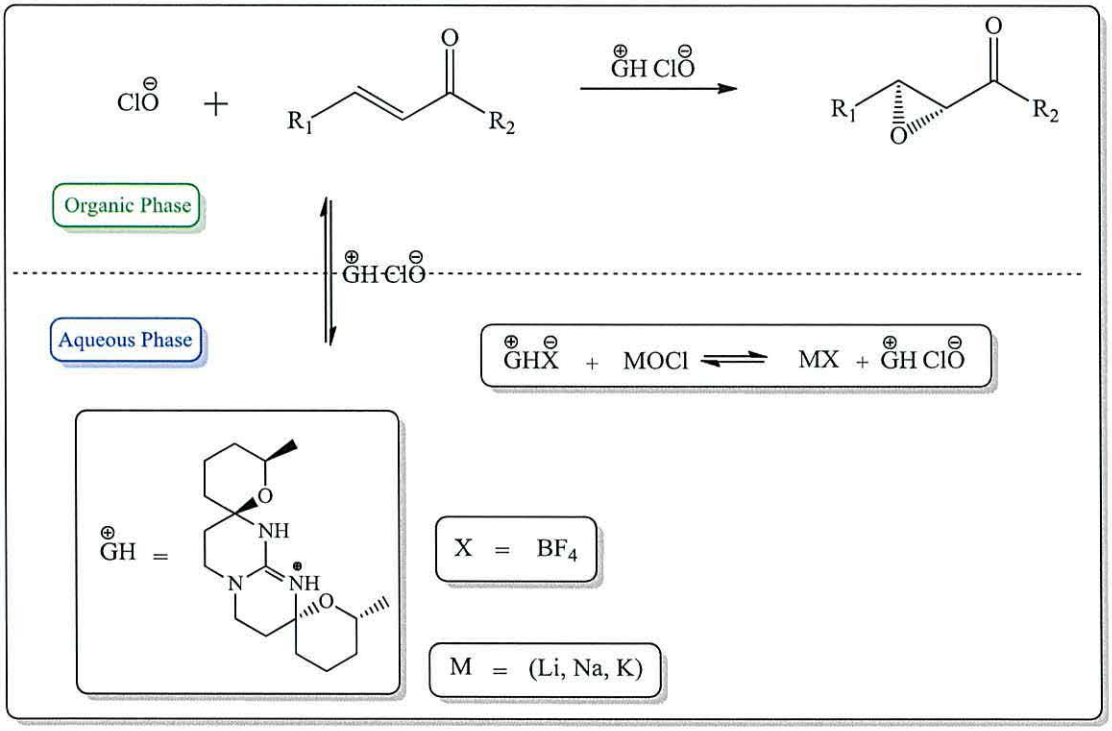

Figure 6. Possible PTC mechanism of (**7**) – epoxidation.

However unlike other phase transfer reagents the guanidinium species employed in this reaction is a protonated salt as opposed to a quaternary ammonium species. This means that under the basic reaction conditions, which are in the pH range of 11-14, the catalyst could be deprotonated by the hypochlorite or hydroxide ions leading to a neutral guanidine species (G) which would not be able to partake in the phase transfer of hypochlorite. We

could thus speculate that an alternate mechanism where the metal hypochlorite could be being transferred to the organic phase and the guanidine is acting as a chelate ligand (Figure 7.).

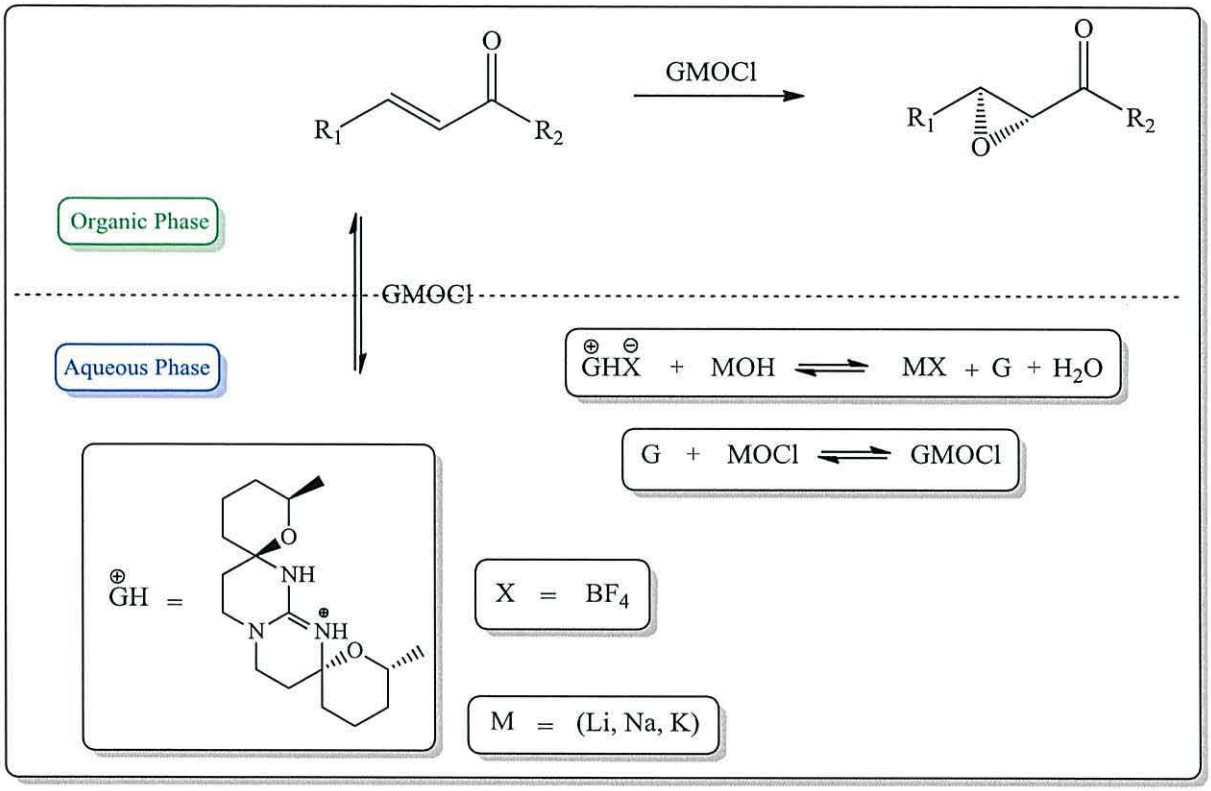

Figure 7. Potential PTC epoxidation mechanism which could occur at pH's where a neutral guanidine species might be formed.

Quantitative determinations of the pK_a's of these guanidine catalysts should give vital information on the mechanism of the reaction and allow a better understanding of the potential for future developments.

1.1.2.3. Synthesis of a novel C_2-Symmetric Guanidinium Salt 53

Conclusions from previous studies using X-ray crystallography indicated that the substituents placed on the pyran rings in Murphy's catalyst act as conformational "locks" for the system driving the known equilibrium to give a single enantiomer for the catalyst (Figure 8.).

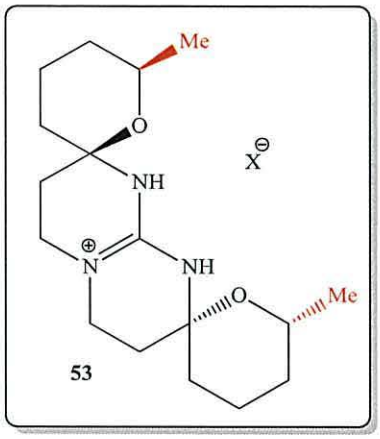

Figure 8. Murphy's catalyst with pyran ring substituents highlighted red.

One hypothesis is that replacement of the pyran oxygens with -NMe groups would lead to the alternate structure **35** which might be an equilibrium mixture between **35**, ent-**35** and meso-**35**, this mixture might be resolvable under kinetic conditions with a chiral acid (A*H) to give a single enantiomer (or indeed either enantiomer by using the enantiomeric acid shown in Scheme 9.). The enone required for this route should be accessible from δ-valerolactam **32** in a reaction similar to that previously reported using δ-valerolactone.[11]

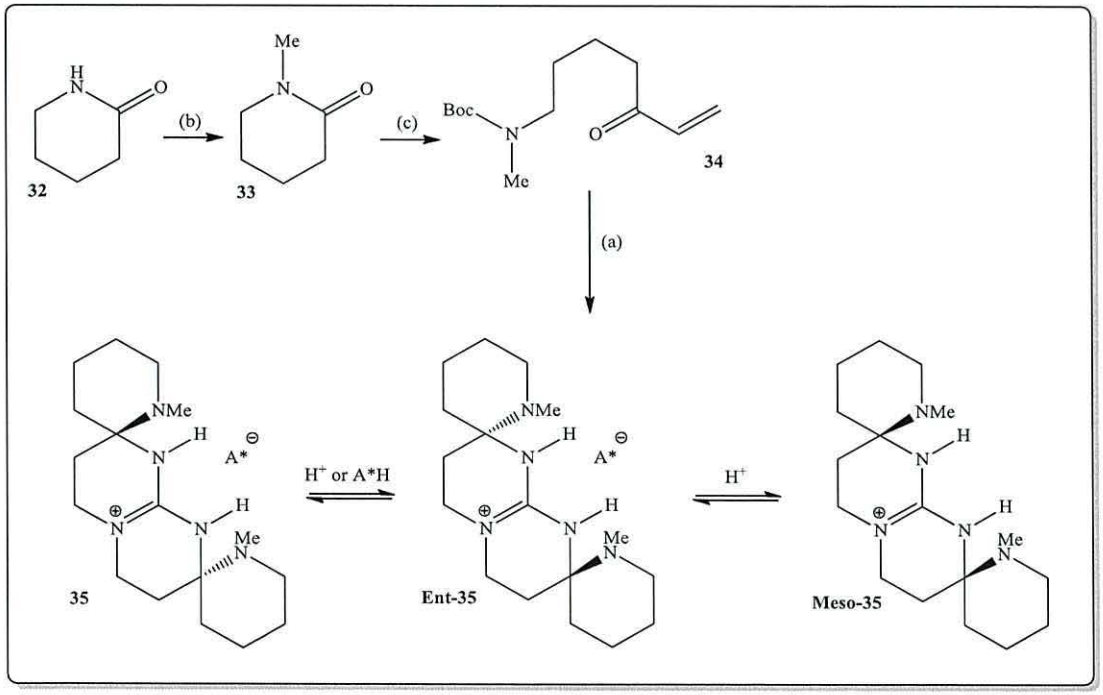

Scheme 9. (a) *n*-BuLi / MeI / THF / -78°C; (b) (i) 2 Eqv. CH_2=PPh_3 / Boc_2O; (ii) CH_2O / DCM.(c) 0.5 Eqv. Guanidine / H^+ / $NaBF_4$ (aq).

1.1.2.4. List of Synthetic Aims (Summary) –

- Synthesis of Murphy's catalyst **7** (BF_4^- anion) for pK_a analysis.
- Synthesis of **16** (BPh_4^- anion) and subsequent Michael addition catalytic testing.
- Synthesis of new C_2-Symmetric guanidine base catalyst **35**.

1.2. Results and Discussion

1.2.1. Synthesis of the Sensitive Compound Guanidine (Methodology 1a.)

Successful preparation of pure guanidine is vitally important as the cyclisation step is capricious and impure guanidine or guanidine that is wet with methanol used in the preparation can lead to a greatly diminished yield. The guanidine used in this reaction must be a solid on freezing at -20°C and must be methanol free (Scheme 10.).

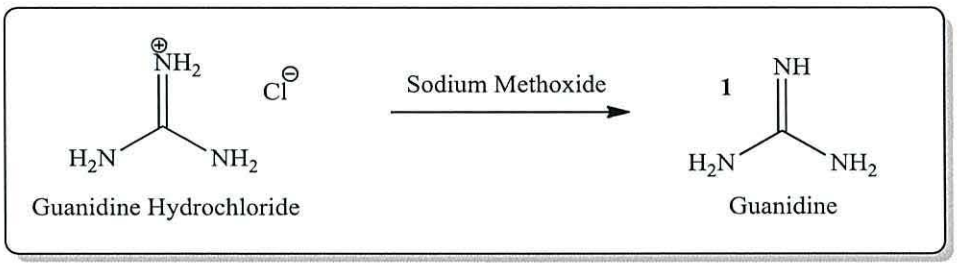

Scheme 10. Preparation of Guanidine from Guanidine hydrochloride.

Guanidine **1** is prepared by reaction of $Na_{(metal)}$, which is washed free of mineral oil with hexane and dried on a paper towel, with anhydrous MeOH at 0°C under a flow of argon (Figure 9a.). After the $Na_{(metal)}$ dissolved and the $H_{2(g)}$ evolution had ceased, dried (P_2O_5) guanidine hydrochloride was added to the mixture and the reaction vessel was fitted with a rubber septum, an argon balloon and then stirred at room temperature overnight. Stirring was then stopped, the mixture given a few minutes to allow the $NaCl_{(ppt)}$ to settle and was then carefully filtered through an oven-dried glass sintered filter under argon (Figure 9b.).

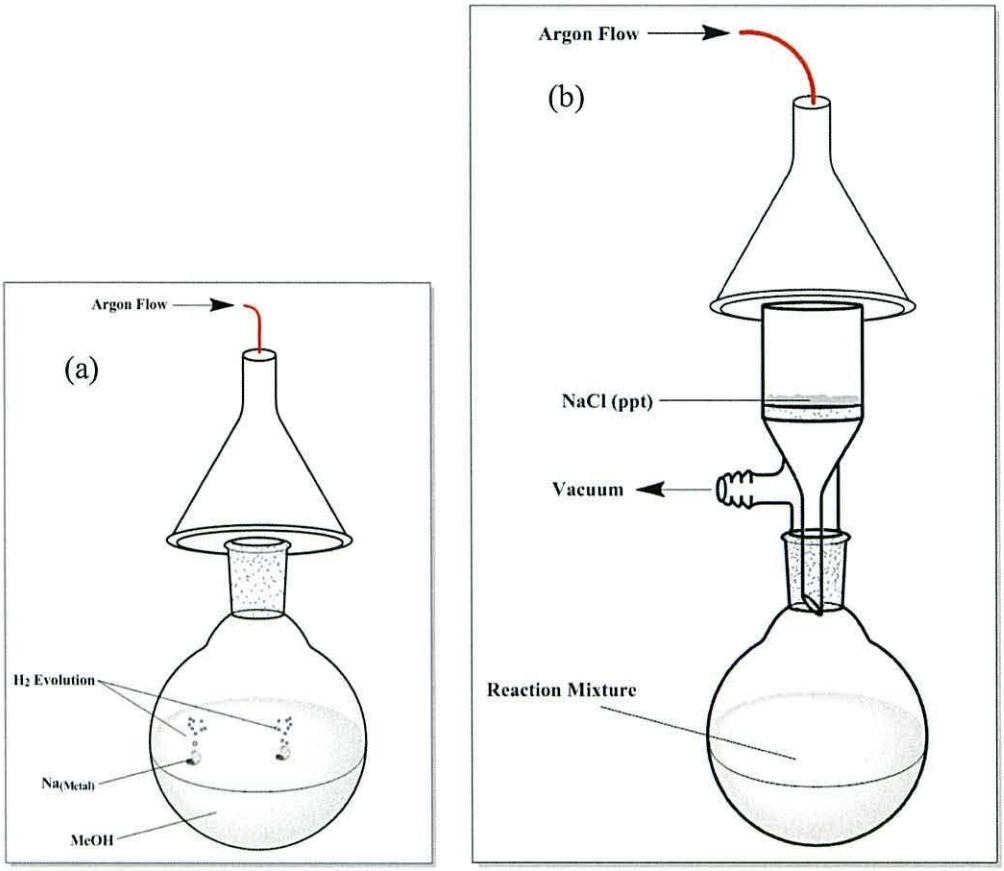

Figure 9.(a) Preparation of sodium methoxide; (b) Filtration of $NaCl_{(ppt)}$ under argon.

A rotary evaporator was washed thoroughly with acetone and then allowed to dry under vacuum, septa and argon balloons were then fitted at the inlet valves to allow an argon flush of the apparatus after evaporation. The mixture was then reduced to ≈ ¼ volume using a hot air gun as the heat source as to avoid any water vapour or steam near the apparatus, care was also taken not to overheat the reaction mixture. The thick solution with visible $NaCl_{(ppt)}$ was again filtered through an oven-dried sintered funnel under argon, followed by complete removal of the solvent *in vacuo*. The product was isolated as a colourless oil, which should be visibly free from any $NaCl_{(ppt)}$ and was placed under a high-vacuum for ≈ 1h. The guanidine was then sealed in a container and placed in the freezer upon which it solidifies into a waxy white solid in high yield (96%).

1.2.2. Synthesis of C_2-Symmetric Guanidine Bases

1.2.2.1. Route to Catalyst 7 (Murphy's Catalyst – Methodology 1b.)

The preparation of the guanidinium salts **37**, **7** and **16** (Scheme 11. X = Cl^- **37**, BF_4^- **7**, BPh_4^- **16**) has been previously reported in the group and requires the modification of ethyl (*R*)-3-hydroxybutyrate **5** over 5 steps as shown in Scheme 11.[13/12/11/27]

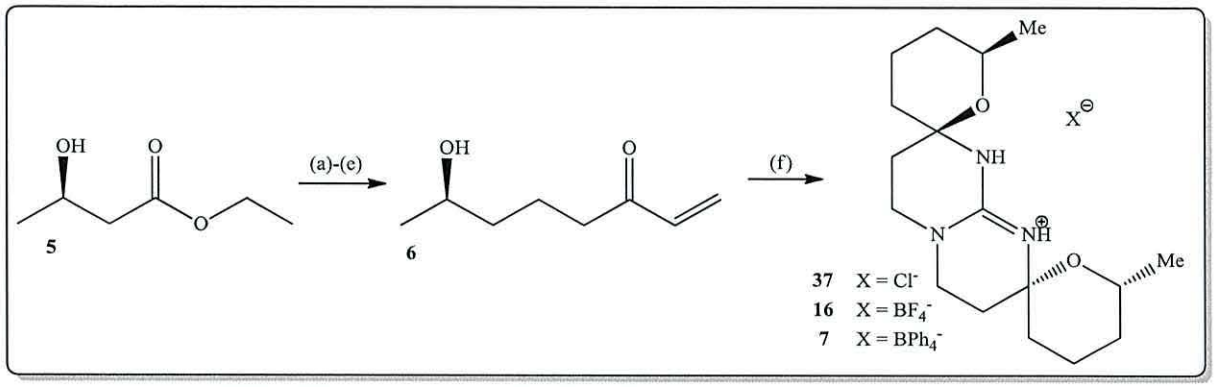

Scheme 11. (a) TBDMSCl / Imid / DMF; 99%; (b) DIBAL / hexane / -78°C; 82%; (c) TosCl / Py; 80%; (d) NaI / acetone; 85%; (e) (i) $CH_3COCHPPh_3$ / *n*-BuLi, (ii) H_2O quench, (iii) excess (aq) formaldehyde; 69%; (f) (i) guanidine / DMF / 0°C / 16h, (ii) HCl / MeOH / 3h, (iii) $NaBF_4$ / DCM; 44%.[12]

The first step (a) (Scheme 12.) was the protection of the alcohol function in **5** using the *tert*-butyldimethylsilane protecting group. Several attempts at this reaction were performed all with very high yields and no varying results. It is worth noting that in each attempt an apparent yield of > 100% was observed, analysis by ^1H and ^{13}C NMR showed that this was due to the presence of trace amounts of the solvent DMF (trace impurity in $CDCl_3$ [^1H – 8.02, 2.96, 2.88 ppm] [^{13}C – 162.62, 36.50, 31.45 ppm]) and also some tert-butyldimethylsilanol by-product due to the excess of TBDMSCl used. Re-dissolving the crude product in DCM and washing with H_2O followed by drying over $MgSO_4$, filtration and removal of solvent under high vacuum resulted in a pure product, however the trace impurities (DMF and silyl alcohol) did not affect the reaction efficiency or yield of the subsequent reduction step (Scheme 13.).

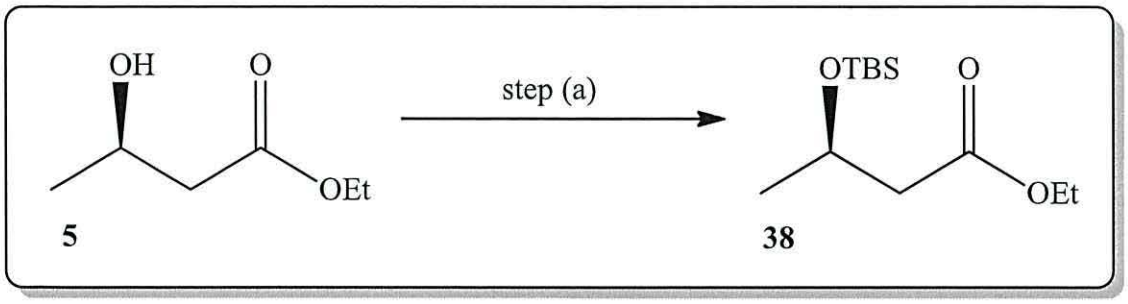

5 **38**

Scheme 12. (a) TBDMSCl / Imid / DMF; 99%.

The second step (b) (Scheme 13.) was the reduction of the protected ester **38** using DIBAL-H (Scheme 13.) at -78°C in anhydrous DCM followed by quenching of the reaction using Rochelle's salt which afforded product **39** (82 - 91% yield in 6 attempts).

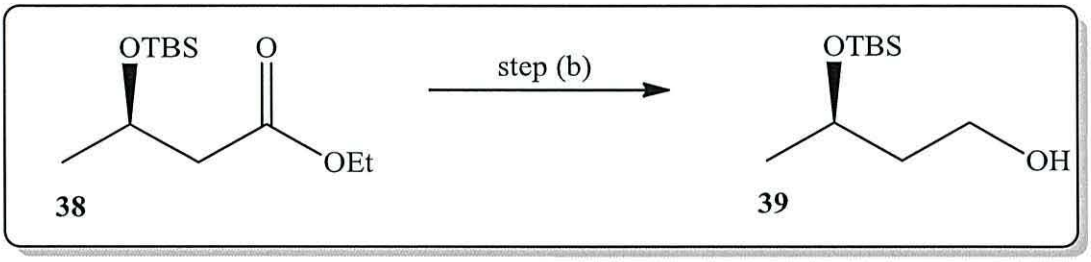

38 **39**

Scheme 13. (b) (i) DIBAH / DCM / -78°C; (ii) Et_2O / Rochelle's Salt; 91%.

The third step (c) (Scheme 14.) was the tosylation of the alcohol function in **39** using *para*-toluenesulphonyl chloride in pyridine. The tosyl group is electron-withdrawing therefore making it an excellent leaving group and pyridine is used as both the solvent and as a base to remove the HCl produced in the reaction. The first attempt at this reaction yielded only a 55% yield of **40** however a second attempt using a larger excess of *para*-toluenesulphonyl chloride and a longer reaction time afforded **40** in 88% yield. All subsequent tosylation reactions involved a slight excess of 1.3 equivalents and gave the product in > 88% yield (55 - 92% in 5 attempts).

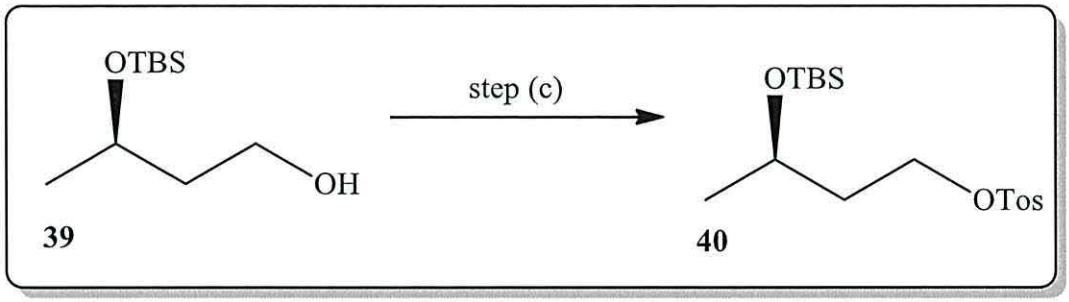

Scheme 14. (c) (i) *p*-Toluenesulphonyl chloride (1.3 eqvs) / Pyridine / 0°C; (ii) DCM / H_2SO_4; 92%.

The next reaction was the iodination of the tosylate **40** to the iodide **41** using NaI in acetone at reflux. The iodination reaction proceeds much smoother if the NaI is added to the reaction as a solution in dry acetone. The crude product was isolated as a yellow oil in 90% yield (range 84 – 90% in 4 attempts) after purification using silica column chromatography (Scheme 15.).

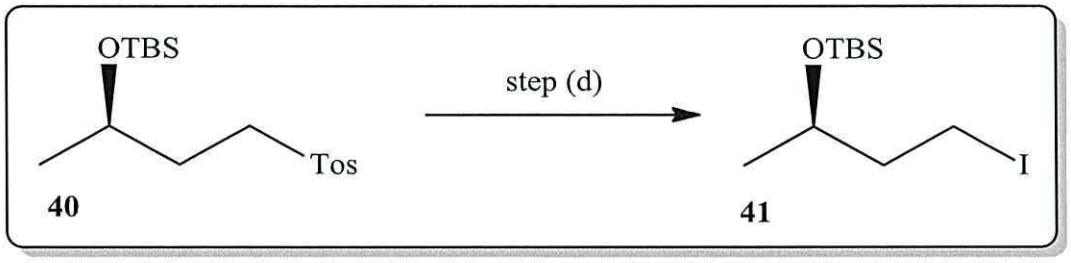

Scheme 15. (d) NaI / acetone; 78%.

The fifth and key step in the synthesis of enone **6** (step (e) Scheme 16.) and involves treatment of acetylmethylenetriphenylphosphorane (AMTP) with *n*-BuLi at -50°C to generate the intermediate anion **42** which is then reacted with the iodide **41** to give the phosphorane **43**, this is then treated with formaldehyde to give the enone **6**.

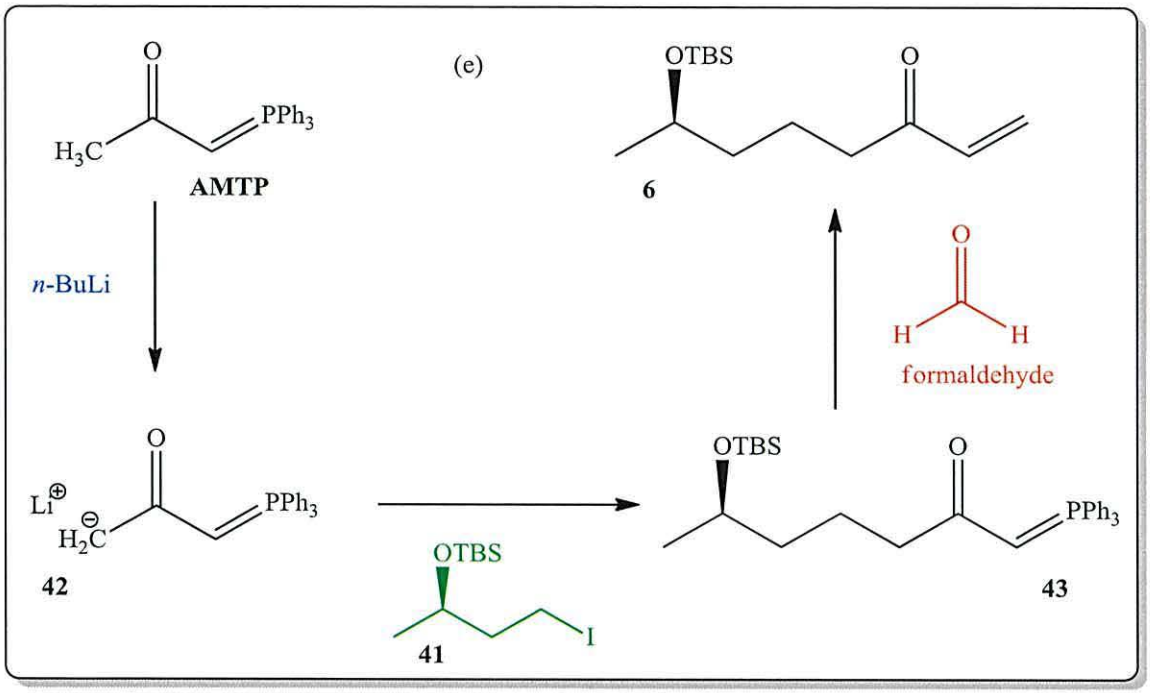

Scheme 16. (e) (i) AMTP / *n*-BuLi / -78°C, (ii) H_2O quench, (iii) excess formaldehyde; 79%.

1.2.2.2. *n*-BuLi Titrations (Methodology 1c.)

The stoichiometry of the first step of this reaction is iodide **41** : *n*-BuLi : AMTP = 1 : 1 : 1.1. In this reaction it is vital to determine the concentration (Figure 10.) of the *n*-BuLi and this was achieved by titration against diphenylacetic acid (DPAA). The volume of dry THF to be used in the titration was determined by using an equimolar ratio of reactant to solvent ie. by determining the molarity of the reaction with respects to the phosphorane and using the same molarity of DPAA. The concentration of the *n*-BuLi varied from reaction to reaction and is dependent on the dryness of the glass-ware, the quality and age of the *n*-BuLi but mainly on the water content of the anhydrous THF. Small amounts of H_2O present in the THF will react with *n*-BuLi to give LiOH and therefore reduces the carefully controlled amount of *n*-BuLi needed for the reaction which can reduce yields. The titration gives good indication of the residual H_2O content of the THF and if the concentration is very low can be a warning to attempt the preparation of dry THF and not to proceed with the reaction.

$$\text{Conc. of } n\text{-BuLi (M)} = \frac{\text{mmol of DPAA}}{\text{ml of } n\text{-BuLi}}$$

Figure 10. *n*-BuLi Titration: DPAA (1mmol, 0.212g) in dry THF (5.3ml).

Discussion Continued -

The enone **6** was purified using silica column chromatography and was typically isolated as a clear oil in 79%. The structure of the enone **6** was assigned by the ^{1}H and ^{13}C NMR's, specifically the ^{1}H ABX splitting pattern associated with the vinylic group (Figure 11.).

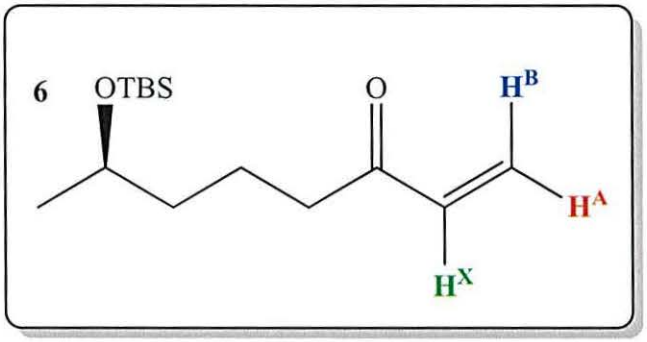

Figure 11. The vinylic ABX protons present in enone **6**.

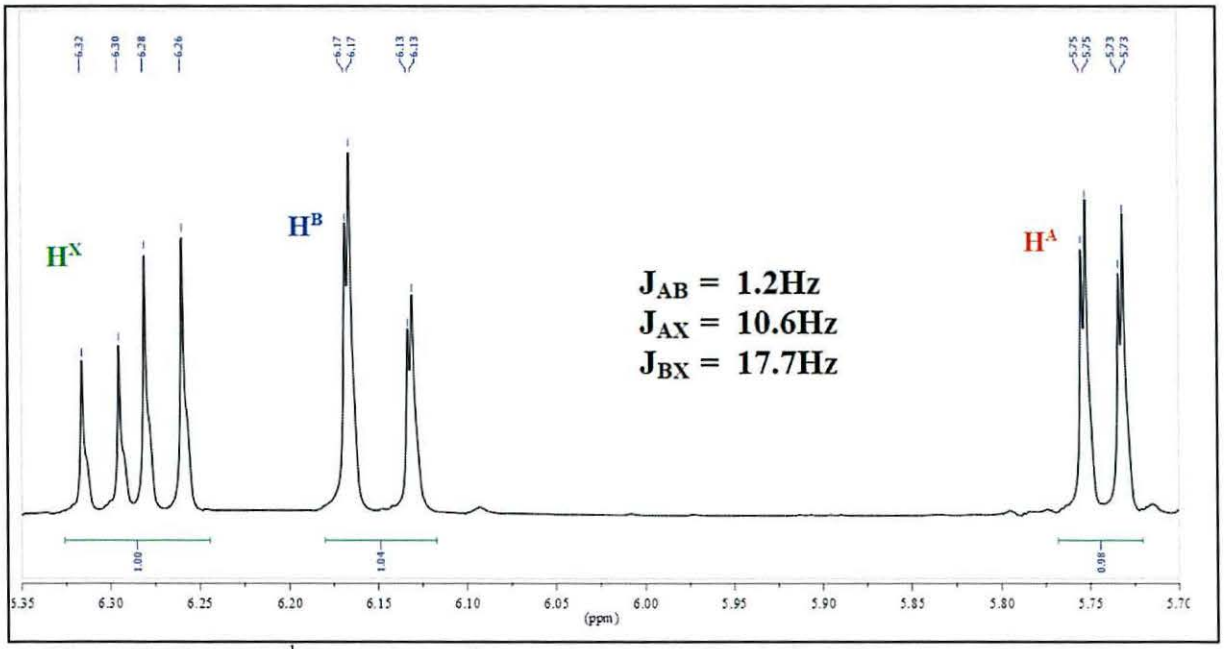

Figure 12. Expanded ^{1}H NMR in the alkene region showing the vinylic ABX proton peaks and J values.

The smallest J value (J_{AB} = 1.2 Hz) arises from the coupling of protons $\mathbf{H^A}$ and $\mathbf{H^B}$ on the same carbon that are different (diastereotopic) due to the fact there is no rotation about the double bond which is also referred to as geminal coupling (or two-bond coupling - ^2J). The largest J value (J_{BX} = 17.7 Hz) is the *trans* coupling between protons $\mathbf{H^B}$ and $\mathbf{H^X}$ whilst the J_{AX} value (10.6 Hz) is the *cis* coupling between protons $\mathbf{H^A}$ and $\mathbf{H^X}$. The chemical shifts are $\mathbf{H^X}$ 6.29 ppm, $\mathbf{H^B}$ 6.15 ppm and $\mathbf{H^A}$ 5.74 ppm (Figure 12.).

Lower yields for this reaction were observed, the cause of which can be attributed to the varying H_2O content of the dry THF. The dry THF used in the reaction with the best yield was obtained from a condenser reflux distillation set-up using $Na_{(metal)}$ wire with benzophenone as an indicator of air and water content (a colour change from blue / black → deep purple indicates good quality anhydrous THF). The benzophenone reacts with $Na_{(metal)}$ producing diphenylketyl anions which give the solution a deep purple colour (blue or purple depending on the solvent). The ketyl anion is soluble in many organic solvents and therefore can easily react with any air or water present giving stable non-volatile products. Distillation of THF from this mixture and immediate use generally gives the best results.

The anhydrous THF from the sodium/benzophenone still gave the highest concentration of *n*-BuLi and a good overall reaction yield (79%). Other attempts at this reaction used dry THF from a multi-solvent purifier system with varying *n*-BuLi concentrations and poor yields (23% - 65%). Reverting to THF from the distillation apparatus once again gave good yields in the production of enone **6**.

With the enone in hand the preparation of catalyst **44** was attempted using the conjugate addition of guanidine to 2 equivalents of enone **6** followed by acid catalysed deprotection of the silyl groups and cyclisation leading to the catalyst **44** (Scheme 17.).

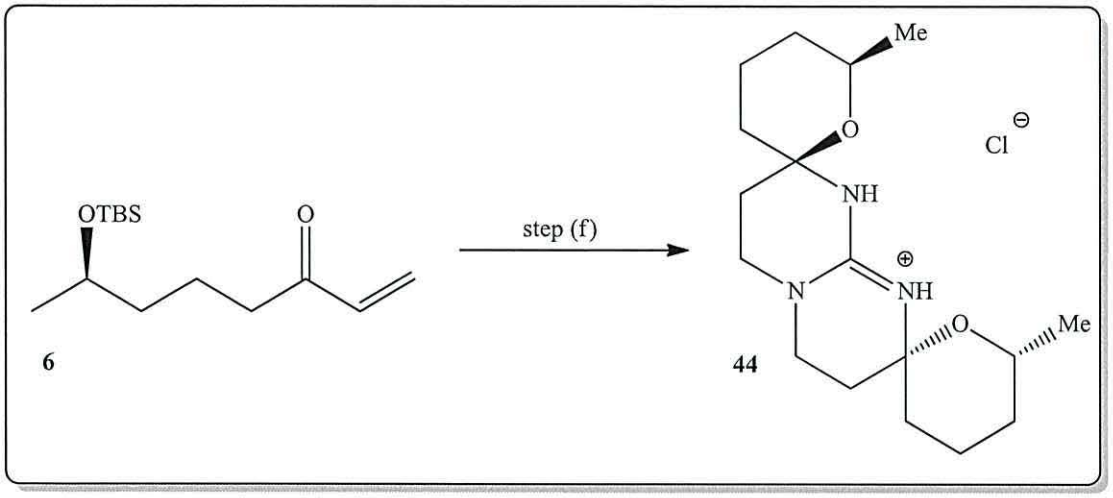

Scheme 17. (f) (i) guanidine / DMF / 0°C / 16h, (ii) HCl / MeOH / 3h, (iii) $NaBF_4$ / DCM; 44%.

The other key step in the synthesis of catalyst **7** is the final conjugate addition of guanidine to enone **6**. Freshly synthesised guanidine was prepared before each attempt and was isolated as a colourless oil which gave a waxy white solid upon freezing (-20°C). It is of importance that all manipulations using guanidine are carried out under an atmosphere of argon as free guanidine is very hygroscopic. Enone **6** was dissolved in dry DMF and cooled to 0°C, at this temperature a solution of guanidine in DMF was added drop-wise over ≈ 5 mins. The mixture was left in the ice bath and allowed to warm to RT overnight. After cooling to 0°C, methanolic HCl is carefully added and the mixture again left to stir for three hours. Water was then added and the product extracted with chloroform and washed with brine, followed by H_2O. The product **44** is obtained as a waxy solid in 8 – 17% yield over 5 attempts.

These yields were disappointing and lower than those previously reported.[12] It is supposed that the yields obtained are dependent on the use of freshly prepared and dried guanidine and the use of good quality anhydrous DMF. The successful preparation of guanidine is achieved using anhydrous conditions, however the most important step appears to be the complete removal of residual MeOH (reaction solvent) which can be achieved using an efficient high-vacuum pump. Unsuccessful guanidine cyclisation reactions were

encountered due to incomplete removal of residual MeOH from the guanidine, which was found to be due to reduced pressure coming from the vacuum pump. This reduction in pressure was rectified by directly connecting the guanidine sample to the high-vac as the Schlenck manifold previously employed gave rise to minute leaks in the system and resulted in pressures not sufficient to fully remove all traces of MeOH (even with gentle heating of the sample).

The presence of the desired compound **7** is easily identified from consideration of the ^{13}C NMR spectra as shown below (Figure 13.) with the signal for the guanidinium carbon appearing at 149.30 ppm and the quaternary carbons for the pyran rings at 78.63 ppm.

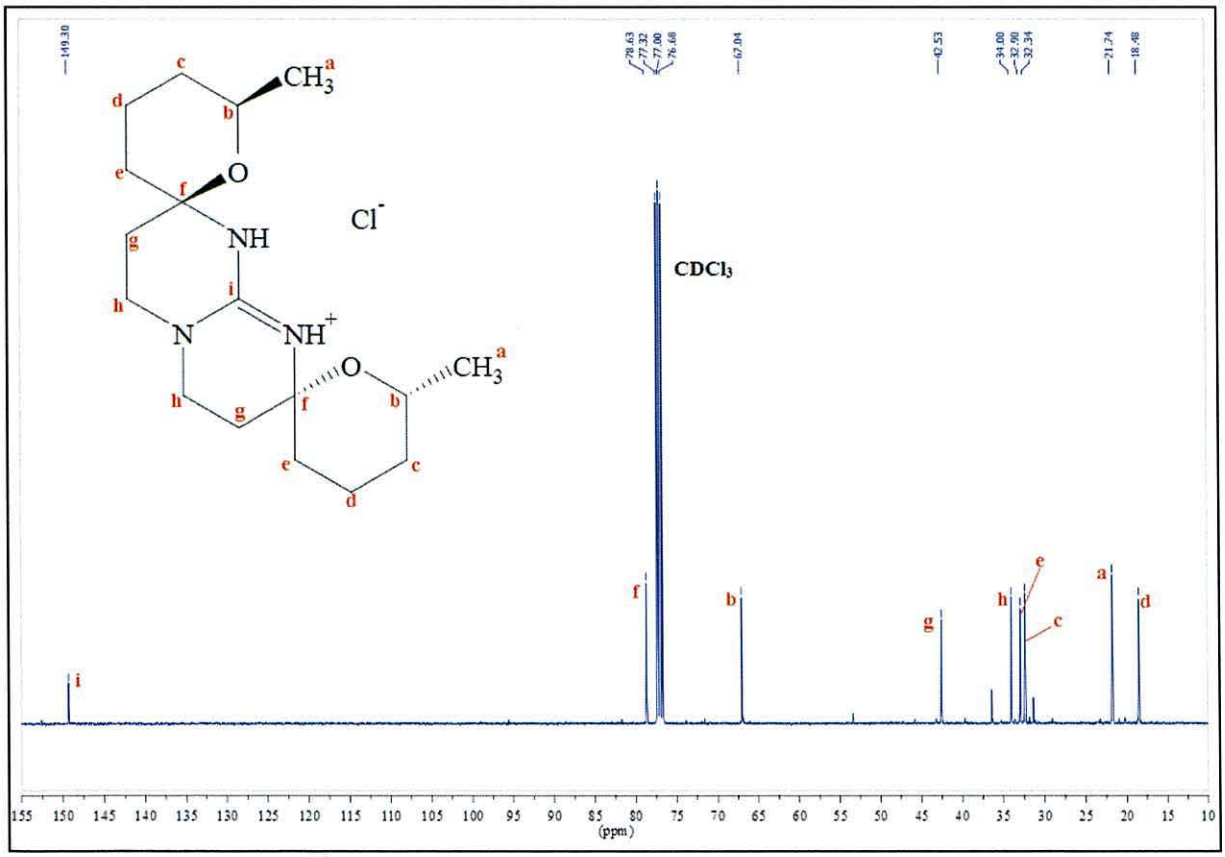

Figure 13. The annotated ^{13}C spectra of guanidinium salt **44** (Spectrum acquired in $CDCl_3$ at 500 MHz).

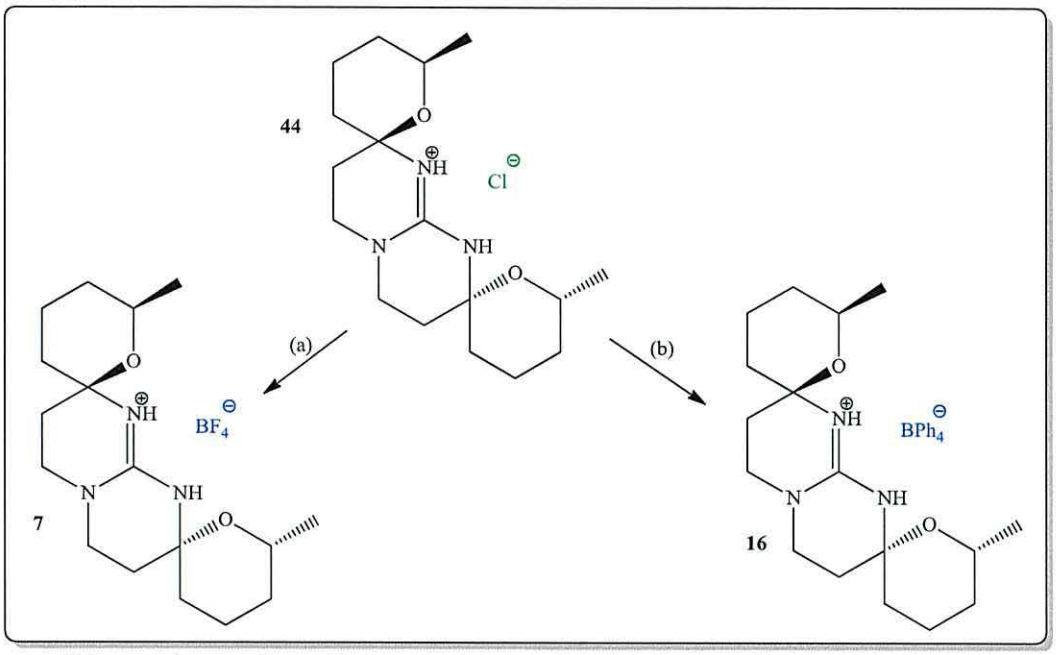

Scheme 18. Ion exchange of guanidinium catalysts. (a) DCM / $NaBF_4$ (aq); 15%; (b) THF / $NaBPh_4$; 88%.

1.2.2.3. Preparation of Catalyst 7 (BF_4^-) (Methodology 1d.)

The final preparation of catalysts **7** and **16** can be achieved by exchange of the chloride ion for the BF_4^- ion or BPh_4^- ion (Scheme 18a.). The ion exchange of Cl^- to BF_4^- is performed by stirring the chloride salt with saturated aqueous $NaBF_4$ solution followed by separation and purification using column chromatography (MeOH : $CHCl_3$, 0% - 3% in 0.25% increments, Rf = 0.16 in 5% MeOH : $CHCl_3$). The product from this column is finally triturated in Et_2O : Hexane (4 : 1) affording the solid catalyst **7** as a free flowing white powder.

1.2.2.4. Preparation of Catalyst 16 (BPh_4^-) (Methodology 1e.)

The exchange of the chloride ions in **44** to give **16** (Scheme 18b.) was achieved by treatment with an excess of $NaBPh_4$ in THF and stirring for 8 h. Evaporation of this solution followed by washing with water removes excess $NaBPh_4$ and the NaCl generated in the ion exchange. The compound was characterised by ^{13}C NMR spectroscopy giving the requisite

signals for the borate counter ion which was also identified in the ^{11}B NMR at -6.3 ppm which is consistent with the literature (Figure 14.)[28]

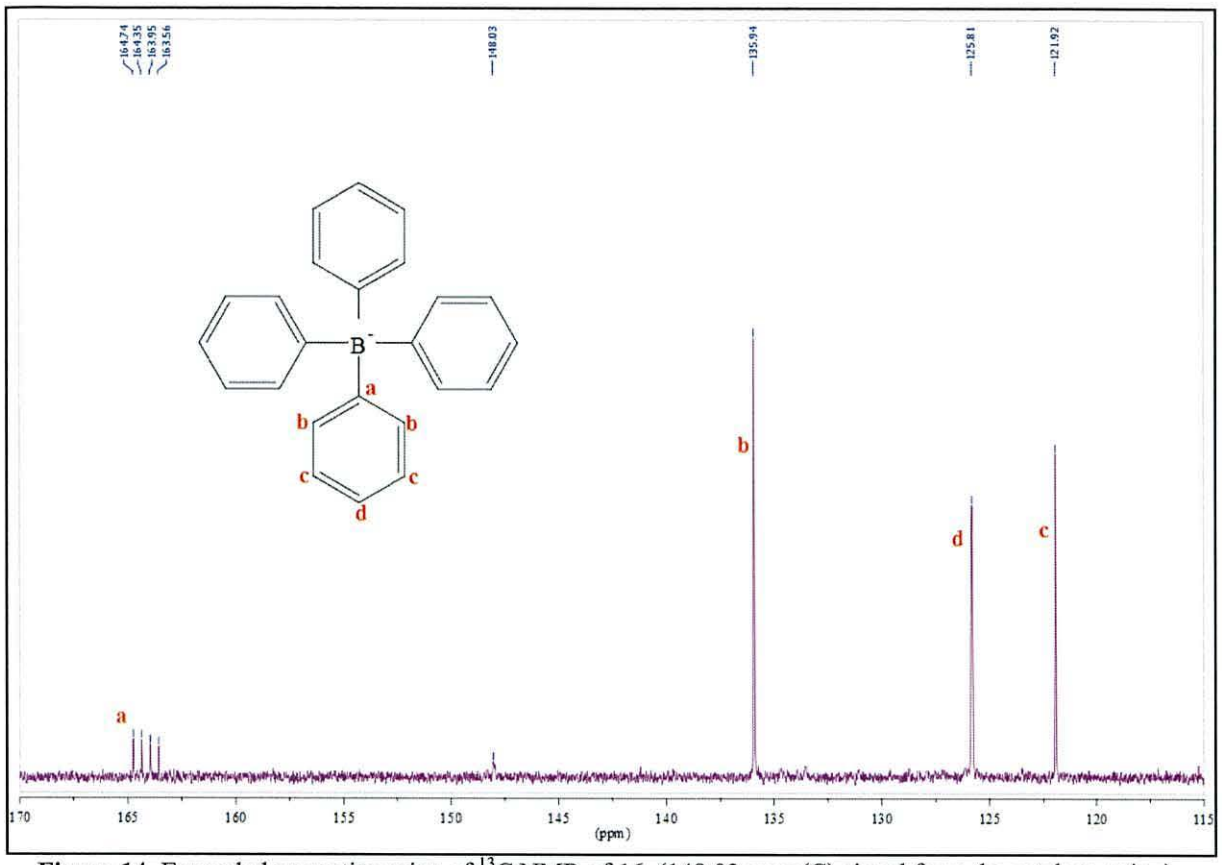

Figure 14. Expanded aromatic region of ^{13}C NMR of **16**, (148.03 ppm (C) signal from the catalyst cation).

1.2.3. pK_a Determination of Catalyst 7 and Related Compounds in DMSO (Methodology 1f.)

One of the major goals of this research was the determination of the pK_a value of the catalyst species G. The method for determination of this value is a bracketing buffer method[29] and was determined in the O'Donohue research group in the Department of Chemistry at Durham University. This method uses UV-Vis spectrophotometric data from which pK_a's can be calculated via the manipulation of the equilibrium constant (K_{eq}) between a buffered solution of the target compound with their corresponding conjugate base (generated *in situ*) and a selected indicating compound (with a known pK_a value up to 2 units either side of the compound under investigation Equation 2.).

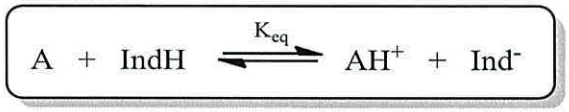

Equation 2. Equilibirum between the buffered compound and an indicator.

The equilibrium constant (K_{eq}) can be defined using Equation 3a., which can also be re-written as Equation 3b., therefore by implementing the observed absorbance change upon ionization at a single analytical wavelength, K_{eq} can be caluculated.

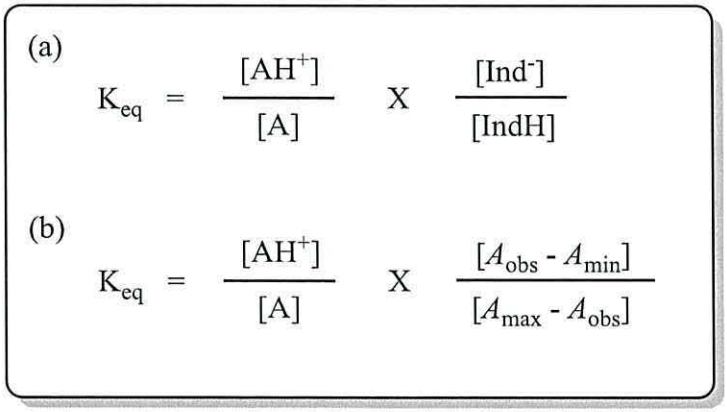

Equation 3. (a) & (b) Definitions of the equilibrium constant K_{eq}.

A_{max} corresponds to the absorbance observed for the fully ionized indicator (Ind^-) at a single analytical wavelength and was obtained using excess potassium dimsyl until there was

no further increase in absorbance. A_{min} corresponds to the minimum absorbance observed for the fully protonated indicator (IndH) at a single analytical wavelength and was obtained by adding excess HCl(aq) (final concentration of HCl was 50 mM, total concentration of H_2O in DMSO was 1% V/V). A_{obs} corresponds to the absorbance observed for a given HA / A^- ratio at a single analytical wavelength. Figure 15. shows graphically how A_{max}, A_{obs} and A_{min} can be obtained from UV-Vis spectra.

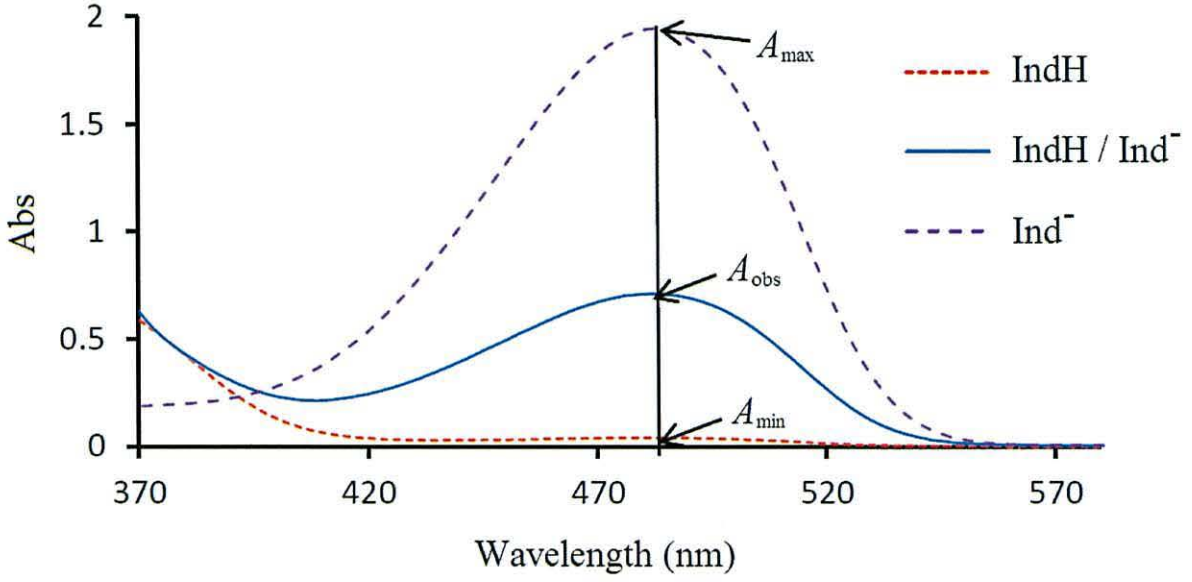

Figure 15. Representative UV-Vis spectra for an indicator in the presence of excess HCl (----), a buffered HA / A^- mixture (—) and an excess of potassium dimsyl (-----).

Using the measured K_{eq} value, pK_a's for the target compounds (Brønsted acids) can be calculated using Equation 4., in combination with the known pK_a value of the relevant indicator used.

$$pK_a(AH^+) = pK_a(IndH) + \log_{10}K_{eq}$$

Equation 4. Determination of pK_a from measured K_{eq}.

Table 4. pK_a values for the indicators used in the spectrophotometric experiments.

Indicator	Structure	pK_a (DMSO) w. Ref
2,4-dinitrodiphenylamine	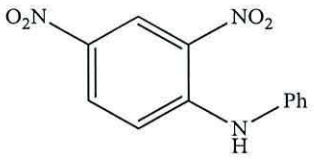	12.74± 0.04[30]
2-naphthol	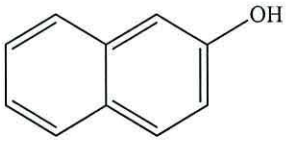	17.10± 0.03[31]

The UV-Vis spectra of 2,4-dinitrodiphenylamine buffered by Brønsted acid solutions of compound **7** can be seen in Figure 16. along with the corresponding data in Table 5. The average value of K_{eq} is quoted with the corresponding standard deviation (Equation 5.).

Equation 5.

$$SK_{eq} = \sqrt{\frac{\Sigma(K_{eq} - K_{eq}^{av})^2}{n-1}}$$

Using the average K_{eq} (K_{eq}^{av}) the pK_a may be calculated using Equation 4. Using Equation 6. the standard deviation may then be calculated for the pK_a.

Equation 6.

$$SpK_a = \sqrt{S_a^2 + S_b^2}$$

Where S_a is the standard deviation quoted for the pK_a of the conjugate acid of the indicator and S_b calculated using Equation 7.

Equation 7.

$$S_b = \frac{(0.434)(SK_{eq})}{K_{eq}^{av}}$$

A range of compounds were also investigated including the previously prepared compounds **10 - 12**,[13] the tricyclic compound **45**[32] which does not possess the 2 axial oxygen substituents and the commercially available guanidines **46** and **47** (Figure 16.). It was hoped that consideration of these results would give some insight into the effects of structure on the basicity of the guanidines.

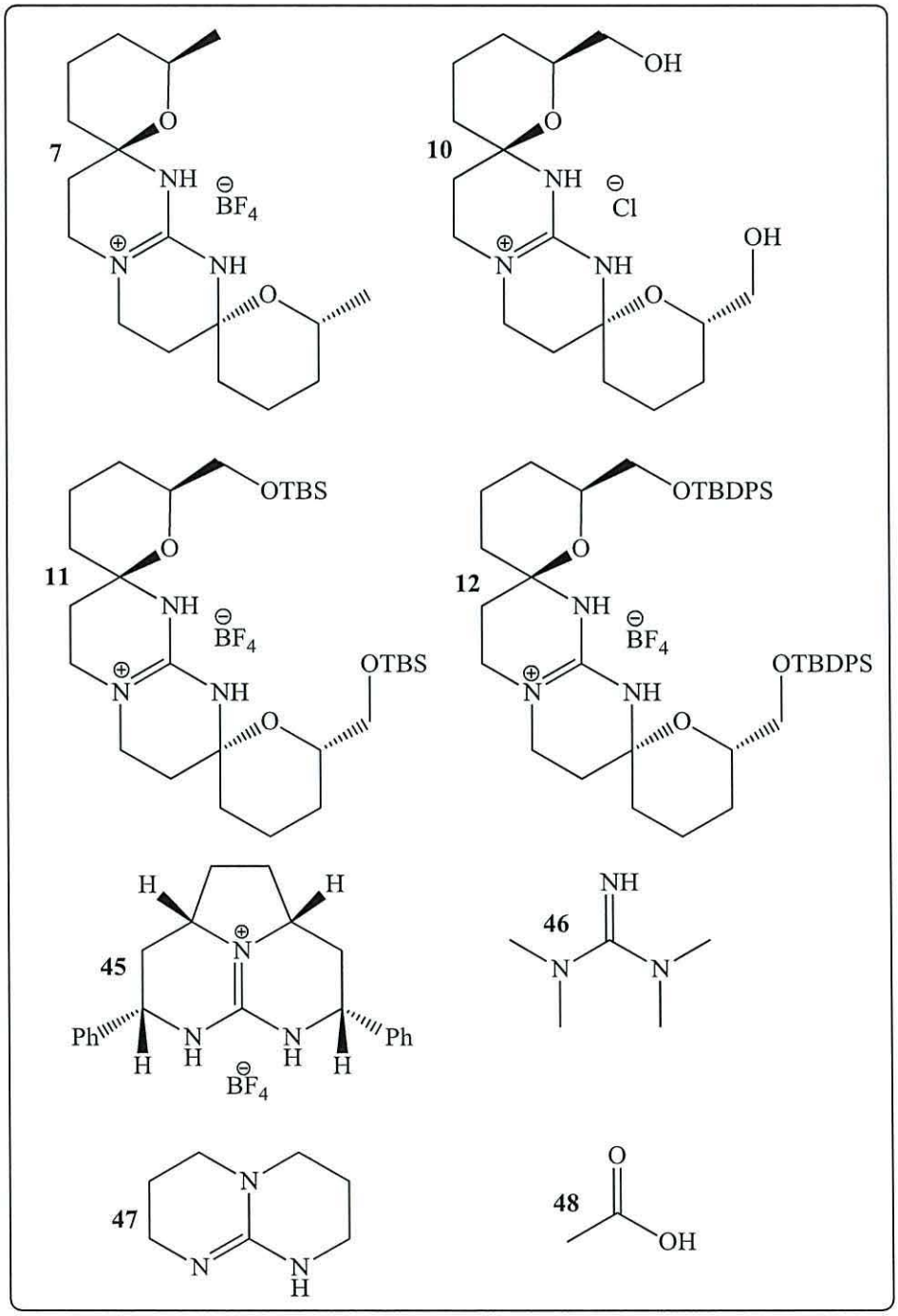

Figure 16. Guanidine compounds for pK_a analysis **7, 10 - 12, 45 – 47** (acetic acid reference **48**).

The UV-Vis bracketing buffer method for compound **7** was then carried out as described in Methodology 1f. (p.26), the results for which are given in Figure 17. and Table 5. below.

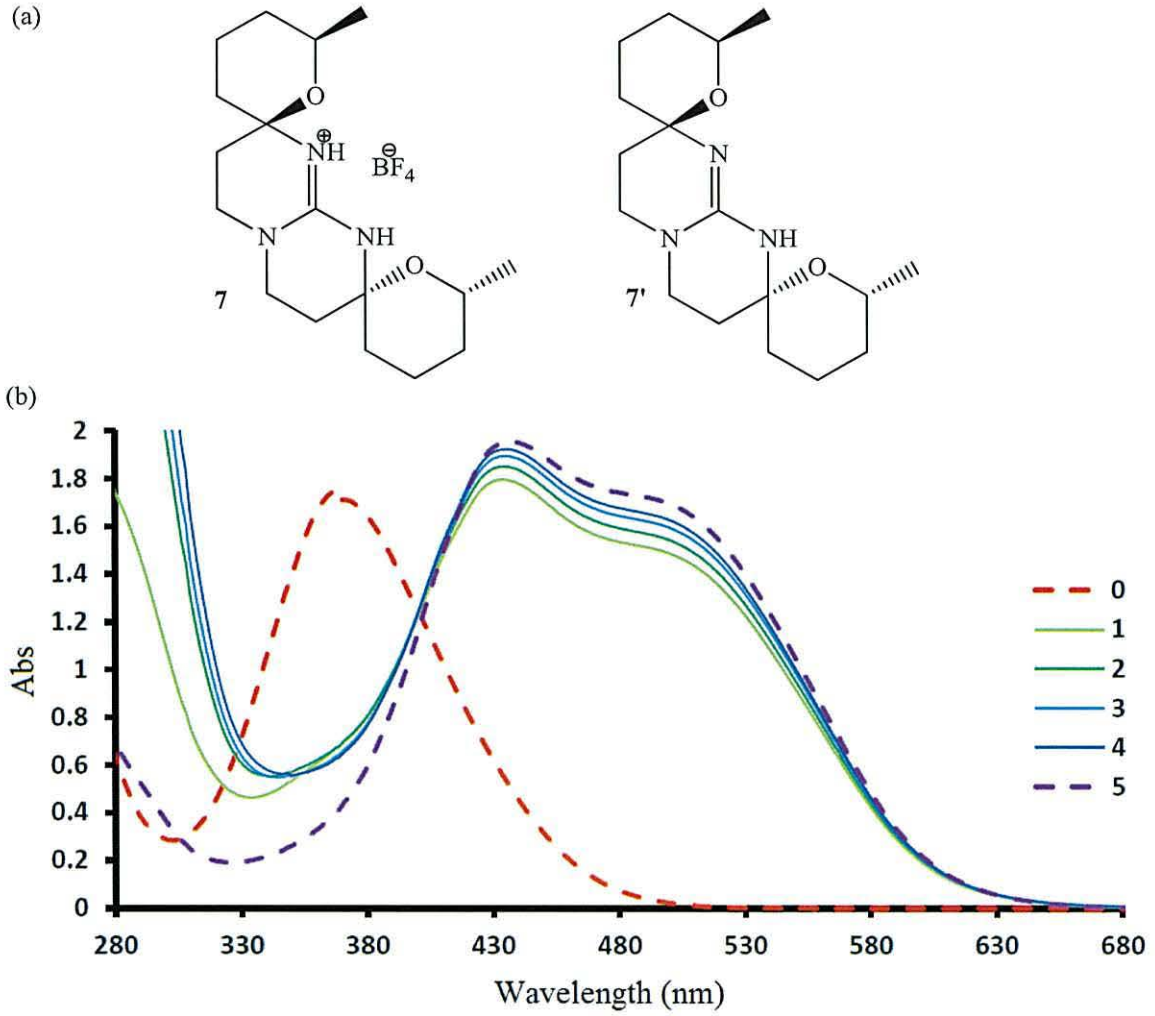

Figure 17. (a) Structure of **7** and **7'**. (b) UV-Vis spectra of 0.1mM 2,4-dinitrodiphenylamine in DMSO using different ratios of **7** and **7'** at 25°C.

Table 5. Absorbance data for 2,4-dinitrodiphenylamine[a] in DMSO at 495 nm at 25°C.

Spectrum No.	[7] (mM)	[7']^{b} (mM)	Abs (495 nm)	K_{eq} ^{c}
0	0.00	0.00	0.033	-
1	2.02	0.98	1.504	14.62
2	1.70	1.30	1.558	12.90
3	1.37	1.63	1.611	13.10
4	1.05	1.95	1.644	12.76
5	0.00	0.00	1.712	-

[a][2,4-dinitrodiphenylamine] = 0.1 mM; spectrum 0 represents fully protonated indicator (IndH) and spectrum 5 fully ionised indicator (Ind—).
[b]Anion 7' was generated *in situ* by addition of potassium dimsyl.
[c]See calculation for K_{eq} Equation 8.

From the data given in Table 5. the K_{eq} was calculated from:

Equation 8.

$$K_{eq} = \frac{[7]}{[7']} \times \frac{(A_{obs} - 0.033)}{(1.712 - A_{obs})}$$

And the average K_{eq} was calculated as 13.34± 0.86 and by using Equation 7. the pK_a is calculated as 13.87± 0.05.

1.2.3.1. pK_a's of Related Guanidine Compounds

UV-Vis spectra and pK_a calculations for the guanidine compounds **10** – **12** and **45** – **47** were then performed analogously (full data is available in the appendix) and the K_{eq} and pK_a results for the compounds shown in Figure 16. are given in Table 6. Also given is the method check calculated pK_a for acetic acid **48** (measured at 12.48) which is used as a reference and was in agreement with the literature (measured at 12.3) both in DMSO at 25°C.[31]

Table 6. Equilibrium constants (K_{eq}) and pK_a's of guanidine compounds (Figure 16.) in DMSO.

Entry	Compound	K_{eq}	pK_a
1	**7**	13.34±0.86	13.87± 0.05
2	**10**	14.96± 2.22	13.91± 0.08
3	**11**	7.63± 0.73	13.62± 0.06
4	**12**	2.88± 0.33	13.20± 0.06
5	**45**	8.85± 0.60	13.69± 0.05
6	**46**	1.98± 0.10	13.04± 0.05
7	**47**	0.11± 0.01	16.14± 0.05
8	**48**	0.55± 0.06	12.48± 0.06

All pK_a's were found to be > 13 (except the acetic acid reference sample **48**). With respect to the tetracyclic compounds (**10 - 12**), it can been seen that an increase in steric bulk at the pendant –OH group position results in a lowering of the pK_a values to a small extent. Literature compound **47** was found to have the highest pK_a and again this was in agreement with the literature .[31/33/34]

1.2.4. Investigation of the Quinone Michael Addition Reaction Catalysed by 16

With the catalyst **16** in hand we next turned to the investigation of its ability as an enantioselective catalyst in the previously investigated Michael reaction between the quinone **29** and nitrostyrene **30** (Scheme 19.). The general method for this reaction was to treat one equivalent of the quinone **29** with an excess of *trans*-β-nitrostyrene initially at 0°C with 0.05 molar equivalents of the catalyst **16** and to monitor the reaction by ^{1}H NMR (Figure 19.).

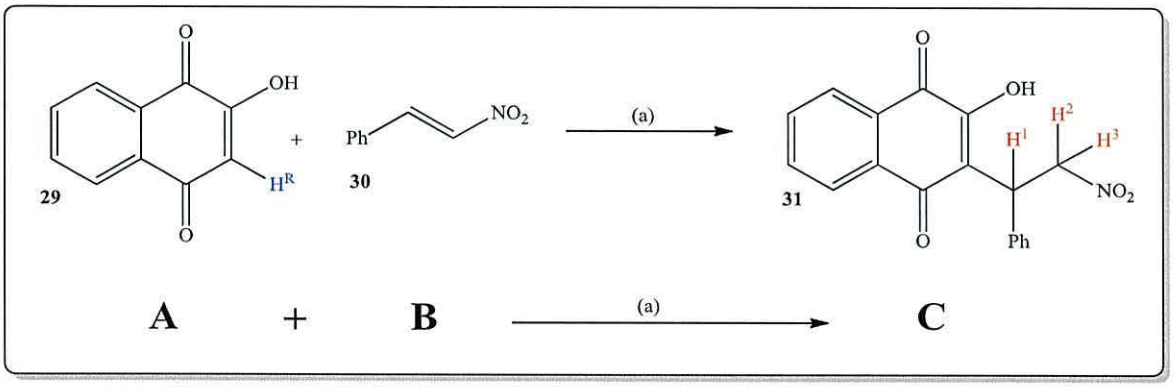

Scheme 19. (a) Catalyst **16** 0.05 eqv / Solvent (THF / EtOH) / 0°C → RT. H^R = hydrogen signal from the reactant. H^1, H^2 & H^3 = hydrogen signals from the product.

In the ^{1}H NMR, the alkene hydrogen signal from the starting material quinone H^R (Figure 19.) was used as a reference peak at 6.30 ppm and the integration of H^R was set to 1.00. An average integration of the three product hydrogen signals H^1, H^2 & H^3 were taken and a ratio of starting material to product calculated. Figure 19. shows the disappearance of the starting material signal H^R and formation of product signals $H^{1/2/3}$ over time. Although many data points were measured, 5 selected stages were taken for the stacked reaction progression NMR below (for full data table see appendix).

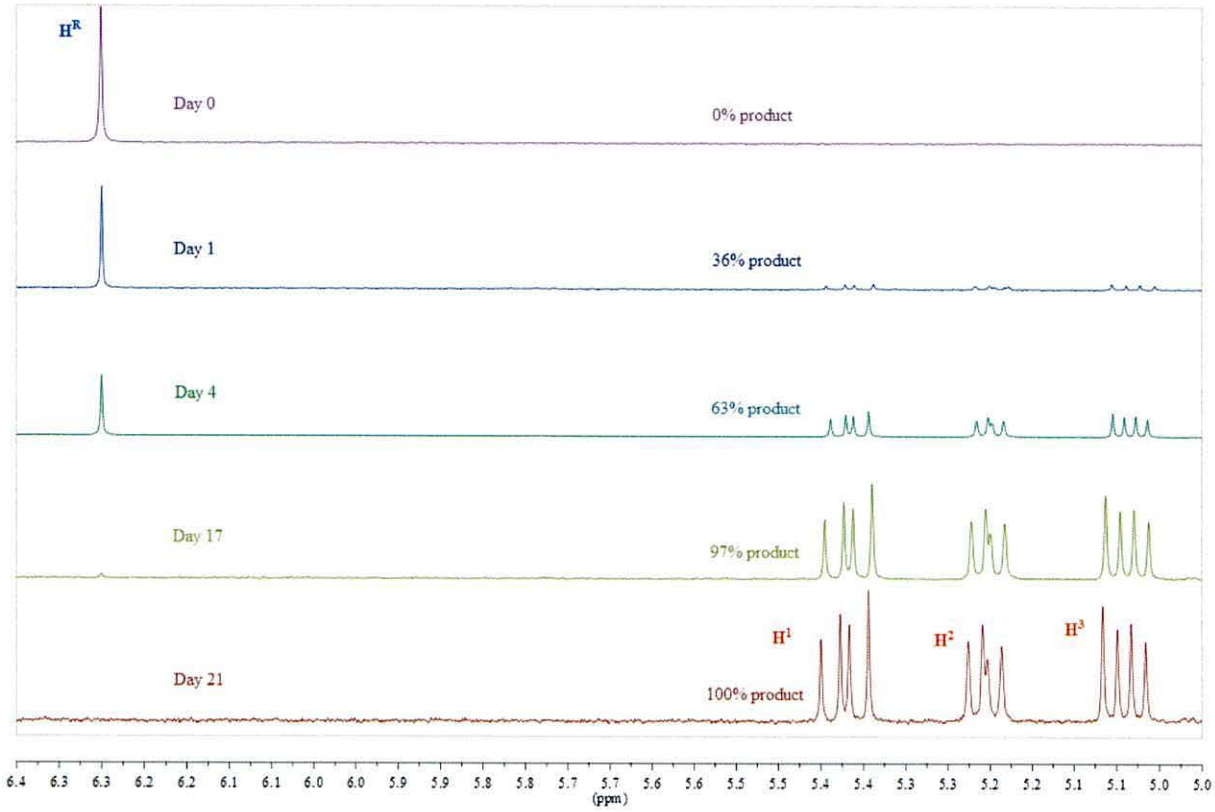

Figure 19. Stacked NMR's showing disappearance of product signal H^R and formation of product signals $H^{1/2/3}$.

1.2.4.1. Purification of Catalysed Michael Addition Products (Methodology 1g.)

When the product formation reached 100% (or sufficient end point had been determined) the reaction solvent was removed *in vacuo* and the product purified using silica gel column chromatography (25% DCM : Petrol followed by 100% DCM). The 25% DCM : Petrol was to separate any unreacted *trans*-β-nitrostyrene which comes off in < 5 column pots and has a high running Rf = 0.89 in 100% DCM. The product can then be eluted in 100% DCM affording the pure bright yellow solid product with an Rf = 0.22 in 100% DCM in high yields. Although visualisation of the TLC's can be achieved in I_2 or PMA, due to the highly coloured nature of both the product and starting material it is extremely clear on the TLC plate even without staining. It is also extremely easy to identify the product and remaining starting material coming through the column (and in the individual column pots) due to their respective colours (*trans*-β-nitrostyrene shows as a translucent green / yellow colour in DCM

and the product a bright yellow) although it should be noted that the colour of column pots is not always a reliable indicator of separation. In both solvents (THF / EtOH) when product formation exceeds ≈ 80% the compound falls out of solution (precipitation) as a fine yellow solid, care was taken to ensure homogenous samples were removed for analysis by NMR to maintain reliability of results.

1.2.4.2. Discussion of Catalytic Results

Time was measured in hours and a table of reaction rates, product formation and e.e.'s (from HPLC) were collated, 5 experiments were performed:

Table 7. Table of results for catalytic reactions.

Entry	Solvent (15ml)	Catalyst	Additive	$T_{1/2}$ h (days)	Time h (days)	Conversion (%)	e.e. (e.r.)
1	THF	None	None	N/A	1699 (71)	< 1	N/A
2	EtOH	None	None	509 (21)	1392 (58)	74.8	N/A
3	EtOH	None	H_2O (0.5ml, 3.3%)	65 (2.7)	712.5 (30)	100	N/A
4	THF	**16**	None	465 (19)	1699 (71)	84.8	(44:56) 12.3%
5	EtOH	**16**	None	39 (1.6)	477 (20)	100	(42.5:57.5) 15.2%

Entry 1 (Table 7.) was the background reaction in THF without catalyst **16** and after 71 days little to no observed reaction had occurred. Entry 2 was the background reaction in EtOH without catalyst **16** and has a $T_{½}$ of 21 days, after 58 days the reaction was halted at 75% completion. Entry 3 was the reaction performed in EtOH with water as an additive, which reached $T_{½}$ in 2.7 days and 100% completion after 30 days and it is clear that water significantly increases the rate of this reaction suggesting that a proton donor is of importance in the mechanism

The reactions involving catalyst **16** (0.05 eqvs) was first attempted in THF and was found to reach $T_{½}$ in 19 days and after 71 days had reached 85 % completion. The reaction

would have eventually reached completion but was halted due to time restraints. Extrapolation of Graph 1 (product formation [C] vs time) gives an estimated 100% conversion time of ≈ 88 days. The enantiomeric ratio (e.r.) was determined by HPLC as 44 : 56 with an e.e. of 12 %. Repetition of this reaction in EtOH (Entry 5) with catalyst **16** (0.05 eqvs) gave a much faster rate of reaction with a $T_{½}$ of only 1.6 days and full conversion to product quinone **31** was achieved in 20 days. The enantiomeric ratio (e.r.) was determined by HPLC and gave an e.r. of 42.5 : 57.5 with an e.e. of 15 %.

It is apparent that the rates of reaction, both catalysed and uncatalysed were significantly faster in EtOH (Entries 2, 3 and 5) and addition of H_2O or the catalyst **16** was found to increase the rate of reaction further. The e.e.'s for these reactions were not spectacular but were higher than those reported for the BF_4^- catalyst suggesting that the more open guanidinium motif on the catalyst leads to an improvement in asymmetric induction.

Determination of the order of reaction and also the rate constant (*k*) (to compare Entries 1 - 5) was achieved by plotting graphs of concentration Vs time.

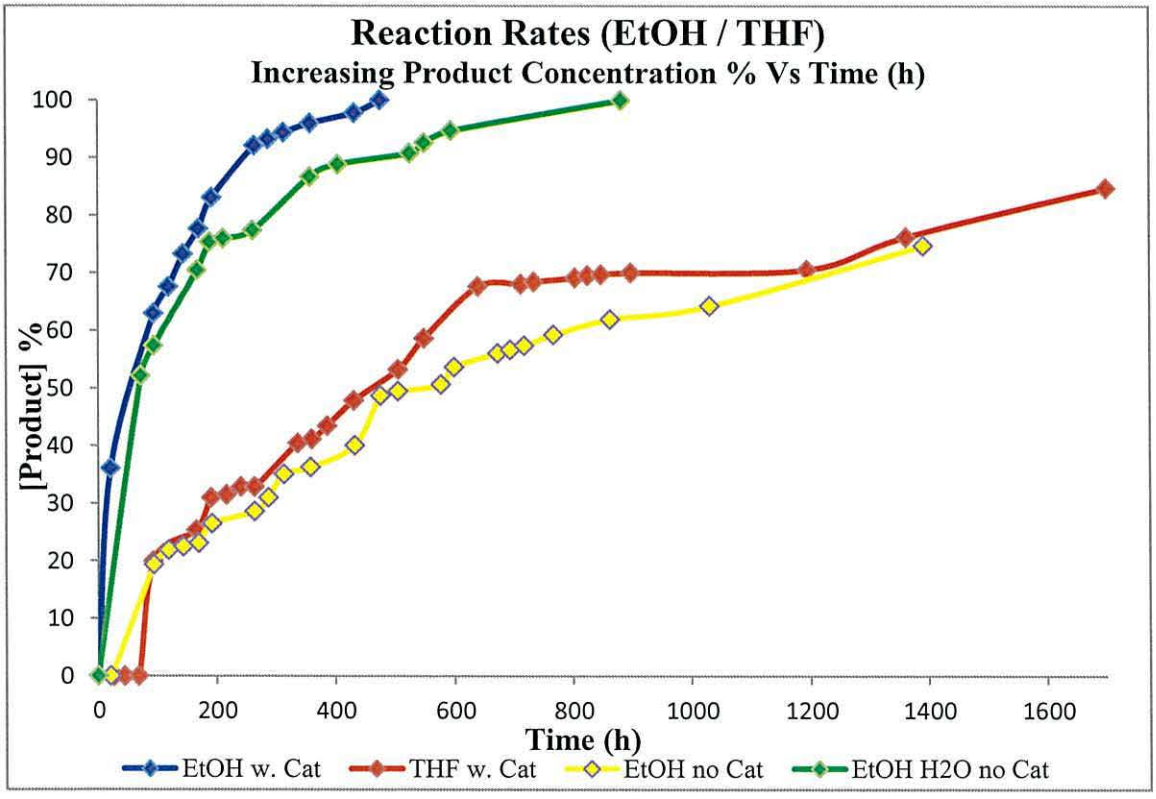

Graph 1. Rate of increasing product concentration (%) against time (h).

Graph 1. shows formation of the product [C] plotted against time (h) and gives a good initial indication of the exponential decrease in rate. However in order to determine the rate constant (k) a plot of decreasing reactant concentration [A] Vs time is needed.

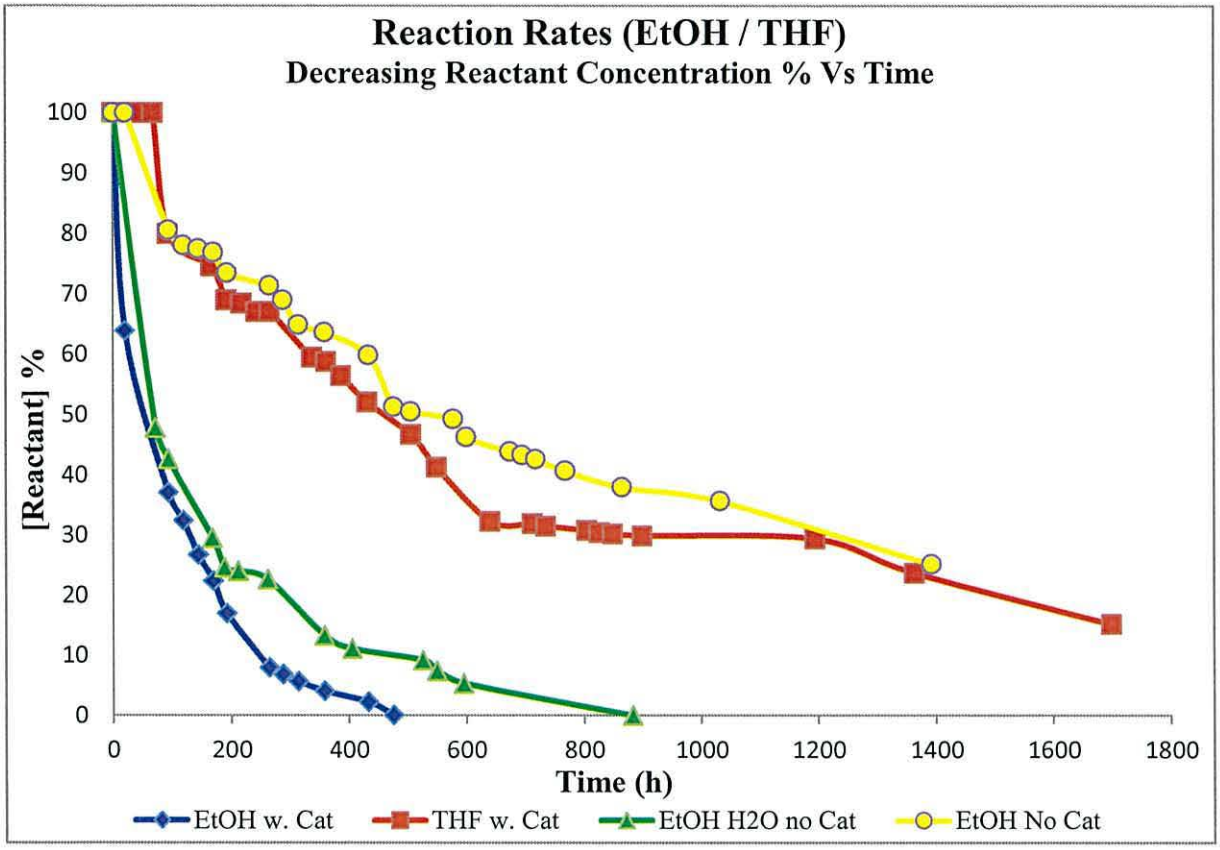

Graph 2. Rate of decreasing reactant concentration (%) against time (h).

Graph 2. shows the decreasing concentration of reactant [A] plotted against time (h) and from the exponential curve we can deduce that the rate of reaction is directly proportional to the concentration of [A] and hence the reaction is first order with respect to A (the rate equation of this first order reaction is shown in Equation 9.). The non-linear graph also tells us that as [A] decreases, the rate of reaction also decreases and in order to find a relationship between [A] and t (time) we must integrate Equation 9. and introduce an integration constant (c).

Equation 9. t = time, k = rate constant and n = order.

$$\text{Rate of reaction} = -\frac{\mathrm{d[A]}}{\mathrm{d}t} = k[\mathrm{A}]^n$$

$$-\frac{\mathrm{d[A]}}{[\mathrm{A}]} = k\mathrm{d}t$$

$$-\int \frac{\mathrm{d[A]}}{[\mathrm{A}]} = \int k\mathrm{d}t$$

$$c - \ln[\mathrm{A}] = kt$$

To find c we apply the condition that when $t = 0$, $[\mathrm{A}] = [\mathrm{A}]_0$. It then follows that $c = \ln[\mathrm{A}]_0$ (which corresponds to the intercept in Graph 3) and therefore the integrated rate equation for a 1st order reaction (with respect to A) is given in Equation 10.

Equation 10. Integrated 1st order rate equation.

$$\ln[\mathrm{A}] = \ln[\mathrm{A}]_0 - kt$$

This equation gives a linear relationship between t and ln[A] from which the rate constant (k) can be determined from the gradient (Graph 3.). Graph 3. shows this linear correlation between t and ln[A] with the units for time in days, the equation labels in Graph 3. represent a rearrangement of Equation 10, eg. y = -0.2083x + 4.4829 is equivalent to $\ln[\mathrm{A}] = -kt + \ln[\mathrm{A}]_0$ (with y = ln[A] and x = t).

Table 8. Summary of rate constants derived using Equation 10 and Graph 3.

Reaction	$\ln[\mathrm{A}]_0$	Equation 10 (t)	k(%day^{-1})
EtOH w. Cat	4.482	$\ln[\mathrm{A}] = 4.482 - 0.008t$	0.21
THF w. Cat	4.479	$\ln[\mathrm{A}] = 4.479 - 0.001t$	0.027
EtOH H_2O no Cat	4.200	$\ln[\mathrm{A}] = 4.200 - 0.004t$	0.10
EtOH no Cat	4.501	$\ln[\mathrm{A}] = 4.501 - 0.001t$	0.027

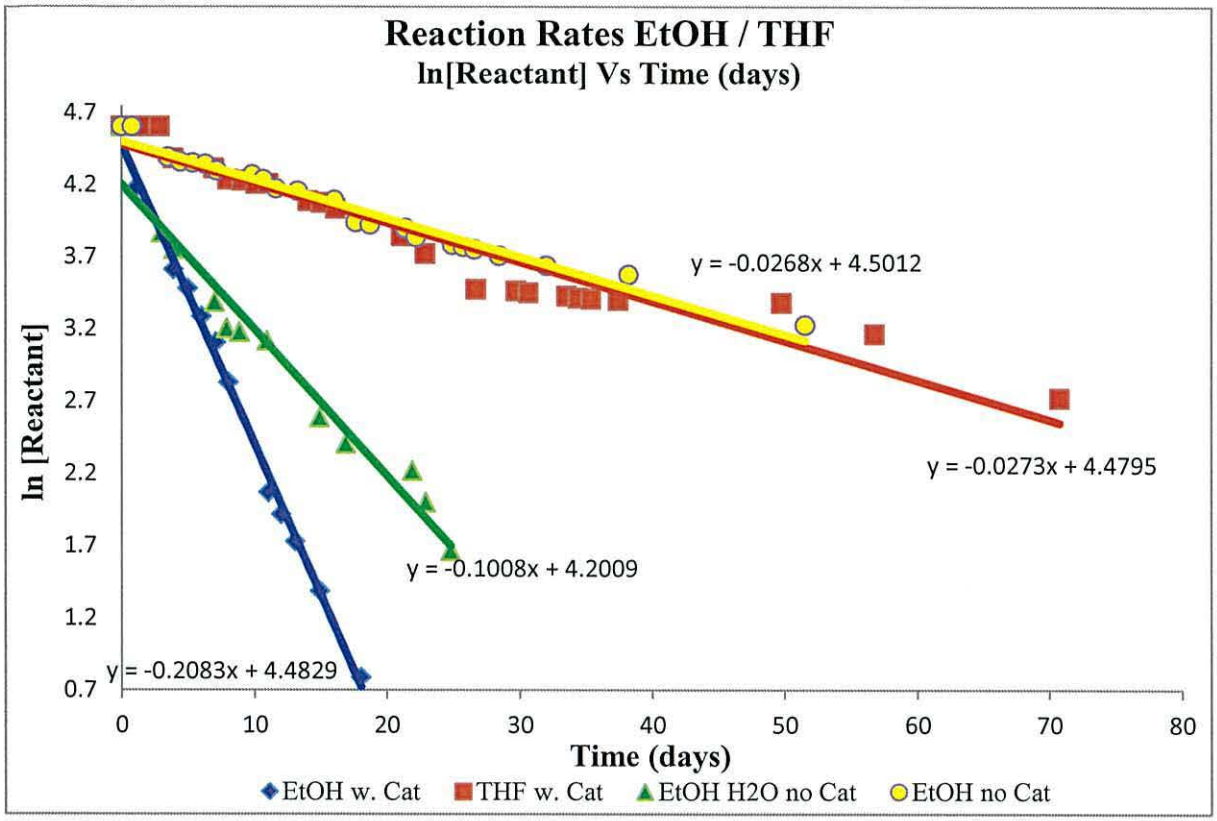

Graph 3. The linear plot of ln[A] against time (days).

The results (rate constant k) shown in Table 8. were as expected. k in EtOH was faster than THF for all experiments, with the catalysed EtOH faster than uncatalysed. With respect to the catalysed reactions EtOH exhibits an 8-fold increase in rate compared to THF. The units for these rates are % conversion per day ($\%day^{-1}$). The catalysed reaction in EtOH gave the highest e.e. compared to the catalysed reaction in THF.

1.2.5. Attempted synthesis of the Catalyst 53

The final stage of this investigation was to attempt the preparation of the amine based catalyst **53**. Our initial strategy utilised the readily available starting material δ-valerolactam (piperidin-2-one) **32** and it was envisaged that N-methylation followed by reaction with methylenetriphenylphosphorane would lead to the ylide **49** which on reaction with formaldehyde will give **34** the precursor to the guanidine base **53** (Scheme 20.).

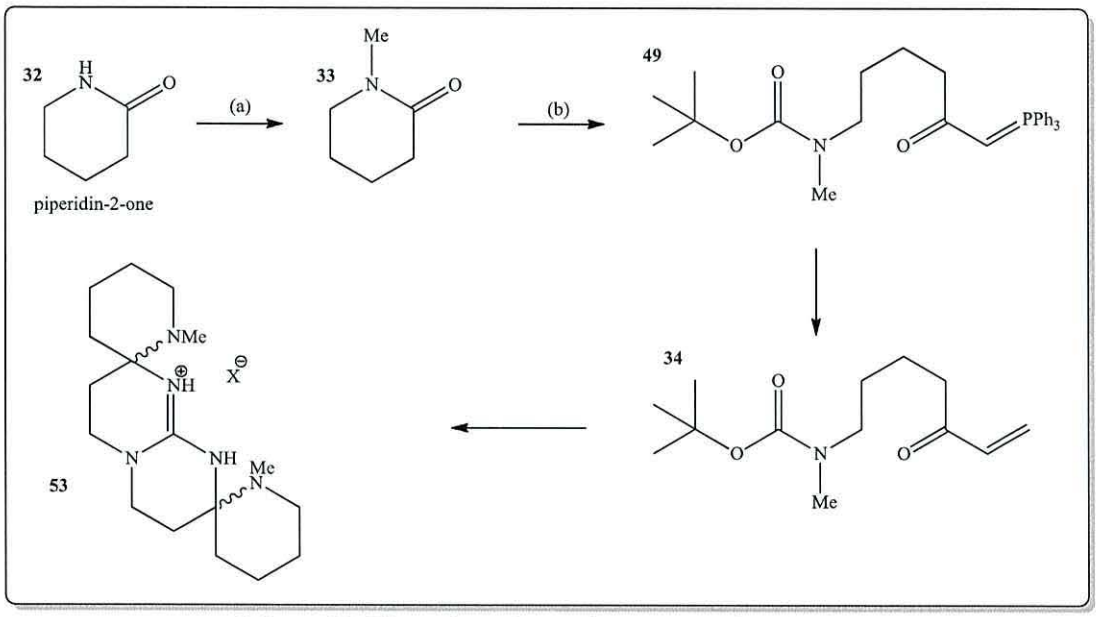

Scheme 20. Planned reaction pathway to novel catalyst **53**.

1.2.5.1. Synthesis of 1-Methylpiperidin-2-one (Methodology 1h.)

The initial step, the methylation of piperidin-2-one **32** has been reported in the literature on numerous occasions and a variety of methods are available for effecting this transformation.[35/36/37/38/39]

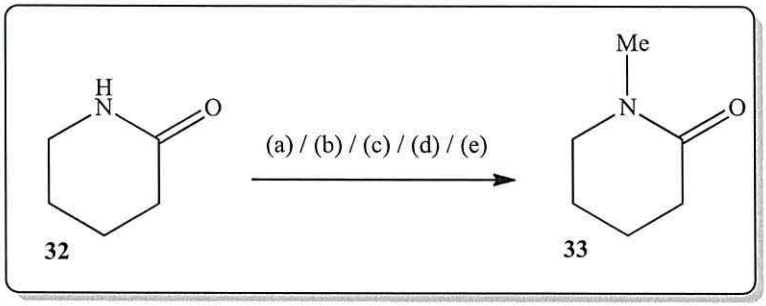

Scheme 21. Literature Reactions (a)[35] $(CH_3O)_2SO_2Na$ / C_6H_6; (b)[36] (i) NaH / MeI / THF; (ii) HCl / 110°C / Dowex / 70%; (c)[37] NaH / MeI / 18-Crown-6 $[C_2H_4O]_6$ / THF / 36%; (d)[38] $(Me_2N)_3P{=}C(Me)_2$ / MeI / THF / -78°C / 60%; (e)[39] (i) *n*-BuLi / THF / Hexane / -30°C; (ii) THF / MeI / -78°C / 88%.

Initial attempts were made using the method reported by by Kawasaki *et al,*[36] which was chosen due to its simple reagents, relatively high yield and it only involving 1 reaction step. This involved the reaction of piperidin-2-one with NaH and MeI in THF at 0°C. The first attempt gave an oily product in 42.8% yield, which was invariably contaminated with mineral oil from the NaH. Removal of this mineral oil before the reaction then gave disappointing yields of ≈ 34%. Literature reaction (e) by Crozet *et al*[39] was then attempted which involved the reaction of *n*-BuLi and piperidin-2-one in THF at -30°C, followed by addition of MeI at -78°C. The mean yield obtained for this reaction was 79% with a highest yield of 87% in 7 attempts (literature yield 88%).[39]

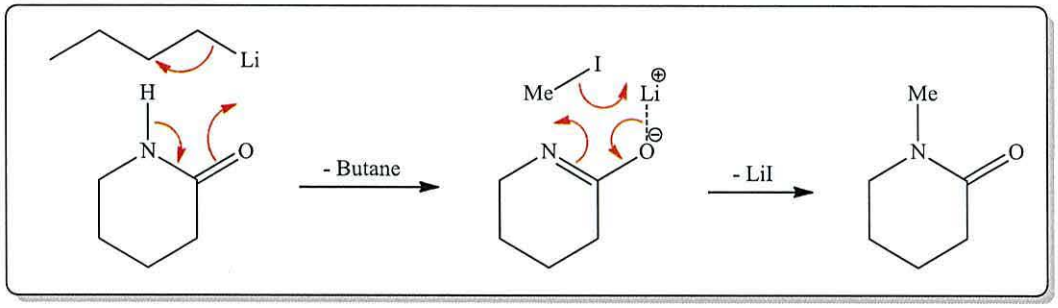

Scheme 22. Methylation of piperidin-2-one using n-BuLi and MeI.

Care was taken to ensure exact amounts of *n*-BuLi were used in this reaction, achieved by performing titrations of *n*-BuLi against DPAA in an equimolar volume of THF (with respect to the experiment). The titration was performed in triplicate and a mean concentration found and utilised, the anhydrous THF used in the experiment was from the same batch used in the titrations and experiments were performed immediately after the results had been obtained and analysed.

The titrations to calculate exact concentrations of *n*-BuLi were necessary due to the sensitivity of the reaction. From early attempts it was clear that not enough *n*-BuLi resulted in

a mixture of the desired product **B** and unreacted starting material **A** (see Figure 20.), which are difficult to separate using either column chromatography or distillation. Conversely too much *n*-BuLi resulted in desired product **B** and the undesirable product **C** in various amounts, also difficult to separate as well as severely reducing yield.

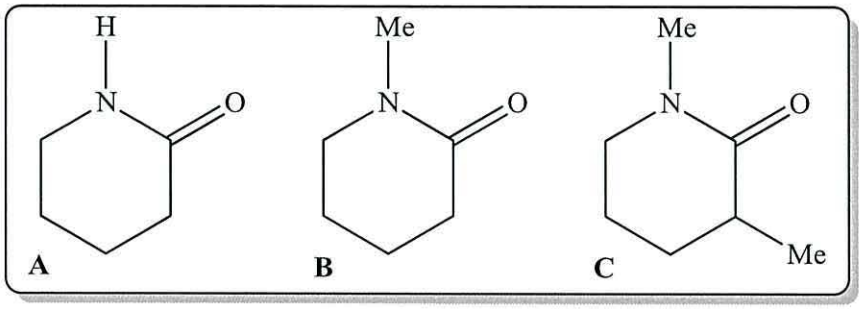

Figure 20. Methylation products A, B and C.

These methylation products were easily deduced from the DEPT spectra by closely examining the number of CH_2 and CH/CH_3 signals. A mixture of **A** and **B** (Figure 21.) resulting from too little *n*-BuLi gave a DEPT spectra with 8 CH_2 (O) signals and 1 CH_3 (□).

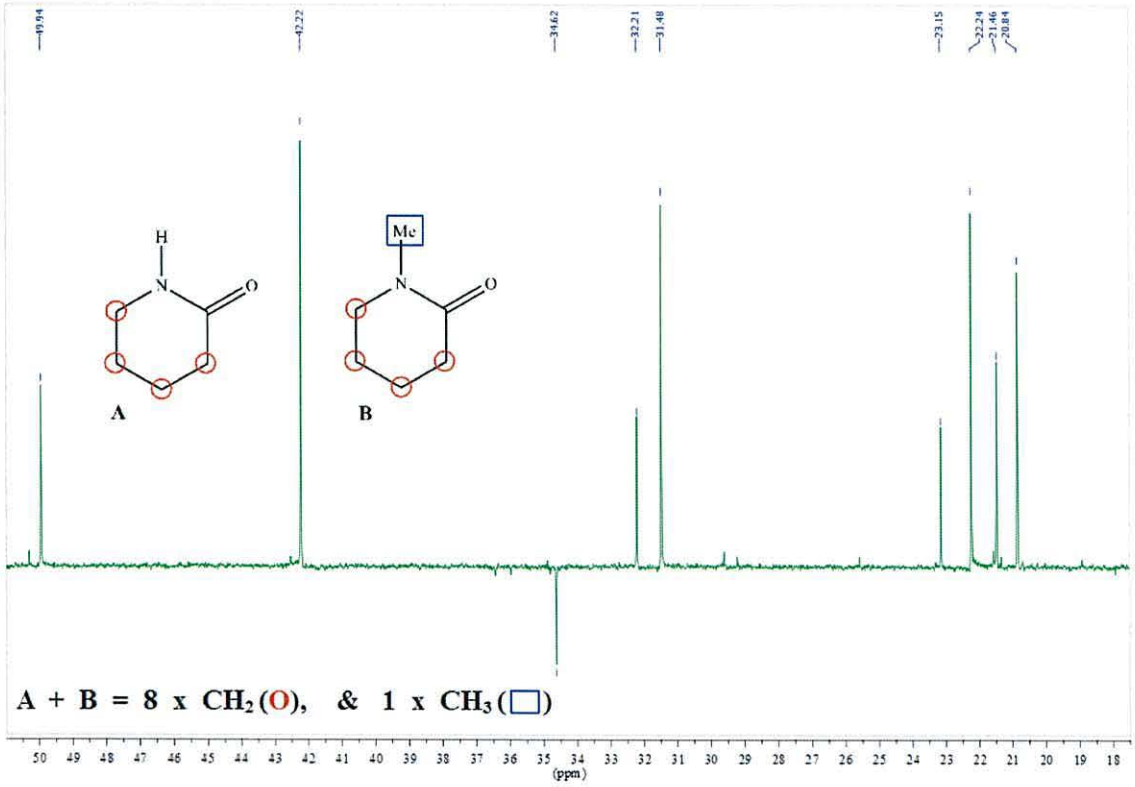

Figure 21. DEPT spectra showing methylation products A & B.

A mixture of **B** and **C** (Figure 22.) resulting from too much *n*-BuLi gave a DEPT spectra with 7 CH_2 (O) signals, 3 CH_3 (□) signals and 1 CH (□).

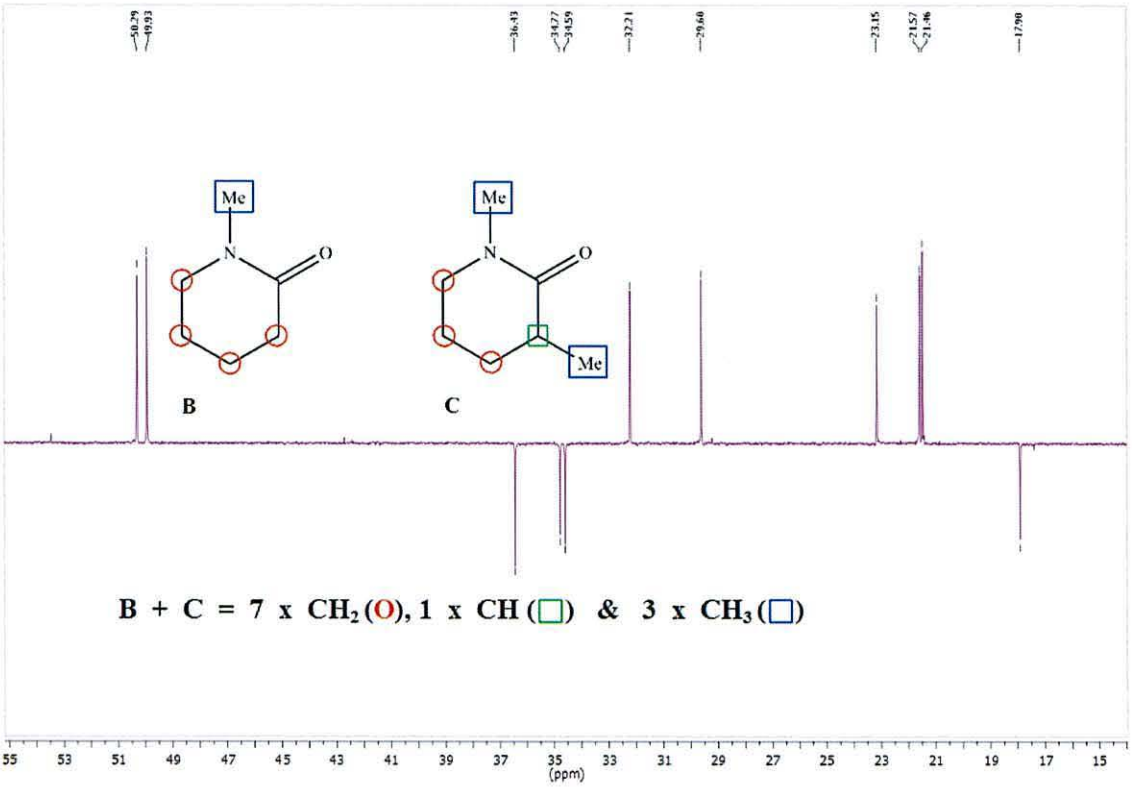

Figure 22. DEPT spectra showing methylation products B & C.

After a few attempts the correct ratio of *n*-BuLi to piperidin-2-one was found to be 1 : 1.1 equivalents and the single desired product **B** was distilled in 87% yield.

1.2.5.2. Ring opening of 1-methylpiperidin-2-one

Step (b) (the ring opening of 1-methylpiperidin-2-one) was attempted in a reaction similar to a previously reported reaction of δ-valerolactone **55** with metheylenetriphenylphosphorane **54**.[11] In this reaction the product is silylated to give the phosphorane **2** (Scheme 23.).

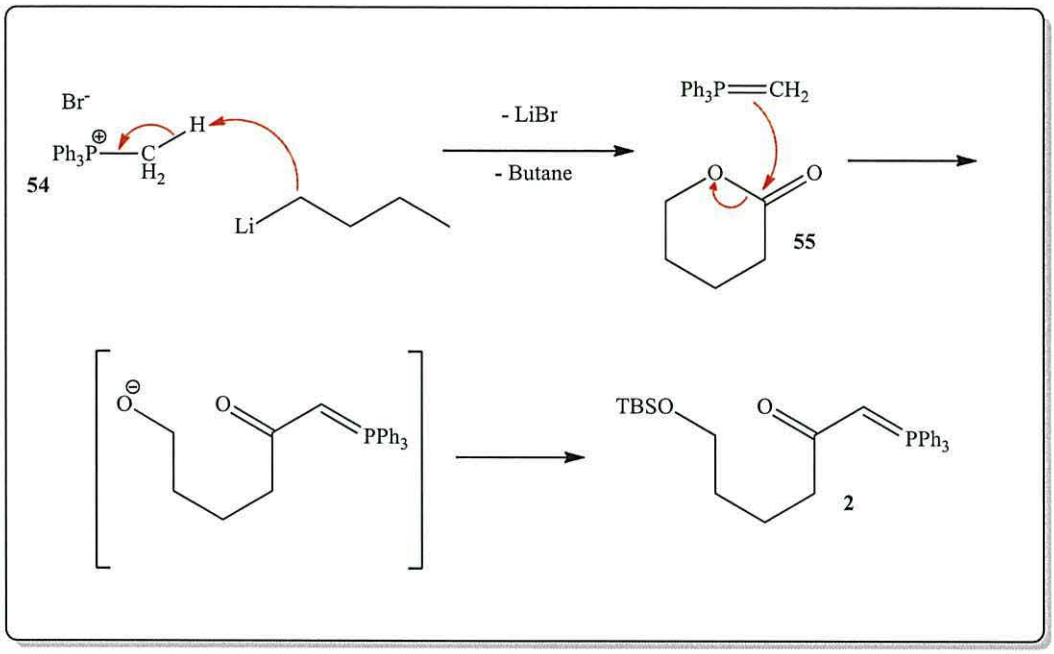

Scheme 23. Ring opening of δ-valerolactone **55.**

It was hoped that the reaction of the phosphorane **56** with the lactam **33** would lead to the intermediate **56** which could be Boc-protected to give **49** (Scheme 24.)

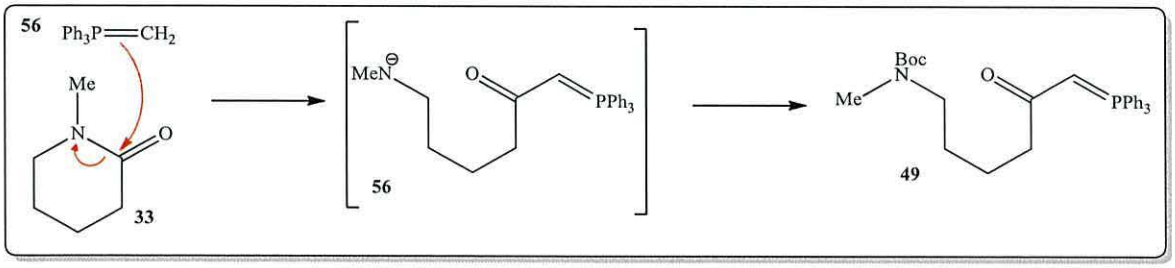

Scheme 24. Ring opening of N-methyl lactam **33**.

This reaction was attempted several times under varying conditions (time, temperature and length of time to generate the ylide) and on all occasions the majority product obtained was recovered starting material. This would seem to suggest that the lactam is unreactive in this reaction and the probable reason for this is the known lower reactivity of amides towards nucleophilic attack. This is largely due to the increased resonance contribution found in amides when compared to esters as represented in Figure 23.

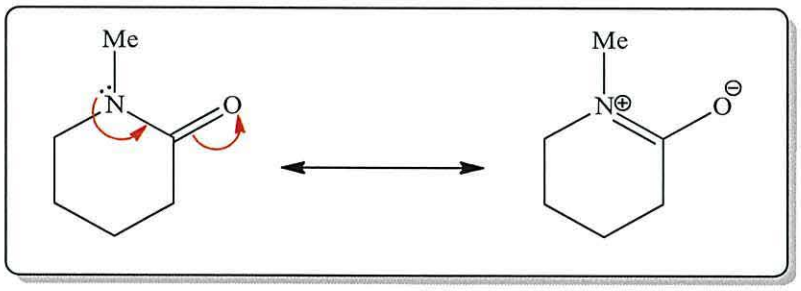

Figure 23. Amide resonance explanation for failed ring-opening.

A second synthetic route to the enone **34** was envisaged which mimics the preparation of enone **6** used in the synthesis of the catalyst **7**. This route begins with 3-chloropropan-1-ol **57** which is converted to the amine **59** in 2 steps which on protection and iodination gives the iodide **61**. The coupling of this iodide with AMTP followed by reaction with formaldehyde will give the desired enone **34** (Scheme 25.).

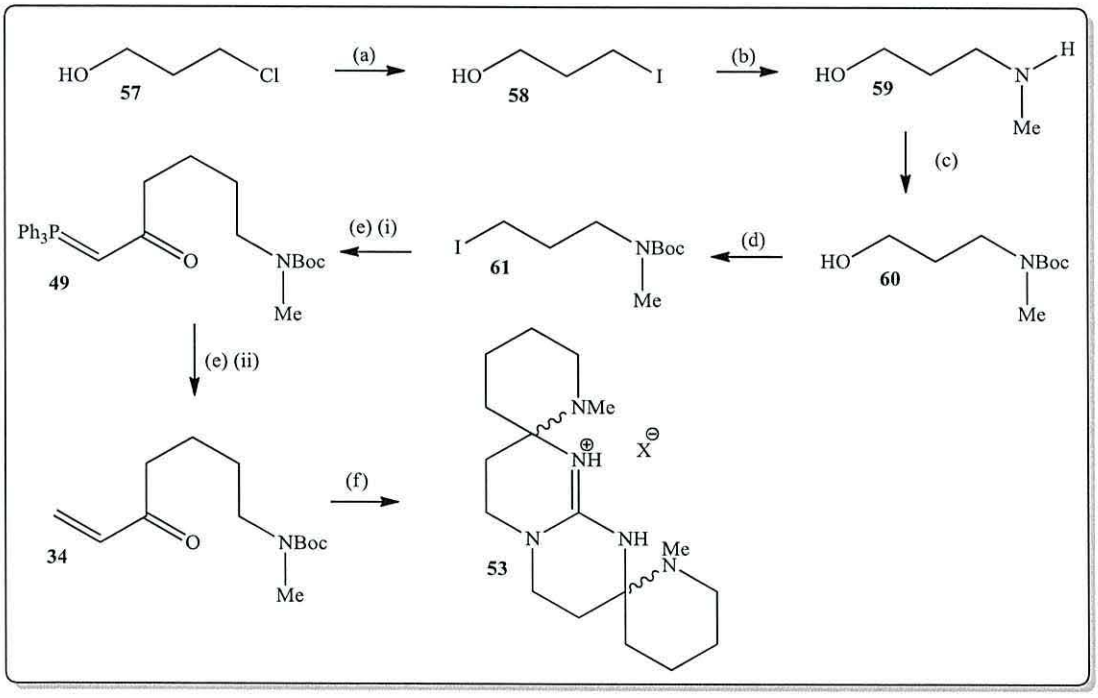

Scheme 25. Alternate planned route to novel catalyst **53**.

In attempting steps (a) and (b) the reaction reported in a patent[40] was repeated which described the reaction of 3-chloropropan-1-ol, NaI and $MeNH_2$ in ethanol, with the presumed

mechanism shown below (Figure 24.). Following this one-pot method, a reasonable crude yield of amine was obtained which was then Boc-protected (step c), to give the desired compound in 10% overall yield which was deemed unacceptable.

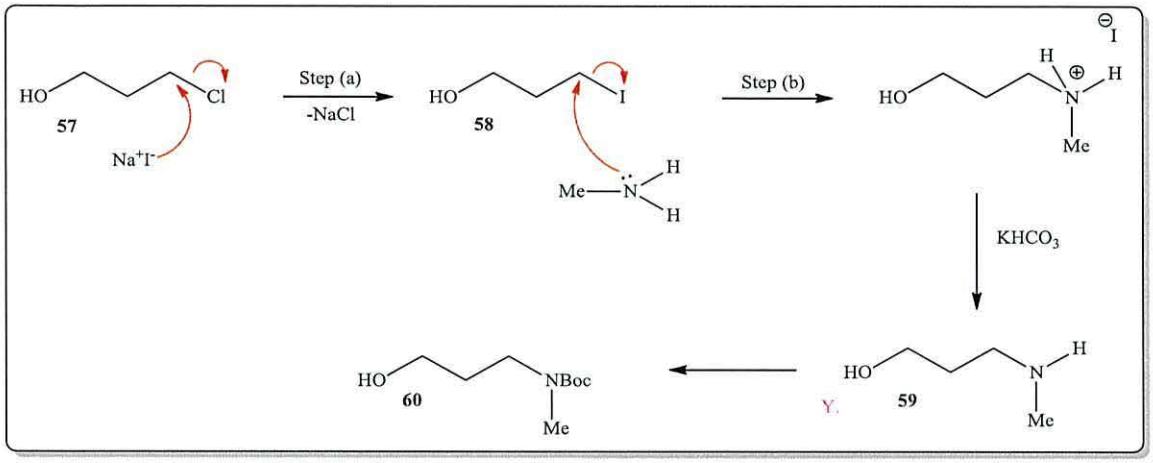

Figure 24. Reaction mechanisms for steps (a) and (b).

In order to improve this process we firstly converted the chloride **57** directly to the iodide **58** in a Finkelstein reaction. Thus 3-chloropropan-1-ol **57** and NaI (1.45 equivalents) were dissolved in acetone and heated under relux at 70°C for 24 h. The reaction was monitored using ^{1}H NMR, showing full conversion (R-Cl → R-I) from the change in chemical shift of the -CH_2 group closest to the halogens (Figure 25.). After purification the iodide **58** was obtained as an almost colourless oil in 68% yield.

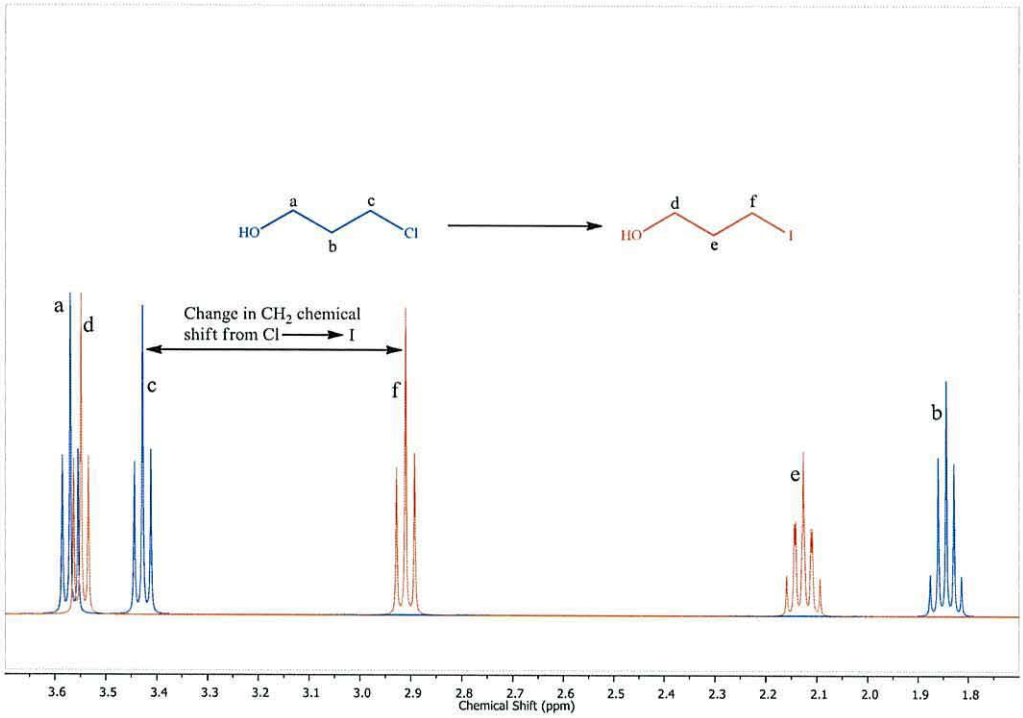

Figure 25. Change in CH_2 chemical shift of ≈ 0.52 ppm from chloro- to iodo- compound.

The 3-iodopropan-1-ol **58** was then reacted with $MeNH_2$ (33% in ethanol) over 48 hours, neutralised (K_2CO_3) and after work up the amine **59** was obtained as a colourless oil in 91% yield. Boc-protection was achieved by reaction of **59** in dichloromethane with di-*tert*-butyl dicarbonate over 12 h. After work up and column chromatography the desired compound **60** was obtained in 55% yield.

Conversion of the alcohol **60** to the corresponding iodide **61** was achieved using a combination of PPh_3, imidazole and iodine in anhydrous DCM over 16 h to give the desired compound in 76% as a colourless oil (Scheme 26.).[41]

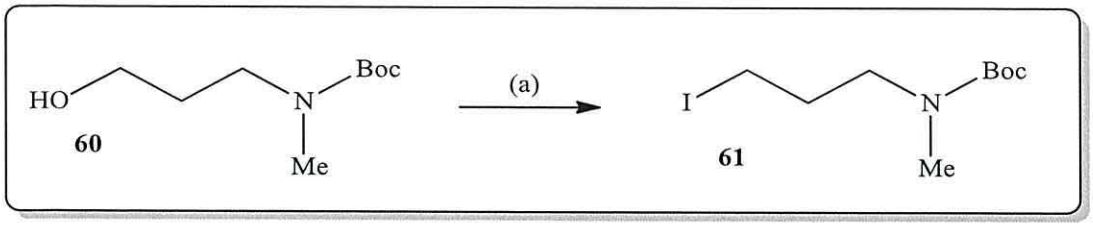

Scheme 26. Synthesis of iodide **61**.

The next step in the synthesis is the reaction of the iodide **61** with the anion generated by the lithiation of AMTP with *n*-BuLi at -50°C. The *n*-BuLi concentration was again determined via titrations against DPAA and care should be taken not to cool the AMTP / THF solution below ≈ -60°C as the AMTP crashes out of solution and does not re-dissolve sufficiently. Thus THF / AMTP / *n*-BuLi mixture was stirred at -60°C for 1 h whereupon the iodide **61** was added as a solution in THF. After work up the ylide **49** was obtained in 77% yield after column chromatography. Reaction of this ylide with formaldehyde in DCM gave the enone **34** as a colourless oil in 71% yield after column chromatography (Scheme 27.).

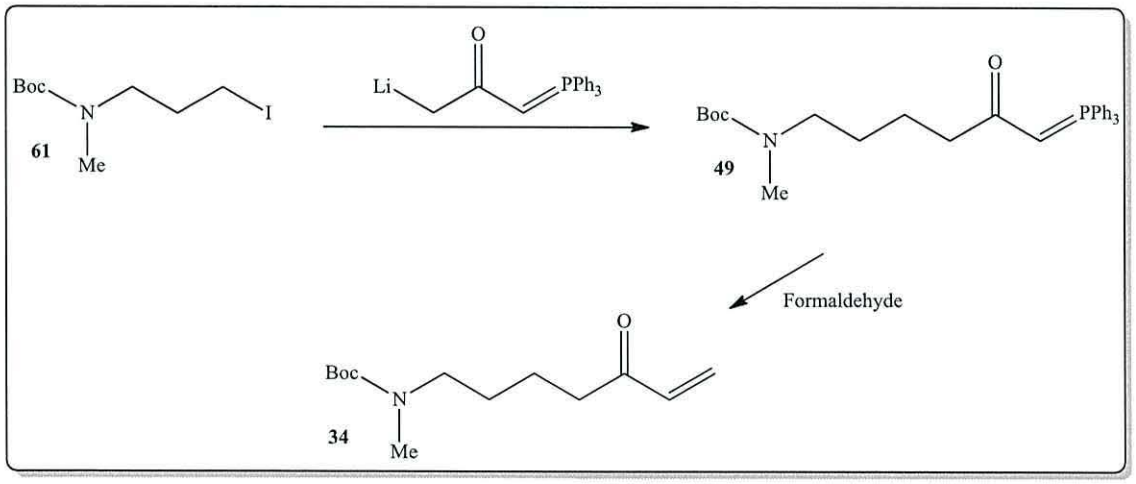

Scheme 27. Synthesis of enone **34** via ylide **49**.

The structure of enone **34** was confirmed by analysis of the ^{1}H and ^{13}C data, specifically the ^{1}H ABX splitting pattern associated with the vinylic group (Figure 26. For full spectra see Appendix).

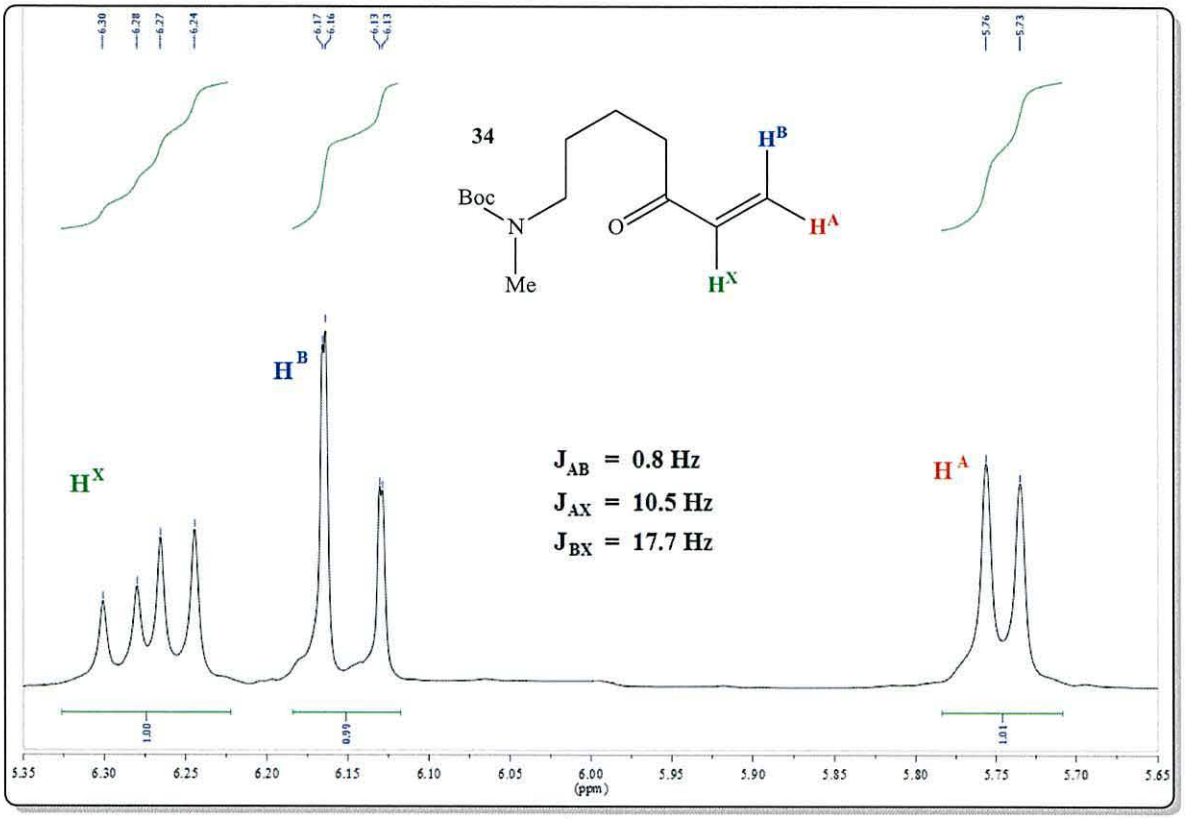

Figure 26. ^{1}H analysis of **34**.

The smallest J value (J_{AB} = 0.8 Hz) arises from the coupling of protons H^A and H^B on the same carbon that are diastereotopic due to the fact there is no rotation about the double bond (germinal coupling). The largest J value (J_{BX} = 17.7 Hz) is the *trans* coupling between proton H^B and H^X, whilst J value of 10.5 Hz corresponds to the *cis* coupling between protons H^A and H^X. The chemical shifts are H^X 6.28 ppm, H^B 6.15 ppm and H^A 5.74 ppm.

With the enone in hand we next attempted to prepare the tetracyclic guanidine **53** by the addition of 0.5 equivalents of guanidine, followed by acidic deprotection (Scheme 28.).

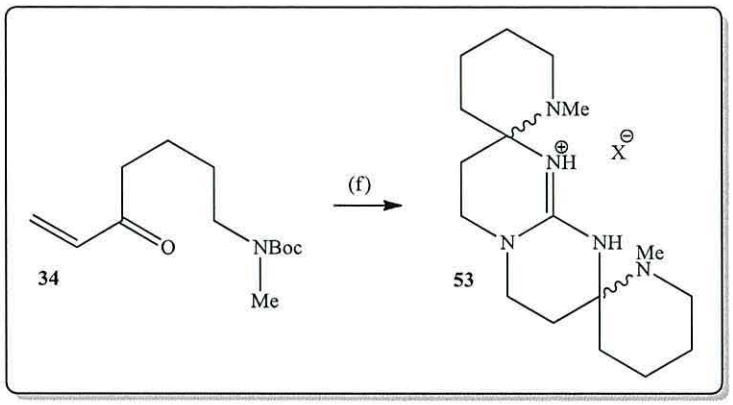

Scheme 28. Preparation of tetracyclic guanidine **53**.

On attempting this reaction a crude compound was obtained which was deprotected by treatment with aqueous HCl (3 M), analysis of the compound obtained on extraction with DCM indicated the presence of N-Boc and analysis by electrospray MS was performed. Analysis of the data indicated a mass at m/z 506.37 [M^+] which corresponds to the bicyclic compound **62** (Figure 27.)

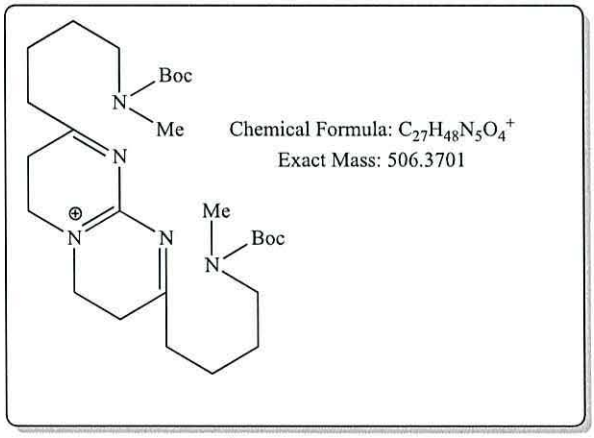

Figure 27. Bicyclic intermediate compound **62**.

Treatment of **62** with methanolic HCl to fully deprotect the intermediate was performed and after extraction with DCM and co-evaporation with toluene a crude yellow oil was obtained which contained a number of compounds as evidenced by ^{1}H NMR. Analysis of this mixture by TLC indicated no clear spots so analysis by electrospray MS was performed. This spectrum indicated the complete disappearance of the m/z: 506.37 peak with the main ion peak present now at m/z: 304.24 this is close to the required mass of 306.26 and might

suggest the presence of an aromatised intermediate such as **63** in which cyclisation has failed to occur or a partly aromatised structure **62** or possibly a combination of both (Figure 28.).

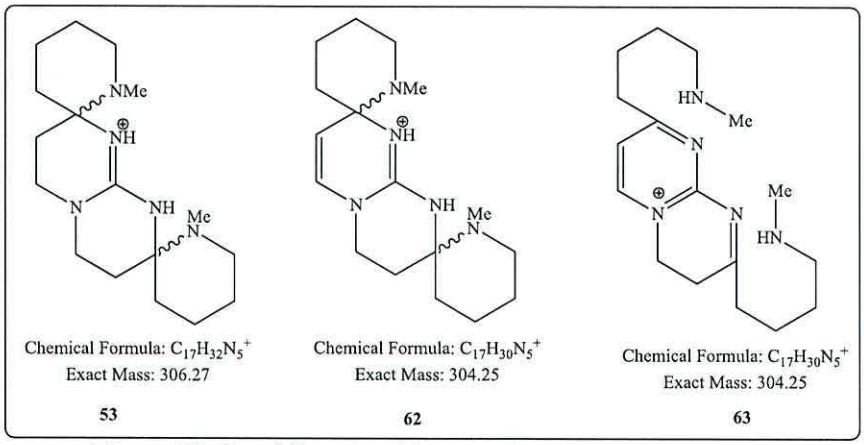

Figure 28. Guanidine **53** and intermediate compounds **62 – 63**.

Attempted purification of the now deprotected reaction mixture using column chromatography (0% - 5% MeOH : $CHCl_3$) gave 3 combined fractions (plus the column flushings) that were sent to the EPSRC National Mass Spectrometry Service Centre (EPSRC - NMSSC), although no significant conclusions could be obtained from the poor MS results.

1.3. Conclusion

1.3.1. Catalyst 7 (BF_4^- anion)

The synthesis of catalyst **7** was achieved successfully with a several minor improvements being made. There are 2 key reactions in this route, one being the formation of the α,β-unsaturated ketone **6**, step (e), from the treatment of AMTP with *n*-BuLi and its subsequent reaction with iodide **41**. The crucial aspect in this reaction is the water content of the dry THF as it has dramatic effects on the yield. THF sourced from a dry multi-solvent dispenser system gave varying results (most likely due to the condition of the filter cartridge inside the system). THF dried using a condenser reflux distillation set-up, over $Na_{(metal)}$ wire (using benzophenone as an indicator) gave consistently the best results, determined from the *n*-BuLi titrations of DPAA performed prior to each reaction and also from the yields of enone **6** (> 60% with the highest yield of 79%). The final step is the conjugate addition of guanidine to enone **6.** The use of anhydrous DMF (reaction solvent) and guanidine free from residual MeOH affords catalyst **7**, after purification via column chromatography (MeOH : $CHCl_3$, 0% - 3% in 0.25% increments) in 8 – 17% yield in 5 attempts.

The pK_a's of catalyst **7** and several previously prepared guanidines **10** – **12** and **45** (and commercially available guanidines **46** and **47**) were determined using a bracketing buffer method which utilises UV-Vis spectrophotometric data as well as manipulation of the equilibrium constant (K_{eq}). The pK_a of acetic acid **48** was calculated as 12.48 using the same procedure and was used as a method check that was found to be in accordance with the literature (12.3).[31/33] The pK_a of 1,1,3,3-tetramethylguanidine **46** was calculated as 13.04 and was also in full agreement with the literature values of 13 in DMSO albeit determined using a different method.[42/43]

The pK_a values for the synthetic guanidines **7**, **10** - **12** and **45** - **46** were all in the range 13.04 – 13.91 except 1,5,7-Triazabicyclo[4.4.0]dec-5-ene **47** which was found to be 16.14. This difference of over 2 magnitudes of basicity is interesting and suggests that the pyran rings and oxygen substutuients of **7**, **10** - **12** have a profound effect on the basicity of these guanidines. Catalysts **7** (-methyl) and **10** (-hydroxymethyl) have close pK_a values and there appears to be a slight decrease in pK_a as the steric bulk of this position on the pyran ring increases from $-CH_2OTBDMS$ in **11** to $-CH_2OTBDPS$ in **12**. This might be a reflection of the lower solvation of the guanidinium ion with increasing bulk of the substituents leading to an increase in acidity.

The Henderson–Hasselbalch equation (shown in Equation 11.) relates pH to the pK_a and the fraction of the species in the acidic / basic forms.

Equation 11.

$$pH = pK_a + \log\left(\frac{[B]}{[BH^+]}\right)$$

When there is 50% ionisation (ie. $[B] = [BH^+]$) then the $pH = pK_a$. If the $[B] / [BH^+]$ ratio is 1/10 then the pH will be one unit below the pK_a.

Utilisation of the pK_a can give an insight into the PTC mechanism, for example in the epoxidation reaction (Scheme 7.) the reactions were carried out at approximately pH = 12 (determined using a pH meter calibrated with buffer solutions). For all the guanidinium species (shown in Table 6. and Figure 16.) the pK_a's were 13-14, so with a reaction run at a pH of 12, there would be a ratio of $[B]/[BH^+]$ which is 1/10 or lower and thus effectively 92% protonation, with this level of protonation further increasing with pKa's higher than 13. This level of protonation indicates that the reaction mechanism of epoxidation involving guanidine catalyst **7** is most likely similar to be a standard PTC mechanism (Figure 6.) where the positively charged guanidinium ion transfers the ^-OCl species into the organic phase allowing the reaction to occur.

1.3.2. Catalyst 16 (BPh_4^- anion)

The successful synthesis of catalyst **16** was achieved as well as its subsequent testing for proficiency at catalysing the quinone Michael addition reaction (Scheme 19). The formation of product [C] and disappearance of reactant [A] were monitored using ^1H NMR. Graph 2. (plot of [A] v *t*) gives rise to an exponentially decreasing curve from which we can deduce the reaction is dependent on the concentration of A and therefore 1st order with respect to A ($[A]^1$ or simply [A]). The plot of ln[A] v *t* (Graph 3.) gives a linear correlation from which the rate constant *k* can be deduced (see Equation 10.). The highest rate of reaction was achieved (as expected) in the protic solvent EtOH with 0.05 equivalents of catalyst **16** with a rate constant calculated as $k = 0.21$ $\%day^{-1}$. Products were isolated in a yield of > 99% and an e.e. of 15.2% after 20 days.

Another reason for the observed improvements of catalyst **16** over catalyst **7** (which is also the basis of our hypothesis) is the effects from the catalysts counter ion (ie. BF_4^- / BPh_4^-) and can be attributed to the interaction shown in Figure 29.

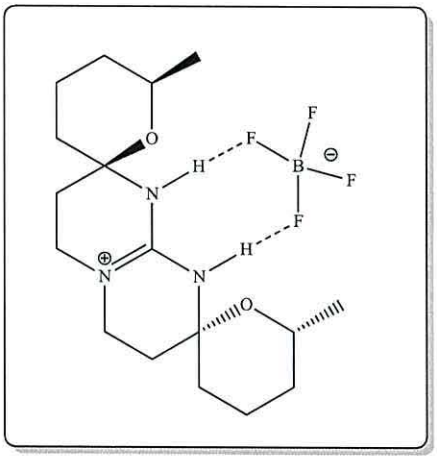

Figure 29. The interaction of the BF_4^- ion with the catalysts active site.

The hydrogen bonding interaction shown in Figure 29. between the BF_4^- counter ion and the guanidinium centre (catalyst **7**) could inhibit catalytic activity due to reactants not

being able to co-ordinate to this active site (due to the steric hindrance from the BF_4^-). Catalyst **16** (BPh_4^- counter ion) showed increased reaction rates and e.e.'s and could be attributed to the larger anion (containing 4 x phenyl rings) not being able to sit near the guanidinium core and therefore does not inhibit reaction around this active site.

1.3.3. Novel Catalyst 53

Guanidine cyclisation and deprotection was attempted in a reaction analogous to that in the synthesis of catalyst **7**. Evidence of partial cyclisation and incomplete deprotection was given by MS results. Further deprotection with methanolic HCl did not result in the desired product after purification using column chromatography.

The testing of this novel catalyst **53**, in relation to the hypothesis that relocation of the Me groups (which act as conformational locks, Figure 8.) would increase the catalytic performance, was not achieved. Although, this gives a promising road to further investigations.

1.4. Experimental

General: All chemicals and solvents were obtained from standard UK chemical suppliers (ie. Sigma Aldrich, Alfa Aesar and Lancaster). Dry solvents were obtained via distillation over sodium wire or obtained from standard UK sources.

Thin Layer Chromatography (TLC): All TLC results were obtained using Kieselgel 60 F_{254} glass silica TLC plates. Visualisation techniques consisted of ultra-violet light, iodine (staining) and phosphomolybdic acid (PMA – staining).

Fourier Transform Infra-Red Spectroscopy (FTIR): All FTIR spectra were obtained using a Bruker Tensor 27 FTIR machine, with results being given in wavenumbers (cm^{-1}). Samples were loaded on via NaCl discs and using either Nujol (mull), chloroform (neat) or potassium bromide (disc), stated where necessary.

Nuclear Magnetic Resonance (NMR): All spectra were obtained using Bruker Advance III Ultrashield 400 and 500 Plus NMR machines, particular frequencies for spectra are given, along with the type of deuterated solvent in which they were run.

Mass Spectrometry (MS): All samples sent to the EPSRC national mass spectrometry service centre in Swansea.

Guanidine 1

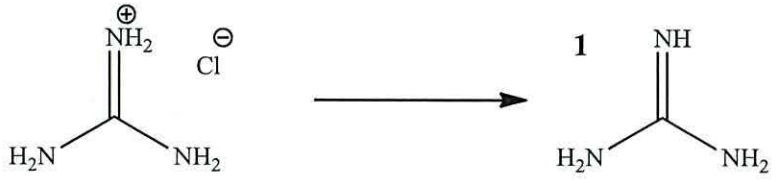

Chemical Formula: CH_6ClN_3
Molecular Weight: 95.53

Chemical Formula: CH_5N_3
Molecular Weight: 59.07

Sodium metal (2.40g, 104.3mmol) was washed in hexane, dried and added in portions to dry MeOH (200 mL) under argon (**CAUTION!** evolution of H_2 (g)). Once the sodium had reacted, pre-dried (P_2O_5) guanidine hydrochloride (10.00 g, 104.7 mmol) was added and the mixture stirred to room temperature overnight. The solution was filtered through a sinter filter apparatus to remove precipitated NaCl and the MeOH reduced *in vacuo* to ca. 1/4 of the original volume. The resultant slurry was then filtered once more to remove further NaCl precipitate and the filtrate was completely evaporated under high vacuum to guanidine as a colourless oil, which solidified to a waxy white solid upon freezing (-20°C) (5.93 g, 100.39 mmol, 96%).

(R)-ethyl 3-(tert-butyldimethylsilyloxy)butanoate 38[13]

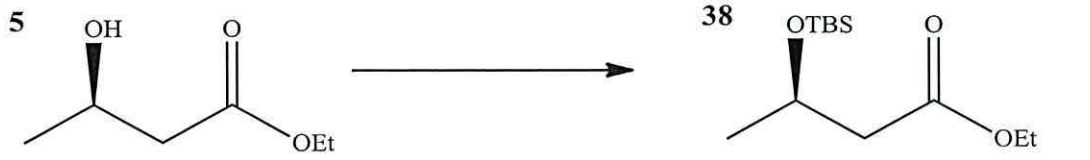

Chemical Formula: $C_6H_{12}O_3$
Molecular Weight: 132.16

Chemical Formula: $C_{12}H_{26}O_3Si$
Molecular Weight: 246.42

Under an atmosphere of argon, alcohol **5** (4.95 g, 37.5 mmol) was dissolved in dry DMF (20 mL) and cooled to 0°C. Imidazole (7.89 g, 116.1 mmol) and *tert*-butyldimethylsilyl chloride (8.47 g, 56.2 mmol) were added carefully. The mixture was stirred and warmed to RT overnight, whereupon water (200 mL) and hexane (100 mL) were added and the mixture separated. The aqueous layer was extracted with hexane (3 x 100 mL), the combined organic layers were dried ($MgSO_4$) and the solvent removed *in vacuo*. The product **38** was isolated as a clear oil (9.15 g, 37.1 mmol, 99%). Data was in agreement with the literature.[12/44]

δ_H (500 MHz, $CDCl_3$); 4.26 (1H, sextet, J = 7.3 Hz CH), 4.09 (2H, m, CH_2), 2.46 (1H, dd, J = 14.5, 7.6 Hz, CH), 2.35 (1H, dd, J = 14.5, 5.3 Hz, CH), 1.24 (3H, d, J = 7.1 Hz CH_3), 1.17 (3H, d, J = 6.1 Hz, CH_3), 0.85 (9H, s, 3 x CH_3), 0.03 (6H, s, 2 x CH_3) ppm.

(R)-3-((tert-butyldimethylsilyl)oxy)butan-1-ol 39[13]

Chemical Formula: $C_{12}H_{26}O_3Si$
Molecular Weight: 246.42

Chemical Formula: $C_{10}H_{24}O_2Si$
Molecular Weight: 204.38

Under an atmosphere of argon, butanoate **38** (10.76 g, 43.67 mmol) was dissolved in dry DCM (100 mL) and cooled to -78°C. DIBAL-H (100 mL, 100 mmol) was added drop-wise over 20 mins. The mixture was left in the cooling bath and allowed to warm slowly to RT overnight. The mixture was then cooled to 0°C and EtOAc (10 mL) was added slowly over 20 mins, followed by MeOH (6 mL) added over 10 mins. The mixture was then diluted with Et_2O (100 mL) and a solution of Rochelle's salt (250 mL) was added dropwise over 30 mins (after ≈ 5 mL the mixture formed a thick cloudy gel which then dispersed upon further addition of Rochelle's salt solution). The mixture was then stirred at RT for 2 h. The mixture was then separated and the (aq) layer further extracted with ether (2 x 100ml). The combined organic layers were washed with H_2O (150 mL) and dried ($MgSO_4$). The solvent was removed *in vacuo* giving the alcohol product **39** as a clear oil (8.06 g, 39.51 mmol, 91%). Data was in agreement with the literature.[12/44]

^{1}H NMR: δ_H (500 MHz, $CDCl_3$); 4.09 (1H, sextet, J = 5.9 Hz, CH), 3.74 (2H, m, CH_2), 1.69 (2H, m, CH_2), 1.18 (3H, d, J = 6.2 Hz, CH_3), 0.88 (9H, s, 3 x CH_3), 0.07 (6H, s, 2 x CH_3) ppm.

(R)-3-((tert-butyldimethylsilyl)oxy)butyl 4-methylbenzenesulfonate 40[13]

Chemical Formula: $C_{10}H_{24}O_2Si$
Molecular Weight: 204.38

Chemical Formula: $C_{17}H_{30}O_4SSi$
Molecular Weight: 358.57

Under an atmosphere of argon, a stirred solution of alcohol **39** (8.42 g, 40.39 mmol) in dry pyridine (35 mL) was cooled to 0°C and *p*-toluenesulphonyl chloride (10.0 g, 52.51 mmol) was added and the mixture stirred overnight. The mixture was then diluted with DCM (100 mL) and H_2O (500 mL) and separated. The aqueous layer was further extracted with DCM (2 x 100 mL) and the combined organic layers washed with H_2SO_4 (400 mL, 0.5 M) and H_2O (2 x 200 mL). The combined organic layers were dried ($MgSO_4$) and the solvent removed *in vacuo* giving the tosylate product **40** as an oil (13.38 g, 37.31 mmol, 92%). Data was in agreement with the literature.[12/44]

^{1}H NMR: δ_H (500 MHz, $CDCl_3$); 7.78 (2H, d, J = 8.2 Hz, 2 x CH), 7.34 (2H, d, J = 8.2 Hz, 2 x CH), 4.09 (2H, m, CH_2), 3.89 (1H, sextet, J = 6.1, CH), 2.44 (3H, s, CH_3), 1.72 (2H, m, CH_2), 1.09 (3H, d, J = 6.1 Hz, CH_3), 0.81 (9H, s, 3 x CH_3), 0.01 (6H, s, 2 x CH_3) ppm.

(R)-tert-butyl((4-iodobutan-2-yl)oxy)dimethylsilane 41[13]

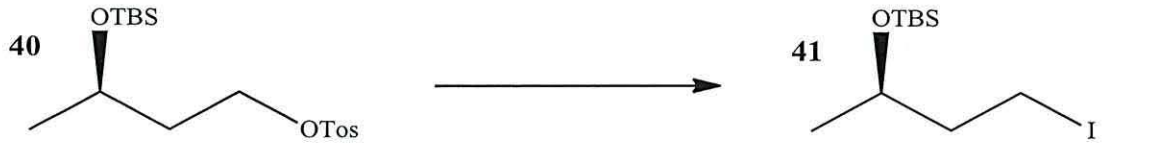

Chemical Formula: $C_{17}H_{30}O_4SSi$
Molecular Weight: 358.57

Chemical Formula: $C_{10}H_{23}IOSi$
Molecular Weight: 314.28

Tosylate **40** (22.55 g, 62.88 mmol) was dissolved in dry acetone (100 mL) and a solution of NaI (47.61 g, 317.63 mmol) in dry acetone (250 mL) was added. The mixture was heated under reflux for 4 h. After cooling to RT the mixture was diluted with ether (150 mL) and filtered. The filtrate was reduced *in vacuo* to a semi-solid mass, which was then triturated with ether (50 mL) followed by addition of petrol (80 mL). The supernatant liquid was filtered from the solid mass and this process repeated a further 3 times (50 mL ether – trituration – 80 mL petrol). The solvent was removed from the combined filtrates *in vacuo* to give the crude product as a yellow oil (17.72 g, 56.38 mmol, 90%). The crude material was purified using column chromatography (5% Et_2O : Petrol, Rf = 0.68 in 5% Et_2O : Petrol) giving the iodide product **41** as a clear oil (17.79 g, 56.59 mmol, 90%). Data was in agreement with the literature.[12/44]

^{1}H NMR: δ_H (500 MHz, $CDCl_3$); 3.89 (1H, sextet, J = 5.7 Hz, CH), 3.24 (2H, m, CH_2), 1.93 (2H, m, CH_2), 1.16 (3H, d, J = 6.1 Hz, CH_3), 0.89 (9H, s, 3 x CH_3), 0.09 (6H, s, 2 x CH_3) ppm.

(R)-7-((tert-butyldimethylsilyl)oxy)oct-1-en-3-one 6[13]

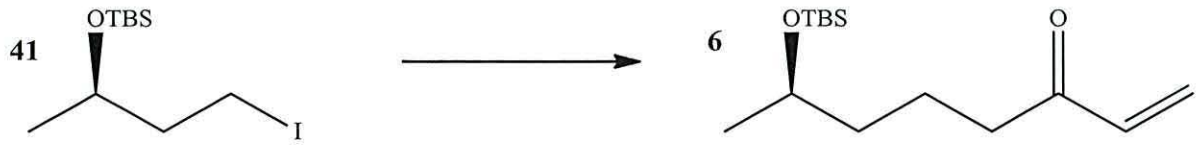

Chemical Formula: $C_{10}H_{23}IOSi$
Molecular Weight: 314.28

Chemical Formula: $C_{14}H_{28}O_2Si$
Molecular Weight: 256.46

Acetylmethylenetriphenylphosphorane (AMTP) (8.26 g, 28.9 mmol) was dissolved in dry THF (140 mL). The solution was cooled to -50°C and *n*-BuLi (2.2 M, 11.9 mL, 26.3 mmol) was added drop-wise over 5 mins. The deep red solution was stirred at -50°C for 1 h. The solution was then cooled to -78°C and iodide **41** (8.26 g, 26.3 mmol) was added. The mixture was left in the cooling bath and allowed to warm slowly to RT overnight with stirring. H_2O (90 mL) and DCM (100 mL) were added, the mixture was then separated and the aqueous layer extracted with DCM (3 x 50 mL). Formaldehyde solution (aqueous formaldehyde (94 mL) with DCM (50 mL) and dried over $MgSO_4$) was added through a funnel with cotton wool and the mixture left to stir overnight. The mixture was then diluted with DCM (60 mL) and washed with H_2O (2 x 60 mL) separated and then dried ($MgSO_4$). The solvent was removed *in vacuo* and the product purified using column chromatography (EtOAc : Petrol 0% - 3% in 1% increments Rf = 0.22 in 6% EtOAc : Petrol). The enone product **6** was isolated as a colourless oil (5.34 g, 20.8 mmol, 79%). Data was in agreement with the literature.[12]

^{1}H NMR: δ_H (500 MHz, $CDCl_3$); 6.29 (1H, dd, J = 17.7, 10.6Hz, CH), 6.15 (1H, dd, J = 17.7, 1.2Hz, CH), 5.74 (1H, dd, J = 10.6, 1.2Hz, CH), 3.75 (1H, sextet, J = 5.9Hz, CH), 2.53 (2H, t, J = 7.3Hz, CH_2), 1.6 (2H, m, CH_2), 1.36 (2H, m, CH_2), 1.07 (3H, d, J = 6.1Hz, CH_3), 0.82 (9H, s, 3 xCH_3), 0.01 (6H, s, 2 xCH_3) ppm.

^{13}C NMR: δ_C (500 MHz, $CDCl_3$); 200.50 (C=O), 136.49 (CH), 127.66 (CH_2), 68.26 (CH), 39.60 (CH_2), 39.02 (CH_2), 25.83 ((CH_3)$_3$), 23.66 (CH_3), 20.14 (C), 18.02 (CH_2), -4.45 (CH_3), -4.80 (CH_3) ppm.

(*6R, 6"R, 2R, 2"R*)-6,6"-Dimethyldispiro [tetrahydropyran-2,2'-(2,3,4,6,7,8-hexahydro-1*H*-pyrimido[1,2-a] pyrimidine)-8',2"-tetrahydropyran]-9'-ium chloride 44[13]

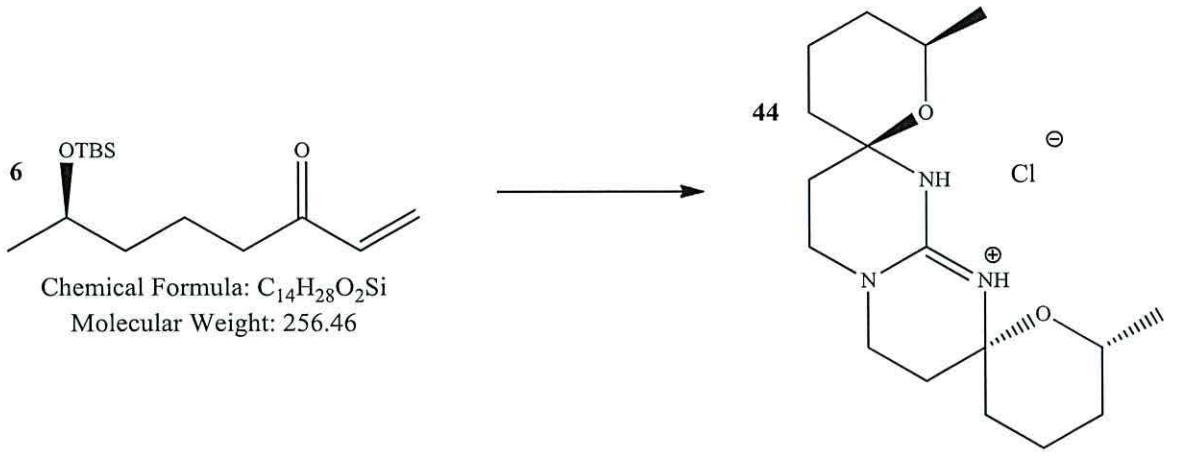

Chemical Formula: $C_{14}H_{28}O_2Si$
Molecular Weight: 256.46

Chemical Formula: $C_{17}H_{30}ClN_3O_2$
Molecular Weight: 343.89

Under an atmosphere of argon, enone **6** (3.30 g, 12.86 mmol) was dissolved in dry DMF (30 mL) and cooled to 0°C. A solution of guanidine (0.38 g, 6.43 mmol) in DMF (1.2 mL) was added drop-wise over 5 mins. The yellowish mixture was stirred at 0°C for 30 mins and then allowed to warm to RT overnight. The reaction mixture was again cooled to 0°C and methanolic HCl (6.6 mL of acetyl chloride in 59.4 mL of dry MeOH) was added carefully and the pinkish mixture warmed to RT and stirred for 3 h. The mixture was then diluted with DCM (150 mL) and washed with brine (2 x 200 mL) and H_2O (2 x 400 mL) and the aqueous layers back extracted with DCM (75 mL). The combined organic layers were dried ($MgSO_4$) and co-evaporated with toluene (2 x 50 mL) at 55°C to remove traces of DMF and the crude oil dried *in vacuo* (3.28 g, 9.54 mmol, 74.2%). The crude oil was purified by column chromatography (MeOH : $CHCl_3$, 0% - 3% in 0.25% increments, Rf = 0.21 in 5% MeOH : $CHCl_3$ run up twice). The guanidine product **44** was isolated as a tacky white solid (0.76 g, 2.21 mmol, 17%). Data was in agreement with the literature.[12]

^{1}H NMR: δ_H (400 MHz, $CDCl_3$); 1.10 (6H, d, J = 6.2Hz, 2 x CH_3), 1.18 (2H, m, 2 x CH), 1.58 (2H, dt, 2 x CH), 1.74 (4H, m, 4 x CH) 1.86 (4H, m, 4 x CH), 1.96 (2H, m, 2 x CH),

2.39 (2H, m, 2 x CH), 3.16 (2H, ddd, J = 12.3, 5.9, 1.4Hz, 2 x CH), 3.68 (2H, dt, J = 12.9, 4.8Hz, 2 x CH), 3.91 (2H, ddq, J = 12.3, 6.2, 2.1Hz, 2 x CH), 9.78 (2H, s, 2 x NH) ppm.

^{13}C NMR: δ_C (400 MHz, $CDCl_3$); 149.30 (C), 78.63 (2 x C), 67.04 (2 x CH), 42.53 (2 x CH_2), 34.00 (2 x CH_2), 32.90 (2 x CH_2), 32.34 (2 x CH_2), 21.74 (2 x CH_3), 18.48 (2 x CH_2) ppm.

(*6R, 6"R, 2R, 2"R*)-6,6"-Dimethyldispiro [tetrahydropyran-2,2'-(2,3,4,6,7,8-hexahydro-1*H*-pyrimido[1,2-a] pyrimidine)-8',2"-tetrahydropyran]-9'-ium tetrafluroborate 7[12]

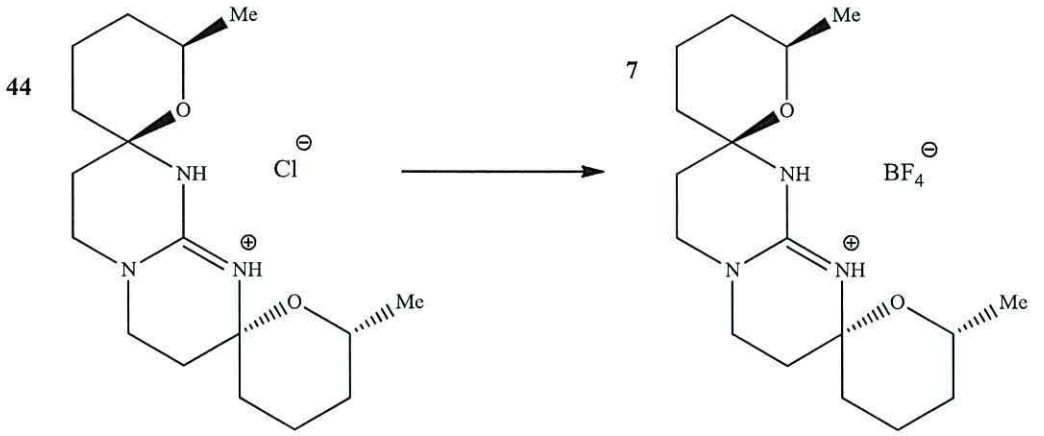

Chemical Formula: $C_{17}H_{30}ClN_3O_2$
Molecular Weight: 343.89

Chemical Formula: $C_{17}H_{30}BF_4N_3O_2$
Molecular Weight: 395.24

Ion exchange: Guanidine chloride salt **44** as a solution in DCM (30 mL) was stirred with $NaBF_4$ (30 equivs) and H_2O added drop-wise until all the solid had dissolved. The white solution was stirred vigorously overnight at RT. The mixture was separated and the organic phase washed with H_2O (3 x 30 mL) and dried ($MgSO_4$). The solvent was removed *in vacuo* and the product isolated by coloumn chromatography (MeOH : $CHCl_3$, 0% - 3% in 0.25% increments, Rf = 0.16 in 5% MeOH : $CHCl_3$). The guanidine tetrafluoroborate salt **7** was purified further by trituration in petrol and precipitated from ether (0.20 g, 0.51 mmol, 15%). Data was in agreement with the literature.[12]

^{1}H NMR: δ_H (400 MHz, $CDCl_3$); 7.50 (2H, br s, 2 x NH), 3.84 (2H, ddq, J = 11.8, 6.1, 2.1Hz, 2 x CH), 3.68 (2H, dt, J = 12.5, 5.0Hz, 2 x CH), 3.22 (2H, ddd, J = 12.5, 5.8, 1.6Hz, 2 x CH), 1.5 - 2.20 (14H, cm), 1.18 (2H, m, 2 x CH), 1.11 (6H, d, J = 6.1Hz, 2 x CH_3) ppm.

^{13}C NMR: δ_C (500 MHz, $CDCl_3$); 148.42 (C), 78.87 (2 x C), 66.93 (2 x CH), 42.72 (2 x CH_2), 33.56 (2 x CH_2), 32.95 (2 x CH_2), 32.12 (2 x CH_2), 21.72 (2 x CH_3), 17.66 (2 x CH_2) ppm.

(*6R, 6"R, 2R, 2"R*)-6,6"-Dimethyldispiro [tetrahydropyran-2,2'-(2,3,4,6,7,8-hexahydro-1*H*-pyrimido[1,2-a] pyrimidine)-8',2"-tetrahydropyran]-9'-ium tetraphenylborate 16

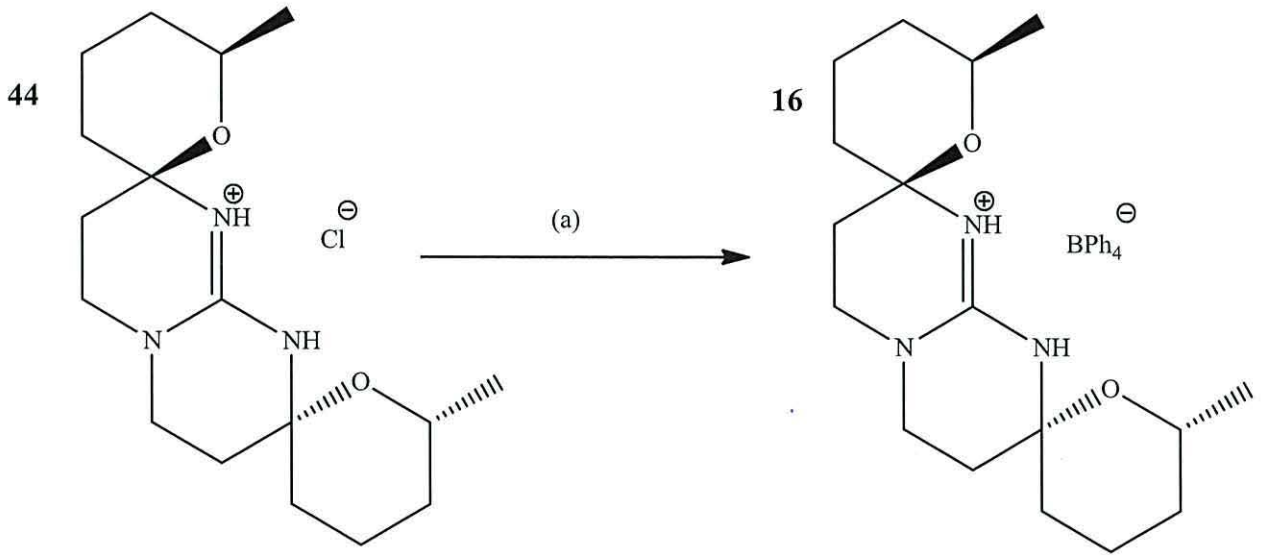

Chemical Formula: $C_{17}H_{30}ClN_3O_2$
Molecular Weight: 343.89

Chemical Formula: $C_{41}H_{50}BN_3O_2^+$
Molecular Weight: 627.67

Ion exchange: Guanidine chloride salte **44** (199.7 mg, 0.581 mmols) was dissolved in dry THF (5 mL) to which $NaBPh_4$ (0.6 g, 1.75 mmols) was added and the reaction followed by TLC until completion. The solvent was removed *in vacuo* and the crude white solid dissolved in DCM (10 mL) washed with H_2O (2 x 50 mL) to remove NaCl and excess $NaBPh_4$. The solution was dried ($MgSO_4$) filtered and the solvent removed *in vacuo* giving the guanidine tetraphenylborate salt **16** as a free-flowing white solid (321.8 mg, 0.513 mmols, 88%). Data was in agreement with the literature.

^{1}H NMR: δ_H (500 MHz, $CDCl_3$); 1.11 (6H, d, J = 6.1Hz, 2 x CH_3), 1.26-1.58 (14H, cm), 1.78 (2H, dd, J = 13.5, 4.3Hz, 2 x CH), 2.92 (2H, dd, J = 12.4, 5.5Hz, 2 x CH), 3.47 (4H, m, 4 x CH), 6.31 (2H, br s, 2 x NH), 6.93 (4H, t, J = 7.2Hz, 4 x CH aromatic), 7.07 (8H, t, J = 7.4Hz, 4 x (2 x CH aromatic)), 7.50 (8H, m, 4 x (2 x CH aromatic)) ppm.

^{13}C NMR: δ_C (500 MHz, $CDCl_3$); 164.74 (C aromatic), 164.35 (C aromatic), 163.95 (C aromatic), 163.56 (C aromatic), 148.03 (C), 135.94 (2 x CH aromatic), 125.81 (2 x CH aromatic), 121.92 (CH aromatic), 78.95 (2 x C), 67.04 (2 x CH), 42.63 (2 x CH_2), 33.26 (2 x CH_2), 32.80 (2 x CH_2), 31.96 (2 x CH_2), 21.69 (2 x CH_3), 18.02 (2 x CH_2) ppm.

^{11}B NMR: δ_B (400 MHz, $CDCl_3$); -6.46 ppm.[28]

General Method for catalyst testing (Quinones – Michael Addition)

2-hydroxy-3-(2-nitro-1-phenylethyl)naphthalene-1,4-dione 31[45]

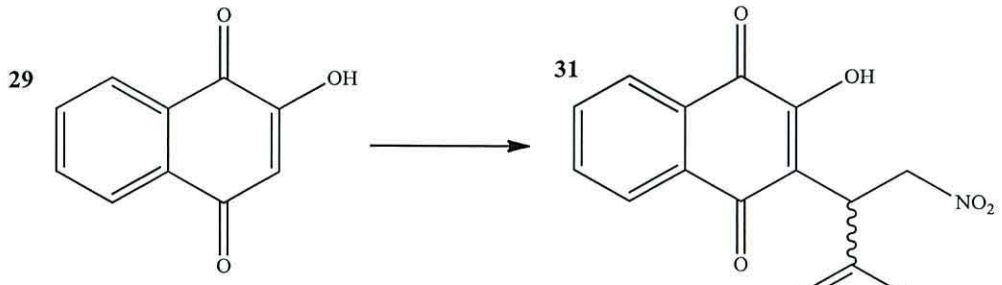

Chemical Formula: $C_{10}H_6O_3$
Molecular Weight: 174.15

Chemical Formula: $C_{18}H_{13}NO_5$
Molecular Weight: 323.30

2-hydroxynaphthalene-1,4-dione **29** (100 mg, 0.574 mmols) and *trans*-β-nitrostyrene **30** (128.5 mg, 0.861 mmols) were dissolved in dry solvent (THF / EtOH 15 mL on separate occasions) and cooled to 0°C. Guanidine catalyst **16** (18 mg, 0.0287 mmols, 0.05 eqv) was added. The reaction progress was followed by ^{1}H NMR (see R&D). The solvent was removed *in vacuo* and the crude yellow solid product was purified by column chromatography (25% DCM : Petrol, followed by 100% DCM). Product **31** was isolated as a bright lemon yellow solid (138.4 mg, 0.428 mmols, 92.1%). Data was in agreement with the literature.[45]

^{1}H NMR: δ_H (400 MHz, $CDCl_3$); 8.15 (2H, ddd, J = 19.1, 7.7, 1.2Hz, 2 x CH), 7.79 (1H, td, J = 7.6, 1.4Hz, CH), 7.71 (1H, td, J = 7.5, 1.3Hz, CH), 7.48 (2H, m, 2 x CH), 7.33 (2H, m, 2 x CH), 7.26 (1H, m, CH), 5.50 (1H, dd, J = 13.3, 9.1Hz, CH), 5.33 (1H, m, CH), 5.16 (1H, dd, J = 13.3, 6.8Hz, CH), 1.58 (1H, s, OH) ppm.

^{13}C NMR: δ_C (400 MHz, $CDCl_3$); 183.68 (C=O), 181.13 (C=O), 160.46 (C-OH), 153.17 (C), 137.50 (C), 135.46 (CH), 133.31 (CH), 132.63 (C), 128.99 (2 x CH), 128.27 (2 x CH), 127.85 (CH), 127.23 (CH), 126.36 (CH), 120.78 (C), 76.34 (CH_2), 39.66 (CH) ppm.

Rf: 0.22 in 100% DCM.

ee from HPLC:

EtOH	(42.4 : 57.6)	15.2%
THF	(43.9 : 56.1)	12.3%

Racemic products were made using THF / EtOH with H_2O (0.5ml) and no catalyst.

Background tests were also carried out without H_2O or catalyst (no noticeable reaction occurred)

1-methylpiperidin-2-one 33[39]

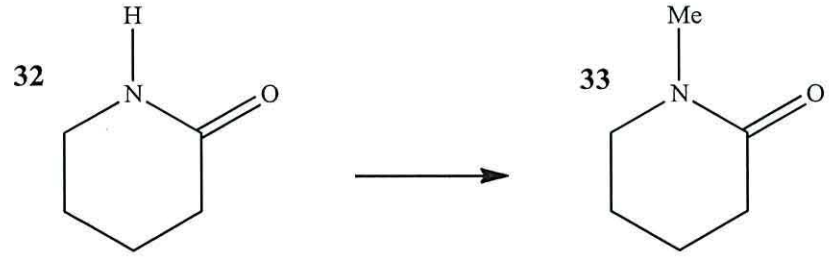

Chemical Formula: C_5H_9NO
Molecular Weight: 99.13

Chemical Formula: $C_6H_{11}NO$
Molecular Weight: 113.16

In an inert atmosphere of argon piperidin-2-one **32** (10 g, 100.88 mmol) in dry THF (100 mL) was cooled to -30°C in an acetone nitrogen bath. To the solution *n*-BuLi (44.4 mL, 110.97 mmol) was added and the mixture stirred for 30 mins. The mixture was then cooled to -78°C and MeI (15.75 g, 110.97 mmol, 6.9 mL) was added, the mixture was then left in the cooling bath overnight and allowed to slowly warm to room temperature. Ether was added (50 mL) and the solvent removed *in vacuo*, H_2O (150 mL) was added and then crude material extracted using DCM (3 x 50 mL). The crude material was dried ($MgSO_4$), filtered and the solvent removed *in vacuo* giving the crude product as an slightly yellow oil (11.07 g). This crude oil was purified via distillation giving the methylated piperidone product **33** as a colourless oil (9.96 g, 87.68 mmol, 87%). Data was in agreement with the literature.[39]

^{1}H NMR: δ_H (500 MHz, $CDCl_3$); 3.20 (2H, t, J = 5.5Hz, CH_2), 2.86 (3H, s, CH_3), 2.29 (2H, t, J = 6.2Hz, CH_2), 1.73 (4H, m, 2 x CH_2) ppm.

^{13}C NMR: δ_C (500 MHz, CDCl3); 169.70 (C=O), 49.75 (CH_2), 34.40 (CH_3), 32.05 (CH_2), 22.97 (CH_2), 21.29 (CH_2) ppm.

3-iodopropan-1-ol 58[40]

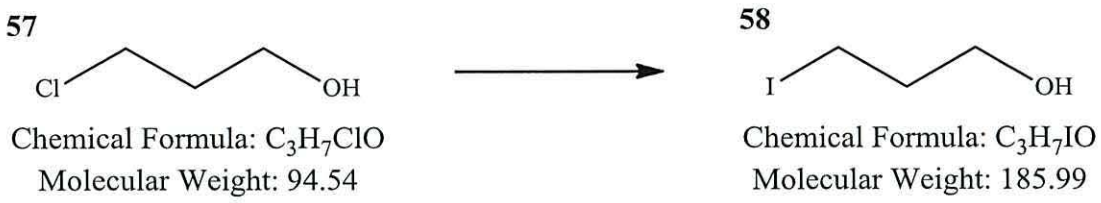

Chemical Formula: C_3H_7ClO
Molecular Weight: 94.54

Chemical Formula: C_3H_7IO
Molecular Weight: 185.99

In an inert argon atmosphere, 3-chloropropan-1-ol **57** (16.8 g, 177.7 mmol) and NaI (38.74 g, 258.27 mmol, 1.45 eqvs) were heated under reflux for 24 h in acetone (200 mL). The mixture was allowed to cool and then filtered through a sintered glass funnel and the $NaCl_{(ppt)}$ cake washed with a small portion of cold acetone (ca. 25 mL). The solvent was removed *in vacuo* giving a crude oil which was purified via trituration in 1:1 ether : petrol and the $NaCl_{(ppt)}$ again removed via filtration. The oil was dissolved in a small amount of ether and washed with H_2O (2 x 200 mL) and brine (2 x 150 mL) and the aqueous layers back-extracted with small portions of ether (2 x 50 mL). The combined organic layers were dried ($MgSO_4$) and the solvent removed *in vacuo* giving **58** as an almost colourless oil (22.42 g, 120.5 mmol, 68%). Data was in agreement with the literature.[40]

1H NMR: δH (500 MHz, $CDCl_3$); 3.74 (2H, t, J = 5.9Hz, CH_2), 3.31 (2H, t, J = 6.7Hz, CH_2), 2.69 (1H, s, OH), 2.03 (2H, pentet, CH_2) ppm.

3-(methylamino)propan-1-ol 59[46]

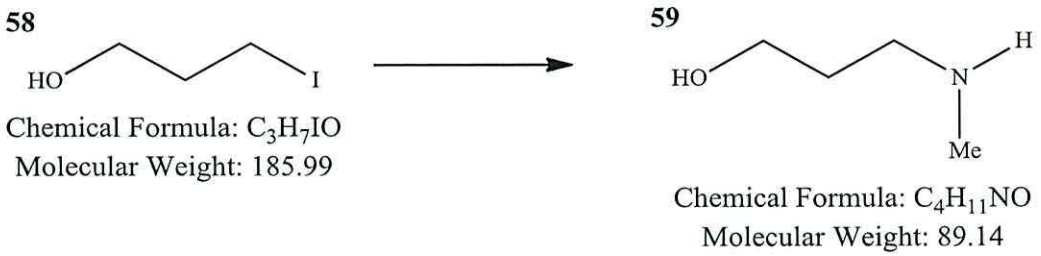

In an inert argon atmosphere 3-iodopropan-1-ol **58** (22.42 g, 120.5 mmol) and $MeNH_2$.EtOH (33% in ethanol, 300 mL, 2.4 moles, 20 equivs) were stirred over a weekend. Small amounts of K_2CO_3 were added until there was no more fizzing and the mixture filtered through a sintered glass funnel. The ethanol was removed *in vauco* and the oil re-dissolved in DCM (200 mL) upon which the $KI_{(ppt)}$ was filtered and the cake washed with cold DCM (50 mL). The DCM was removed *in vacuo* and the alcohol product 59 isolated as an almost colourless oil (9.74 g, 109.66 mmol, 91%). Data was in agreement with the literature.[46]

1H NMR: δ_H (500 MHz, CD_3OD); 3.66 (2H, t, J = 6.1Hz, CH_2), 2.86 (2H, t, J = 7.1Hz, CH_2), 2.52 (3H, s, CH_3), 1.80 (2H, pent, CH_2) ppm.

13C NMR: δ_C (500 MHz, CD_3OD); 61.10 (CH_2), 49.66 (CH_2), 35.26 (CH_3), 31.47 (CH_2) ppm.

tert-butyl (3-hydroxypropyl)(methyl)carbamate 60[47]

Chemical Formula: $C_4H_{11}NO$
Molecular Weight: 89.14

Chemical Formula: $C_9H_{19}NO_3$
Molecular Weight: 189.25

In an inert atmosphere of argon alcohol **59** (4.76 g, 53.39 mmols) was dissolved in a minimum of dry DCM. To this solution di-*tert*-butyl dicarbonate (15.15 g, 69.42 mmols, 1.3 eqvs) in dry DCM (100 mL) was added drop-wise via a pressure equalizing dropping funnel over 30mins. The mixture was stirred at room temperature overnight. The solvent was removed *in vacuo* and the crude mixture was purified using column chromatography (35% EtOAc : Petrol, Rf = 0.27 in 35% EtOAc : Petrol). The protected alcohol product **60** was isolated as a clear oil (5.55 g, 29.33 mmols, 55%). Data was in agreement with the literature.[47]

1H NMR: δH (500 MHz, $CDCl_3$); 4.08 (2H, t, J = 6.5Hz, CH_2), 3.31 (2H, t, J = 6.9Hz, CH_2), 2.86 (3H, s, CH_3), 1.89(2H, pentet, J = 6.5Hz, CH_2), 1.46 (9H, s, 3 x CH_3).

13C NMR: δC (500 MHz, CDCl3); 157.19 (C=O), 79.94 (C), 58.09 (CH_2), 44.22 (CH_2), 34.10 (CH_3), 29.66 (CH_2), 28.34 (3 X CH_3) ppm.

tert-butyl (3-iodopropyl)(methyl)carbamate 61[48]

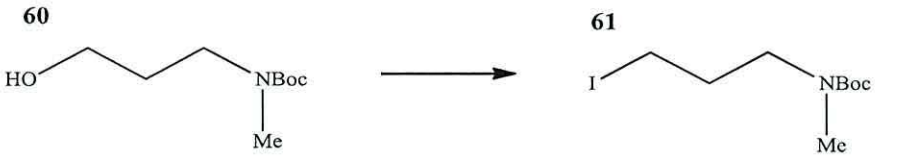

Chemical Formula: $C_9H_{19}NO_3$
Molecular Weight: 189.25

Chemical Formula: $C_9H_{18}INO_2$
Molecular Weight: 299.15

In a 500 mL round bottom flask dry DCM (150 mL) was mixed with (in order) PPh_3 (9.62 g, 33.66 mmol), imidazole (3.08 g, 45.17 mmol) and iodine (11.24 g, 44.29 mmol). In an inert atmosphere of argon a solution of alcohol **60** (5.55 g, 29.33 mmol) in DCM (40 mL) was added. The mixture was stirred overnight at room temperature. An aqueous solution of sodium thiosulfate was added and the mixture separated, the organic layer dried ($MgSO_4$) and the solvent removed *in vacuo*. The crude product was triturated with ether : petrol (removing most residual PPh_3) and purified using column chromatography (20% Et_2O : Petrol, Rf = 0.19 in 30% Et_2O : Petrol). The iodo product **61** was isolated as an almost colourless oil (6.64 g, 22.2 mmol, 76%). Data was in agreement with the literature.[48/49]

1H NMR: δH (500 MHz, $CDCl_3$); 3.25 (2H, t, J = 6.8Hz, CH_2), 3.11 (2H, t, J = 6.9Hz, CH_2), 2.82 (3H, s, CH_3), 2.02 (2H, apparent pentet, CH_2), 1.42 (9H, s, 3 x CH_3) ppm.

tert-butyl methyl(5-oxo-6-(triphenylphosphoranylidene)hexyl)carbamate 49

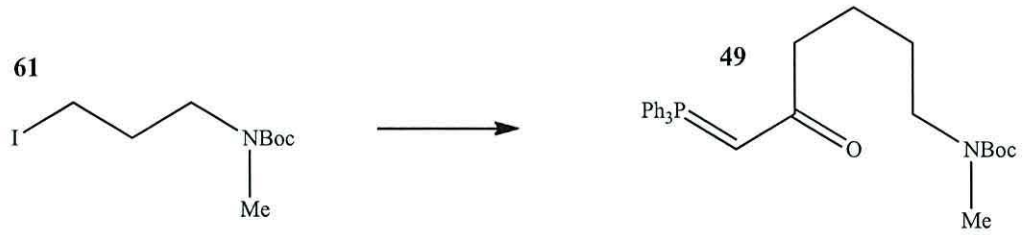

Chemical Formula: $C_9H_{18}INO_2$
Molecular Weight: 299.15

Chemical Formula: $C_{30}H_{36}NO_3P$
Molecular Weight: 489.59

In an inert atmosphere acetylmethylenetriphenylphosphorane AMTP (1.18 g, 3.69 mmol) was dissolved in dry THF (50 mL) and cooled to -50°C. *n*-BuLi (1.34 mL, 3.35 mmol) was added drop-wise and the deep red coloured mixture stirred at -60°C for 1h. The reaction was then cooled to -78°C and a solution of iodide **61** (1.00 g, 3.35 mmol) in a minimum of THF was added. The mixture was stirred in the cooling bath and allowed to warm up slowly to room temperature overnight. H_2O (100 mL) was added and the mixture separated and the aqueous layer extracted with DCM (3 x 50 mL). The combined organic layers were dried ($MgSO_4$) and the solvent removed *in vacuo* giving the crude product as an oil (2.1 g). The crude product was purified by column chromatography (0% - 80% EtOAc : Petrol, Rf = 0.17 in 80% EtOAc : Petrol) giving the phosphorane product **49** as a colourless oil (1.26 g, 2.57 mmol, 77%). Compound **49** was unstable to storage and used in the next step immediately.

1H NMR: δH (500 MHz, $CDCl_3$); 7.66 (6H, m, 3 x (2 X CH aromatic), 7.56 (3H, m, 3 x CH aromatic), 7.47 (6H, m, 3 x (2 x CH aromatic), 3.22 (2H, unresolved triplet, CH_2), 2.83 (3H, s, CH_3), 2.35 (2H, unresolved triplet, CH_2), 1.65 (2H, m, CH_2), 1.58 (2H, m, CH_2), 1.44 (9H, s, 3 x CH_3) ppm.

13C NMR: δ_C (500 MHz, $CDCl_3$); 155.77 (C=O), 132.99 (3 x (2 x CH aromatic), 131.99 (3 x CH aromatic), 128.75 (3 x (2 x CH aromatic), 78.83 (C), 48.79 (CH_2), 41.12 (CH_2), 33.84 (CH_3), 28.38 (3 x CH_3), 27.81 (CH_2), 24.12 (CH_2) ppm.

tert-butyl methyl(5-oxohept-6-en-1-yl)carbamate 34

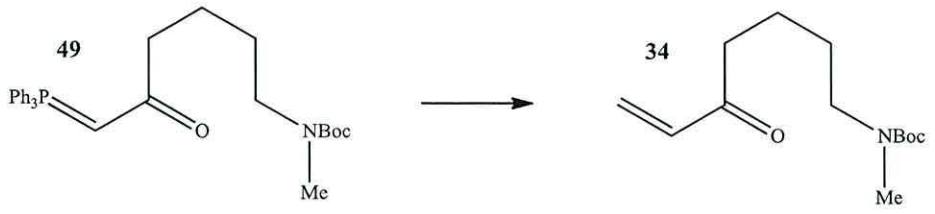

Chemical Formula: $C_{30}H_{36}NO_3P$
Molecular Weight: 489.59

Chemical Formula: $C_{13}H_{23}NO_3$
Molecular Weight: 241.33

Phosphorane **49** (1.26 g, 2.57 mmol) was dissolved in DCM (50 mL) and stirred in formaldehyde (Aqueous formaldehyde solution (47 mL) was diluted with DCM (25 mL) and dried ($MgSO_4$)). The mixture was stirred overnight at room temperature. The mixture was then diluted with DCM (100 mL), washed with H_2O (2 x 150 mL), separated and dried ($MgSO_4$). The solvent was removed *in vacuo* and the crude product purified using column chromatography (15% EtOAc : Petrol, Rf = 0.15 in 15% EtOAc : Petrol) giving the desired enone **34** as a slightly yellow oil (0.44 g, 1.82 mmol, 71%). Compound **34** was unstable to storage and used in the next step immediately.

1H NMR: δH (500 MHz, $CDCl_3$); 6.28 (1H, dd, J = 17.7, 10.5 Hz, CH), 6.15 (1H, dd, J = 17.7, 0.8 Hz, CH), 5.75 (1H, d, J = 10.5 Hz, CH), 3.15 (2H, unresolved triplet, CH_2), 2.75 (3H, s, CH_3), 2.55 (2H, t, J = 7.0Hz, CH_2), 1.56-1.43 (4H, m, 2 x CH_2), 1.37 (9H, s, 3 x CH_3) ppm.

Attempted reaction

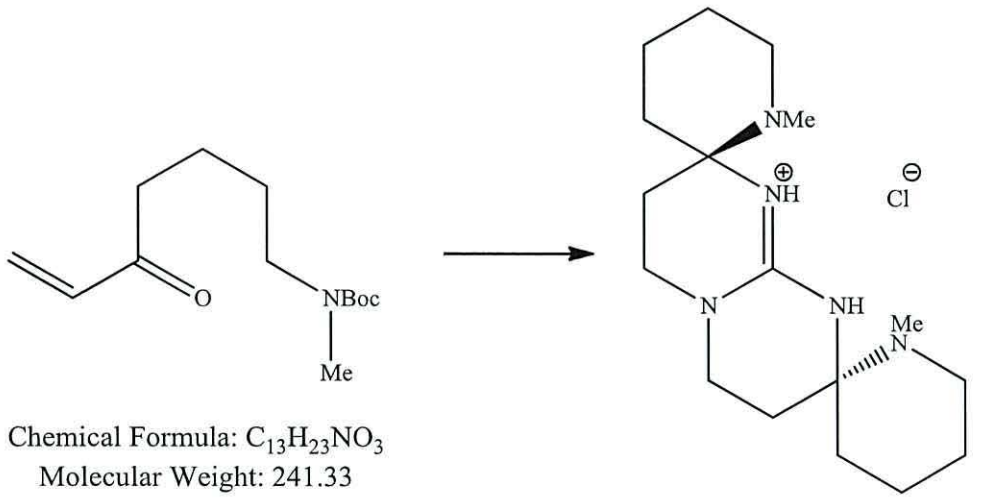

Chemical Formula: $C_{13}H_{23}NO_3$
Molecular Weight: 241.33

Chemical Formula: $C_{17}H_{32}ClN_5$
Molecular Weight: 341.92

In an inert atmosphere of argon enone **34** (0.73 g, 3.03 mmol) was dissolved in dry DMF (5 mL) and cooled to 0°C. Guanidine as a solution in DMF (0.1 g, 1.67 mmols, 0.75 mL solution) was added slowly and the reaction mixture stirred to room temperature over 72 h. The mixture was cooled to 0°C and HCl (3 M, 10 mL) (and alternate attempts using Methanolic HCl) was added drop-wise. A sticky polymer formed which was re-dissolved with MeOH (8 mL) and the mixture stirred overnight. The MeOH was removed *in vacuo* and the mixture extracted with DCM (25 mL) and washed with brine (50 mL). The residual DMF was removed by co-evaporation with toluene (3 x 20 mL). The purification was attempted using column chromatography (0% - 5% MeOH : $CHCl_3$).

1.5. References

1. R. Noyori, *Chemical Communications (Cambridge, England)*, 2005, 1807–11.

2. U.S. Climate Change Technology Program, *INDUSTRIAL PROCESS EFFICIENCY Technology Options for the Near and Long Term*, 2005.

3. A. Schmid, J. S. Dordick, B. Hauer, A. Kiener, M. Wubbolts, and B. Witholt, *Nature*, 2001, **409**, 258–68.

4. R. Noyori, *Nature Chemistry*, 2009, **1**, 5–6.

5. R. Noyori, *Advanced Synthesis and Catalysis*, 2001, **343**, 1.

6. A. Strecker, *Justus Liebigs Annalen der Chemie*, 1861, **118**, 151–177.

7. J. Clayden, N. Greeves, S. Warren, and P. Wothers, *Organic Chemistry*, New York, 1st edn., 2001.

8. H. Tapiero, G. Mathé, P. Couvreur, and K. . Tew, *Biomedicine & Pharmacotherapy*, 2002, **56**, 439–445.

9. *US Pat.*, US20080286165, R. K. Graupner, D. J. Hultine, and J. A. Van Vechten, 2007.

10. Y. Sawayama, *Synlett*, 2011, 651–654.

11. P. J. Murphy, H. L. Williams, D. E. Hibbs, M. B. Hursthouse, and K. M. A. Malik, *Tetrahedron*, 1996, **52**, 8315–8332.

12. A. Howard-Jones, P. J. Murphy, D. A. Thomas, and P. W. R. Caulkett, *The Journal of Organic Chemistry*, 1999, **64**, 1039–1041.

13. M. Allingham, A. Howard-Jones, P. Murphy, D. Thomas, and P. Caulkett, *Tetrahedron Letters*, 2003, **44**, 8677–8680.

14. V. Alcazar, J. R. Moran, and J. de Mendoza, *Tetrahedron Letters*, 1995, **36**, 3941–3944.

15. H. Nishida, N. Takada, and M. Yoshimura, *Bulletin of the Chemical Society of Japan*, 1984, **57**, 2600–2604.

16. L. A. K. Staveley and T. Davies, *Transactions of the Faraday Society*, 1957, **53**, 19–30.

17. C. Najera, R. Chinchilla, and P. Sanchez-Agullo, *Tetrahedron Asymmetry*, 1994, **5**, 1393–1402.

18. D. Ma and K. Cheng, *Tetrahedron Asymmetry*, 1999, **10**, 713–719.

19. B. M. Trost and V. S. C. Yeh, *Angewandte Chemie International Edition*, 2002, **41**, 861–863.

20. P. Bakó, L. Toke, and Z. Bajor, *Journal of the Chemical Society Perkin Transactions I*, 1999, 3651–3655.

21. T. Ooi and K. Maruoka, *Angewandte Chemie (International ed. in English)*, 2007, **46**, 4222–66.

22. S. Shirakawa and K. Maruoka, *Angewandte Chemie (International ed. in English)*, 2013, **52**, 4312–48.

23. C. M. Starks, *Journal of the American Chemical Society*, 1971, **93**, 195–199.

24. R. M. Owens and C. M. Starks, *Journal of the American Chemical Society*, 1973, **95**, 3613–3617.

25. B. Lygo and P. G. Wainwright, *Tetrahedron*, 1999, **55**, 6289–6300.

26. P. M. Harper, MSc Thesis, University of Wales, Bangor, 2011.

27. P. J. Murphy, H. L. Williams, M. B. Hursthouse, and K. M. A. Malik, *Journal of the Chemical Society, Chemical Communications*, 1994, 119.

28. J. D. Odom, L. W. Hall, and P. D. Ellis, *Organic Magnetic Resonance*, 1974, **6**, 360–361.

29. P. Christ, A. G. Lindsay, S. S. Vormittag, J.M. Neudörfl, A. Berkessel, and A. C. O'Donoghue, *Chemistry - A European Journal*, 2011, **17**, 8524–8.

30. M. R. Crampton and I. A. Robotham, *Journal of Chemical Research*, 1997, 22–23.

31. G. Bordwell, *Accounts of Chemical Research*, 1988, **21**, 3305–3312.

32. G. P. Black, P. J. Murphy, and N. Walshe, *Tetrahedron*, 1998, **54**, 9481–9488.

33. C. D. Ritchie and R. E. Uschold, *Journal of the American Chemical Society*, 1967, **89**, 1721–1725.

34. C. F. Lemaire, J. J. Aerts, S. Voccia, L. C. Libert, F. Mercier, D. Goblet, A. R. Plenevaux, and A. J. Luxen, *Angewandte Chemie (International ed. in English)*, 2010, **49**, 3161–4.

35. L. Malek, *Collection of Czechoslovak Chemical Communications*, 1951, **16/17**, 23–31.

36. M. Maeda, S. Okusada, and K. Kawasaki, *Chem. Pharm. Bull.*, 1984, **32**, 4157–4160.

37. T. Endo and A. Nabeya, *J. Org. Chem*, 1991, **56**, 3194–3197.

38. O. Guerret, H. Gornitzka, J. B. Cazaux, D. Bigg, F. Palacios, G. Bertrand, and S. Gourmi-Magnet, *J. Org. Chem*, 1999, **64**, 3741–3744.

39. O. Jentzer, P. Vanelle, M. Crozet, J. Maldonado, and M. Barreau, *European Journal of Medicinal Chemistry*, 1991, **26**, 687–697.

40. *US Pat.*, US20060293521C, M. Kausch, K. Yongsin, R. R. Thomas, and D. L. Hardman, 2006.

41. P. J. Garegg and B. Samuelsson, *Journal of the Chemical Society Perkin Transactions I*, 1980, 2866–2869.

42. K. Bowden, *Journal of Chemical Research: Miniprint*, 1990, 377.

43. W. K. Warburton and S. J. Angyal, *Journal of the Chemical Society*, 1951, 2492–2494.

44. C. G. Moore, P. J. Murphy, H. L. Williams, A. T. McGown, and N. K. Smith, *Tetrahedron*, 2007, **63**, 11771–11780.

45. S. B. Woo and D. Y. Kim, *Beilstein Journal of Organic Chemistry*, 2012, **8**, 699–704.

46. P. Sheldrake, E. Tyrrell, S. Mintias, and I. Shahid, *Synthetic Communications*, 2003, **33**, 2263–2268.

47. B. H. Lee and M. J. Miller, *The Journal of Organic Chemistry*, 1983, **48**, 24–31.

48. *Br Pat.*, GB6242470A, Baxter, S. Brough, T. McInally, and M. Mortimore, 2001.

49. *US Pat.*, US4717728A, M. Furukawa and M. Sato, 1983.

Chapter 2: Introduction to Neutron Scattering

2.1. Introduction to Neutron Scattering

Discovered by Chadwick in 1932,[1/2] neutrons are powerful tools that have advantages over other radiation techniques applied to the study of matter (structure / dynamics). A neutron is an uncharged or electrically neutral sub-atomic particle with a mass of 1.009 amu, 1,839 times that of an electron that also has a magnetic moment.

2.1.1. Why Use Neutrons?

Due to its uncharged nature, the neutron interacts with the nucleus of an atom as opposed to interactions with the surface layers or electron cloud (as with techniques such as XRD, Raman and IR). This means the scattering power or intensity of spectra is not related to the atomic number (Figure 1.), which differs from X-ray or electron based techniques in which scattering power increases in proportion to the number of electrons in the atom. This gives rise to the ability to study or probe lighter atoms (such as hydrogen, the most abundant element in our galaxy) in the presence of heavier atoms. It also allows atoms next to each other in the periodic table to be distinguished due to them having vastly different scattering cross sections.

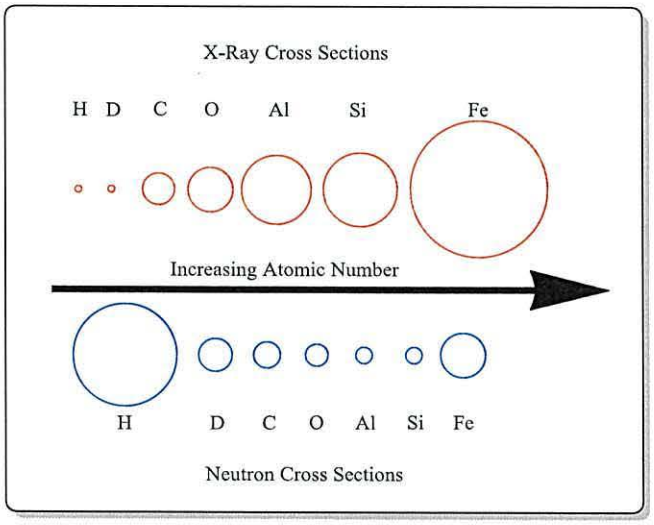

Figure 1. Neutron and X-ray scattering cross sections of particular atoms.

Another useful property of neutron based techniques is that isotopes exhibit substantially different scattering lengths (see Figure 1. – comparison of neutron cross sections of Hydrogen [H] & Deuterium [D]), which allows the use of isotopic labelling (or isotopic substitution) to label specific or different parts of the molecule (due to nuclear dependence on scattering).

The interaction of a neutron with the nucleus of an atom is weak (but not negligible) so as well as being an extremely powerful and penetrating probe, these weak interactions mean that it is also a non-destructive technique (even with highly sensitive compounds such as active catalysts or with complex samples such as biological / polymeric materials).

Neutron scattering is an experimental technique started over 50 years ago[3] and now has applications in crystallography,[4] physics,[5] physical chemistry,[6] biophysics[7] and materials research.[8]

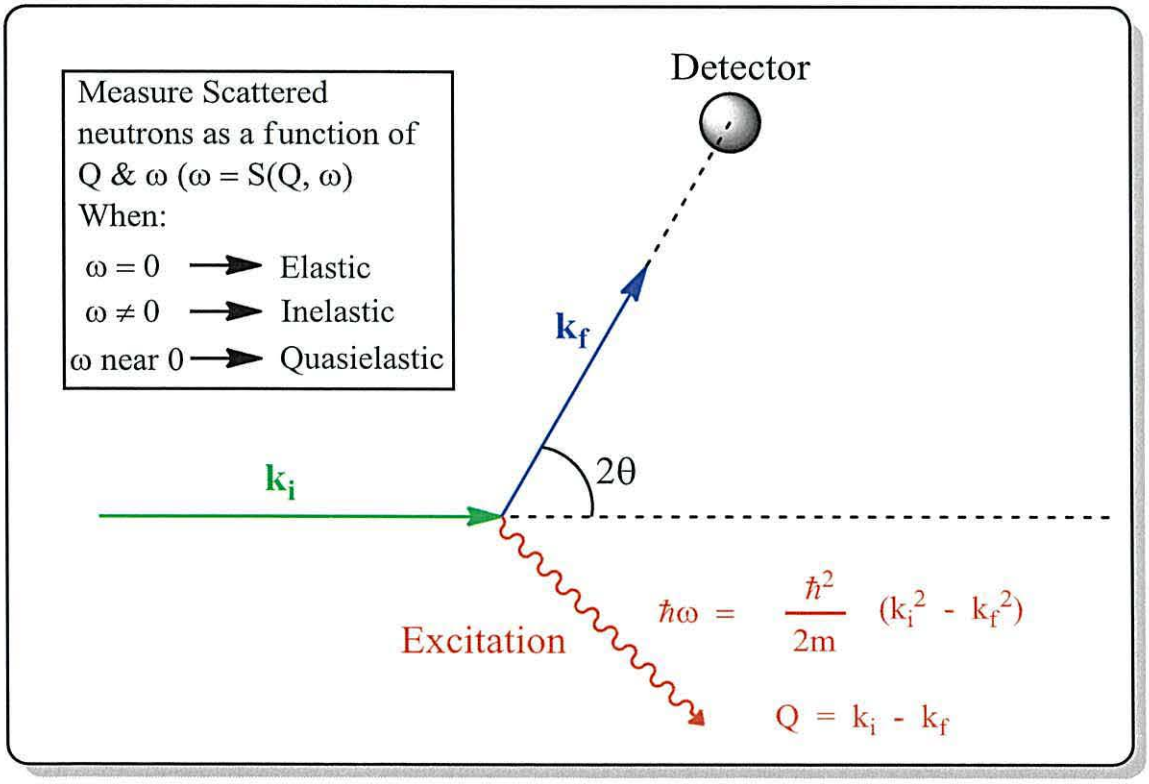

Figure 2. Neutron scattering experimental schematic diagram.

2.1.2. Elastic Neutron Scattering – (Neutron Diffraction or ENS)

A sample is placed in a beam of neutrons and a diffractogram is produced that provides information on the atomic and or magnetic structure of the sample material. Due to the different cross sections or scattering properties (Figure 1.) the information derived is complementary to that from X-ray scattering (XRD) but can be thought of as a similar technique. In ENS a momentum is transferred from the neutron to the sample. This transfer leads to a miniscule translation of the entire sample but leaves the internal state of the sample unchanged.[9]

Equation 1. The momentum (Q) transfer.

$$Q = \underline{k}_i - \underline{k}_f$$

$$\underline{k} = \frac{2\pi}{\lambda}$$

Q = momentum
$\underline{k}$ = wavefactor ($Å^{-1}$)
i / f = incident / final values
λ = wavelength of the neutron

2.1.3. Inelastic Neutron Scattering – (Neutron Spectroscopy or INS)

Applied to the study of atomic vibrations and other excitations. A sample is placed in a beam of neutrons and upon interaction (neutron on matter) the neutron remains uncharged and can be treated as a "billiard ball" scattering from the atomic nuclei.

An atoms nucleus is $\approx 1/1000^{th}$ of the diameter of the atom hence the neutrons are highly penetrating. Neutrons are best described as quantum mechanical entities, exhibiting both particle- and wave- like properties.[10]

In INS vibrational spectroscopy an inelastic scattering event results in significant transfers of energy (E, cm^{-1}) and momentum (Q, $Å^{-1}$). The momentum (Q) calculated as in Equation 1., with the energy transfer (E_T) calculated as follows.[11]

Equation 2. The energy transfer (E_T).

$$E_T = E_i - E_f$$

INS produces vibrational spectra not dissimilar to those derived using IR and Raman, but with hydrogenous modes particularly emphasised. INS spectra are also affected by an absence of selection rules, which does not apply to optical spectroscopy. Vibrational spectra can be placed into two broad classes:

Those in which a photon with the correct energy excites a vibrational transition (absorbed or emitted) such as IR. Those in which a particle is inelastically scattered by a material, where the particles energy changes in an amount equal to that of the vibrational transition. Examples of techniques where said particle is:

A photon (Raman scattering), an atom (Helium atom scattering), an electron (High-resolution electron energy loss spectroscopy / Inelastic electron tunnelling spectroscopy) and a neutron (Inelastic neutron spectroscopy).[11]

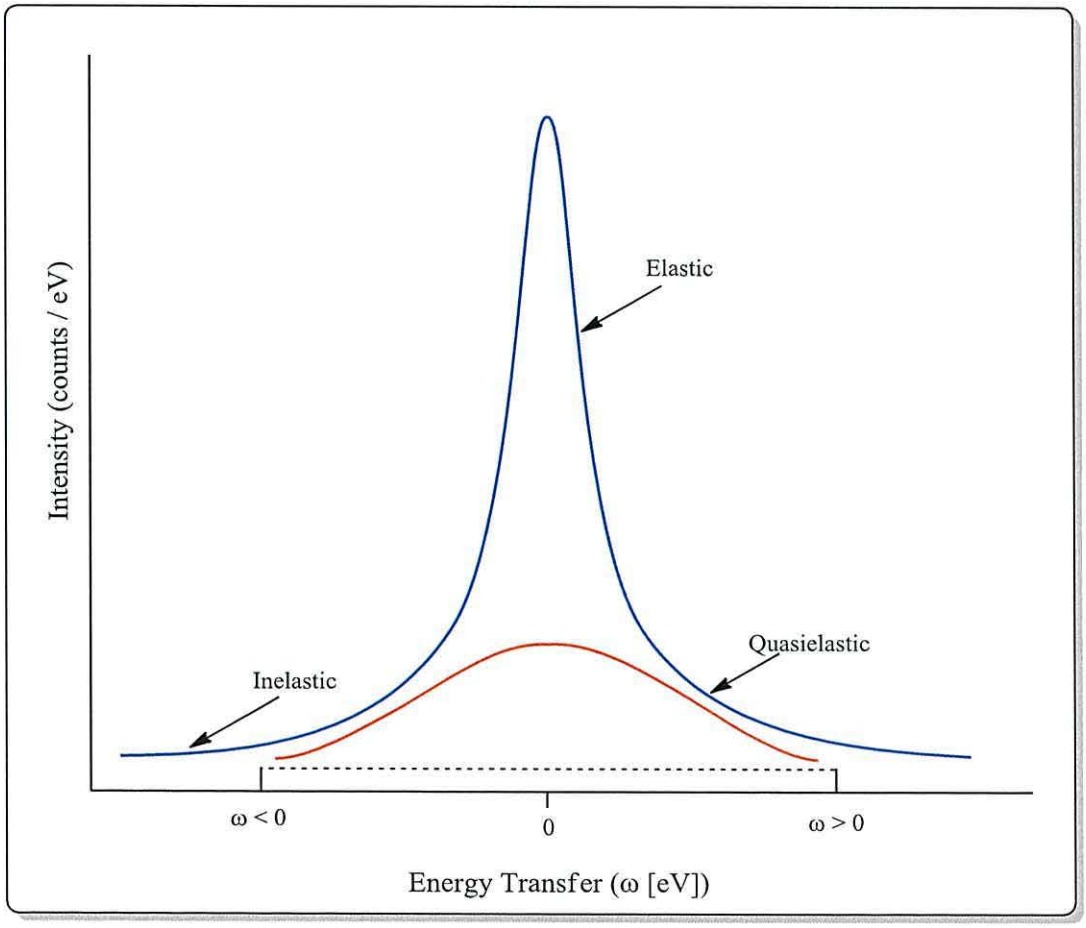

Figure 3. Elastic line representation

Neutron spectroscopy measures the atomic and magnetic motions of atoms, it has proven itself to be extremely useful in studying the structure of materials and the nature of dynamic processes. Using the change in energy of a neutron as it scatters from a sample, a wide variety of physical phenomenon (such as diffusional or hopping motions of atoms, the rotational modes of molecules, sound modes and molecular vibrations, recoil in quantum fluids, magnetic and quantum excitations or even electronic transitions) can be observed.[12]

The time and size scales available via neutron spectroscopy range from sub-picoseconds to nanoseconds and from fractions of interatomic distances (<1Å) to diameters of large molecular clusters (up to ≈ 1000Å). Structure is not the only property of molecules that can effect physical phenomenon, the often overlooked dynamics of the surrounding medium (solvent) and solute can also be very accurately characterised by the neutron, another great facet of such types of spectroscopy.[13]

Although often knowing the atomic structure will be sufficient in understanding the nature of a molecule, sometimes a deeper understanding of the physics of a phase change is necessary to understand the atomic dynamics. Whereas the most common forms of vibrational spectroscopy (IR/R spec) are cheap and readily available they are only sensitive to certain vibrational modes and the calculation of the scattered intensity is also prone to much error. These light scattering techniques are often used to "fingerprint" a compound, this can be done more accurately with INS which can also be used as a tool to understand the physics of a system. Due to the unique way neutrons scatter, among others uses it is a great technique for understanding and measuring the vibration or diffusion of a compound or material. The 1994 Nobel Prize in Physics was awarded for pioneering contributions to the field of neutron scattering to B. N. Brockhouse (Neutron Spectroscopy) and C. G. Shull (Neutron Diffraction).

2.1.4. Neutron Sources

The most important aspect of performing neutron scattering experiments is the neutron source itself, INS is a flux-limited technique and any major advances in this area will be dependent upon increasing the intensity of the neutron beam source.[14] There are two methods for the production of a sufficient flux of neutrons (> 10^{14} neutrons cm^{-2} s^{-1}), one being ^{235}U fission (Figure 4.) at a nuclear research reactor and the other being nuclear spallation.

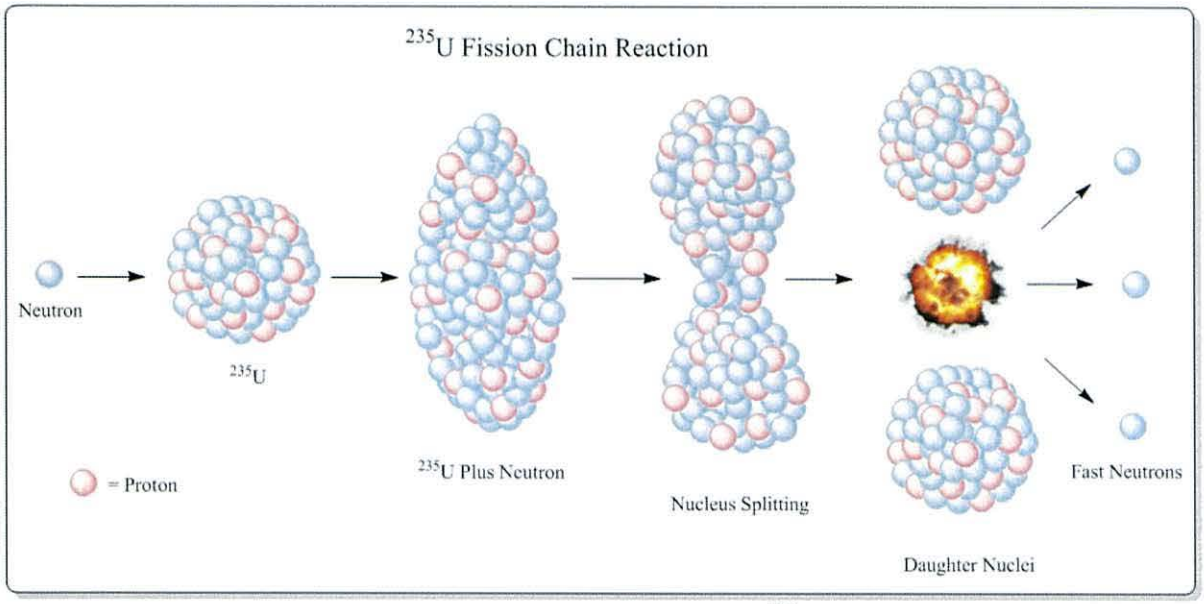

Figure 4. Schematic representation of neutrons produced from ^{235}U fission in a research reactor.

The incident neutron is fired into the ^{235}U nucleus where it is absorbed, the nucleus then becomes unstable and splits immediately forming daughter nuclei and releasing fast neutrons which initiate the fission of more ^{235}U nuclei in a continuous flow chain reaction (2 neutrons / fission are generated, one is used to sustain the chain reaction, the other is available for science).

When neutrons are produced via spallation (Figure 5.) a proton is accelerated (to ≈ 84% the speed of light) and fired into a heavy metal target and high energy particles are

scattered. These particles consist of protons, neutrons and alpha particles (composed of 2 protons and 2 neutrons) which then collide with other nuclei causing similar reactions (extranuclear cascade). In this process up to 20 / 30 neutrons are emitted for each proton which can then be guided towards the sample (via moderators which regulate the neutrons energy).

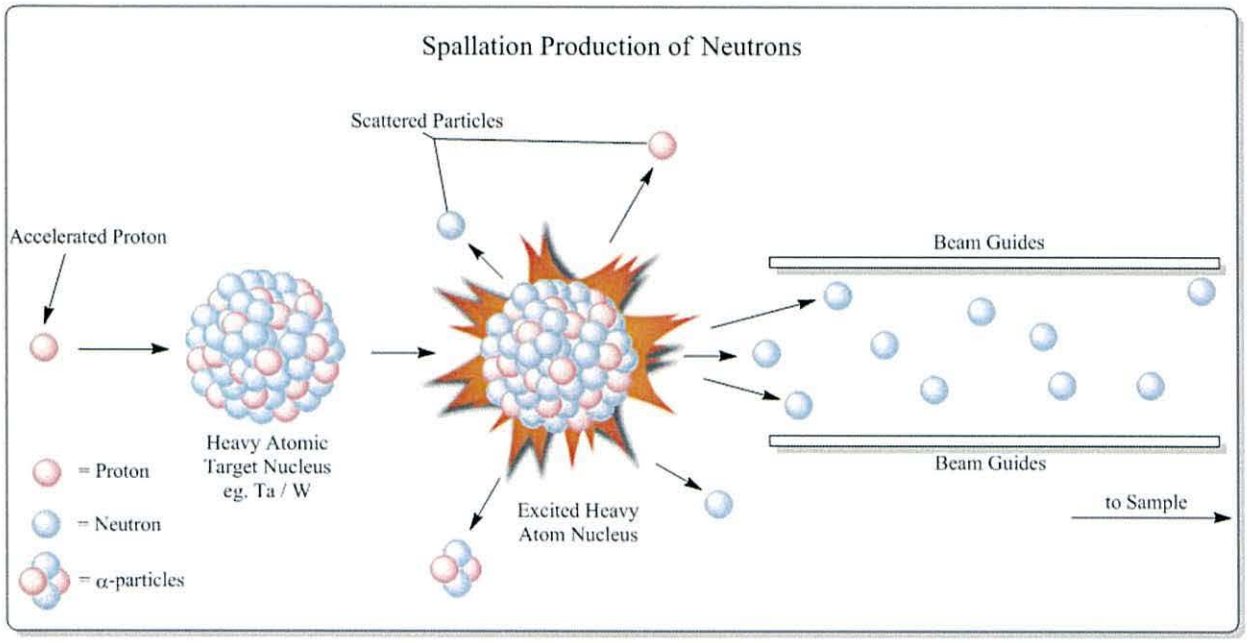

Figure 5. Schematic representation of neutrons produced via spallation.

The accelerated proton beam is pulsed (generally 40 – 60 Hz) and therefore time-of-flight (TOF) is the most common form of analysis. The future of INS will consist of spallation sources as, at present, research reactors "are close to the limit of the heat load generated by the fission process…that can be handled".[14] The use of spallation sources in the future of INS research will be favoured in part due to political worldwide concerns about nuclear-weapon proliferation and also concerns over environmental issues (cf. Fukushima Daiichi disaster).

There are three centres worldwide that boast neutron sources; SNS (Spallation Source at Oak Ridge in Tennessee USA),[15] J-PARC (Proton Accelerator Research Complex in Tokai

Japan)[16] and ISIS (Spallation Source at the Rutherford-Appleton Laboratories in Oxford UK).[17]

"The ISIS pulsed neutron and muon source at the Rutherford Appleton Laboratory in Oxfordshire is a world-leading centre for research in the physical and life sciences. It is owned and operated by the Science and Technology Facilities Council."[18]

ISIS produces beams of neutrons and muons that allow scientists to probe materials and compounds on the atomic scale using a wide variety of experiments.[19] Techniques and instruments (Figure 6.) include Muon spectroscopy (ARGUS, EMU, HIFI and MuSR),[20] Reflectometry (CRISP, INTER, OFFSPEC, POLREF and SURF),[21] Small angle scattering (LOQ, SANS2D, NIMROD and Sandals),[22] Neutron diffraction (GEM, ENGIN-X, HRPD, NIMROD, OSIRIS, PEARL, POLARIS, ROTAX, DANDALS, SXD, WISH and INES)[23] and Neutron Spectroscopy (IRIS, MARI, MERLIN, VESUVIO, LET, OSIRIS, MAPS and TOSCA).[24]

The instruments are located in 2 different target stations optimised to produce high energy (TS1 - short wavelength) and low energy (TS2 - long wavelength) neutrons respectively (Figures 6. & 7.).

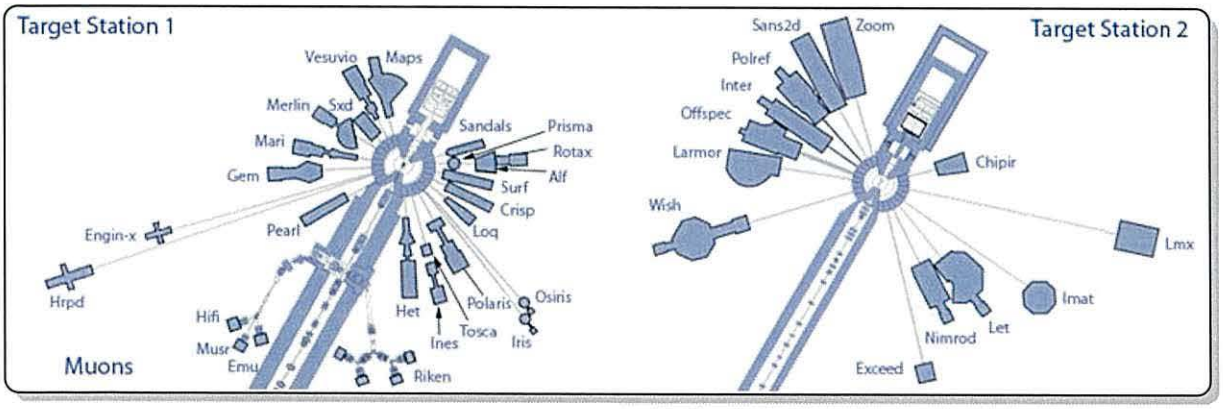

Figure 6. Target stations 1 & 2 with location of instruments.[19]

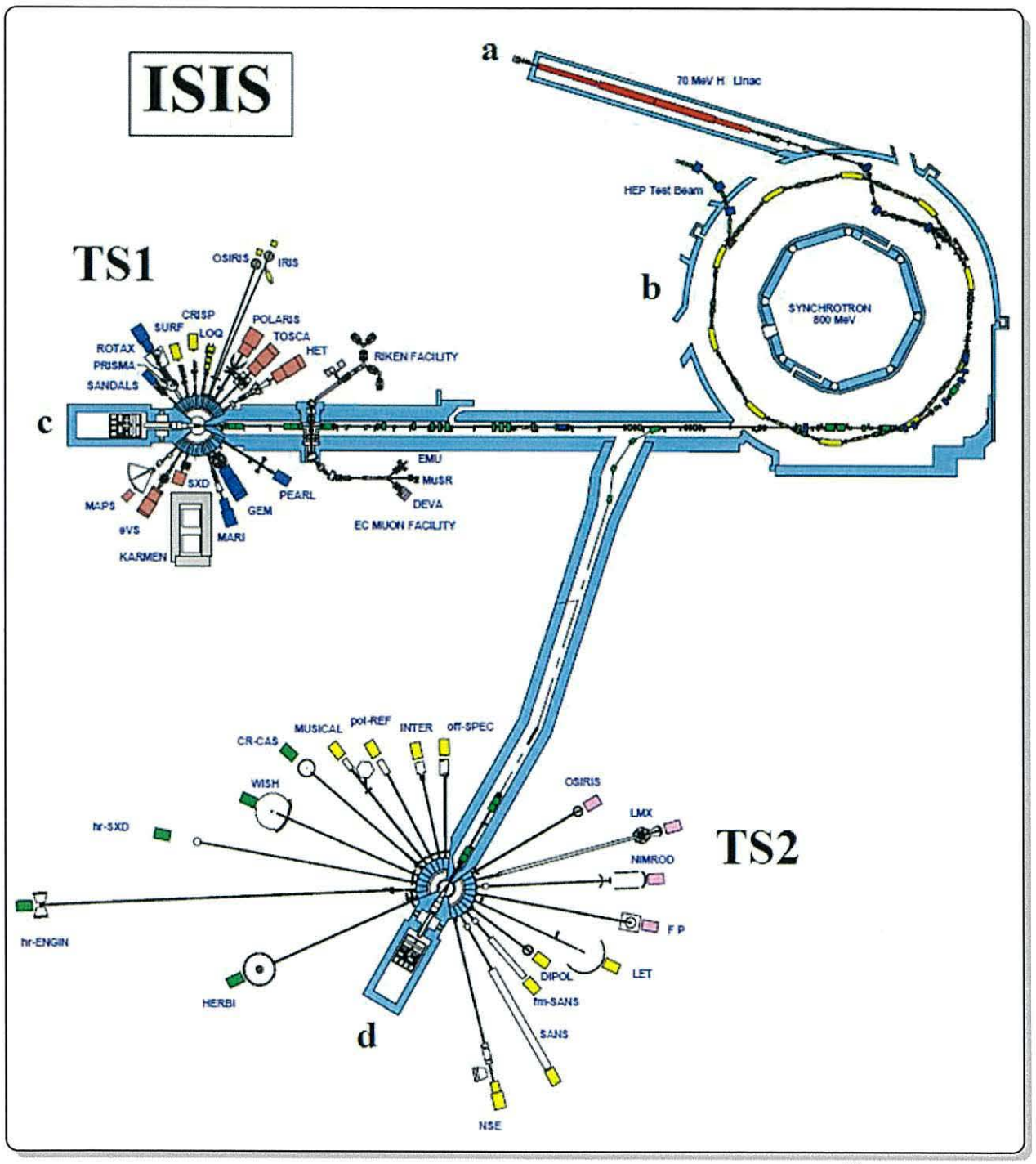

Figure 7. Aerial schematic of ISIS (a) Source; (b) Synchrotron; (c) TS1; (d) TS2.[18]

2.1.5. How ISIS Works

Negative hydrogen ions (H^-) are produced at the injector ion source (Figure 7a.) from hydrogen gas and hot caesium vapour, using an electric discharge. The stream of negative ions is fed into a Radio Frequency Quadrupole (RFQ) which accelerates, bunches and focuses the H^-'s into discrete packages 4.94 ns apart. The ion bunches are then fed into the Linac

which consists of four 10 m long copper lined electrode tubes which progressively accelerate the ions to a speed of ≈ 37% the speed of light. The beam of ions is then fed into the synchrotron (Figure 7b.) which consists of a circular ring of powerful magnets with a circumference of 163 m that bend and focus the beam even further. The inside of the synchrotron contains thin sheets of alumina foil that strip away the electrons creating a beam of protons that are then accelerated by radio-frequency electric fields and after ≈ 10,000 revolutions the proton beam has separated into two large bunches that have been accelerated to ≈ 84% of the speed of light. Fast kicker magnets eject the extracted proton beam (EPB) towards the neutron and muon targets, with the process being repeated 50 times a second producing a beam current of 200 μA.

TS1 (Figure 7c.) consists of 18 beam lines that feed the neutron scattering instruments (9 on each side). Neutrons are made when the EPB hits the heavy metal target (thick tungsten plates coated with tantalum to prevent corrosion) upon which water cooling channels and multiple neutron energy moderators are used to create a beam of neutrons with the correct energies for the particular experiments. The muon target is also located in TS1 and consists of a 10 mm thick carbon target that upon collision with the EPB releases pions (with an average lifetime of 26 ns) that decay into muons, the muon target uses 2 - 3% of the proton beam. TS2 is optimised for the proton beam line producing lower energy (cold) neutrons with longer wavelengths upon collision with a 2nd tungsten target (Figure 7d.) leading to instruments that produce spectra with greater functionality and higher resolution.

This study will focus on spectra obtained from the instruments TOSCA, MAPS and SANDALS located in TS1 at the ISIS pulsed neutron and muon source (Rutherford Appleton Labs) and can be seen in Figures 6. and 7.

2.1.5.1. TOSCA

TOSCA is an indirect geometry spectrometer which is optimised for the study of molecular vibrations.[25] It was designed to replace the previous instrument TXFA in 1998 which had reached its limitations in relation to INS spectrometry.[26] Spectra obtained using TOSCA are similar to those obtain using the optically analogous techniques IR and Raman which can also be used complementarily. TOSCA has been used to study catalysts, hydrogen storage materials, hydrogen bonded systems, advanced materials, biological samples and organic compounds (such as drugs). It has many advantages over other vibrational techniques, including the sensitivity of studying hydrogen vibrations (due to the large H cross-section see Figure 1.). Another useful advantage is the sample environment, neutrons are able to penetrate deeply into materials and easily pass through sample holders generally made from metals such as aluminium, which allows completely sealed (in aluminium holders sealed with indium wire) highly sensitive samples to be studied freely and non-destructively. The INS spectrometer TOSCA is able to cover the whole range of molecular vibrations (0 – 4000 cm^{-1} or 0 – 500 meV).

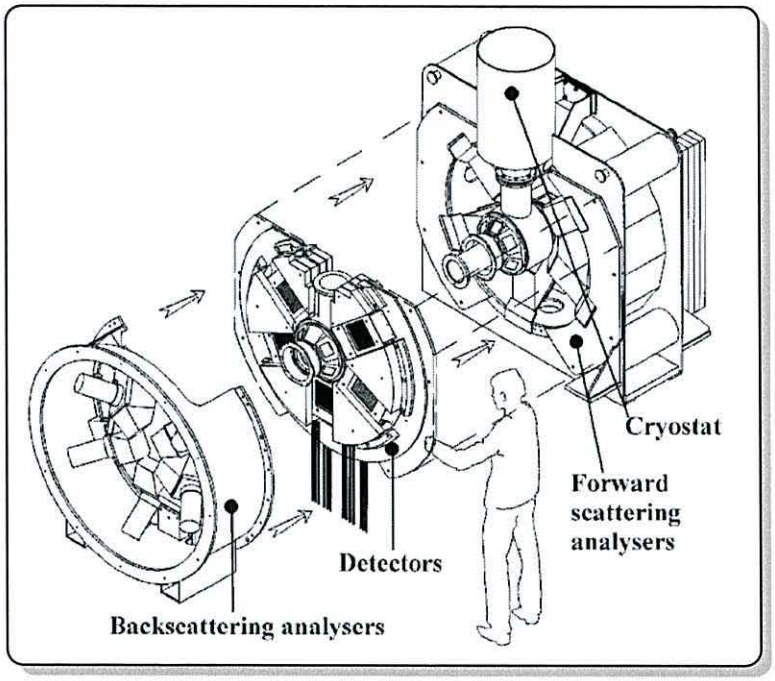

Figure 8. TOSCA diagram showing detectors for forward and back scattering.[27]

The presence of detector banks for forward and backward scattering (Figure 8.) leads to increases in sensitivity and the larger size of TOSCA (in comparison to its predecessor TXFA 1985-1998) meant that it had to be moved downstream creating a larger primary flight path from 12m to 17m. This increase in flight path gave rise to significant improvements in resolution which, historically, allows access to new areas of science and innovation.[28/27]

2.1.5.2. MAPS

MAPS is a time-of-flight (TOF) chopper spectrometer customized for high energy magnetic excitations in single crystals.[29] It is located in TS1 at ISIS (Figures 6. & 7.) and boasts a vast array of position sensitive detectors that are capable of mapping regions in the Brillouin zone. Inelastic coherent neutron scattering occurs if the momentum (Q) transferred to the scattering system is entirely taken up by collective particle motions.[30] This allows single excited states of such motions to be observed in liquids, powders and polycrystals in a similar fashion to single crystals. The high resolution and broad energy range achieved using MAPS allow for minimal gaps in coverage and make it able to observe broad features which could otherwise be dismissed as background.[31] Its versatility makes it able to accommodate a large range of sample environments including furnaces, cryostats and also with the ability to perform *in situ* measurements.

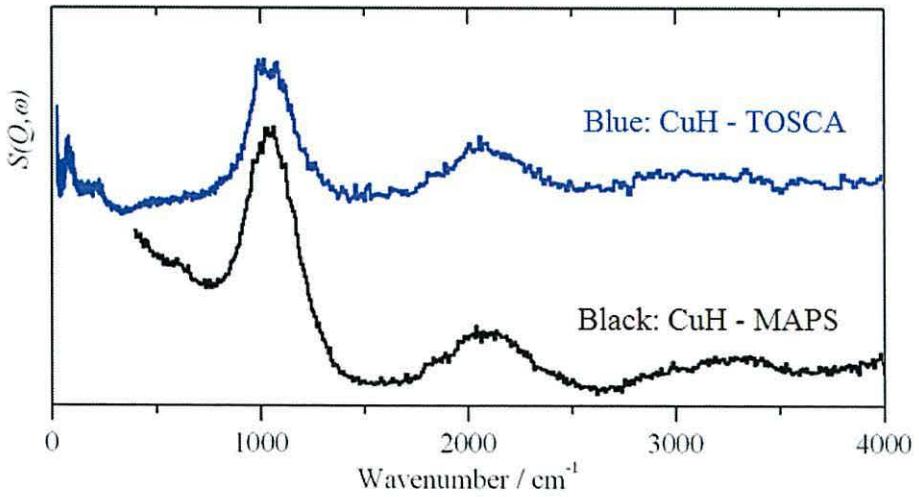

Figure 9. The spectra of CuH from MAPS and TOSCA.

Resolution in MAPS spectra decrease towards to the lower energy region (energies < 800 cm^{-1}) which can be seen in Figure 9. by the black trace tailing upwards, but with good resolution at higher energies. This is the opposite of TOSCA (in which resolution decreases at energies approaching 4000 cm^{-1}) which can be seen by the 'square shaped' peaks at energies > 3000 cm^{-1}, but used in conjunction they can be an extremely powerful tool with a very broad energy range (Figure 9.).

2.1.5.3. SANDALS

SANDALS is a small angle neutron diffractometer optimised to study the structure of liquids and amorphous samples (Figure 10.).[32] First operational in 1989 and with a significant refurbishment in 2005, SANDALS combines the pulsed neutron source and a large array of small angle detectors to measure structure factors (S(Q)) and is especially adept at measuring S(Q) for light atoms (such as hydrogen and deuterium). It has been applied to the disciplines of nanotechnology, polymers, clays, ionic liquids, biomolecules in solution and gas absorbed on solid catalysts. SANDALS employs the powerful technique of isotopic substitution to elucidate in depth structural analysis on the atomic scale.[33]

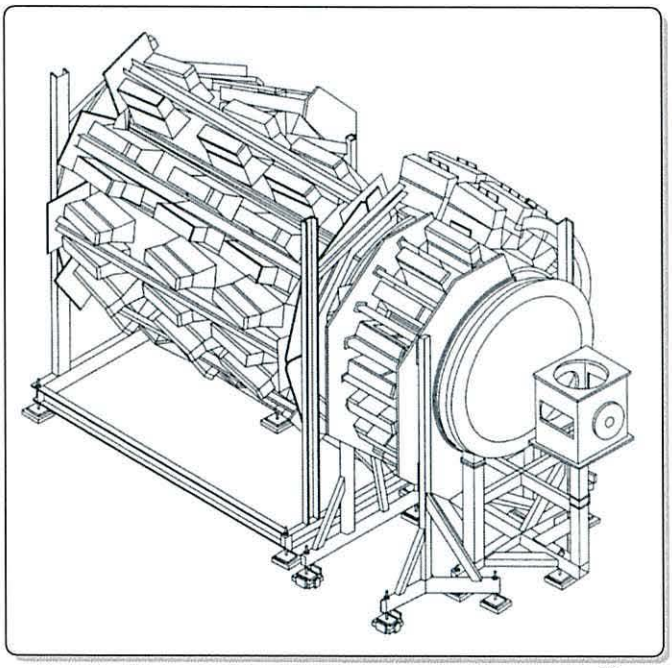

Figure 10. Drawing of the instrument SANDALS.[33]

The field of neutron scattering is ever growing with many countries investing in this relatively new technique. The emphasis is currently on increasing detectors[34] but with spallation sources still having considerable potential that is, as yet, unlocked.

2.2. References

1. J. Chadwick, *Proceedings of the Royal Society A: Mathematical, Physical and Engineering Sciences*, 1932, **136**, 692–708.

2. J. Chadwick, *Proceedings of the Royal Society A: Mathematical, Physical and Engineering Sciences*, 1933, **142**, 1–25.

3. T. I. Taylor, R. H. Anderson, and W. W. Havens, *Science*, 1951, **114**, 341–355.

4. D. M. Novak, L. S. Smirnov, A. I. Kolesnikov, V. I. Voronin, I. F. Berger, N. M. Laptash, A. D. Vasil'ev, and I. N. Flerov, *Crystallography Reports*, 2013, **58**, 129–134.

5. Y. Matsuda, H. Sakaguchi, H. Takeda, S. Terashima, J. Zenihiro, T. Kobayashi, T. Murakami, Y. Iwao, T. Ichihara, T. Suda, T. Ohnishi, Y. Watanabe, H. Otsu, K. Yoneda, Y. Satou, K. Ozeki, and M. Kanazawa, *Physical Review C*, 2013, **87**, 034614.

6. M. F. Collins and B. C. Haywood, *The Journal of Chemical Physics*, 1970, **52**, 5740–5745.

7. S. F. Parker, R. Jeans, and R. Devonshire, *Vibrational Spectroscopy*, 2004, **35**, 173–177.

8. V. Paul-Boncour, S. F. Parker, H. Hagemann, S. M. Filipek, R. Wierzbicki, and M. Latroche, *Faraday Discussions*, 2011, **151**, 307.

9. C. C. Wilson, *Single Crystal Neutron Diffraction From Molecular Materials*, World Scientific, Singapoore, 2000.

10. S. F. Parker and P. I. Haris, *Spectroscopy*, 2008, **22**, 297–307.

11. S. F. Parker, D. Lennon, and P. W. Albers, *Applied Spectroscopy*, 2011, **65**, 1325–1341.

12. www.isis.stfc.ac.uk/instruments/neutron-spectroscopy4761.html, 8/4/13.

13. P. C. H. Mitchell, S. F. Parker, A. J. Ramirez-Cuesta, and J. Tomkinson, *Vibrational spectroscopy with neutrons, with applications in chemistry,biology, materials science and catalysis*, World Scientific, Singapore, 2005.

14. S. F. Parker, *Encyclopaedia of Spectroscopy and Spectrometry*, Academic Press, 2000, Vol. 2, 905–915.

15. www.sns.gov, 8/4/13.

16. www.j-parc.jp/, 8/4/13.

17. www.isis.stfc.ac.uk, 25/2/13.

18. www.isis.stfc.ac.uk/about-isis/aboutisis.html, 8/4/13.

19. www.isis.stfc.ac.uk/instruments/instruments2105.html, 8/4/13.

20. www.isis.stfc.ac.uk/instruments/muon-spectroscopy4762.html, 8/4/13.

21. www.isis.stfc.ac.uk/instruments/reflectometry2594.html, 8/4/13.

22. www.isis.stfc.ac.uk/instruments/small-angle-scattering2573.html, 8/4/13.

23. www.isis.stfc.ac.uk/instruments/neutron-diffraction2593.html, 8/4/13.

24. www.isis.stfc.ac.uk/instruments/neutron-spectroscopy4761.html, 8/4/13.

25. www.isis.stfc.ac.uk/instruments/tosca, 20/2/13.

26. Z. . Bowden, M. Celli, F. Cilloco, D. Colognesi, R. . Newport, S. . Parker, F. . Ricci, V. Rossi-Albertini, F. Sacchetti, J. Tomkinson, and M. Zoppi, *Physica B: Condensed Matter*, 2000, **276-278**, 98–99.

27. D. Colognesi, M. Celli, F. Cilloco, R. J. Newport, S. F. Parker, F. Sacchetti, J. Tomkinson, V. Rossi-Albertini, and M. Zoppi, *Applied Physics A: Materials Science and Processing*, 2002, **74**, 64–66.

28. F. P. Ricci, F. Sacchetti, M. Zoppi, S. F. Parker, C. J. Carlile, J. Tomkinson, R. J. Newport, and C. Andreani, *Physica B: Condensed Materials*, 1998, **241**, 154–156.

29. U. Steigenberger and A. Soper, *ICANS XII Meeting*, 2006, **5**, 3–5.

30. H. Stiller, T. Plesser, and B. Dorner, *Disscussions of the Faraday Society*, 1967, **43**, 160–168.

31. www.isis.stfc.ac.uk/instruments/maps, 20/2/13.

32. www.isis.stfc.ac.uk/instruments/sandals, 25/2/13.

33. C. Benmore and A. Soper, *RAL Technical Reports*, 1998, **006**, 1–39.

34. M. Moon, S. S. Desai, J. Cheon, and C. Lee, *Nuclear Instruments and Methods in Physics Research Section A: Accelerators, Spectrometers, Detectors and Associated Equipment*, 2009, **600**, 213–216.

Chapter 3: Synthesis and Structural Studies of Copper (I) Hydrides

3.1. Introduction

3.1.1. Copper (I) Hydride (CuH) – A 170 Year Old Problem

Copper (I) hydride (CuH) was first prepared by Charles-Adolphe Würtz in 1844[1] and published in the journal *Comptes rendus de l'Académie des Science* (Figure 1. Below) English: Proceedings of the Academy of Sciences) a French scientific journal that has been in press since 1666.

Charles-Adolphe Würtz
1817 - 1884

Académie des sciences (France).
Comptes rendus hebdomadaires des séances de l'Académie des sciences.
1844.

CHIMIE. — *Sur l'hydrure de cuivre; par* M. ADOLPHE WURTZ. (Extrait.)

« En examinant l'action de l'acide hypophosphoreux sur les sels de cuivre, j'ai reconnu, dans certaines circonstances, la formation d'un hydrure de cuivre, qui possède tous les caractères d'un composé défini. On peut préparer ce corps de la manière suivante :

Figure 1. Extract from A. Würtz, *Comptes Rendus*, 1844.[1] Reprinted in *Annales de Chimie,* 1844.[2]

Translated as "examining the action of hypophosphorous acid on the salts of copper, which in certain circumstances leads to the formation of a hydride of copper, which possesses the characteristics of a definite compound". Formed by the reaction of hypophosphorous acid with copper sulphate in sulphuric acid (Equation 1.), this CuH is unique among the binary metal hydrides as it can be synthesized at room temperature in aqueous solutions and as a result retains variable amounts of water (ie. CuH.xH2O) which if removed is said to result in spontaneous and exothermic decomposition.[3]

$$4Cu^{+} + 6H_2PO_2^{-} + 6H_2O \xrightarrow{H^{+}} 4CuH_{(ppt)} + 6H_2PO_3^{-} + 8H^{+}$$

Equation 1. Route (1): Würtz reaction equation with spectator ions omitted.

Although the Würtz method still remains the most established means of preparation (Würtz modern synthetic method reported by Fitzsimons *et al*[3]) several other routes have also been published. Another aqueous route involves the reduction of copper sulphate solutions with sodium borohydride (Equation 2.) and was proposed by Travers and Ray in 1912.[4] This CuH compound was described and characterized as the same $CuH.H_2O$ as prepared via route (1).

$$2Cu_2^{+} + 2BH_4^{-} + 6H_2O \longrightarrow 2CuH + 2B(OH)_3 + 2H^{+} + 5H_2$$

Equation 2. Route (2): Redox reaction of $NaBH_4$ with $CuSO_4$.

Another CuH was reported, first by Warf and Feitknecht in 1950[5] and then by Wiberg and Henle in 1952.[6] This method involved the $LiAlH_4$ reduction of CuI in pyridine (Equation 3.) and was reported in significantly greater detail in 1968 by Dilts and Shriver.[7]

$$3CuI + LiAlH_4 \longrightarrow 3CuH + AlI_3 + LiH$$

Equation 3. Route [3]: $LiAlH_4$ reduction of CuI in pyridine.

There has been considerable interest in these copper (I) hydrides synthetically and structurally over the last 170 years, Figure 2. shows a timeline of copper hydride investigations.

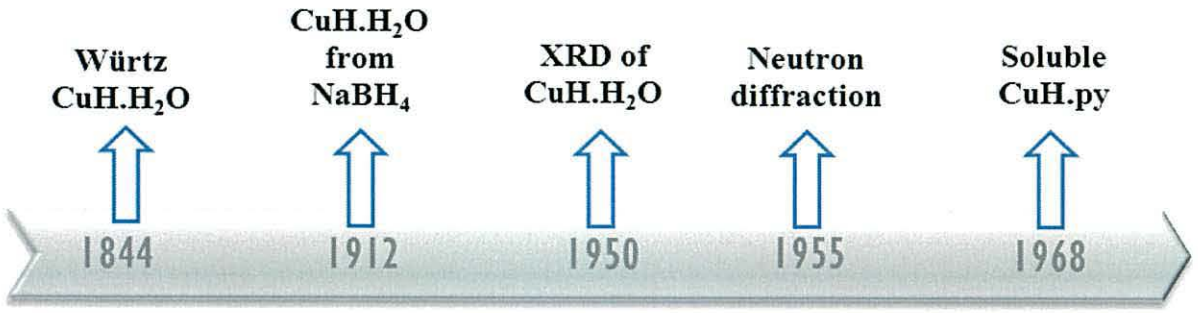

Figure 2. The timeline of synthetic and structural investigations into various CuH preparations.

Fascinatingly the problem with CuH is that all three routes apparently give different compounds:

Route (1): Würtz reaction – This insoluble $CuH.H_2O$ appears as rust-red coloured particles and can be hydrolysed by base. The compound has a "shell" of water that is essential to its stability as removal of this shell results in the full exothermic decomposition of CuH.[3] The bulk structure is well defined with X-ray[8/9] and neutron diffraction studies.[8] Binary metal hydrides usually adopt the same crystal structure as the pure metal (with some lattice expansion to accommodate the interstitial hydrides), CuH (prepared by this method) however adopts the Würtzite structure rather than face-centered cubic structure that pure copper exhibits.[10] The shell is said to be amorphous and has not been located or observed by diffraction studies.

Route (2): $NaBH_4$ reaction – This insoluble $CuH.H_2O$ appears as coffee coloured particles. This route leads to a CuH that is apparently more stable than the others as it is reported by Mahanti *et al* to be able to survive in boiling water for > 1h.[11]

Route (3): Reduction of CuI in pyridine – This blood-red/brown CuH.py is obtained via a non-aqueous reaction in the organic solvent pyridine and is soluble in "soft" donor solvents such as alkylphosphines, phosphites, alkyl sulphides and pyridines. CuH.py is reported to retain 4-20% weight pyridine. The particle size of CuH.py from this route is said to be significantly smaller.[7]

3.1.1.1. Uses and Investigations of Copper Hydride (CuH) in the Literature:

There are many instances of CuH in the literature, in 1969 Whitesides *et al* published a study showing how copper(I) hydride formed by the reduction of CuBr in pyridine (and precipitated by ether) was a good reducing agent for σ-organometallic compounds. Although their attempts to detect any copper-hydrogen stretching vibration using IR or any hydride signal using NMR failed.[12] Negeshi and Yoshida followed this study with an example of copper(I) hydrides reducing other organic substances (mainly aromatic halides).[13]

It has also been identified as an intermediate phase in the dissolution of brass in H_2SO_4 by Burzyńska and Zembura in the 1990's utilizing XPS and XRD.[14/15]

The use of CuH in catalysis has been of great interest, specifically as a route to active copper catalysts by synthesizing CuH in contact with catalytically interesting acidic and basic supports such as silica, ceria and alumina, followed by the novel low temperature decomposition of copper hydride to metallic copper. The study utilized XRD / TEM and was published in *Catalysis Letters* by Fitzsimons *et al* in 1992.[16]

The chemisorption of hydrogen on copper was investigated between 1974-1995 with emphasis on determination of activation barriers and dynamics.[17/18] This led to the proposal that hydrogen is stored subsurface in the $Cu/Zn/Al_2O_3$ methanol synthesis catalyst.[19]

In a 1998 study by Vaškelis *et al*, *in situ* XRD analysis into the autocatalytic Cu^{2+} reduction by BH_4^- was used as an electrochemical investigation that showed the formation and decomposition of CuH (Equation 4.).[20]

(a) CuH Formation -

$$4Cu^{+} + BH_4^{-} + 4OH^{-} \longrightarrow 4CuH + B(OH)_4^{-}$$

(b) CuH Decomposition -

$$2CuH \longrightarrow 2Cu + H_2$$

(c) Overall Process -

$$2Cu_2^{+} + BH_4^{-} + 4OH^{-} \longrightarrow 2Cu + B(OH)_4^{-} + 2H_2$$

Equation 4. CuH formation and decomposition equations.[20]

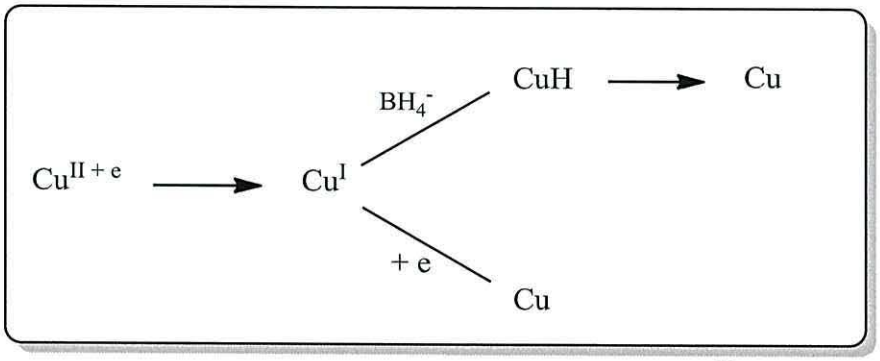

Scheme 1. Historic representation of CuH formation.[20]

In 1999 Tanaka *et al* explored the use of CuH as a catalyst in organic synthesis, it was found that the *in situ* generation (and subsequent reaction) of the highly reactive CuH species in a copper (I) chloride-tributyltin hydride-DMF system (Equation 5.) led to the successful synthesis of 3-norcephalosporin (Figure 3.), which is a promising precursor to orally active drugs.[21]

$$Bu_3SnH + CuCl \longrightarrow \text{"CuH"} + Bu_3SnCl$$

Equation 5. The copper (I) chloride-tributyltin hydride catalytic system in the highly polar solvent DMF (*in situ* generation of CuH). Early description of CuH.[21]

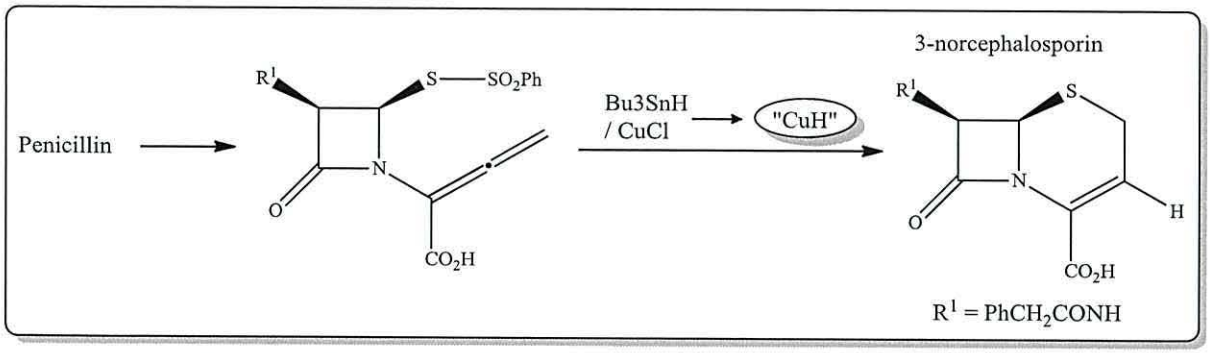

Figure 3. Copper (I) hydride species in the synthesis of 3-norcephalosporin.[21]

It is interesting to note the use of quotation marks for "CuH" when written in this paper,[21] giving it an air of mystery or at least indicating to the nature of its unknown properties and stoichiometry. The complex lengths that were undertaken to generate this *in situ* "CuH" by transmetallation of tributyltin hydride with copper(I) salts, give an indication not only to its potential as a catalyst but also to its highly reactive yet rapid and explosive decomposition. However no direct spectral evidence for CuH was obtained, instead it was indirectly determined from the formation of hydrogen gas and metallic copper (Equation 6.).

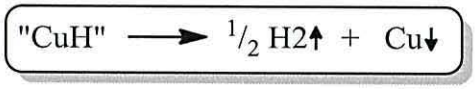

Equation 6. Indirect determination of CuH by its decomposition products.[21]

In 2004 Tkacz *et al* reported the synthesis of a new phase of copper hydride by the high pressure (14.4Gpa) reaction of elemental copper and hydrogen in a diamond anvil cell using XRD as the analytical method.[22] This new CuH phase was said to adopt the fcc crystal structure instead of the hexagonal Würtzite structure reported in other preparations of copper hydride. Their goal was to obtain completely pure CuH, free from the copper oxides, copper metal and water commonly present in previous synthetic methods. This new phase CuH was found to "act as an explosive at room temperature"[22] although estimations from the lattice expansion by hydrogen (compared to pure copper metal) gave a Cu : H atomic ratio of 1 : 0.4.

Another study published in 2004 by Nowak *et al* involved ^{2}D and ^{63}Cu NMR experiments with the aim of investigating "the stability of copper hydride and its unusual non-stoichiometric behaviour [which] are still very important issues for the better understanding of the properties of this oldest known hydride".[23] Their conclusions stated that Würtz CuH / CuD exhibits covalent type bonding, is non-metallic in nature and exists non-stoichiometrically as $Cu_1 : H_{0.7\text{-}1.0}$.

In 2007 a paper by Lineberger *et* al stated that the "numerous theoretical and experimental studies... are important for understanding hydrogen onto metal in heterogeneous catalysis".[24] Although their photoelectron spectroscopic study of copper monohydride (CuH) and copper dihydride (CuH_2) found no reported isolation of CuH_2 and only provided evidence for CuH.

In 2012 Wu and Hasin published the sonochemical synthesis of CuH, which was reported to be the first time a metal hydride has been synthesized through sonochemistry. The experimental sample was free from common copper hydride impurities such as CuO, Cu_2O and $Cu_{(metal)}$, with the only impurity being TiO_2 which they attributed to being from the titanium ultrasonic horn used.[25] The limiting factor for the synthetic yield was controlled by the concentration of available hydrogen atoms, not the concentration of Cu^{2+}, however the quantity of CuH produced is comparatively low compared to standard chemical routes. The proposed mechanism for this synthesis is shown in Equation 7.

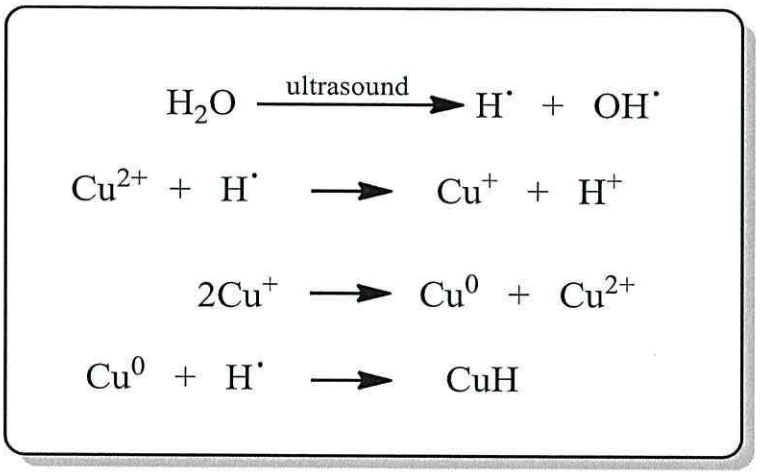

Equation 7. Proposed reaction mechanism for sonochemical synthesis of CuH.[25]

Due to its insolubility, synthetic impurities and its unstable explosive nature (even when prepared by elemental high-pressure reactions or sonochemically) a limit was imposed on the research potential of CuH to be used as a mild reducing agent or catalytically and it has been superseded by the ligand stabilized copper hydride complex Stryker's reagent.

3.1.2. The Stoichiometric Copper(I) Hydrido Species Stryker's Reagent - $[HCu\{P(C_6H_5)_3\}]_6$

Hydrido(triphenylphosphine) copper(I) hexamer (aka Stryker's reagent or Osborn complex - $[HCu\{P(C_6H_5)_3\}]_6$) was prepared by Osborn *et al* in 1971 and was the first truly stoichiometric copper hydride species.[26] They reported the reaction of tetrameric triphenylphosphinocopper chloride $[PPh_3CuCl]_4$ (also the corresponding bromide, iodide, cyanide and thiocyanate) with sodium trimethoxyborohydride $[(NaB(OCH_3)_3H]$ in DMF yielded hexameric triphenylphoshinocopper(I) hydride $H_6Cu_6(PPh_3)_6$.DMF (Equation 8.).

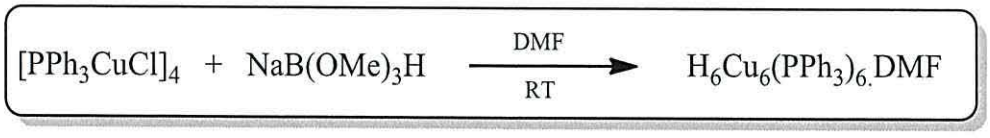

Equation 8. Preparation of Osborn's complex DMF solvate.[26]

Initial studies failed to identify or assign the hydrides using IR, NMR and X-rays with the follow up using non-direct chemical analysis of the gaseous decomposition products (H_2 and HD) to assign $x = 6$ in $H_xCu_6(PPh_3)_6$. However again "no absorptions attributable to Cu-H vibrational modes were observed in the infrared spectrum, nor were any resonances attributable to hydride ligands seen in a ^1H NMR spectrum of the complex".[27]

Initially published work on the exact structure of $H_6Cu_6(PPh_3)_6$ determined by single crystal X-ray diffraction was unable to locate the hydrides directly, (Figure 4.) but found a distorted octahedron of copper atoms with six short (2.52 Å average) and six long (2.68 Å average) Cu–Cu edges, giving six small and two large faces, with each vertex capped by a phosphine ligand.

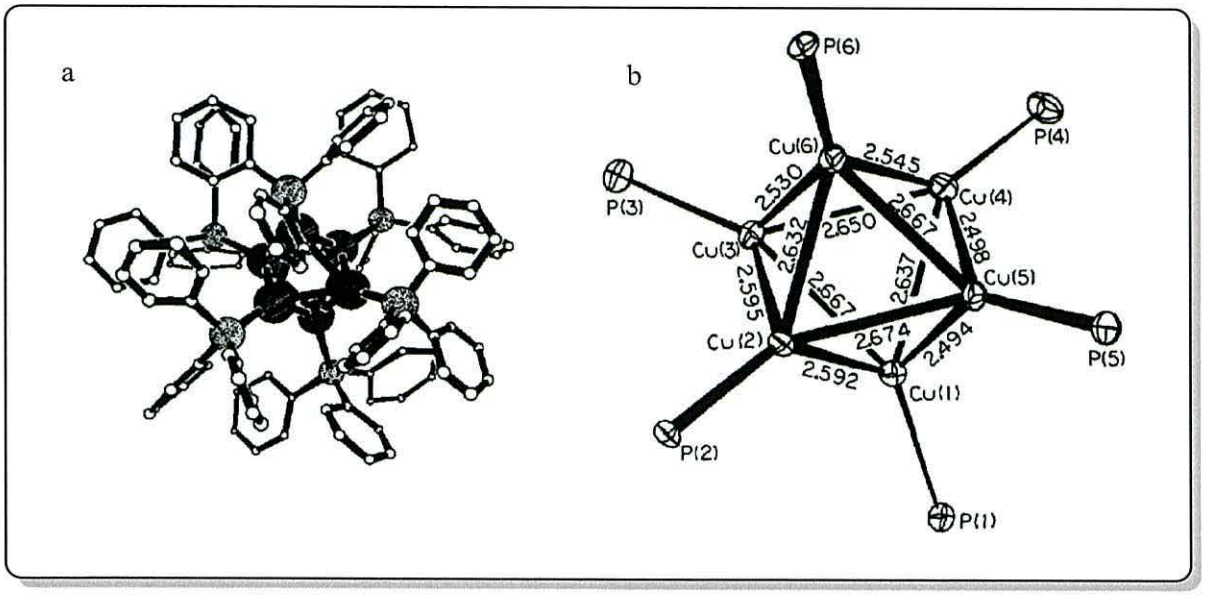

Figure 4. (a) Stereochemistry of the $H_6Cu_6(PPh_3)_6$ cluster (hydrogen atoms omitted).[26] (b) Copper-copper distances within the $H_6Cu_6(PPh_3)_6$ cluster.[27]

In 1984 Bau and Ho discussed that the "elusive nature of the H atoms in $H_6Cu_6(PPh_3)_6$ has resulted in two different views for the M-H bonding in this cluster hydride" and attempted to locate the hydrides using neutron diffraction, although they were not able to grow suitably large crystals for such a study.[28] These two different views for the M-H's were

suggested to be two-fold bridging across the short edges of the Cu-Cu bonds and three-fold bridging above the small faces. The face-bridging approximation was favoured due to the different hexameric copper clusters $H_6Cu_6[P(NMe_2)_3]_6$ and $H_6Cu_6[P(p\text{-toly1})_3]_6$ being characterised as having face bridging hydrogens.[29/30]

In 1988 Stryker *et al* published a simplified one-pot reaction (Equation 9.) for the synthesis of $[(Ph_3P)CuH]_6$ which was highly cited (70 times) and required no preparation or purifying of species that are difficult to handle and could be performed on the bench-top with significantly improved yields (71%) to that of Osborn *et al* (20 - 52% with carefully controlled stoichiometry) and is the reason for it now being commonly referred to as Stryker's reagent and not Osborn complex.[31]

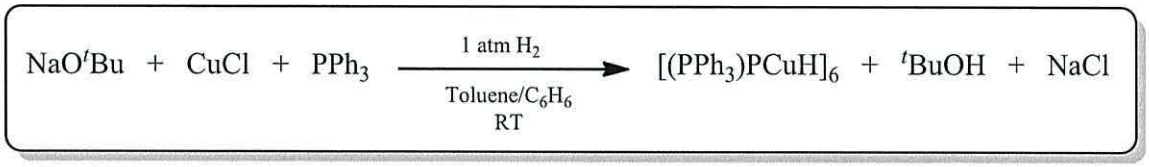

Equation 9. Stryker's one-pot procedure of the synthesis of $[(Ph_3P)CuH]_6$.[31]

This synthetic method (Equation 9.) allowed swift and efficient access to Stryker's reagent and gave (after several days) "crystals of the compound formed as large hexagonal plates" as reported in the X-ray study by Healy *et al* in 1989.[32] Answers to the location of the hydrides however were still not found although it was again suggested that a face-centered location was preferred.

In 2003 Chiu *et al* reported an improved synthetic method similar to that of Stryker's preparation (Equation 10.).[33]

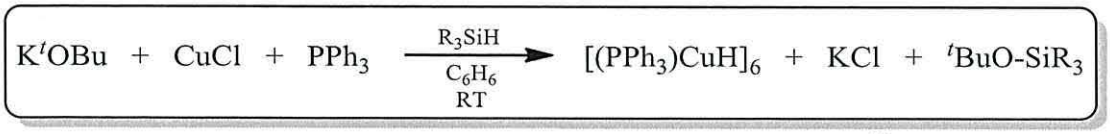

Equation 10. An expedient preparation of Stryker's reagent.[33]

This route utilized various silanes as the reducing agent and had significantly improved reaction times (from 24 h to 1-2 h) as well as greater yields, with the highest being 88% (Table 1.)

Table 1. Synthesis of Stryker's reagent using various silanes as reducing agents – results.[33]

Entry	Silane	CuCl:KO^{t}Bu:PPh_3:Silane	Time (h)	Yield (%)
1	PMHS	1:1:1:1.2	2.2	47[a]
2	PMHS	1:1:1:2	1.5	68[a]
3	PMHS	1:1:2:2	1.5	82[a]
4	Et_3SiH	1:1:1:1.2	2.5	30[a]
5	Et_3SiH	1:1:2:2	2.75	31[a]
6	Ph_2SiH_2	1:1:2:0.75	1.0	53[b]
7	$PhMe_2SiH$	1:1:2:2	2.0	88[b]
8	TMDS	1:1:1:0.6	2.2	60[a]
9	TMDS	1:1:2:1	1.0	80[b]

[a]Reaction in Toluene (polymethylhydrosiloxane = PMHS)
[b]Reaction in Benzene (tetramethyldisiloxane = TMDS)

Table 1. shows the results for reaction times and yields using the various silanes as reducing agents. Good reaction times and yields were achieved using the silane polymethylhydrosiloxane (PMHS), however, analysis using ^{1}H NMR showed extraneous broad upfield signals corresponding to silylated polymeric by products. The use of $PhMe_2SiH_2$ (Entry 7) however afforded a very pure deep red crystalline product, with Stryker's reagent being fully characterised using ^{1}H NMR including the signal corresponding to the metal-hydrogen (Cu-H cf. 3.53 ppm below).

^{1}H NMR Literature (400MHz, C_6D_6): δ 7.67 (t, J = 8.1 Hz, 36H), 6.95 (t, J = 7.3 Hz, 18H), 6.74 (t, J = 7.5 Hz, 36H), 3.53 (br s, 6H).[33]

In 2005 Lee and Yun published a direct synthesis of Stryker's reagent from a copper (II) salt. This method was even more convenient than the previous route proposed by Chiu *et al* due to no KCl (or NaCl) by-product removal being required, as well as no preparation of CuCl from $CuCl_2$ (due to the moisture and air sensitivity of $CuCl_2$) being necessary. The synthetic route involved the reaction of copper(II) acetate with triphenylphosphine in the presence of the organosilane Ph_2SiH_2 (Equation 11.). The reaction was carried out in benzene and the red crystalline product $[(Ph_3P)CuH]_6$ was obtained in high purity (analysed by ^1H NMR) in 82% yield.

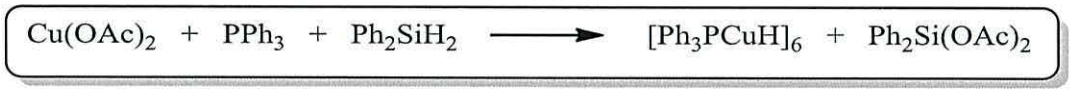

Equation 11. Synthesis of Stryker's reagent from a Cu (II) salt.

3.1.2.1. Instances and Uses of Stryker's Reagent in the Literature

There are many uses of Stryker's reagent in the literature, used both stoichiometrically and catalytically. In 1988 (the same year the simplified one-pot reaction was published) Stryker *et al* reported that $[(Ph_3P)CuH]_6$ was effective for the selective conjugate hydride addition to α-β-unsaturated carbonyl compounds (with some of the most interesting results shown in Table 2. Entries 1 - 4) and also that $[(Ph_3P)CuH]_6$ was chemically compatible with Me_3SiCl and afforded an efficient procedure for reductive silylations (Table 2. Entries 5 & 6).

Table 2. Conjugate reductions / silylations of α-β-unsaturated carbonyl compounds.[34]

Entry	Substrate	$[(Ph_3P)CuH]_6$ Equivs	Time (h)	Product	Yield (%)	
1	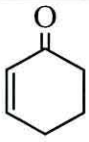	0.16	0.25	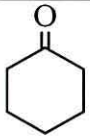	94[a]	
2	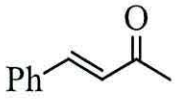	0.24	0.33	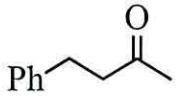	93[a]	
3	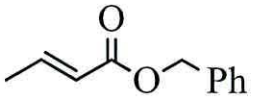	0.24	0.50	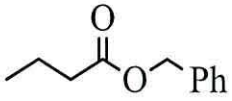	97[a]	
4	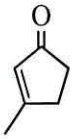	0.32	24	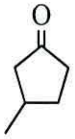	96[a]	
5	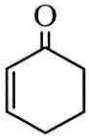	0.18	<0.25	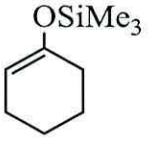	95[b]	
6	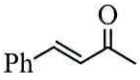	0.32	<0.10	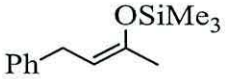	95[b]	

[a]Reaction at RT, C_6D_6, H_2O (1 equiv per hydride)
[b]Reaction at RT, C_6D_6, Me_3SiCl (1.5 equiv per hydride)

In 1990 Stryker *et al* published how stoichiometric (and excess) quantities of $[(PPh_3)CuH]_6$ (0.2 – 0.6 equivalents) could similarly be applied to the conjugate reduction of polyfunctional α-β-unsaturated carbonyl compounds that contained halogen, sulfonate, γ-oxygen and sulfur substituents with high yields (generally > 90%). This began to demonstrate not only the selectivity and efficiency of Stryker's reagent, but also its wide compatibility with various substituents.[35]

Stryker's wide use, high selectivity, tolerance for functional groups and mild reaction conditions lead it to be named "Reagent of the Year" in 1991 by e-EROS (*Encyclopedia of Reagents for Organic Synthesis*).[36]

In 1998 Lipshutz *et al* published a study showing how convenient and efficient methods for conjugate reductions could be achieved using catalytic quantities of Stryker's reagent, as low as 0.5 mol% (Scheme 2.).[37] These reactions proceed with high yields and can be run at room temperature, in common solvents and can be used with compounds containing a good variety of substituents, although no mechanism for these reactions was proposed.

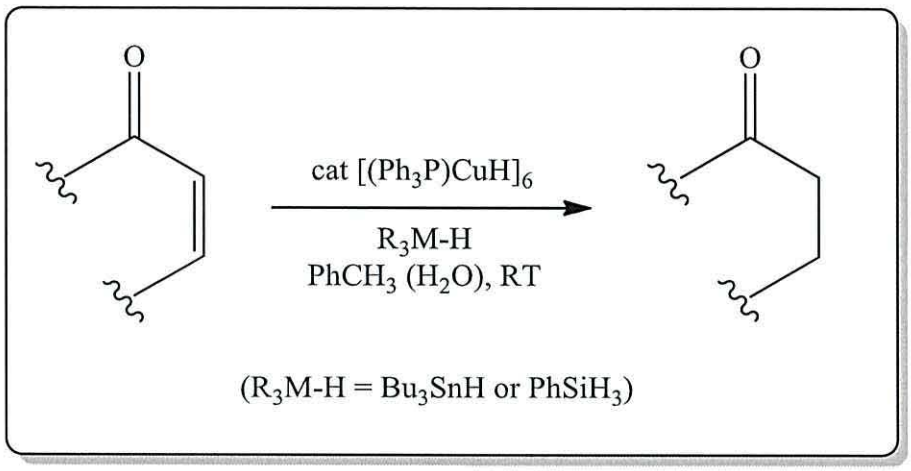

Scheme 2. Reaction conditions for catalytic Stryker's conjugate reductions.[37]

Another study showing the efficiency of $[(PPh_3)CuH]_6$ to catalyse hydrogenations (an example of which is shown in Scheme 3.) was published by Stryker *et al* in 2000.[38] The catalytic use of Stryker's reagent was highly chemoselective (simply by varying the ancillary ligand added to the reaction mixture) and also included the regioselective 1,2-reduction of α-β-unsaturated ketones and aldehydes to allylic alcohols. In addition, the active catalyst was shown to be equally active when formed *in situ* by the reaction of copper (I) chloride, sodium *tert*-butoxide and dimethylphenylphosphine under hydrogen, a great advantage for synthesis using catalytic quantities of Stryker's reagent, which is sensitive to air and highly sensitive when in solution.

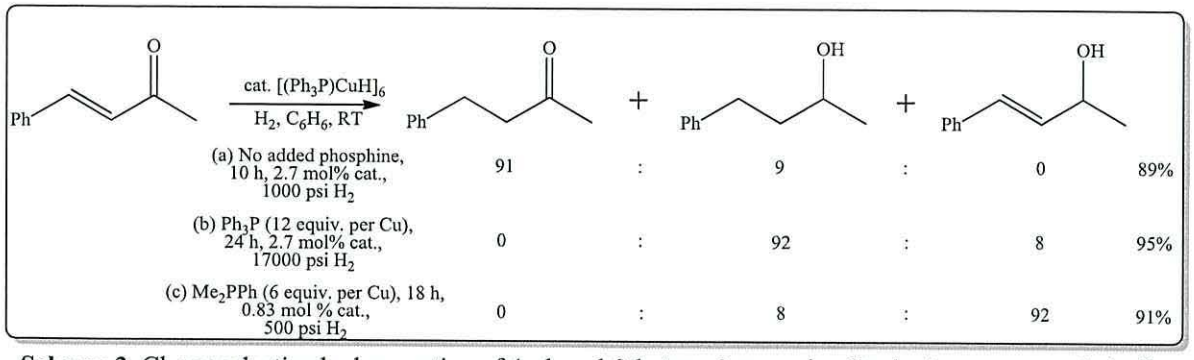

Scheme 3. Chemoselective hydrogenation of 4-phenyl-3-butene-2-one using Stryker's reagent catalytically.

As well as Stryker's reagent being shown to catalyse reactions with high chemoselectivity in 2000 Stryker *et al* demonstrated the stereoselectivity and regioselectivity of copper (I) hydride-catalysed ($[(PPh_3)CuH]_6$) hydrogenations of ketones and α-β-unsaturated ketones and aldehydes (including stabilization effects of the ancillary phosphine ligand).[39] The combination of Stryker's reagent with commercially available phosphine ligands gave access to high stereo- / regio-selective transformations, with the active catalytic species also able to be generated *in situ*.

The asymmetric total synthesis of lucinone (Scheme 4.) by the tandem conjugate reduction-aldol cyclisation using Stryker's reagent was published by Chiu *et al* in 2001.[40] Lucinone (first isolated in 1995) is a natural product traditionally used as an antispasmodic drug[41] and although it has an apparently small structure is contains five stereocenters. Treatment of the enedione with two equivalents of Stryker's reagent (Scheme 4. step (g)) in toluene at 0°C to RT, results in an aldol in which 4 of the 5 stereocenters have been installed with a yield of 99%. This synthesis gives a good example of the efficiency and stereoselectivity achieved when using Stryker's reagent as a tool for organic synthesis.

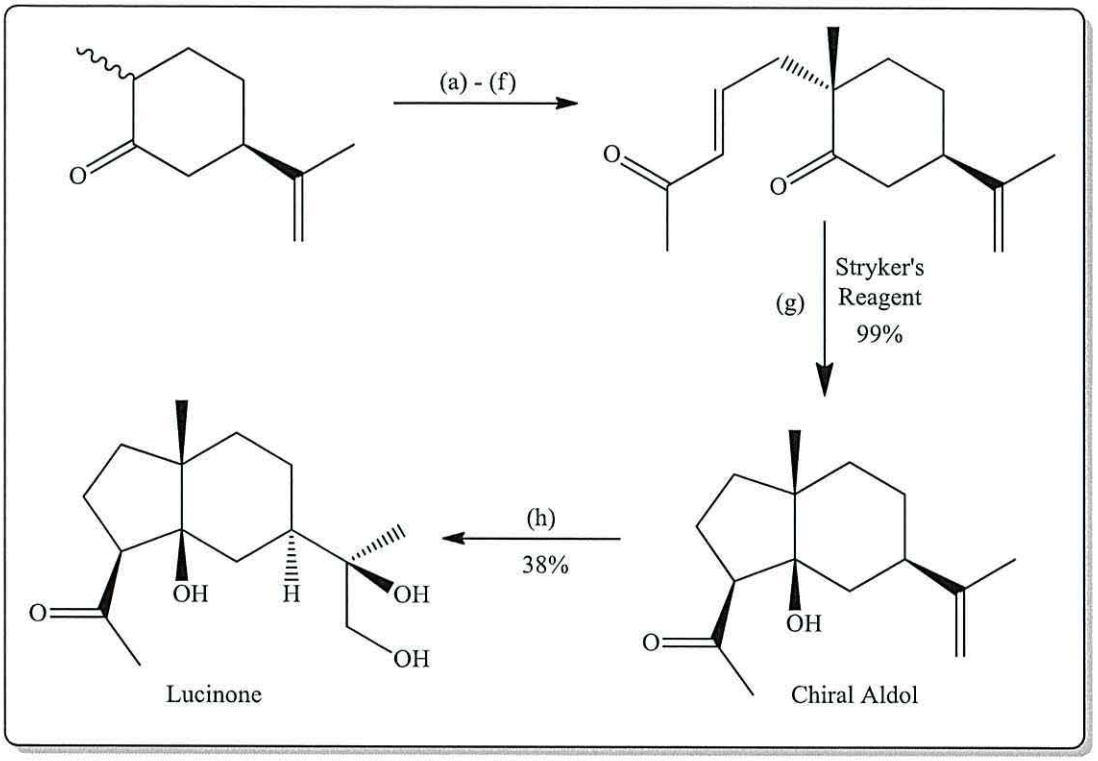

Scheme 4. (a) (+)-Methylbenzylamine / PhMe / reflux; (b) (i) phenyl vinyl sulfone / 35°C; (ii) AcOH / H_2O; (c) ethylene glycol / PhH, reflux; (d) (i) *n*-BuLi / THF / HMPA / -78°C; (ii) 3-iodo-2-(methoxymethoxy)prop-1-ene; (iii) 1% H_2SO_4 / RT; (e) Et_3N / CH_2Cl_2; (f) H_2SO_4 / SiO_2 / CH_2Cl_2; (g) Stryker's reagent, PhMe; (h) cat. OsO_4 / $K_3Fe(CN)_6$.[40]

Other instances of Stryker's reagent in the literature include the highly selective biomimetic conversion of furanheliangolides into eremantholides [42] and a recent theoretical DFT study published by Hu *et al* in 2012,[43] investigating the mechanism of a copper hydride ($[(Ph_3P)CuH]_6$) catalysed hydrosilylation reaction of 3-methylcyclohex-2-enone in which a proposed mechanistic cycle is shown in Scheme 5. (with (Ph_3PCuH) considered to be the active catalytic component). The two critical steps in the catalytic cycle are:

(1) The addition of Ph_3P-CuH to the C=C bond on the substrate (**A** → **C**).
(2) The regeneration of the Ph_3P-CuH catalyst assisted by TMDS (**D** → **A**).

The steric bulk of the triphenylphosphine ligands were found to help stabilize the central Cu atom and promote the co-ordination of this Cu atom with the substrate.

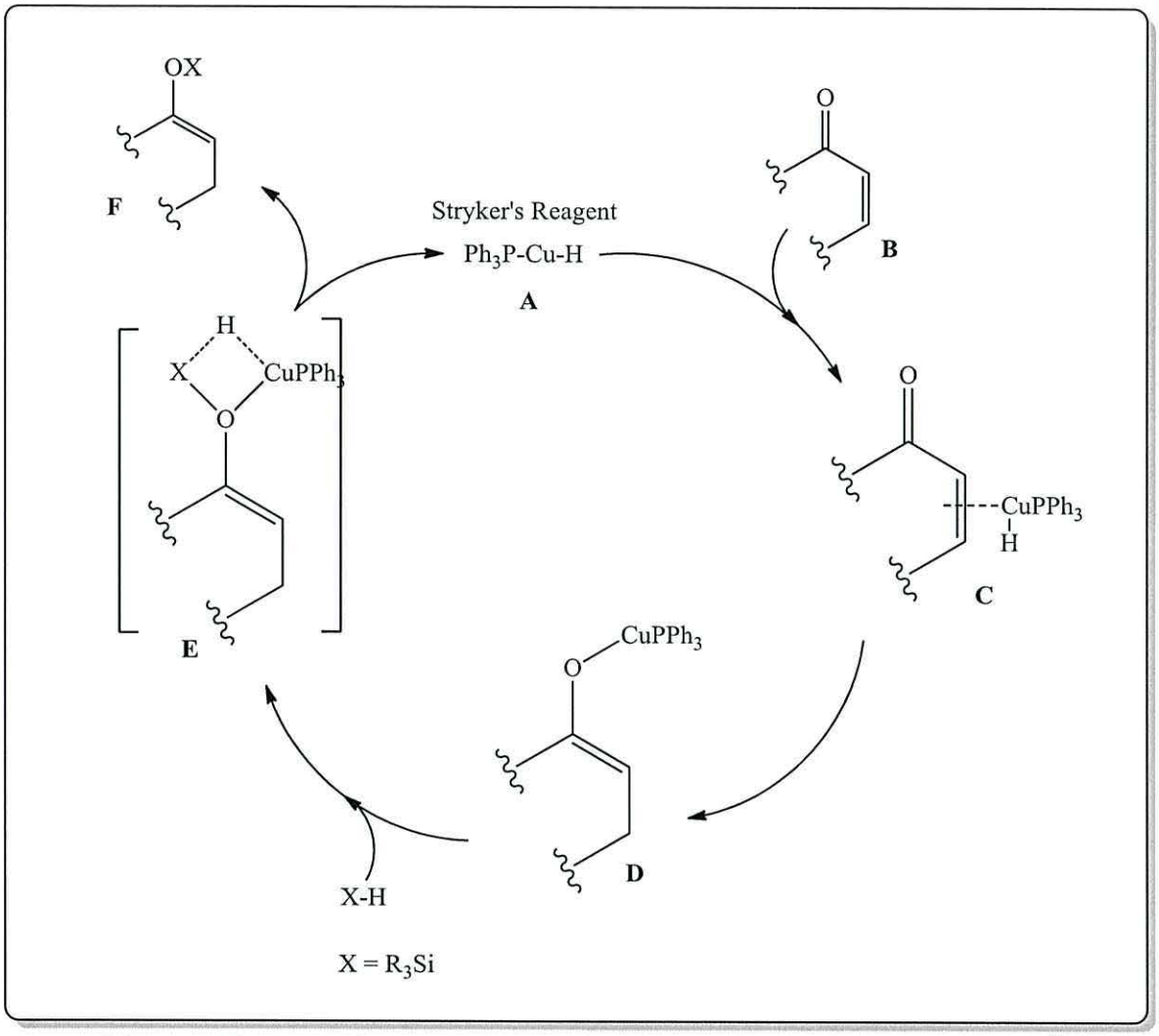

Scheme 5. The proposed mechanism of the hydrosilylation catalysed by Stryker's reagent.[43]

3.1.3. Aims & Hypothesis

3.1.3.1. Copper (I) Hydride ($CuH.H_2O$ / CuH.py)

Synthesis:

1) Synthesis of copper hydride prepared via the Würtz method ($CuH.H_2O$ Route (1) / Equation 1.) will be undertaken as well as the exchange of the surface species H_2O for D_2O, to better observe the CuH bond (see Chapter 2 - Introduction to Neutron Scattering).

2) Synthesis of copper hydride prepared via the $NaBH_4$ reduction method ($CuH.H_2O$ Route (2) / Equation 2.) will be undertaken and again the exchange of surface H_2O for D_2O will be performed.
3) Careful drying of both $CuH.H_2O$'s (Routes (1) & (2)) will be attempted to fully remove any residual water and see if a stable CuH (without the reported rapid exothermic decomposition) exists without its protective shell or whether any hydroxyls remain on the surface.
4) Synthesis of copper hydride prepared via the $LiAlH_4$ reduction of CuI in pyridine method (CuH.py Route (3) / Equation 3.) will be undertaken. Also exchange of the pyridine shell for d_5-pyridine will be attempted.

Spectroscopy:

CuH's prepared by all three routes will be analysed using various spectroscopic techniques (including INS, IR, Raman and XRD). Emphasis will be aimed towards observation of the metal-hydrogen vibrations (Cu-H) using the inelastic neutron spectrometers TOSCA and MAPS. Estimation of CuH particle size (Equation 12.) from all routes (using XRD) combined with investigations into the type / role of the surface species will be performed in an attempt to explain the difference in properties (such as colour, nature of protective sheath and solubility).

Estimation of Particle Size from XRD - Scherrer Equation (Methodology 3a.)

The Scherrer equation is used in XRD and crystallography and relates the broadening of the peaks in an XRD diffraction pattern to particle size (Equation 12.).

Equation 12. The Scherrer Equation.

$$\tau = \frac{K\lambda}{\beta \cos\theta}$$

τ is the apparent crystallite size
K is the Scherrer constant
λ is the X-ray Wavelength
β is the line broadening at ½ max intensity (FWHM)
θ Bragg angle

The most likely structure for CuH consists of a crystalline core with a disordered shell of H_2O / pyridine, similar to that found in hydrous metal oxides (such as $RuO_2.H_2O$,[44] $PdO.H_2O$[45] and $Co_3O_4.xH_2O$[46]).

Comparison of experimentally derived spectra with theoretically calculated spectra (performed in collaboration with the Computational Science and Engineering Department at ISIS) for various ratios of Cu : H in the copper hydride series will be performed to better understand the stoichiometric (or non-stoichiometric) nature of copper(I) hydride.

3.1.3.2. Stryker's Reagent – $[(Ph_3P)CuH]_6$

Synthesis:

Synthesis of Stryker's reagent $[(Ph_3P)CuH]_6$ prepared by the 2005 method reported by Lee and Yun[47] (Equation 11. direct synthesis from a Copper(II) salt) will be performed as well as the synthesis of 2 different deuterium analogues (Stryker's D_1 $[(Ph_3P)CuD]_6$ and Stryker's D_2 $[(C_6D_5)_3PCuH]_6$).

Spectroscopy:

Emphasis will be placed on the metal-hydrogen bonds (Cu-H) which have been observed with ^1H NMR[33] but have not yet been detected by vibrational spectroscopy or X-ray studies.[27] The neutron diffraction study of a similar copper hydride hexamer $[HCuP(p\text{-tolyl})_3]_6$[30] (and X-ray study of $[HCuP(NMe_2)_3]_6$)[29] did locate hydrides and described all six to be face-capping and threefold-bridging. The aim of this study is too characterize the hydrides in Stryker's reagent $[(Ph_3P)CuH]_6$ by a combination of vibrational spectroscopy and neutron diffraction and determine whether a face-bridging or edge-bridging approximation is correct.

3.2. Results and Discussion

3.2.1. Copper(I) Hydrido Species

3.2.1.1. Cuprous Hydride ($CuH.H_2O$) - Würtz (1844)

Although first synthesised by Würtz in 1844[1], the method employed is a modification of the literature method of Fitzsimons *et al*[3] and is based on the following equation:

$$4Cu^{+} + 6H_2PO_2^{-} + 6H_2O \xrightarrow{H^{+}} 4CuH_{(ppt)} + 6H_2PO_3^{-} + 8H^{+}$$

Equation 13. Würtz reaction equation with spectator ions omitted.

An optimum pH of ≈ 1 was achieved using 0.75 M $H_2SO_{4(aq)}$. All solvents and aqueous solutions were degassed using argon for 2 h prior to use. All reactions steps and subsequent manipulations were performed under either an inert argon atmosphere or a constant blanket of argon gas.

Preparation of Würtz $CuH.H_2O$ (Methodology 3b.):

$H_3PO_{2(aq)}$(1.6M, 600ml, 956.25mmol) was placed into a two-necked 1L round bottom flask whilst a mixture of $CuSO_{4(aq)}$ (1M, 150ml, 150mmol) and $H_2SO_{4(aq)}$ (0.75M, 30ml, 22.5mmol) were placed in a pressure equalising dropping funnel and the solutions argon-purged for ≈ 2h (Figure 4.).

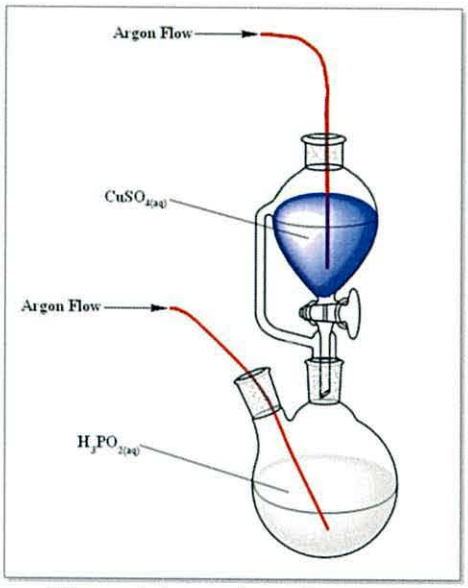

Figure 4. Argon degassing set-up.

After the de-aeration period, the top of the dropping funnel was sealed and the bottom argon tube moved slightly out of the solution but continued to maintain a constant flowing blanket of argon. The reaction flask was warmed accurately to 55°C using a paraffin oil bath and the $CuSO_{4(aq)}$ solution was added drop wise to the $H_3PO_{2(aq)}$ over 15mins.

An observable colour change from pale blue → pale green → olive green → reddish brown (ppt) gave an indication of reaction progress (Figure 5. ≈ 30mins).

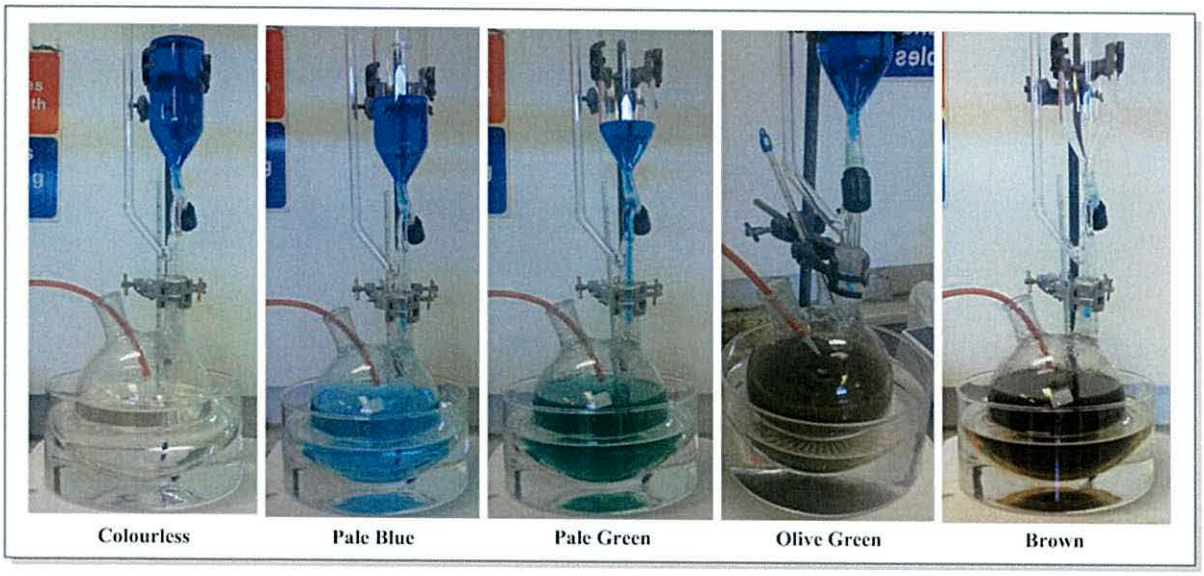

Figure 5. Colour change of the Würtz reaction.

After the reddish brown precipitate ($CuH.H_2O$) was clearly visible the reaction vessel was stirred for a further 45mins and then cooled in ice for ≈ 30mins (Figure 6. left) and then filtered through a sintered glass vacuum filter with a medium porosity (G02) under flowing argon (Figure 6. right). The filtrate is of a pale blue colour due to the slight excess of $CuSO_{4(aq)}$ that was used.

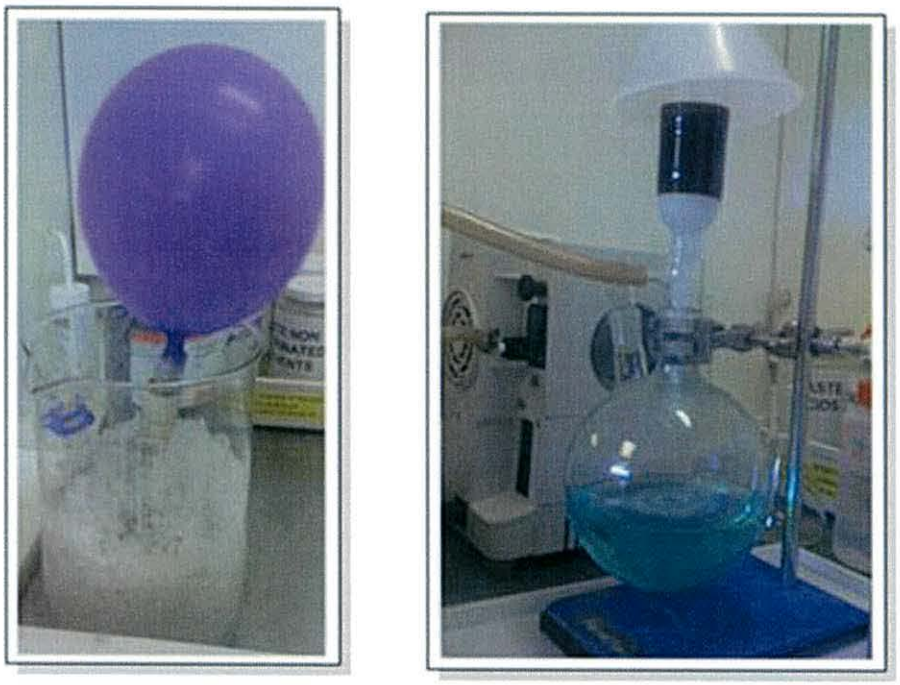

Figure 6. Reaction cooling in ice under argon and subsequent filtration set-up.

After filtration, the $CuH.H_2O$ cake was washed with previously degassed solvents (argon purged 2h) in the following order: H_2O (de-ionised) → Ethanol → Ether. The order is vitally important and the reasoning is as follows; H_2O is to remove any remaining un-reacted starting materials, which are all water soluble, the ethanol was used to remove any excess water and the ether to remove any residual ethanol left and to aid the drying process (argon-aspiration) due to the low vapour pressure of ether.

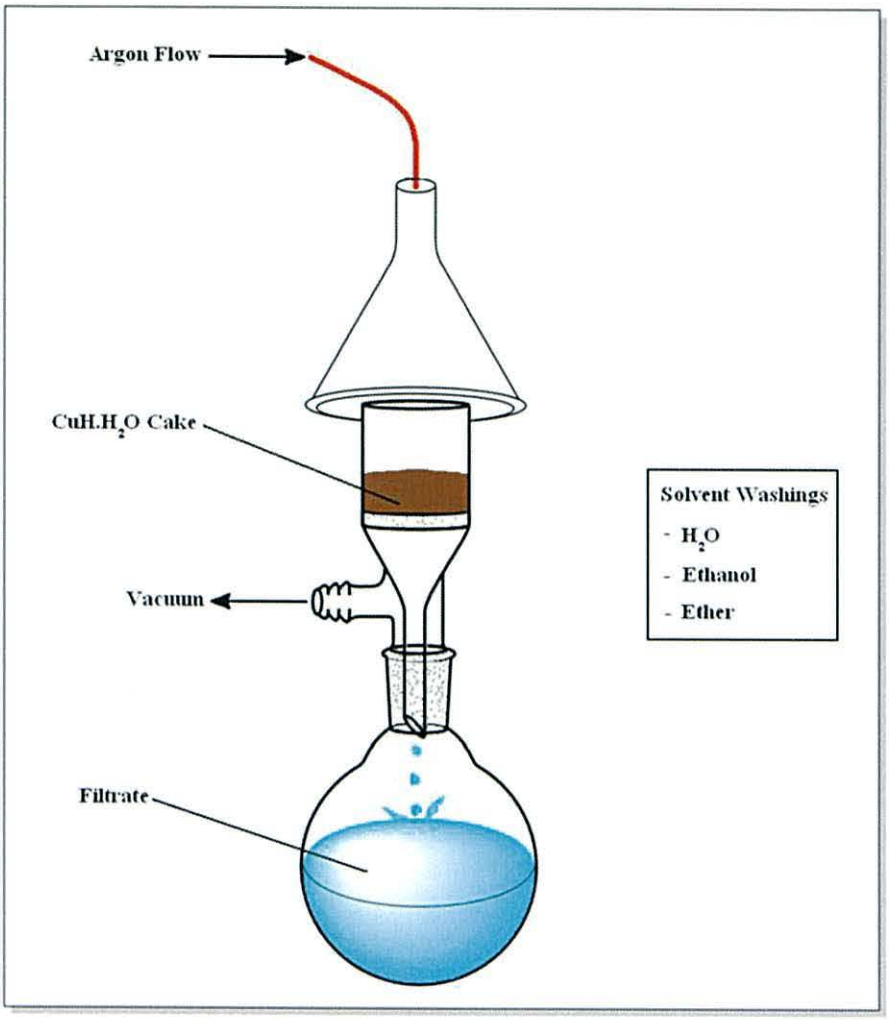

Figure 7. Solvent washing under an argon blanket.

After the washing process the sintered glass filter containing the $CuH.H_2O$ cake was transferred to a sealed argon filled glove bag. The cake was broken apart and dried via aspiration using flowing argon until completely void of ether, the product not being placed under vacuum due to its explosive nature (spontaneous exothermic decomposition).[48] The $CuH.H_2O$ product was then weighed (11.5g) and placed into the necessary sample holders for neutron characterisation (SANDALS, MAPS and TOSCA), XRD and also Raman.

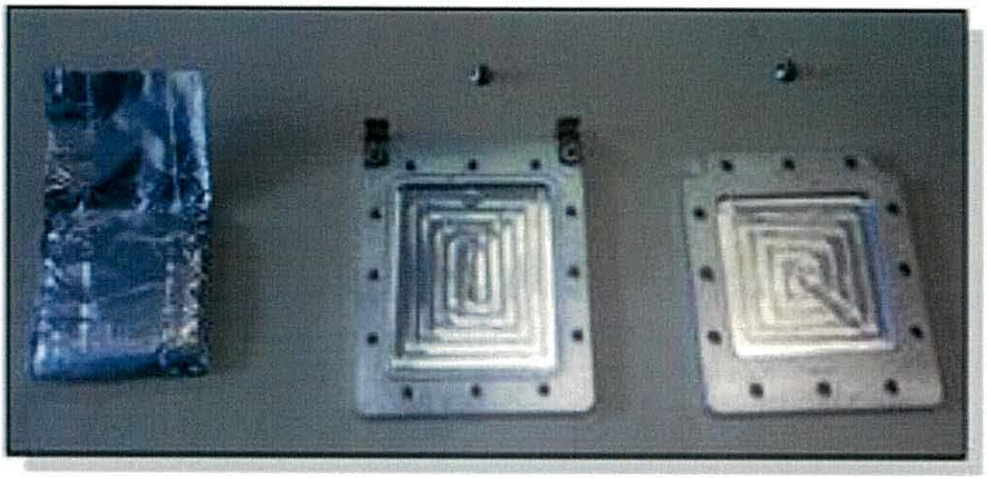

Figure 8. Aluminium foil packet (filled with sample) and Al sample holder (MAPS & TOSCA).

CuH.D_2O was prepared by taking half of the final product which was then stirred for ≈ 12h in D_2O under an atmosphere of argon. The mixture was filtered / dried and loaded into the necessary sample holders for neutron characterisation. A small amount of this product was loaded into 1mm quartz glass capillary tubes for XRD and Raman analysis.

Observational Remarks:

At temperatures below 55°C the reaction still occurs but at a slower rate (deduced from the speed of the colour changes), according to the literature,[49] at temperatures above 60°C the sample is invariably contaminated with copper metal which was confirmed by XRD (see Figure 15.). Samples need to be completely free from any hydrogen containing solvents (ie. H_2O, EtOH and Et_2O) due to them being clearly visible via neutron spectroscopic methods and can therefore overlap or mask regions of particular interest (0 - 4000 cm^{-1}).

After the washing stage (Figure 7.) the argon drying procedure must be performed in a completely oxygen free atmosphere and the residual Et_2O must be dried under flowing gas slowly, too quickly and the endothermic process involved in the evaporation of Et_2O freezes the glass sinter and CuH cake where upon melting exothermic decomposition is likely (even more likely in the presence of O_2). This decomposition results in large quantities of the red solid Cu_2O plus significant heat released in the conversion. CuH left open to the atmosphere at room temperature steadily decomposes (although not exothermically) to the black solid CuO.

3.2.1.2. Spectroscopy of Würtz CuH.H_2O/D_2O:

Initial neutron spectroscopic data for the Würtz CuH showed signals corresponding to hydrogens from the solvents used to wash the final product (H_2O, EtOH and Et_2O). These signals overlapped or masked some regions of interest, so a specialised aluminium sample holder able to be inserted into the MAPS instrument was created (Figure 9.). It was fitted with the ability to blow gases (argon, nitrogen and hydrogen) through the sample (held in place with glass wool) and was also fitted with a real time mass spectrometer. The MS was tuned to detect particular masses from the exhaust tube (H_2O 18, EtOH 46, Et_2O 74 etc.) and the sample was dried under flowing hydrogen until all unwanted exhaust fumes had disappeared and a pure CuH sample was obtained. The dry product did not spontaneously decompose if dried slowly and all further preparations were dried using this method on a larger scale in the lab (using argon).

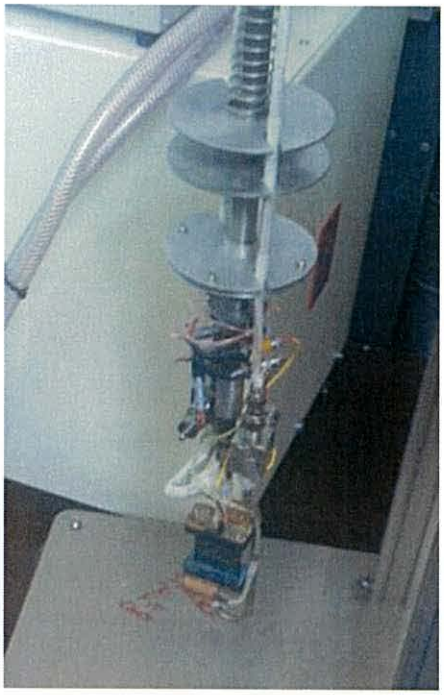

Figure 9. MAPS flow cell / sample drying holder and MS.

Ab initio calculations (CASTEP – performed by the Computational Science and Engineering Department at ISIS) gave dispersion curves (see appendix) which can give accurate INS prediction spectra (Figure 10. generated using aCLIMAX – ISIS in house software)[50].

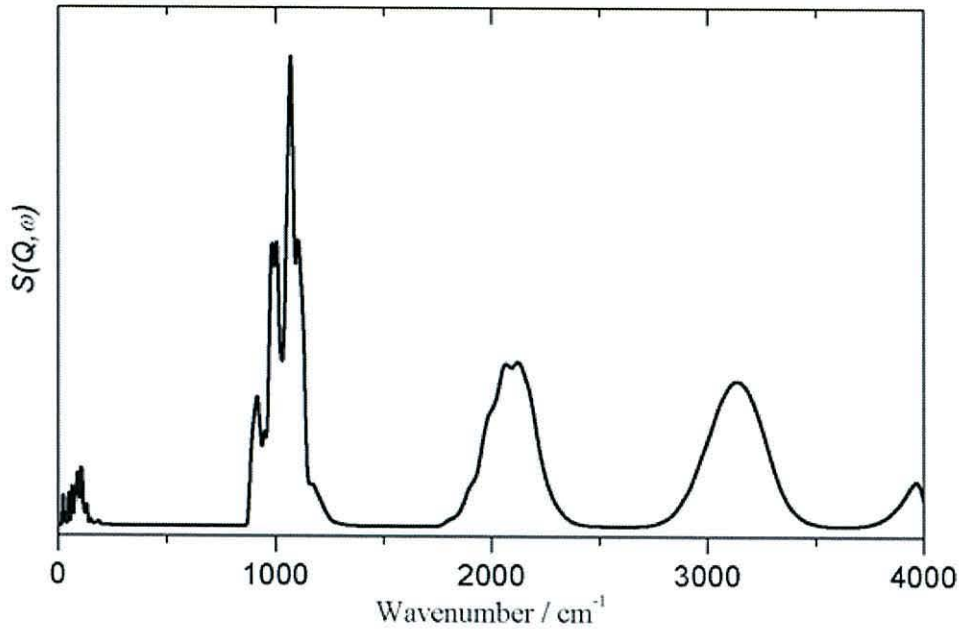

Figure 10. Predicted INS spectra for CuH.

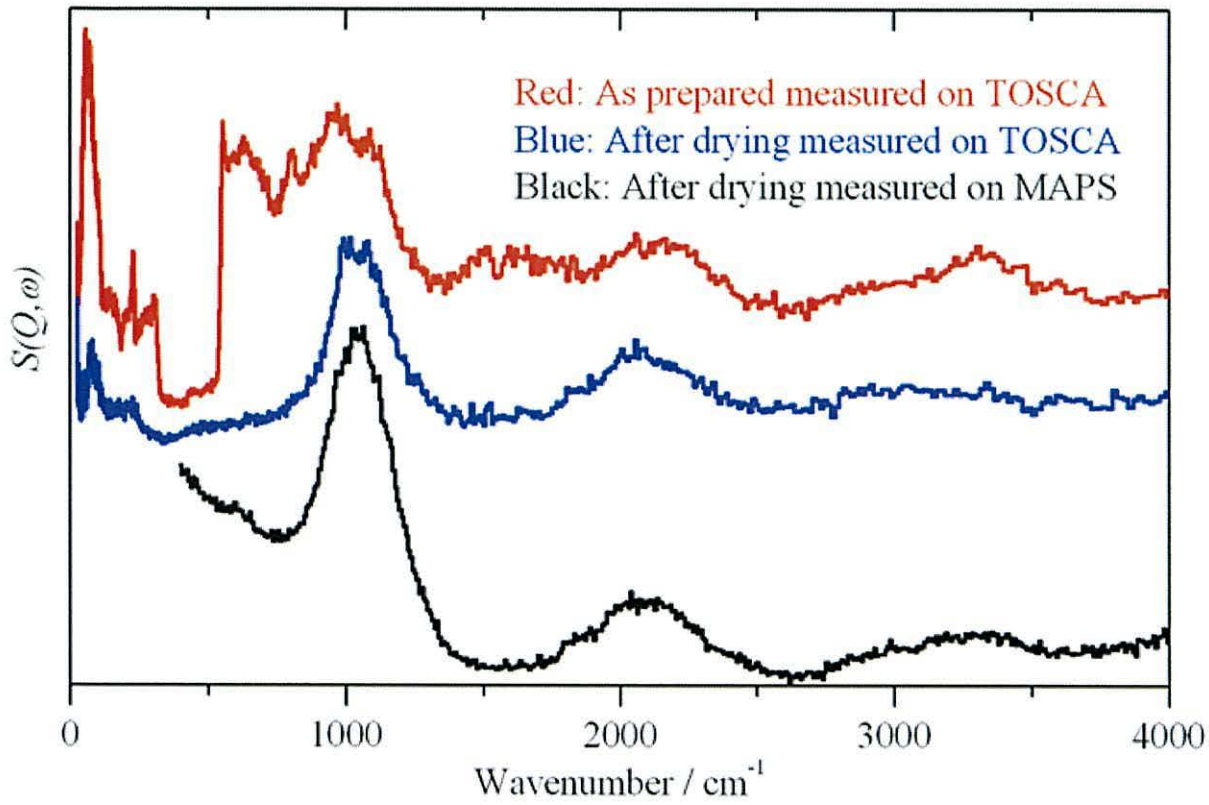

Figure 11. INS MAPS & TOSCA spectra of CuH Würtz before and after drying process.

All samples in Figure 11. show strong broad signals at 1048cm^{-1} (0 → 1 transition of CuH see Figure 17.) with overtones at 2087 (0 → 2) and 3152 cm^{-1} (0 → 3) which are in excellent agreement with the predicted spectrum. The loss of resolution at the higher end of the spectra (> 2500 cm^{-1}) in the TOSCA spectra (Figures 11. red / blue traces) can be seen by the formation of square shaped peaks which is consistent with the theory of the instrument.[51] Conversely the MAPS[52] spectrum (Figure 11. black trace) gives better resolution in the higher energy region with loss of resolution observed in the low energy region < 700 cm^{-1}.

The "cliff-edge" signal in the wet sample (Figure 11. red trace) just above 500 cm^{-1} can be assigned to H_2O as ice I_h.[27] The disappearance of this signal is clearly visible in the dried samples. After removal of the residual H_2O it was hoped that O-H stretches might be observed providing confirmation of hydroxyls present on the shell of CuH.H_2O, this was not the case and further experiments were performed.

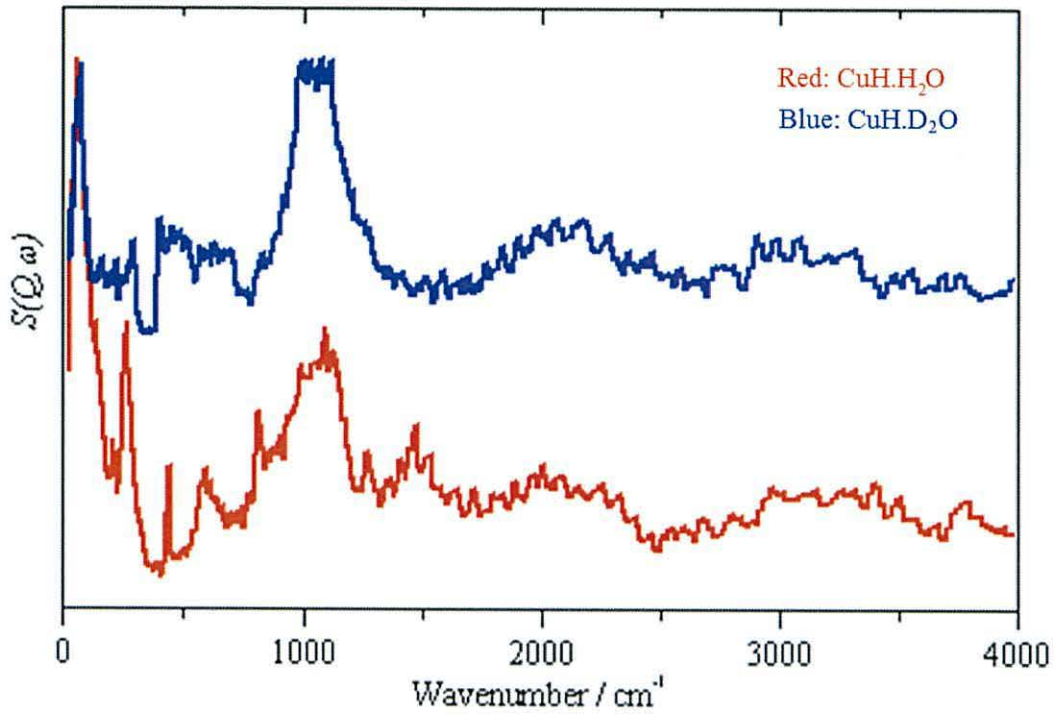

Figure 12. INS TOSCA spectra of Würtz $CuH.H_2O$ (red) and $CuH.D_2O$ (blue) samples.

The comparison of $CuH.H_2O$ with $CuH.D_2O$ (Figure 12.) showed (as expected) the same CuH signals with the addition of D_2O as ice I_h above 500 cm^{-1}. The decomposition of CuH is clearly visible in the MAPS spectra measured at time intervals (Figure 13. below).

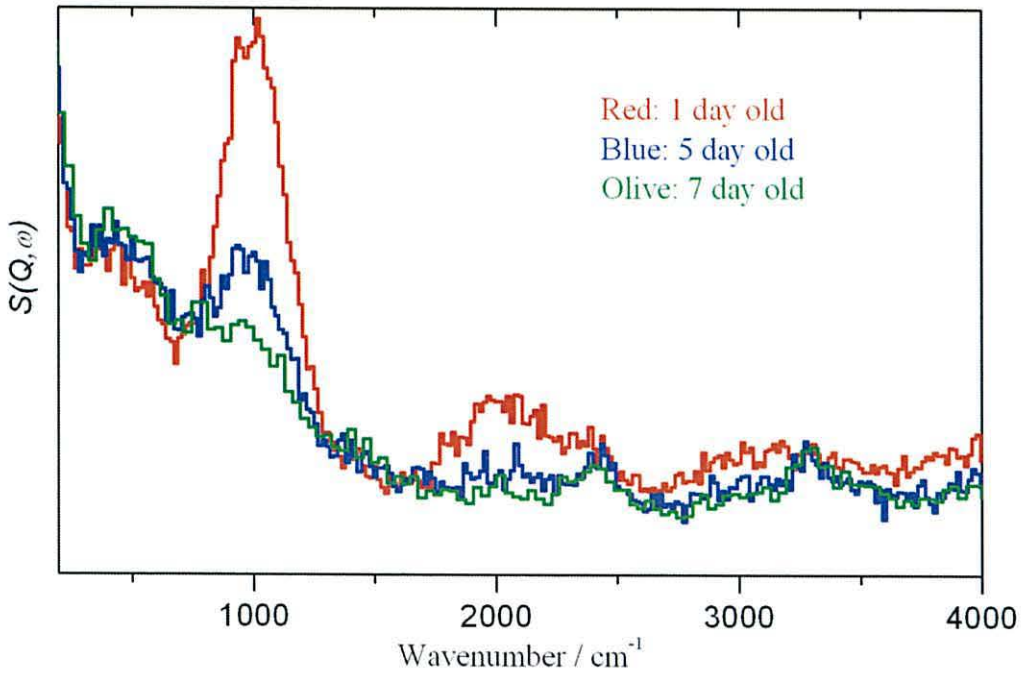

Figure 13. INS MAPS spectra of Würtz CuH at time intervals showing decomposition.

After 4 days the product had decomposed to the black solid CuO (confirmed by XRD in Figure 15.) by approximately half, however it should be noted that the samples were kept in an aluminium sample holder and sealed with indium wire and that decomposition would be significantly faster if left in the open atmosphere.

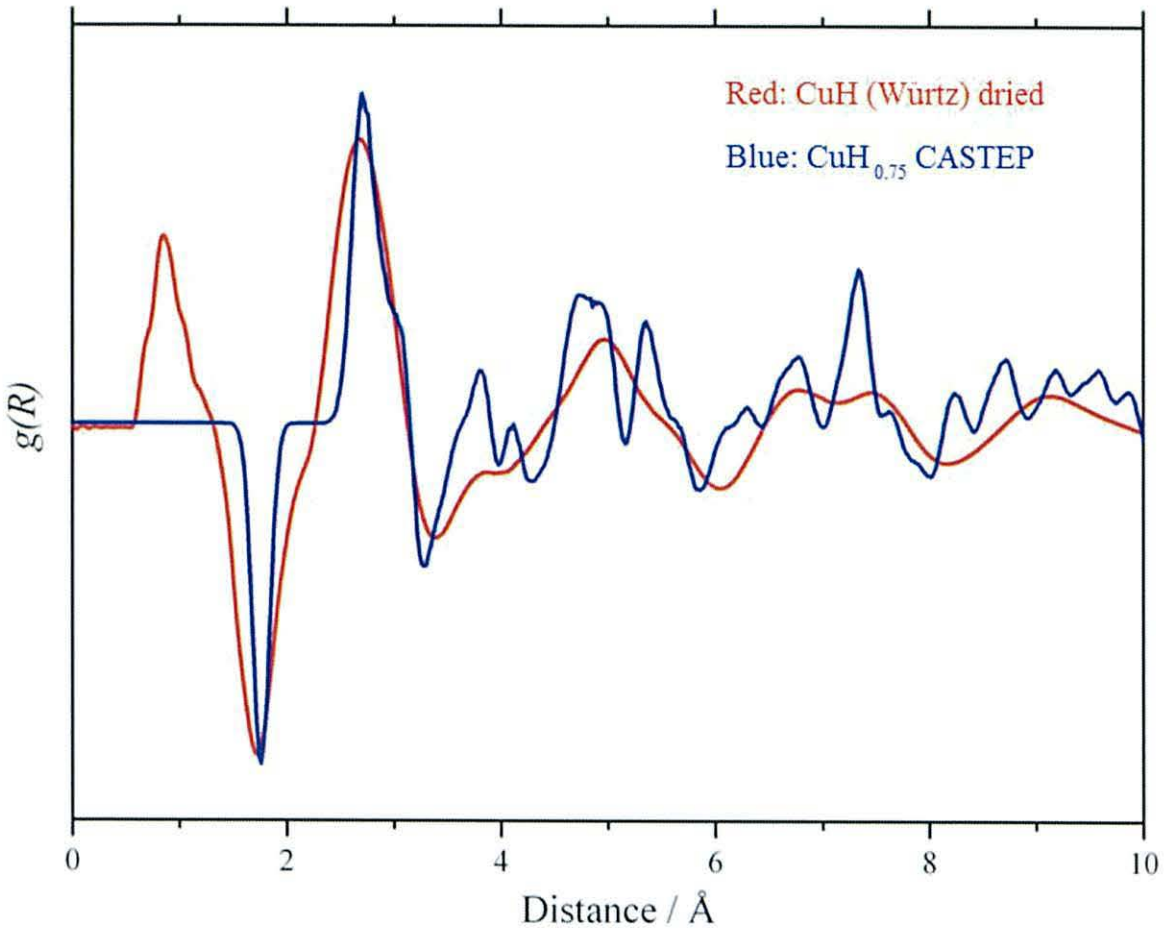

Figure 14. SANDALS diffraction spectrum of Würtz CuH and calculated $CuH_{0.75}$ CASTEP overlay.

The SANDALS diffractogram above (Figure 14.) shows a strong negative peak at 1.81Å which is consistent with the calculated $CuH_{0.75}$ (non-stoichiometric) trace providing further evidence of the Cu-H bond and also clues into the stoichiometry of CuH.

The XRD diffractogram (Figure 15.) confirms the presence of CuH in the Würtz sample, along with the contaminants copper oxide and copper metal which is in full accordance with the literature.[8] Reductions in copper metal traces were achieved in all

subsequent preparations by not exceeding a reaction temperature of 55°C and reductions in CuO can be achieve by maintaining an inert atmosphere throughout all manipulations and reducing time between preparation and analysis.

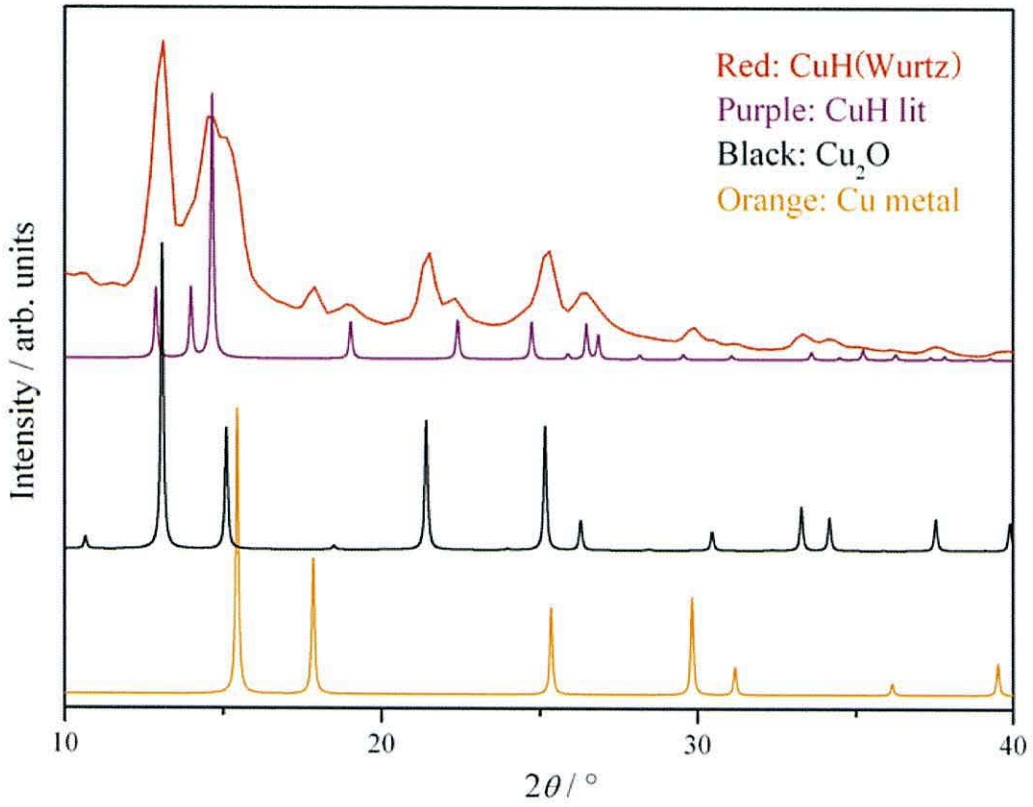

Figure 15. XRD diffractogram of CuH (Würtz) with CuH Lit. (Acta. Cryst.) and impurity references.[53]

Further dried samples of Würtz CuH were prepared and these measured on MAPS. Expansion of the high energy region (> 1750 cm^{-1} Figure 17.) gave interesting results into the Cu-H vibrational transitions and also the bending / stretching frequencies of H_2O (Figure 16.).

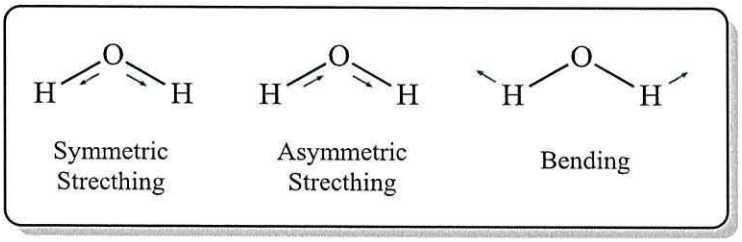

Figure 16. Stretching and bending modes of H_2O.

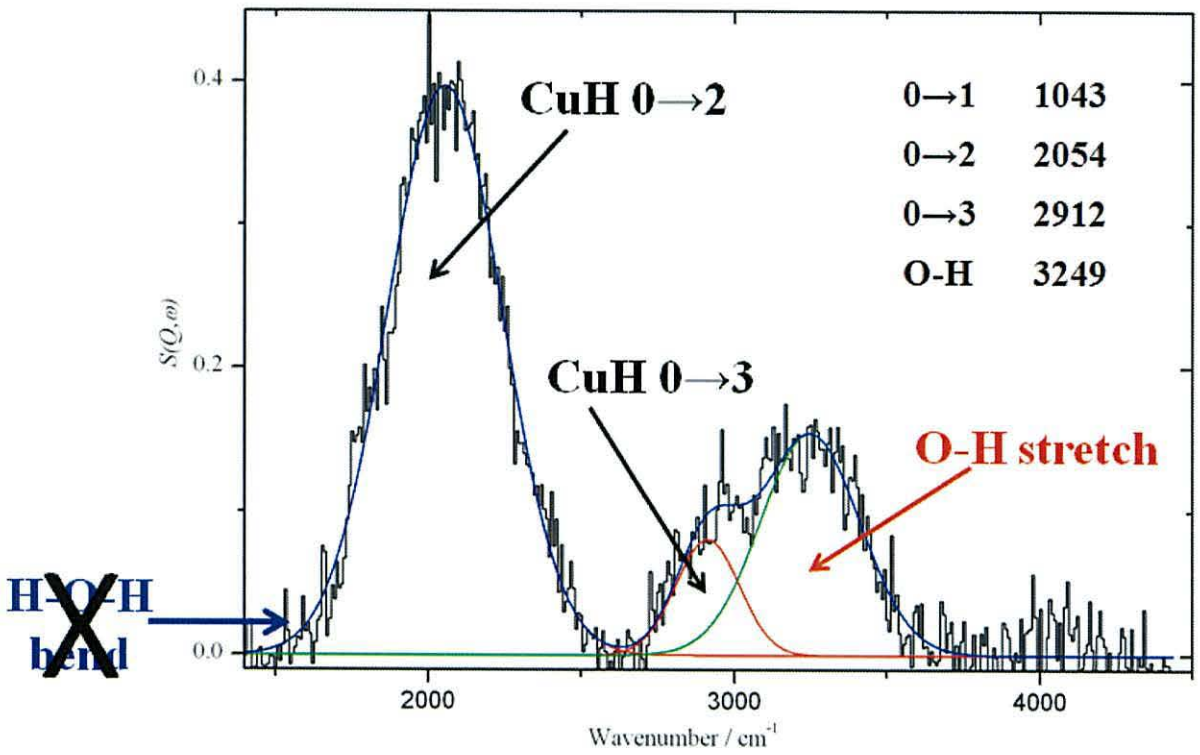

Figure 17. INS MAPS spectrum of dried Würtz CuH in the high energy region.

Figure 17. shows the signals corresponding to particular Cu-H vibrational transitions from 0 (ground state) to higher levels (1-3). In Raman and IR, only the fundamental transition (0 → 1) is seen, whilst higher order transitions (0 → 2 etc.) are forbidden in the harmonic approximation (they are much weaker ≈ 1/100 the intensity of the fundamental transition due to anharmonicity). However, with neutron vibrational spectroscopy (such as MAPS / TOSCA) these higher order transitions are allowed in the harmonic approximation so they may have appreciable intensities.

Figure 17. also shows us that no signal attributed to the H-O-H bending mode (1650 - 1850 cm^{-1}) is observed whilst the O-H stretches (3249 cm^{-1}) are clearly visible giving us proof of hydroxyls present on the surface of $CuH.H_2O$.

3.2.1.3. Cuprous Hydride ($CuH.H_2O$) – $NaBH_4$ (1912)

Although first reported in 1912 by Travers and Ray[4] the method employed was a modification of the literature method of Mahanti *et al*[11] and is based on the following equation:

$$2Cu_2^{+} + 2BH_4^{-} + 6H_2O \longrightarrow 2CuH + 2B(OH)_3 + 2H^{+} + 5H_2$$

Equation 14. Redox reaction of $NaBH_4$ with $CuSO_4$.

All reactions steps and subsequent manipulations were performed under either an inert argon atmosphere or a constant blanket of argon gas.

Preparation of $CuH.H_2O$ from $NaBH_4$ (Methodology 3c.):

In a 2-necked 1 L round bottom flask, $CuSO_4.5H_2O$ (40 g, 160.2 mmol) was fully dissolved in a minimum of $H_2SO_{4(aq)}$ (2 M). The aqueous mixture was degassed with argon for 2 h and warmed slowly to 30°C upon which $NaBH_4$ (6.06 g, 160.2 mmol) was added in small portions. The vigorous exothermic reaction instantaneously results in coffee coloured particles of CuH and also copper metal. The reaction vessel was then sealed with rubber septa, in an inert argon atmosphere and stirred at 30°C for 2 h.

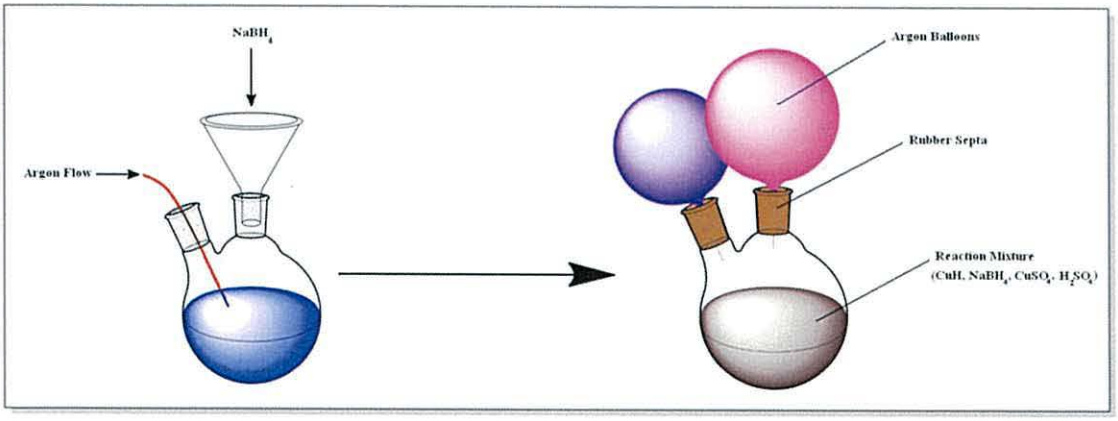

Figure 18. $NaBH_4$ + $CuSO_4$ reaction and stirring at 30°C.

The mixture was then filtered through a sintered glass vacuum filter with a medium porosity (G02) under a flowing argon blanket, the filtrate was blue due to the presence of un-reacted $CuSO_{4(aq)}$. The CuH cake was washed with de-gassed room temperature H_2O to remove any remaining soluble starting materials, followed by 30°C H_2O to remove some free boric acid ($B(OH)_3$) crystals that form upon cooling.

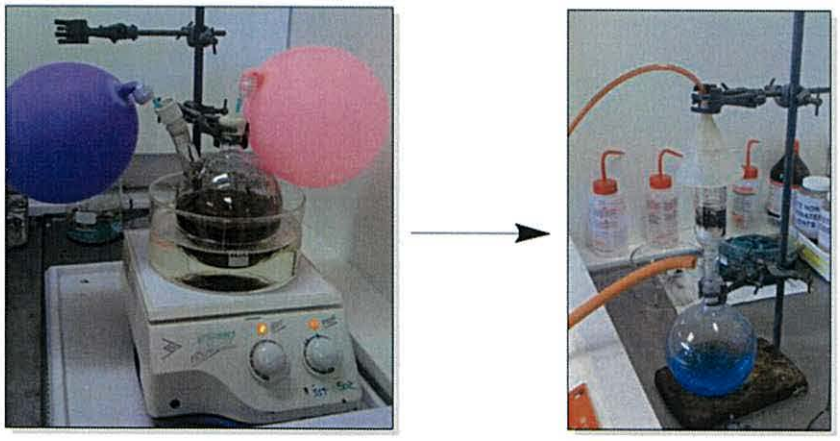

Figure 19. Reaction stirring at 30°C, followed by vacuum filtration in an inert atmosphere.

After being filtered and washed, the product and the sintered glass filter was transferred into a sealed argon filled glove bag. It was then weighed (7.8 g) and loaded into the necessary sample holders for neutron characterisation (TOSCA, MAPS & SANDALS). A small amount (< 0.3 g) was taken and treated with ether, then dried under argon aspiration to obtain a dry powder which could be sufficiently loaded into 1 mm QGCT for XRD and Raman analysis.

$CuH.D_2O$ was prepared by taking the remaining CuH product (≈ 3.5 g) and stirring for ≈ 12 h in D_2O under an atmosphere of argon. The mixture was filtered, dried via vacuum filtration / aspiration and again loaded into the necessary sample holders for neutron characterisation and XRD.

Observational Remarks:

Although a 1 : 1 stoichiometry of $CuSO_4$ to $NaBH_4$ was used it was clear from the colour of the un-reacted filtrate (deep blue) that the limiting factor in this reaction is the $NaBH_4$. It is also worth noting that increasing the quantity of the reactants (ie. 160.2 mmol → 400.5 mmol) in the hope of increasing the mass yield, gave arise to filtering and aspiration problems (ie. filter blockage and decomposition during drying).

The instant vigorous, effervescent and exothermic reaction that occurs upon addition of the $NaBH_4$ gives off enough localised heat to allow small amounts of decomposition to copper metal. Minute but visible amounts of copper metal can been seen in the reaction mixture and in the dried product (shown in the XRD diffractogram Figure 20.). By adding the $NaBH_4$ as an aqueous solution this instantaneous reaction resulting in formation of copper metal is reduced, however there are also serious reductions in yield and reaction time and the product is invariably contaminated with CuO. Post filtration and upon cooling, crystals of free $B(OH)_3$ are visible, according to Mahanti *et al*[11] full removal of this free boric acid can be achieved by stirring the crude CuH product in boiling water for 1 h. Addition of 70-75°C de-ionised H_2O instantly resulted in CuH decomposition to the black solid CuO (proven by XRD), 1 h in boiling would almost definitely result in full decomposition.

3.2.1.4. Spectroscopy of $CuH.H_2O/D_2O$ from $NaBH_4$ Route:

The XRD diffractogram of $CuH.H_2O$ from the $NaBH_4$ route (Figure 20.) shows the same CuH compound as the Würtz reaction albeit contaminated with more $Cu_{(metal)}$ which were visible as minute specs in the reaction mixture and dried product. Copper metal (obviously void of hydrogen) is invisible to the neutron techniques utilised in this experiment and will not affect the results. All free $B(OH)_3$ crystals were removed by purification in H_2O. Application of the Scherrer equation indicates a particle size of 31Å (Equation 12).

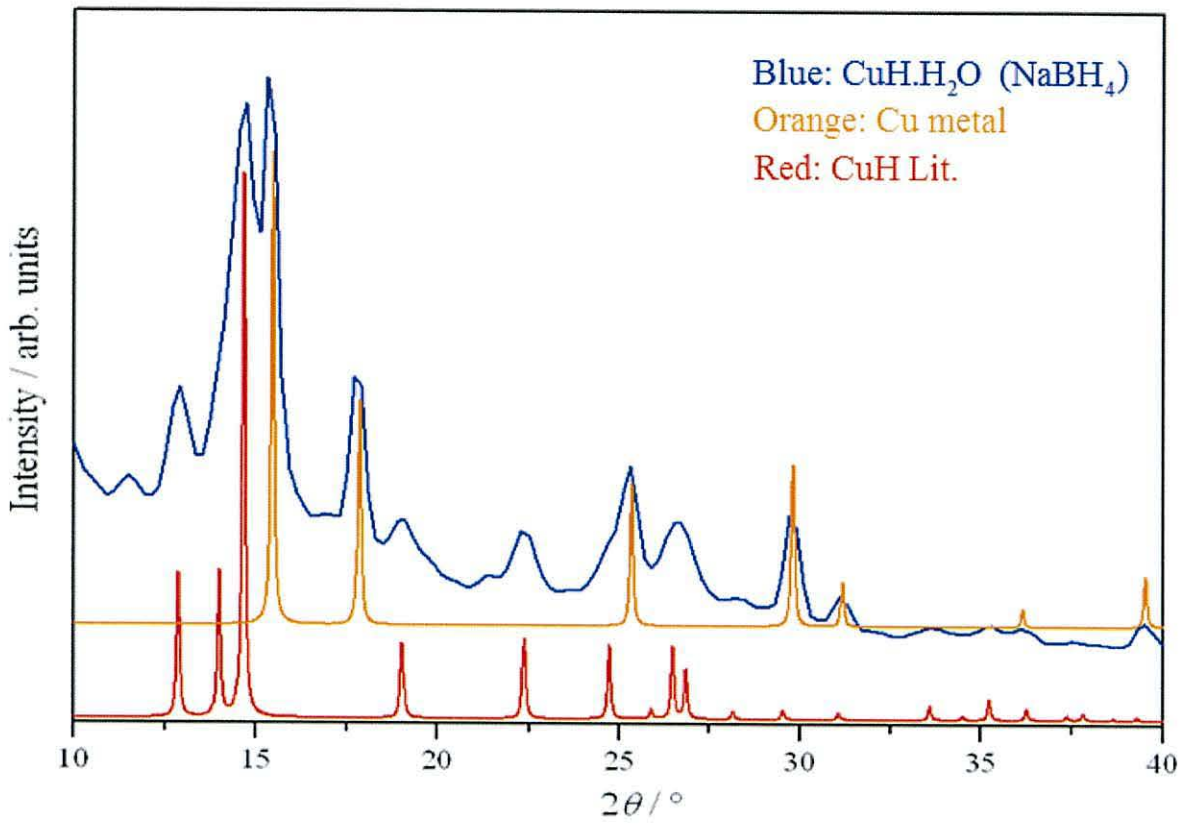

Figure 20. XRD diffractogram of $CuH.H_2O$ from $NaBH_4$ with Cu metal impurity and CuH lit.[53]

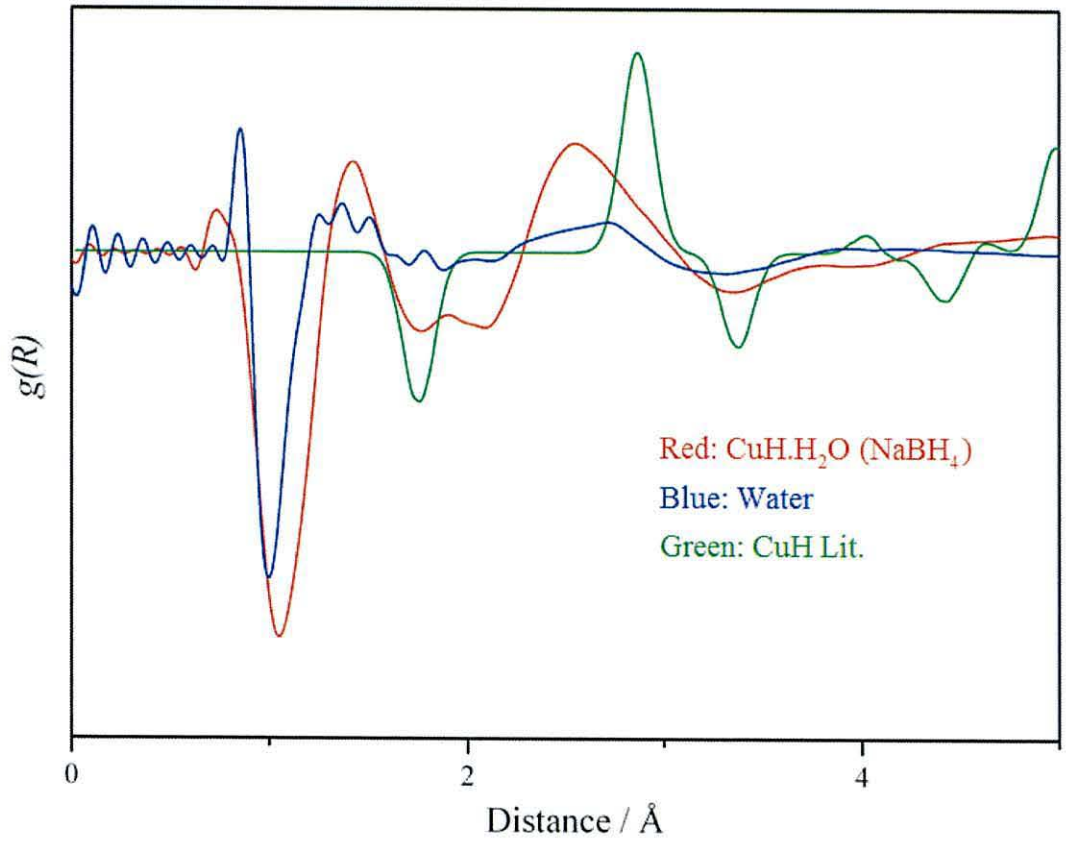

Figure 21. SANDALS diffraction spectra for $CuH.H_2O$ ($NaBH_4$) with reference spectra.[53]

The SANDALS diffraction spectra (Figure 21.) show the $CuH.H_2O$ trace and CuH Lit. trace both having negative peaks at 1.76 Å exactly as expected for Cu-H and further confirmed by the absence of this peak in the water trace. The $CuH.H_2O$ trace and the water trace both show a negative peak at ≈ 1 Å which is characteristic of O-H. This data provides further evidence that both Cu-H and O-H are present in the sample consistent with the core-shell model.

3.2.1.5. Soluble Copper (I) Hydride (CuH.py) - $LiAlH_4$ (1968)

Although the synthesis was first reported by Wiberg and Henle in 1952[6], the method employed is a modification of the literature method of Dilts and Shriver[7] and is based on the following equation:

$$3CuI + LiAlH_4 \longrightarrow 3CuH + AlI_3 + LiH$$

Equation 15. $LiAlH_4$ reduction of CuI in pyridine.

All reactions steps and subsequent manipulations were performed under either an inert argon atmosphere or a constant blanket of argon gas.

Preparation of CuH.py (Methodology 3d.):

$LiAlH_4$ (1 M in ether, 14.75 mmol, 14.75 ml) was placed in the top of a pressure equalising dropping funnel, while CuI (7.62 g, 40 mmol) was dissolved in anhydrous pyridine (180ml) in a 500ml round bottom flask. The $LiAlH_4$ was added to the CuI solution drop wise over 15 mins and the reaction stirred at room temperature for 8 h.

The mixture was then filtered through a sintered glass filter containing a pad of Celite® (filter aid, to avoid blockages) which removes a vast majority of the insoluble AlI_3 and LiH salts.

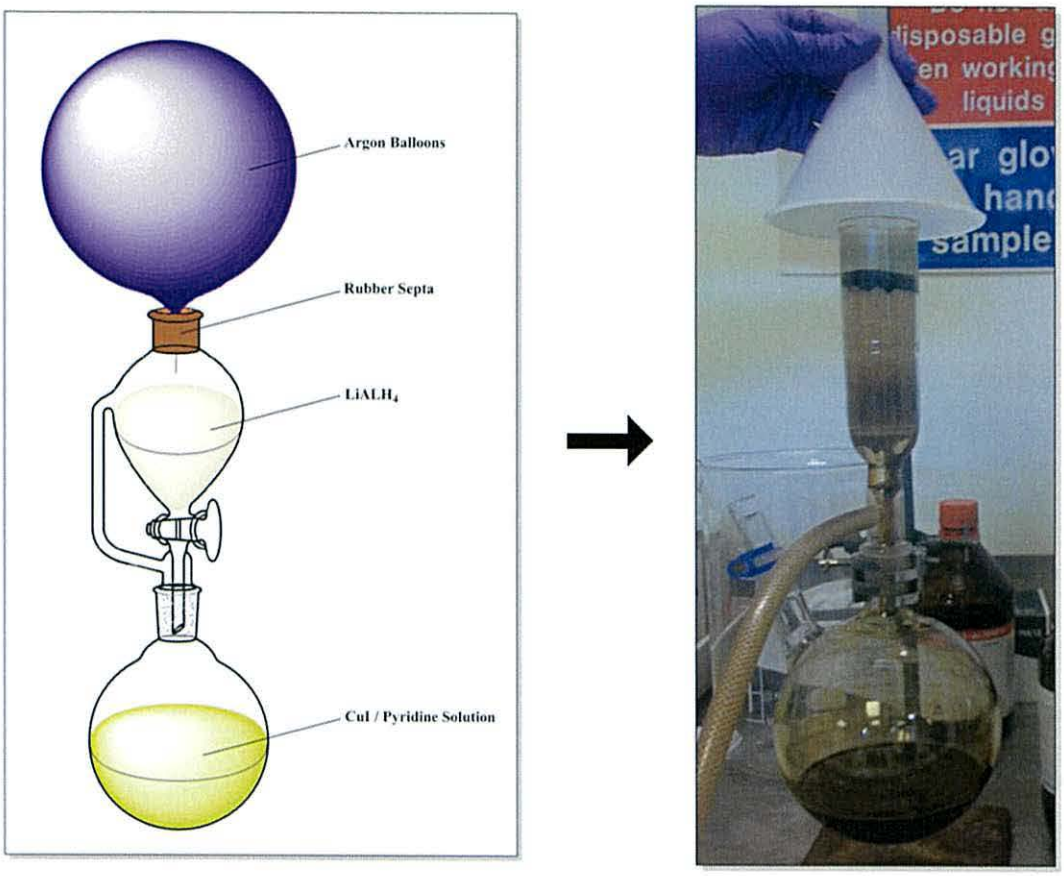

Figure 22. $LiAlH_4$ reduction of CuI in pyridine (left) and Filtration though Celite® pad under argon.

To the filtrate an equal volume of anhydrous ether was added which initiates the precipitation of the CuH product. The mixture was briefly stirred and the brown solid precipitate allowed to settle revealing a pale yellow / green top layer which was carefully decanted (mixture of ether / pyridine). Another portion of anhydrous ether was added and this process repeated several times until the top layer was completely colourless and therefore void of pyridine, with the CuH precipitate clearly visible at the bottom. The mixture was then filtered through a sinter and the product dried *in vacuo* until completely void of ether.

The flask containing the CuH product was transferred into a sealed argon filled glove bag and then loaded into the necessary sample holders for neutron characterisation. A small amount (< 0.3 g) was taken and loaded into 1 mm QGCT for XRD and Raman analysis.

CuH.d_5-py was prepared by taking half the CuH.py product and re-dissolving in d_5-pyridine and followed by stirring at room temperature for ≈ 12 h. The product was again precipitated from ether (several cycles) and dried via argon aspiration. The deuterated sample was then loaded into the necessary samples holders for neutron characterisation and also loaded into 1 mm QGCT for XRD and Raman analysis.

Observational Remarks:

During the filtration stage, using the Celite® filter aid is essential as without it there are instantaneous and serious blockages. This is due to the inorganic salt by-products but most likely also due to the smaller particle size of the CuH.py product getting trapped in the glass sinter. Multiple cycles of ether precipitation are also vital as if there is too much residual pyridine left during the drying stage the result is a sticky pyridine paste that requires further treatment with ether where loss of purity due to exposure to air can seriously affect the product.

3.2.1.6. Spectroscopy of CuH.py/d_5-py:

The XRD diffractogram of CuH.py (Figure 23.) shows a strong resemblance between the experimental and calculated patterns (both stoichiometric and non-stoichiometric) which initially confirms the presence of CuH in the sample.

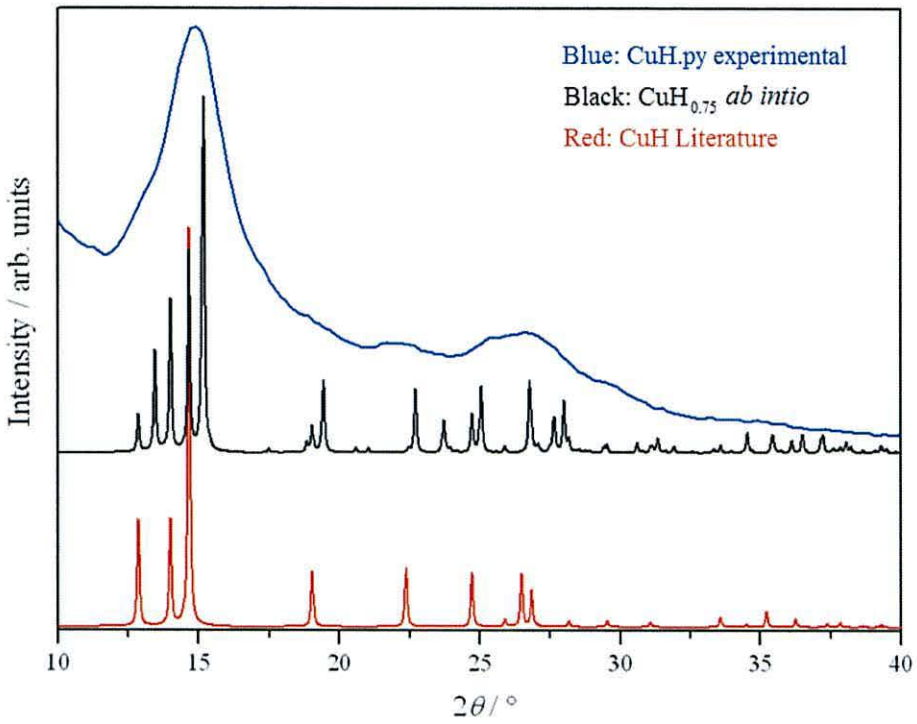

Figure 23. XRD diffractogram of CuH.py, CuH literature and calculated structures (CASTEP).[53]

The width of the CuH.py experimental line prevents any deduction into stoichiometery although a crude estimate of particle size derived from the Scherrer equation is found to be ≈ 13 Å (Methodology 3a. Equation 12).

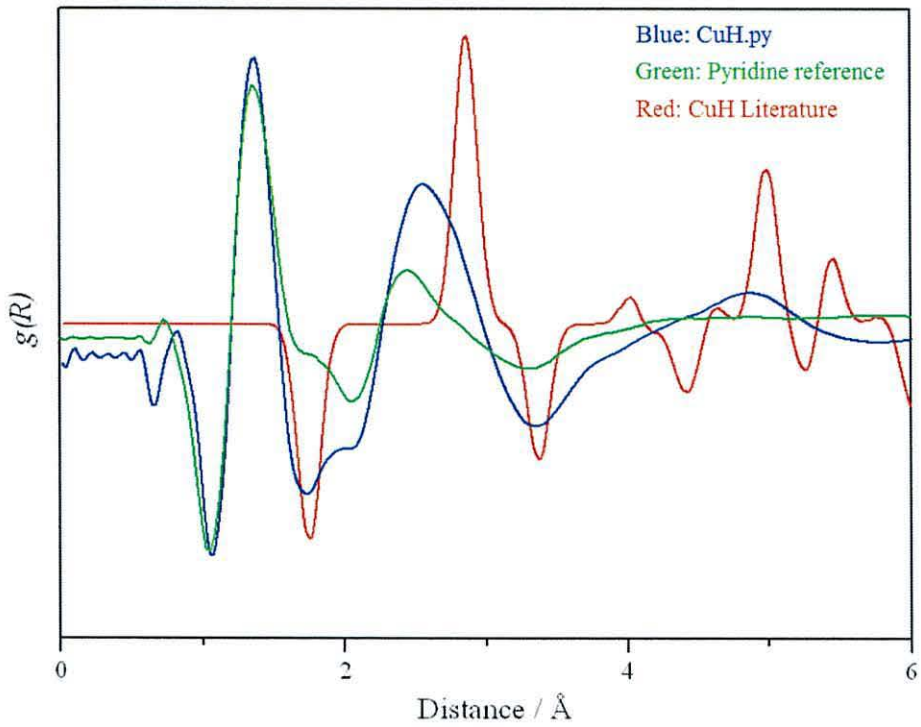

Figure 24. SANDALS diffraction spectra for CuH (experimental and literature) and pure pyridine.[53]

Figure 24. shows the expanded SANDALS spectra (short range 0 – 6 Å for full CuH.py SANDALS diffraction spectrum see appendix) due to the pyridine reference trace only showing correlations < 10 Å which is as expected for liquid samples. The negative peaks at ≈ 1.8 Å confirm the presence of Cu-H and also pyridine which is consistent with the core-shell model hypothesised.

Figure 25. below shows the expanded fingerprint region of various vibrational spectra (INS – TOSCA, IR and Raman) for the CuH.py sample compared to pure pyridine.

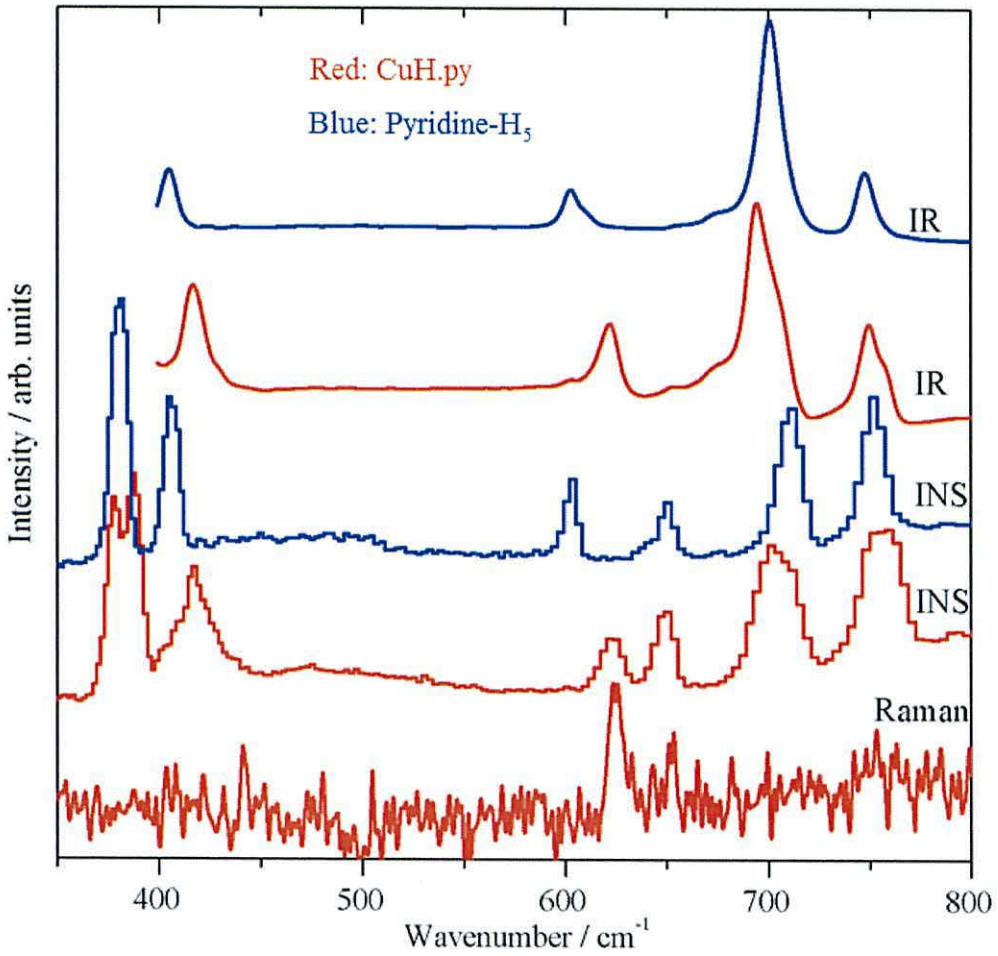

Figure 25. Expanded fingerprint region of vibrational spectra for CuH.py and Pyridine-H_5.

Remarkably some of the peaks related to pyridine in the CuH.py sample are shifted in the INS (TOSCA) traces. These shifts can be observed at 405 to 417 cm^{-1}, 602 to 640 cm^{-1} and 711 to 700 cm^{-1} also confirmed by the IR spectra. These shifts of the vibrational peaks

are classic for co-ordinated pyridine which has been extensively studied[54/55] further confirming the core-shell model of Cu-H with co-ordinated pyridine.

As noticed in the XRD (Figure 23.) the non-stoichiometric nature of CuH modifies the spectral patterns which can also be observed in Figure 26. (below) and also shown previously in Figure 14.

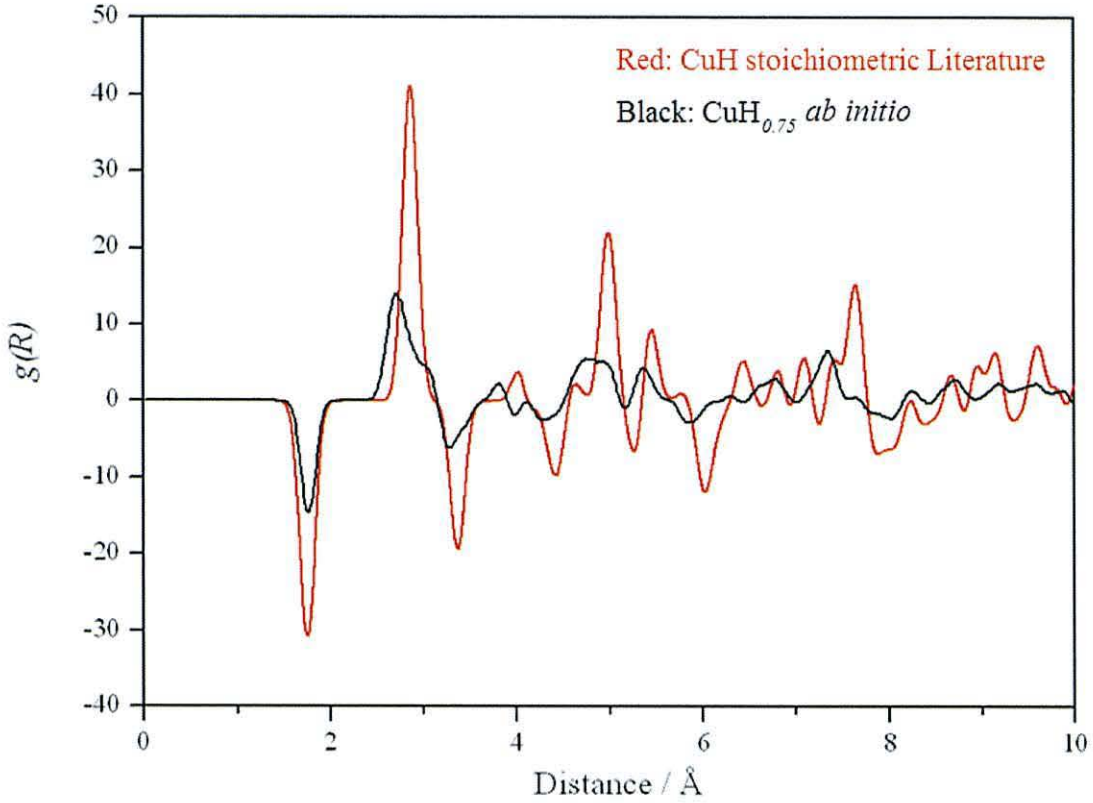

Figure 26. Calculated radial distribution functions for stoichiometric and non-stoichiometric CuH.

This alteration of the pattern (seen in XRD and SANDALS data) due to non-stoichiometry can be confirmed by the comparison of calculated $CuH_{0.75}$ to the CuH.py sample but with pure pyridine subtracted from the data (ie. CuH.py – pyridine-H_5). This subtraction allows us to examine the radial distribution function for the CuH.py sample but with the effects from the pyridine shell removed. This agreement (Figure 27.) strongly supports assignment of CuH_x ($x = < 1$) rather than CuH, which is consistent with several literature findings.

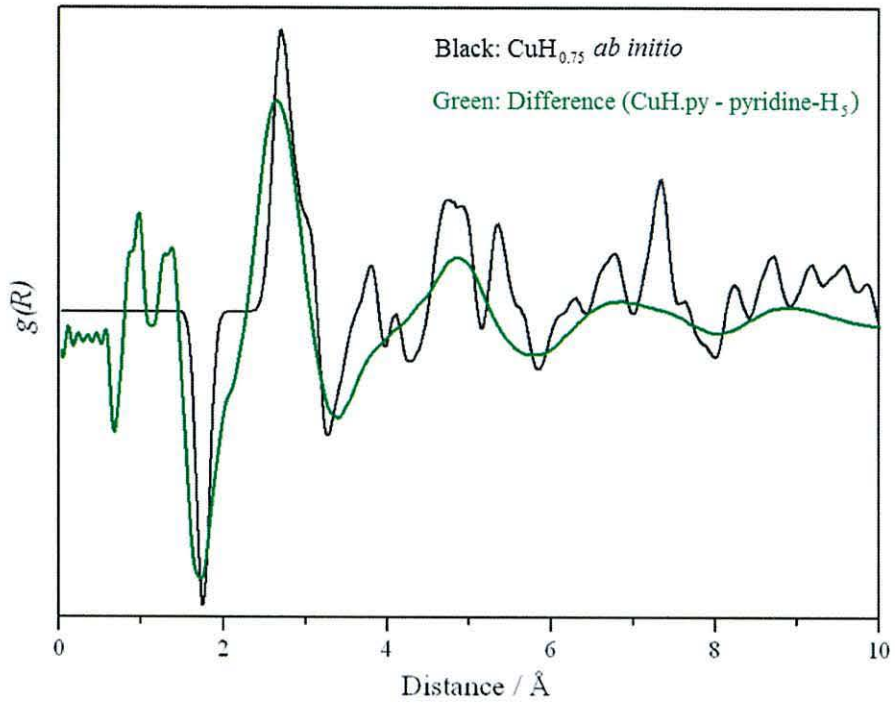

Figure 27. Comparison of non-stoichiometric $CuH_{0.75}$ to experimental SANDALS data for CuH.py (with pyridine subtracted).

Figures 14., 26. and 27. explain the variances in the experimentally derived spectra when compared to stoichiometric CuH from the literature (Acta. Cryst.). The change in pattern can be attributed to the non-stoichiometric nature of the copper hydrides.

3.2.2. Stoichiometric Copper(I) Hydrido Species

3.2.2.1. Osborn Complex aka Stryker's Reagent $[HCu\{P(C_6H_5)_3\}]_6$

The first truly stoichiometric copper hydride, although first prepared by Osborn *et al* in 1971[26] the method employed is modification of the modern literature procedure by Lee and Yun[47] and is based on the following equation.

$$Cu(OAc)_2 + PPh_3 + Ph_2SiH_2 \longrightarrow [Ph_3PCuH]_6 + Ph_2Si(OAc)_2$$

Equation 16. Synthesis of Stryker's reagent from a Cu (II) salt.

3.2.2.2. Preparation of Stryker's Reagent $[HCu\{P(C_6H_5)_3\}]_6$ (Methodology 3e.):

In an argon filled Schlenk flask, $Cu(OAc)_2$ and PPh_3 (1 : 2 ratio) were dissolved in 20 ml of anhydrous benzene, Ph_2SiH_2 (1.2 equivalents) was added to the mixture. Upon stirring at room temperature a colour change (Figure 28.) occurs over ≈ 1 h. The reaction mixture was then stirred for a further 1 h, followed by concentration *in vacuo* to ≈ ½ its volume, where upon the red/orange suspension was allowed to settle and anhydrous acetonitrile was carefully layered on top allowing full crystallisation to occur over night.

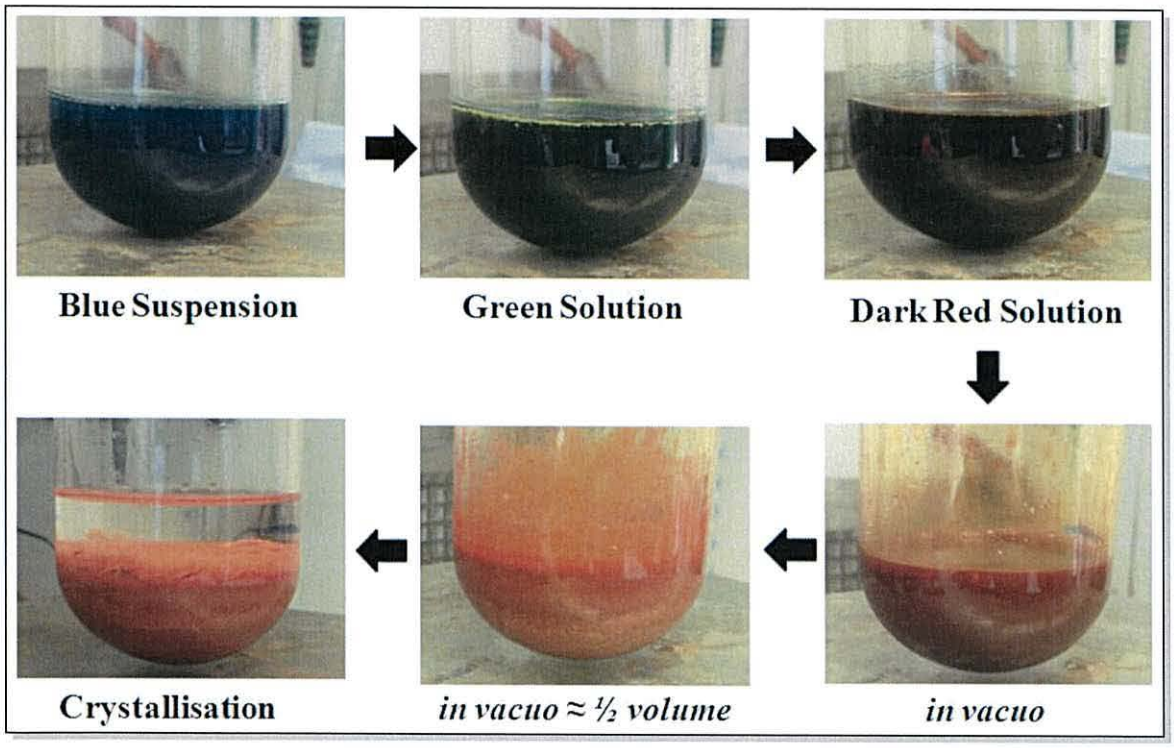

Figure 28. Preparation of Stryker's reagent colour change and concentration under vacuum.

The benzene / acetonitrile slurry was filtered and further slurried with a mixture of 50 : 50 benzene / acetonitrile, which fully removes any unreacted PPh_3 and the $Ph_2Si(OAc)_2$ white solid by-product. The product is purified by washing with several portions of acetonitrile. The filtration system involved a filter tip inserted into the apparatus and driven

by an external vacuum (Figure 29.), this allow multiple washing and filtration steps without ever opening the system to the atmosphere which leads to decomposition.

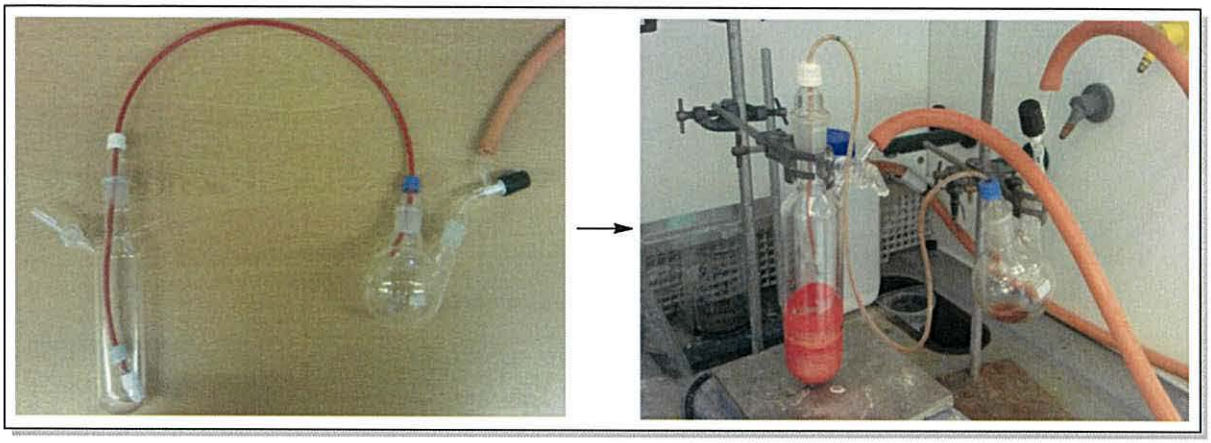

Figure 29. Filtration in an enclosed argon flushed system.

The final product was then dried *in vacuo* obtaining the red crystalline Stryker's reagent completely void of solvent in 79% yield. Initial attempts at this reaction yielded an apparently pure crystalline product that even when kept in a completely sealed argon environment decomposed to a brown / turquoise solid mass after 2 / 3 days, that did not agree with the literature.[31] Later attempts and after analysis by ^{1}H NMR (see Spectroscopy) was found to contain traces of the solvent acetonitrile. Fully removal of this solvent was achieved by very slightly warming the flask (to ≈ room temperature) during the final drying stage *in vacuo*. The product was then stable in an atmospheric gas free environment for > 3 weeks, when all the sample was then analysed but would presumably last longer if kept under argon, which is consistent with the literature.

3.2.2.3. Deuterated Stryker's Reagent $[DCu\{P(C_6H_5)_3\}]_6$ & $[HCu\{P(C_6D_5)_3\}]_6$

The deuterated Stryker analogues were prepared using the same method but exchanging the relevant starting material with the correct deuteride source:

$[DCu\{P(C_6H_5)_3\}]_6$ – **(Methodology 3f.)**

Equation 17. Stryker's synthesis using diphenyl silane D_2.

$[HCu\{P(C_6D_5)_3\}]_6$ – **(Methodology 3g.)**

Equation 18. Stryker's synthesis using deuterated triphenylphosphine D_{15}.

The deuterated reactions proceeded identically to the hydrido reaction with the only observable difference being the time taken for the colour change to occur (significantly faster). This is most likely due to the quality of the starting materials for these reactions, both involved new high quality anhydrous starting materials as well as the deuterium reagents themselves being of a high purity.

3.2.2.4. Spectroscopy of Stryker's Reagent:

NMR –

Due to the sensitive nature of the complex, the Stryker's reagent samples synthesised for study by neutrons were not immediately analysed by NMR and instead remained sealed in the argon flushed Schlenk flasks and were never opened to the atmosphere. After the neutron

spectra were obtained at ISIS (Rutherford Appleton Laboratories) the samples were repackaged in the Schlenk flasks (inside a dry glovebox) and sealed in multiple bags containing positive pressures of argon in an attempt to minimise decomposition. Upon return, although it was still possible to assign the correct signals in the ^{1}H NMR, too much decomposition had occurred for clean spectra to be obtained. However ^{1}H NMR spectra of Stryker's reagent from earlier synthetic attempts (although containing unwanted signals from the solvent CH_3CN and a small amount of the starting material Ph_2SiH_2) were sufficient to provide enough detail for assigning $[(Ph_3P)CuH]_6$ in accordance with the literature[47]. These earlier synthetic attempts at Stryker's complex contained some unwanted CH_3CN solvent due to caution being taken when drying such copper hydride compounds under vacuum (CuH reported to spontaneously and exothermically decompose)[3] however, after several attempts and a test on small scale it was found that dry samples could be obtained without any product combustion. The small amount of Ph_2SiH_2 starting material being left in the first synthetic attempts were rectified by slightly altering the stoichiometry, ie. making PPh_3 a very slight excess leaving no unreacted Ph_2SiH_2 and allowing the PPh_3 to be successfully removed in the multiple C_6H_6 : CH_3CN washing and filtration steps.

^{1}H NMR -

^{1}H NMR Literature (400MHz, C_6D_6):[47] δ 7.67 (t, J = 8.1 Hz, 36H), 6.95 (t, J = 7.3 Hz, 18H), 6.74 (t, J = 7.5 Hz,36H), 3.53 (br s, 6H).

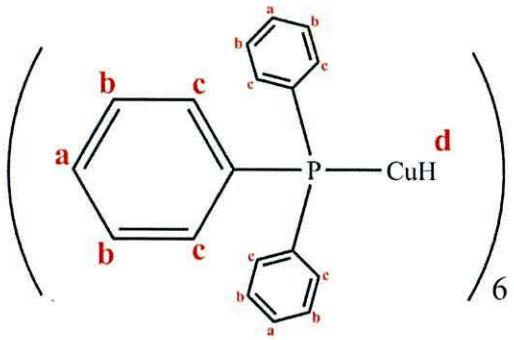

Figure 30. Simplified $[(Ph_3P)CuH]_6$ structure with labelled peaks for NMR (see **Figure 31.** below).

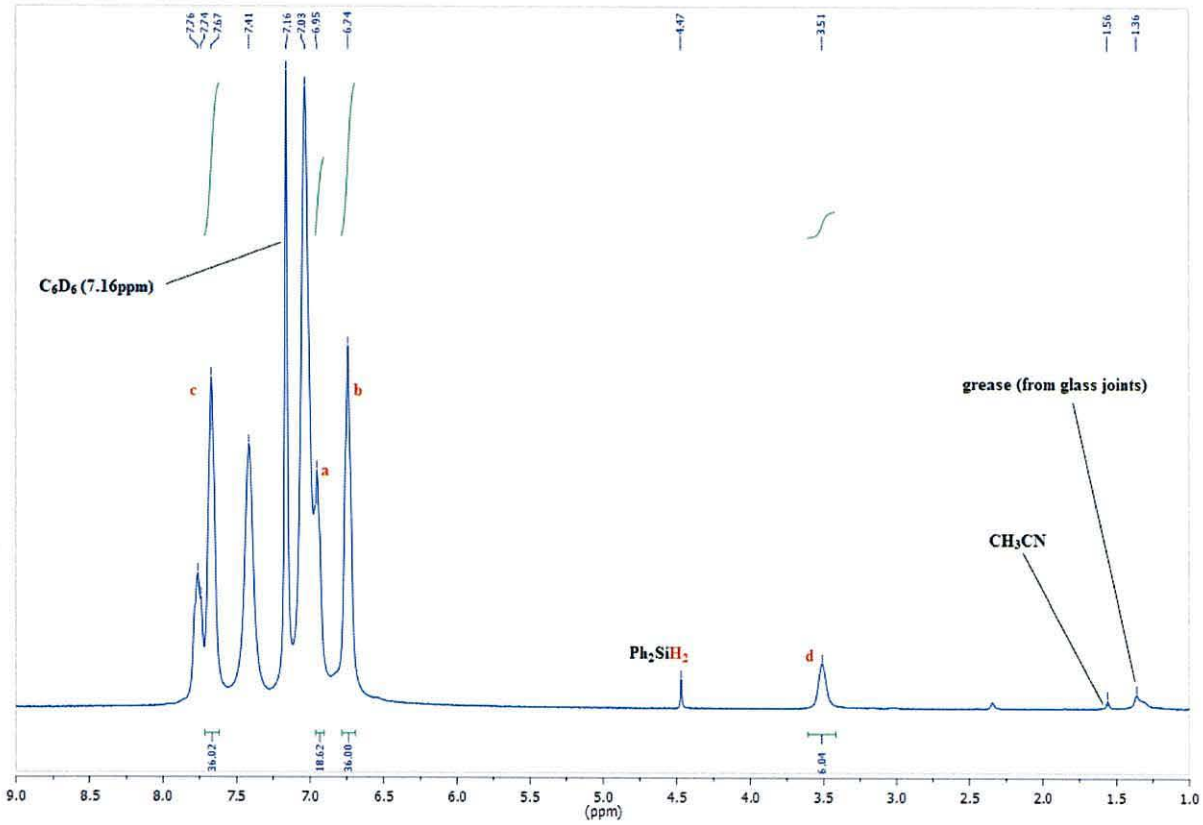

Figure 31. ^1H NMR of $[(Ph_3P)CuH]_6$ in C_6D_6, showing the integration and relevant chemical shifts (ppm).

Integration total 96. Cu-H (6), and 90 aromatic H's (18 from the para- position, 36 from meta- and 36 from ortho-, see Figure 30.) in accordance with the literature[47]. The signals (**a**, **b** & **c**) should be split into triplets but the resolution was not enough to show this, another ^1H NMR was run with increased scans (from 16 to 32) which shows the triplet splitting (Figure 32., it is also worth noting that the time between these spectra being obtained is enough for some decomposition to be visible especially in the Cu-H signal at 3.51ppm).

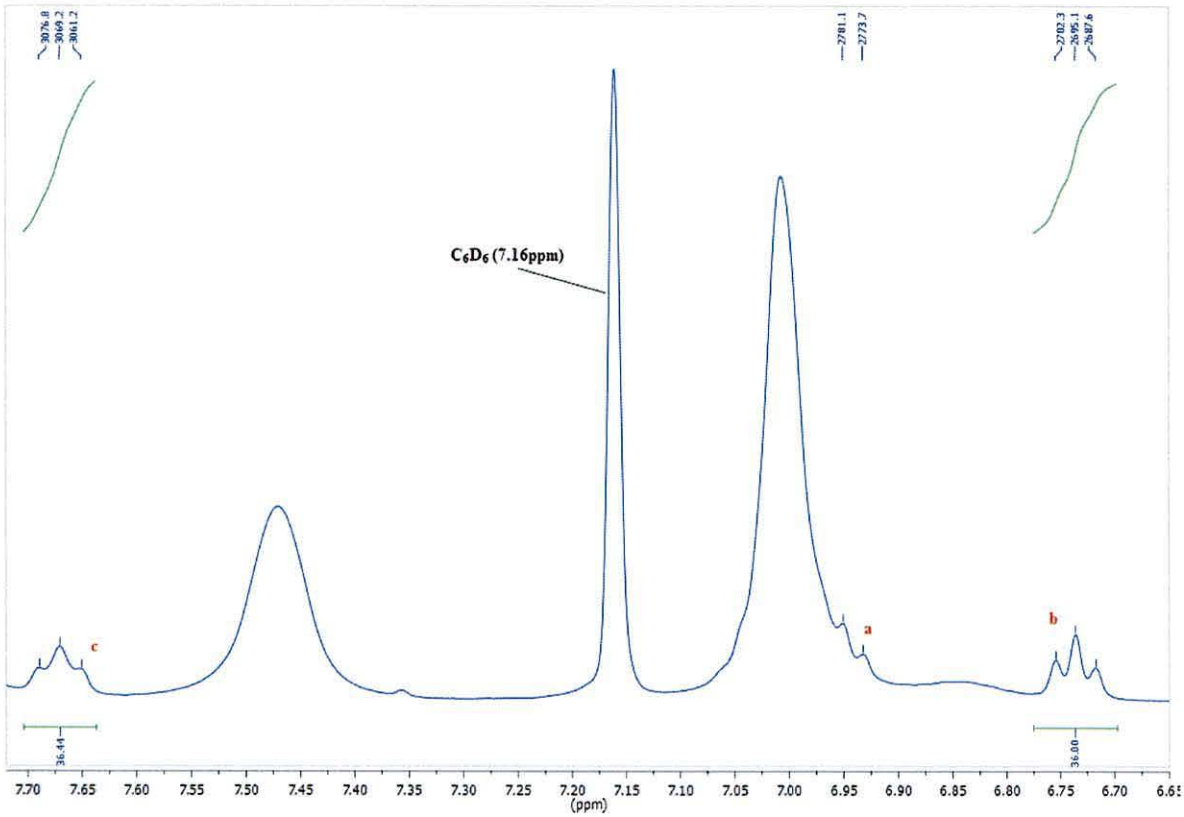

Figure 32. ^{1}H NMR of $[(Ph_3P)CuH]_6$ in C_6D_6, showing relevant aromatic triplet peaks in Hz to give J-values.

Table 3.

Entry	Peak (ppm)	Literature Peaks (ppm)	Peaks (Hz)	J-value (Hz)	Literature J-values (Hz)	*I*	*I* (Literature)
a	6.95	6.95	2781.1 – 2773.7	7.4	7.3	18.62	18
b	6.74	6.74	2702.3 – 2695.1	7.2	7.5	36.00	36
			2695.1 – 2687.6	7.5			
c	7.67	7.67	3076.8 – 3069.2	7.6	8.1	36.44	36
			3069.2 – 3061.2	8.0			
d (Cu-H)	3.51	3.53	singlet	N/A	N/A	6.04	6

The correct integrations, chemical shifts, splitting and J-values are observed for this compound albeit with unwanted peaks from Ph_2SiH_2 (δ 4.47 ppm), minute traces of CH_3CN and glass joint grease (δ 1.56 & 1.36 ppm) but mainly decomposition signals containing aromatic substituents. Following attempts produced pure samples of Stryker's reagent but were not analysed by NMR due to minimum exposure pre-neutron spectroscopy being of the utmost importance, the structure and purity were confirmed using INS.

^{2}H Deuterium NMR -

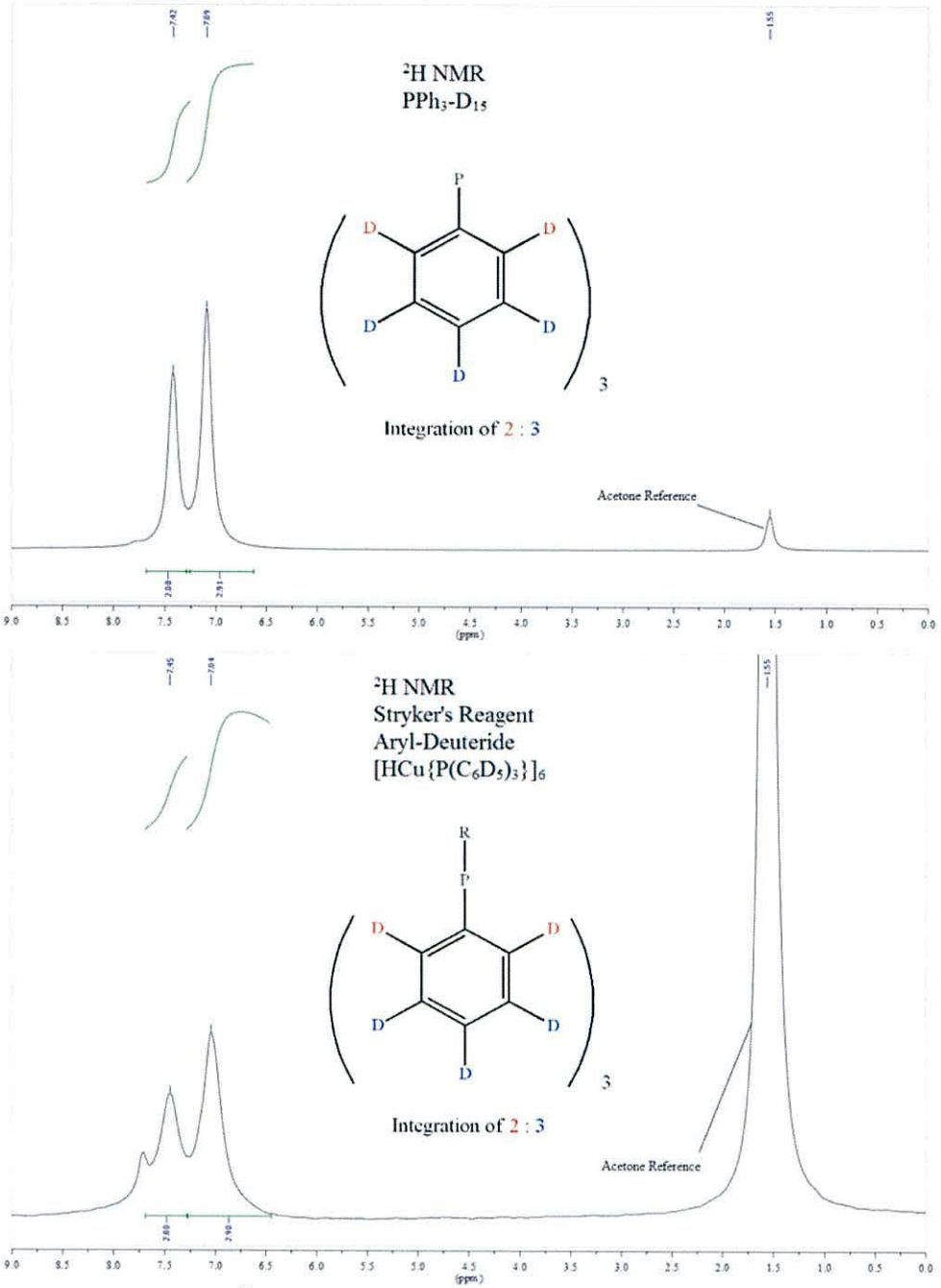

Figure 33. ^{2}H Deuterium NMR of $P(C_6D_5)_3$ and $[HCu\{P(C_6D_5)_3\}]_6$.

These ^{2}H NMR's use C_6H_6 as the solvent with a drop of acetone-D_6 as the reference peak set to 1.55 ppm[56] and show correct integrations for the aromatic C-D signals but with less resolution compared to ^{1}H NMR as expected. The disappearance of these aromatic C-D signals in the ^{1}H NMR for $[HCu\{P(C_6D_5)_3\}]_6$ (see appendix) also confirms successful synthesis of the deuterated compounds for INS.

Neutron Diffraction (SANDALS) –

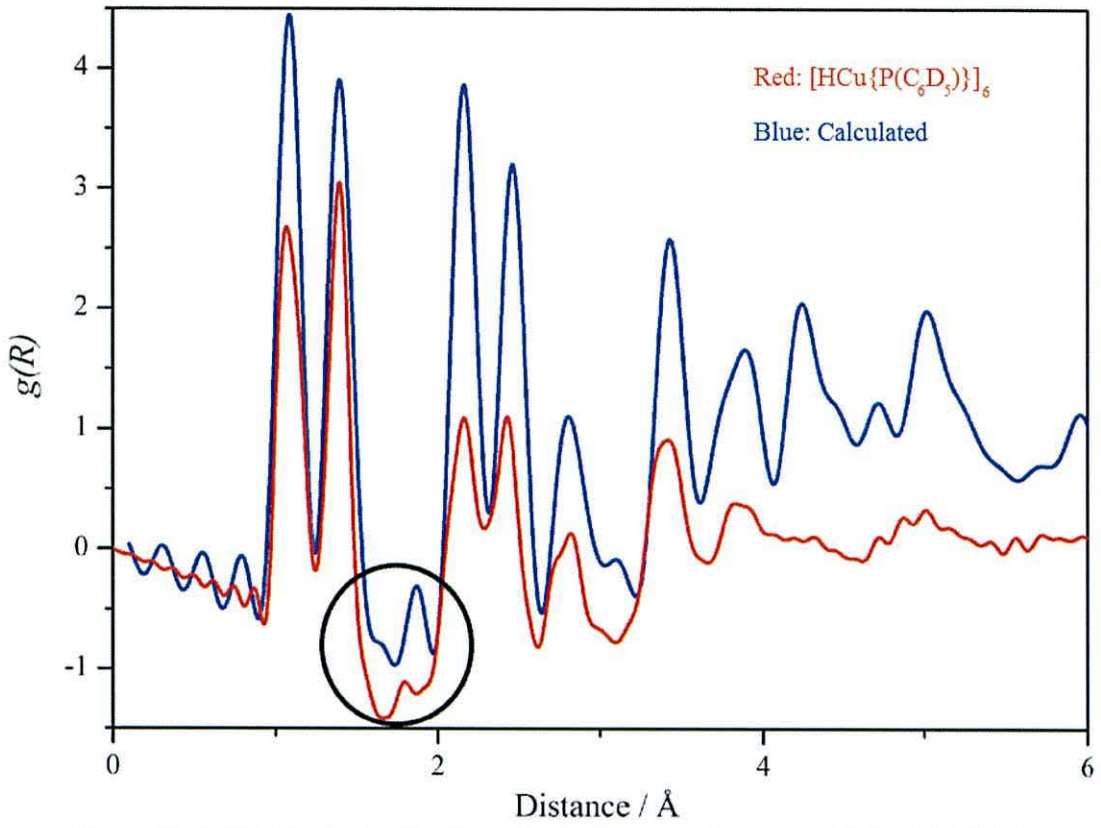

Figure 34. Radial distribution functions of experimental and calculated $[HCu\{P(C_6D_5)_3\}]_6$.

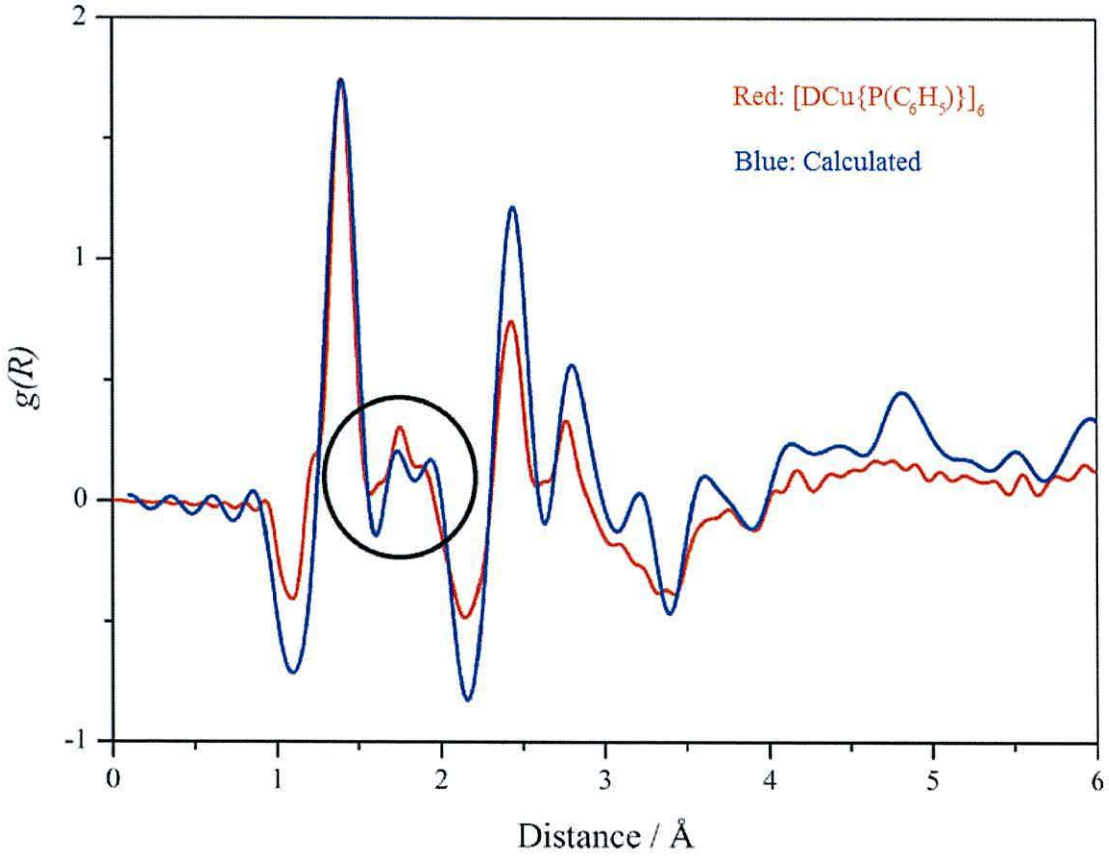

Figure 35. Radial distribution functions of experimental and calculated $[DCu\{P(C_6H_5)_3\}]_6$.

The SANDALS neutron diffraction data shown in Figures 34. & 35. compare results for experimental and calculated $[HCu\{P(C_6D_5)_3\}]_6$ and $[DCu\{P(C_6H_5)_3\}]_6$ which are in excellent agreement. Hydrogen (^1H) has a negative (-) scattering length (related to the neutron undergoing an 180° phase shift upon scattering) while deuterium, carbon, phosphorous and copper have positive (+) scattering lengths. Therefore the (-) peaks are distances involving hydrogen, most noticeable for the peak at 1.09Å which is positive in Figure 34. and negative in Figure 35. corresponding to the C-H and C-D signals from the phenyl rings in $[HCu\{P(C_6D_5)_3\}]_6$ and $[DCu\{P(C_6H_5)_3\}]_6$ respectively. This is further confirmed by the C-C bond peaks at 1.40 Å which are (+) going in both samples.

The black circled areas in both figures are related to the Cu-H & Cu-D distances in the complexes. Figure 34. shows (-) peaks at 1.67 & 1.92 Å corresponding from the 2 different Cu-H distances in $[HCu\{P(C_6D_5)_3\}]_6$, whilst Figure 35. shows (+) peaks at 1.75 & 1.89 Å from the 2 different Cu-D distances.

Table 4. Different Cu-H/D distances in Stryker's reagents $[HCu\{P(C_6D_5)_3\}]_6$ and $[DCu\{P(C_6H_5)_3\}]_6$.

Complex	Cu-H/D Distance 1 (Å)	Cu-H/D Distance 2 (Å)	Cu-H/D Distance 3 (Å)
Stryker's Reagent D1 – Metal-deuteride $[DCu\{P(C_6H_5)_3\}]_6$	1.75	1.75	1.89
Stryker's Reagent D2 – Aryl-deuteride $[HCu\{P(C_6D_5)_3\}]_6$	1.67	1.67	1.92

These 2 different copper hydride / deuteride distances indicate that an edge-bridging hydrogen approximation (Figure 36a.) is correct, instead of the face-bridging hydrogen structure (Figure 36b), consistent with the literature.[27/28]

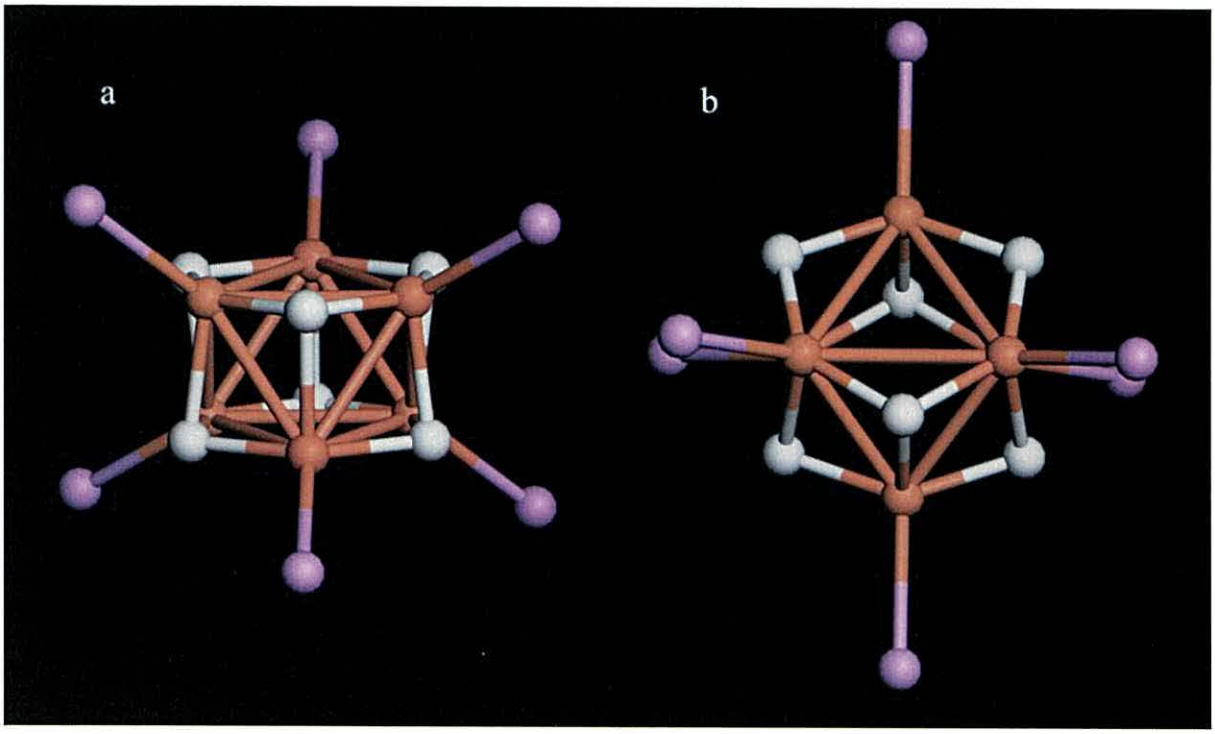

Figure 36. Edge-bridging (a) and face-bridging (b) Stryker's reagent structures.[27/28]

3.3. Conclusion

3.3.1. Copper (I) Hydrides ($CuH.H_2O$ / CuH.py)

(a) Würtz reaction (aqueous)

$$4Cu^{+} + 6H_2PO_2^{-} + 6H_2O \xrightarrow{H^{+}} \boxed{4CuH} + 6H_2PO_3^{-} + 8H^{+}$$

(b) Redox reation of $NaBH_4$ with $CuSO_4$ (aqueous)

$$2Cu_2^{+} + 2BH_4^{-} + 6H_2O \longrightarrow \boxed{2CuH} + 2B(OH)_3 + 2H^{+}\ 5H_2$$

(c) $LiAlH_4$ reduction of CuI (organic)

$$3CuI + LiAlH_4 \longrightarrow \boxed{3CuH} + AlI_3 + LiH$$

Equation 18. (a), (b) and (c) 3 routes to copper hydride.[1/11/7]

Contrary to the literature it is possible to obtain a dried sample of CuH from all three routes by careful aspiration using hydrogen or argon (and presumably other inert gasses e.g. nitrogen), although exothermic decomposition is more likely to occur when drying the aqueously prepared routes (a) and (b) as opposed to the organically prepared route (c). This rapid exothermic combustion (observed when the hydride is placed under a strong vacuum or heated beyond ≈ 45°C) results in the complete copper hydride decomposition to a fine red solid powder identified as Cu_2O (Copper (I) oxide). A slow decomposition (shown in the time interval measured MAPS spectra Figure 13.) occurs at standard room temperatures and pressures and eventually results in full copper hydride decomposition to the black solid CuO (Copper (II) oxide). Indirect quantitative CuH analysis in the literature (hydrogen gas evolution)[57] would have significant error from the copper oxide content as well as the H_2O

shell. The non-metallic nature of CuH reported in the NMR study by Nowak *et al*[23] can most likely be attributed to spectral contributions from the H_2O shell.

The synthetic procedure reported by Mahanti *et al*[11] for the preparation of $CuH.H_2O$ from $NaBH_4$ (b) was found to be incorrect, they state that "the precipitate was mixed with 50 mL of water and boiled for 1 h to dissolve any free boric acid". Any addition of water at temperatures above $\approx$ 45°C results in instant decomposition, confirmed by the visible evolution of gas (hydrogen), addition of 100°C (boiling) H_2O would instantly give the fully oxidized copper product CuO.

Even after the removal of residual H_2O, the expanded high energy region in the INS MAPS spectra of dried CuH Würtz (Figure 17.) shows evidence for O-H, while the residual H_2O bending modes are not apparent, thus confirming the presence of hydroxyls in the outer shell. This is also observed in the SANDALS diffraction spectra in Figure 21. (which compares $CuH.H_2O$, CuH Lit. and water) again confirming the presence of O-H and Cu-H in the sample.

Although prepared via different routes the facile exchange of D_2O for H_2O in the Würtz (a) and $NaBH_4$ (b) samples confirms our basic hypothesis about the structure of copper hydride. It has a crystalline core with a disordered shell of H_2O or pyridine around it. The CuH core is the same in all three routes and adopts the Würtzite structure confirmed from the literature.[19]

The difference in properties observed between Würtz (a) and $NaBH_4$ (b) routes compared to the pyridine route (c) can be attributed to the nature of the shell and also particle size. The aqueous preparations (a) and (b) contain a disordered shell of H_2O and have an approximate particle size of 31 Å (derived using the Scherrer equation from the XRD diffractograms). The soluble CuH.py (c) contains a shell of pyridine attached via the nitrogen and has a significantly smaller particle size of approximately 13 Å, although this could be

much smaller due to the possibility of an agglomerate of particles. This is also confirmed in the synthesis, specifically during filtration using a porous sintered glass filter. The aqueous CuH products were filtered without complications, whilst the CuH.py product became clogged in the sinter due to its significantly smaller particle size now confirmed with XRD. The location of the pyridine shell was confirmed for CuH.py in the vibrational spectra (INS TOSCA & IR Figure 25.) which show a pattern of band shifts corresponding to co-ordinated pyridine and together with the smaller particle size most likely account for its soluble nature in certain organic solvents.[7]

All CuH's were found to be non-stoichiometric which is in agreement with several comments found in the literature. The slight variation between the experimental neutron spectroscopic data compared with that for calculated CuH arises from the theoretical spectra being predicted for CuH_x (x = 1). Figure 37. (below) shows how non-stoichiometry can affect the spectral pattern, which can also be confirmed in the SANDALS spectra shown in Figures 26. & 27. Most likely the compound is a mixture of stoichiometries CuHx (x = 0.5 - 0.9).

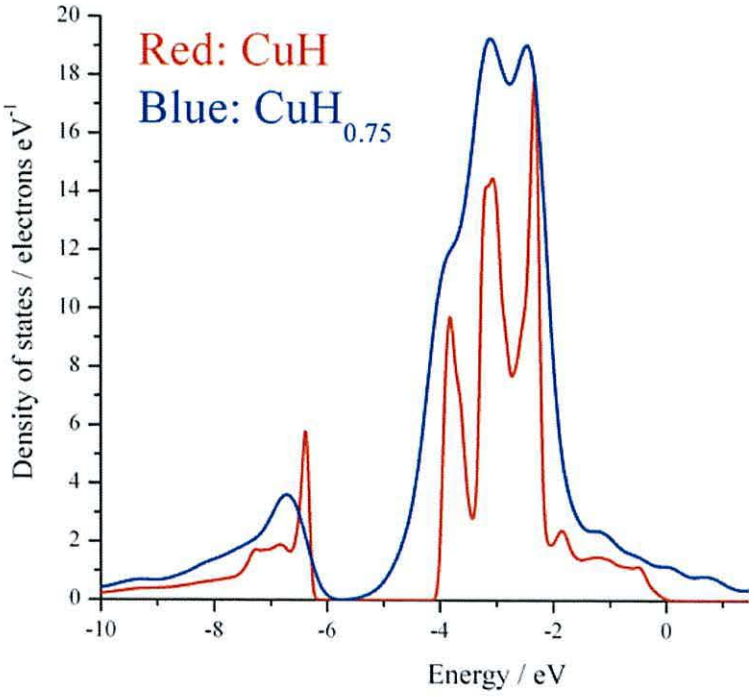

Figure 37. Calculated CuH Vs $CuH_{0.75}$.

3.3.2. Stryker's Reagent – $[HCu\{P(C_6H_5)_3\}]_6$

Although several different preparations of Stryker's reagent are available, the method by Lee and Yun[47] (Equation 20.) requires simple preparation of readily available starting materials and allows synthesis of the deuterated Stryker analogues ($[DCu\{P(C_6H_5)_3\}]_6$ and $[HCu\{P(C_6D_5)_3\}]_6$) to be easily achieved by replacement of the relevant reagent for its deuterated counter-part.

(a) Stryker's Reagent - H (Hydride)

$$Cu(OAc)_2 + PPh_3 + Ph_2SiH_2 \longrightarrow [Ph_3PCuH]_6 + Ph_2Si(OAc)_2$$

(b) Stryker's Reagent - D_1 (Metal - deuteride)

$$Cu(OAc)_2 + PPh_3 + Ph_2SiD_2 \longrightarrow [Ph_3PCuD]_6 + Ph_2Si(OAc)_2$$

(c) Stryker's Reagent - D_2 (Aryl - deuteride)

$$Cu(OAc)_2 + (C_6D_5)_3P + Ph_2SiH_2 \longrightarrow [(C_6D_5)_3PCuH] + Ph_2Si(OAc)_2$$

Equation 20. (a), (b) and (c) Equations for synthesis of Stryker's reagent and its deuterium analogues.

The time taken for the reactions colour change to occur (Blue suspension → Green solution → Red solution Figure 28.) was significantly shorter for the deuterated (b) and (c) preparations when compared to preparation (a) (≈ 30 mins instead of 1 h). This is due to the new, high quality starting materials used in preparations (b) and (c), which contained less traces of water. It can then be concluded that water content can slow the reaction and affect purity and yield.

Samples in solution or samples containing traces of solvent undergo significant decomposition to a green / black waste solid. Care was taken when drying the final products

due to other copper hydride species being exothermically combustible although it was deemed unnecessary caution when trialled on a smaller scale. Completely dry final compounds for (a) - (c), free from by-products and solvent impurities, were achieved in the latter syntheses and no decomposition was observed when stored in an inert atmosphere (argon filled glovebox with < 0.1 ppm of O_2 and H_2O).

Analysis of $[HCu\{P(C_6H_5)_3\}]_6$ (a) by ^1H NMR gave results consistent with the literature[33] and ^2H NMR of $[HCu\{P(C_6D_5)_3\}]_6$) (Figure 33.) also confirmed successful synthesis (as well as the INS data in Figures 34. & 35.).

Location of the hydrogen (or deuterium) bridges in the core cage structure has been achieved from the SANDALS neutron diffraction spectra (Figures 34. & 35.) which also confirm the successful synthesis of the Stryker's deuterated analogues by comparison of experimental and calculated spectral patterns. Analysis of these spectra give 2 different Cu-H / Cu-D distances which implies an edge-bridging location of the H's or D's instead of face-bridging which would show only 1 bond distance as the three bonds would be symmetrical and therefore the same (Figure 38.).

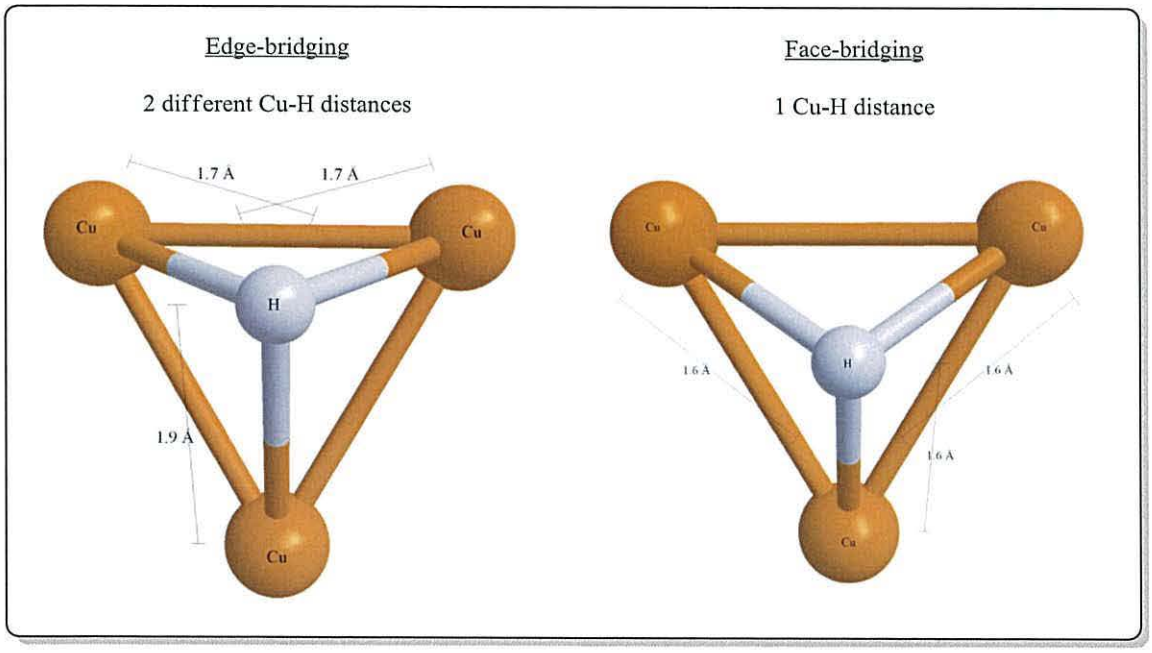

Figure 38. Example bond distances in Edge / Face –bridging structures.

3.4. Experimental

Materials: All chemicals and solvents were obtained from standard UK chemical suppliers (ie. Sigma Aldrich / Alfa Aesar). Dry solvents were obtained via distillation over sodium wire. All compounds were synthesized by variations of the literature. In all cases exclusion of air is essential and achieved with all solvents and aqueous solutions being degassed with argon for 2h prior to use. All reactions steps and subsequent manipulations (including the loading of samples into relevant holders) were performed under either an inert argon atmosphere or a constant blanket of argon gas. Argon filled glove bags and a dry glove box (containing < 1ppm of O_2 and H_2O) were utilised were necessary. **Caution: the dried product may decompose explosively.**

X-ray diffraction: Samples were loaded into silica glass capillaries of internal diameter 1.0mm, and X-ray diffraction (XRD) measurements were made using a Panalytical X'Pert Pro Multi-purpose Diffractometer, running in capillary mode, with a silver anode source (wavelength 0.560885 Å). Measurements were also made on an empty capillary and the empty instrument and a full set of experimental corrections and an absolute normalisation were made using in-house software, GudrunX[58].

Neutron diffraction: Time-of-flight neutron diffraction measurements were performed using the diffractometer, SANDALS[59], at ISIS[60]. The samples were loaded into 2 mm thick plate TiZr cells in an argon glovebox. Data reduction was carried out using the Gudrun[61] package. Simulated radial distribution functions (rdf) were generated with PDFgui.[62]

Inelastic Neutron Scattering (INS) Spectroscopy: INS spectra were recorded with the spectrometers TOSCA[63/64] and MAPS[52/65] at ISIS. The operating principles of the two instruments are described in detail elsewhere.[66] Samples were loaded (in an argon filled

glovebox containing < 0.1ppm of O_2 and H_2O) into aluminum cans, sealed with indium wire and put into a closed cycle cryostat, cooled to ~20 K (liquid helium) and the spectra recorded for 8-12 h.

Nuclear Magnetic Resonance (NMR): All spectra were obtained using Bruker Advance III Ultrashield 400 and 500 Plus NMR machines, particular frequencies for spectra are given, along with the type of deuterated solvent in which they were run.

CuH.H_2O / CuH.D_2O (Würtz route)[1/3]

$$CuSO_4 + H_2SO_4 + H_3PO_2 \longrightarrow CuH_{(ppt)}$$

All solutions, acids and solvents were de-gassed using argon for 1 h prior to use. A mixture of $CuSO_4.5H_2O$ (1 M, 150 mL, 150 mmol) and H_2SO_4 (0.75 M, 30 mL, 22.50 mmol) was added drop wise over 15 mins at 55°C to H_3PO_2 (1.6 M, 600 mL, 956.25 mmol). The reaction mixture changed colour (colourless → pale blue → pale green → olive green → red brown) and was then immediately cooled to 0°C. The mixture was then filtered through a sintered glass filter and the cake subsequently washed with H_2O (250 mL), EtOH (250 mL) and Et_2O (250 mL) with all filtration and washing steps performed under flowing argon. The brown solid CuH product was carefully dried via aspiration (argon) and the CuH product isolated as a red brown solid (11.51 g). The product was immediately placed in an argon environment and sealed into the aluminium sample holder (using indium wire) to prevent decomposition. Approximately half of this solid product was stirred in D_2O (200 ml) at RT overnight and then filtered yielding CuH.D_2O as a brown solid (again all manipulations were performed in an inert atmosphere).

(**CAUTION!** spontaneous and exothermic decomposition possible).

$CuH.H_2O$ / $CuH.D_2O$ ($NaBH_4$ route)[4/11]

$$CuSO_4 + H_2SO_4 + NaBH_4 \longrightarrow CuH_{(ppt)}$$

All solutions, acids and solvents were de-gassed using argon for 1 h prior to use. $CuSO_4.5H_2O$ (40.00 g, 160.19 mmol) was dissolved in the minimum of H_2SO_4 (2 M). $NaBH_4$ (6.06 g, 160.19 mmol) was then added to the solution in small portions and the mixture stirred at 30°C for 2 h under a positive pressure of argon (**CAUTION!** evolution of $H_{2(g)}$). The precipitated brown CuH product was then filtered through a sintered glass filter and washed with several portions of H_2O (3 x 150 mL at RT, 2 x 150 mL at 60°C) followed by EtOH (200 mL) and Et_2O (200 mL) all performed under a blanket of flowing argon. The $CuH.H_2O$ product was dried via aspiration with argon and isolated as a red brown solid (7.8 g), immediately placed into an argon environment and sealed into an aluminium sample holder (using indium wire).

Approximately half was stirred in D_2O (200 mL) at RT overnight and then filtered yielding $CuH.D_2O$ as a brown solid (again all manipulations were performed in an inert atmosphere). (**CAUTION!** spontaneous and exothermic decomposition possible).

CuH.py / CuH.d_5-py (Pyridine route)[6/7]

$$CuI + LiAlH_4 \longrightarrow CuH$$

Under an inert argon atmosphere $LiAlH_4$ (1 M in ether, 14.75 mL, 14.75 mmol) was added drop-wise over 15 mins to a solution of CuI (7.62 g, 40 mmol) in anhydrous pyridine (180 mL). The mixture was stirred at RT for 8 h and then filtered through a pad of Celite® using a sintered glass filter. To the filtrate an equal volume of anhydrous ether was added and the precipitated solution allowed to settle, the supernatant liquid was then decanted / filtered (again using a sintered glass filter) and the process repeated several times or until the supernatant liquid was completely colourless. The final product was filtered (using a sintered glass filter with a medium porosity G02) under a flowing blanket of argon and then dried *in vacuo*. The CuH.py product was isolated as a fine brown solid. The sample was loaded into the aluminium sample holder in a glovebox (< 0.1 ppm of H_2O and O_2) and sealed with indium wire.

Approximately half of the product was re-dissolved in d5-pyridine and stirred at RT overnight in an inert atmosphere. It was then re-precipitated from ether and dried via argon aspiration / *in vacuo* yielding CuH.d5-py as a fine brown solid (again all manipulations were performed in an inert atmosphere).

[(Ph$_3$P)CuH]$_6$ Stryker's Reagent[47]

[(Ph$_3$P)CuH]$_6$

In a Schlenk flask Cu(OAc)$_2$ (1.74 g, 9.53 mmol) and PPh$_3$ (5.00 g, 19.06 mmol) were dissolved in anhydrous benzene (20 mL). To the mixture Ph$_2$SiH$_2$ (2.11 g, 11.44 mmol) was added. After the colour change from a blue suspension → green → dark red solution (≈ 1 h) the reaction mixture was stirred for a further 1 h. The reaction mixture was then concentrated to ½ its volume *in vacuo* upon which the thick bright red/orange suspension was allowed to settle. The system was then filled with argon, anhydrous acetonitrile (50 mL) was carefully layered on top and crystallisation allowed to occur overnight. The red crystals were filtered inside the Schlenk flask using a cannula fitted with a filter apparatus, washed with further portions of anhydrous acetonitrile (5 x 50 mL) and dried under vacuum yielding [Ph$_3$PCuH]$_6$ (2.46 g, 7.53 mmol, 79.0% yield). All filtration and washing steps were performed in an inert argon atmosphere.

δ_H (400 MHz, C_6D_6) δ 7.67 (t, 36H, J = 8.0Hz), 6.95 (t, 18H, J = 7.4Hz), 6.74 (t, 36H, J = 7.5Hz), 3.51 (br s, 6H) ppm.

Deuterated Stryker's Reagent Complexes

[(Ph$_3$P)CuD]$_6$ was prepared via the same method but replacing Ph$_2$SiH$_2$ with deuterated diphenylsilane-d$_2$ Ph$_2$SiD$_2$ (2.13 g, 11.44 mmol).

[(C$_6$D$_6$)$_3$PCuH]$_6$ was prepared via the same method but replacing PPh$_3$ with deuterated triphenylphosphine-d$_{15}$ (C$_6$D$_6$)$_3$P (5.29 g, 19.06 mmol).

3.5. References

1. A. Würtz, *Comptes Rendus*, 1844, **44**, 702.

2. A. Würtz, *Annales de Chimie*, 1844, **3**, 250.

3. N. P. Fitzsimons, W. Jones, and P. J. Herley, *Journal of the Chemical Society, Faraday Transactions*, 1995, **91**, 713.

4. M. W. Travers and R. C. Ray, *Proceedings of the Royal Society A: Mathematical, Physical and Engineering Sciences*, 1912, **87**, 163–179.

5. J. C. Warf and W. Feitknecht, *Helvetica Chimica Acta*, 1950, **33**, 613–639.

6. E. Wiberg and W. Henle, *Z. Naturforsch B*, 1952, **7b**, 250.

7. J. A. Dilts and D. F. Shriver, *Journal of the American Chemical Society*, 1968, **90**, 5769–5772.

8. J. A. Goedkoop and A. F. Andersen, *Acta Crystallographica*, 1955, **8**, 118–119.

9. H. Müller and A. J. Bradley, *Journal of the Chemical Society*, 1926, 1669–1673.

10. Y. Fukai, in *The Metal-Hydrogen System*, Springer-Verlag, Berlin, 1993, p. Chapter 1.

11. M. Dasgupta and M. K. Mahanti, *Oxidation Communications*, 2010, 88–92.

12. G. M. Whitesides, J. S. Filippo, E. R. Stredronsky, and C. P. Casey, *Journal of the American Chemical Society*, 1969, **91**, 6542–6544.

13. T. Yoshida and E. Negishi, *Journal of the Chemical Society, Chemical Communications*, 1974, 762–763.

14. L. Burzyńska, J. Stoch, and Z. Zembura, *Solid State Ionics*, 1990, **38**, 179–186.

15. L. Burzyńska, J. Karp, and Z. Zembura, *Solid State Ionics*, 1994, **73**, 35–40.

16. N. P. Fitzsimons, W. Jones, and P. J. Herley, *Catalysis Letters*, 1992, **15**, 83–94.

17. M. Balooch, M. J. Cardillo, D. R. Miller, and R. E. Stickney, *Surface Science*, 1974, **46**, 358–392.

18. J. M. Campbell and C. T. Campbell, *Surface Science*, 1991, **259**, 1–17.

19. A. J. Elliott, J. Tabatabaei, K. C. Waugh, F. W. Zemicael, R. A. Hadden, and B. Sakakini, *Journal of the Chemical Society, Faraday Transactions*, 1995, **91**, 3659–3662.

20. A. Vaškelis, J. Juškėnas, and J. Jačiauskienė, *Electrochimica Acta*, 1998, **43**, 1061–1066.

21. H. Tanaka, Y. Yamaguchi, S. Sumida, M. Kuroboshi, M. Mochizuki, and S. Torii, *Journal of the Chemical Society, Perkin Transactions 1*, 1999, **3468**, 3463–3468.

22. R. Burtovyy and M. Tkacz, *Solid State Communications*, 2004, **131**, 169–173.

23. B. Nowak, R. Burtovyy, and M. Tkacz, *Journal of Alloys and Compounds*, 2004, **384**, 71–75.

24. R. M. D. Calvi, D. H. Andrews, and W. C. Lineberger, *Chemical Physics Letters*, 2007, **442**, 12–16.

25. P. Hasin and Y. Wu, *Chemical communications (Cambridge, England)*, 2012, **48**, 1302–4.

26. S. A. Bezman, M. R. Churchill, J. A. Osborn, and J. Wormald, *Journal of the American Chemical Society*, 1971, **93**, 2063–2065.

27. M. R. Churchill, S. A. Bezman, J. A. Osborn, and J. Wormald, *Journal of Inorganic Chemistry*, 1972, **11**, 1818–1825.

28. D. M. Ho and R. Bau, *Inorganica Chimica Acta*, 1984, **84**, 213–220.

29. T. H. Lemmen, K. Folting, J. C. Huffman, and K. G. Caulton, *Journal of the American Chemical Society*, 1985, **107**, 7774–7775.

30. R. C. Stevens, M. R. Mclean, R. Bau, and T. F. Koetzle, *Journal of the American Chemical Society*, 1989, **111**, 3412–3413.

31. D. M. Brestensky, D. E. Huseland, C. McGettigan, and J. M. Stryker, *Tetrahedron Letters*, 1988, **29**, 3749–3752.

32. C. F. Albert, P. C. Healy, J. D. Kildea, C. L. Raston, B. W. Skelton, and A. H. White, *Inorganic Chemistry*, 1989, **28**, 1300–1306.

33. P. Chiu, Z. Li, and K. Fung, *Tetrahedron Letters*, 2003, **44**, 455–457.

34. W. S. Mahoney, D. M. Brestensky, and J. M. Stryker, *Journal of the American Chemical Society*, 1988, **110**, 291–293.

35. M. Koenig, J. F. Daeuble, D. M. Brestensky, and J. M. Stryker, *Tetrahedron Letters*, 1990, **31**, 3237–3240.

36. J. M. Stryker and J. F. Daeuble, in *Encyclopedia of Reagents for Organic Synthesis (e-EROS)*, 1991.

37. B. H. Lipshutz, J. Keith, P. Papa, and R. Vivian, *Tetrahedron Letters*, 1998, **39**, 4627–4630.

38. J. X. Chen, J. F. Daeuble, D. M. Brestensky, and J. M. Stryker, *Tetrahedron*, 2000, **56**, 2153–2166.

39. J. X. Chen, J. F. Daeuble, and J. M. Stryker, *Tetrahedron*, 2000, **56**, 2789–2798.

40. P. Chiu, C. P. Szeto, Z. Geng, and K. F. Cheng, *Tetrahedron Letters*, 2001, **42**, 4091–4093.

41. L. Villaescusa Castillo, A. M. D. Lanza, R. Faure, L. Debrauwer, R. Elias, and G. Balansard, *Phytochemistry*, 1995, **40**, 1193–1195.

42. D. C. Sass, V. C. Gomes Heleno, J. L. Callegari Lopes, and M. G. Constantino, *Tetrahedron Letters*, 2008, **49**, 3877–3880.

43. L. Dong, S. Qin, H. Yang, Z. Su, and C. Hu, *Catalysis Science & Technology*, 2012, **2**, 564.

44. W. Dmowski, T. Egami, K. E. Swider-lyons, C. T. Love, and D. R. Rolison, *Journal of Physical Chemistry B*, 2002, **106**, 12677–12683.

45. S. F. Parker, K. Refson, A. C. Hannon, E. R. Barney, S. J. Robertson, and P. Albers, *The Journal of Physical Chemistry C*, 2010, **114**, 14164–14172.

46. E. C. Spencer, N. L. Ross, S. F. Parker, B. F. Woodfield, J. Boerio-Goates, S. J. Smith, R. E. Olsen, a I. Kolesnikov, A. Navrotsky, and C. Ma, *Journal of Physics. Condensed Matter: An Institute of Physics Journal*, 2011, **23**, 205303.

47. D. Lee and J. Yun, *Tetrahedron Letters*, 2005, **46**, 2037–2039.

48. P. J. Herley, N. P. Fitzsimons, and W. Jones, *Journal of the Chemical Society, Faraday Transactions*, 1995, **91**, 719–724.

49. R. Burtovyy, *Thermochimica Acta*, 2000, **363**, 157–163.

50. A. J. Ramirez-Cuesta, *Computer Physics Communications*, 2004, **157**, 226–238.

51. www.isis.stfc.ac.uk/instruments/tosca, 20/2/13.

52. www.isis.stfc.ac.uk/instruments/maps, 20/2/13.

53. http://cds.dl.ac.uk/cds/datasets/crys/icsd/llicsd.html and (Inorganic Cyrstal Structure Database - ICSD).

54. D. T. Lundie, A. R. Mcinroy, R. Marshall, J. M. Winfield, P. Jones, C. C. Dudman, S. F. Parker, C. Mitchell, and D. Lennon, *Journal of Physical Chemistry B*, 2005, **109**, 11592–11601.

55. E. P. Parry, *Journal of Catalysis*, 1963, **2**, 371–379.

56. H. E. Gottlieb, V. Kotlyar, and A. Nudelman, *J. Org. Chem*, 1997, **62**, 7512–7515.

57. G. V Goeden and K. G. Caulton, *Journal of the American Chemical Society*, 1981, **103**, 7354–7355.

58. www.isis.stfc.ac.uk/support-laboratories/xrd/data-analysis/xrd-data-analysis9203.html, 25/2/13.

59. www.isis.stfc.ac.uk/instruments/sandals, 25/2/13.

60. www.isis.stfc.ac.uk, 25/2/13.

61. www.isis.stfc.ac.uk/instruments/sandals/data-analysis/gudrun8864.html, 25/2/13.

62. C. L. Farrow, P. Juhas, J. W. Liu, D. Bryndin, E. S. Božin, J. Bloch, T. Proffen, and S. J. L. Billinge, *Journal of physics. Condensed matter : an Institute of Physics journal*, 2007, **19**, 335219.

63. F. P. Ricci, F. Sacchetti, M. Zoppi, S. F. Parker, C. J. Carlile, J. Tomkinson, R. J. Newport, and C. Andreani, *Physica B: Condensed Materials*, 1998, **241**, 154–156.

64. D. Colognesi, M. Celli, F. Cilloco, R. J. Newport, S. F. Parker, F. Sacchetti, J. Tomkinson, V. Rossi-Albertini, and M. Zoppi, *Applied Physics A: Materials Science and Processing*, 2002, **74**, 64–66.

65. S. F. Parker, D. Lennon, and P. W. Albers, *Applied Spectroscopy*, 2011, **65**, 1325–1341.

66. P. C. H. Mitchell, S. F. Parker, A. J. Ramirez-Cuesta, and J. Tomkinson, *Vibrational Spectroscopy with Neutrons, with Applications in Chemistry,Biology, Materials Science and Catalysis*, World Scientific, Singapore, 2005.

Chapter 4: Synthesis and Neutron Characterisation of Organometallic Catalysts

4.1. Introduction

Transition metal catalysed cross-coupling reactions[1] involving the formation of carbon-carbon and carbon-heteroatom bonds have had a massive influence in organic synthesis since the 1970's.[2/3] Recently, transition metal catalysts (M = Ni, Pd and to a lesser extent Pt) in combination with organic ligands[4] can provide pathways to complex molecules, drugs and materials with excellent yields and e.e.'s.[5/6] These reactions involve organometallic reagents with a variety of functionality (alkyl, aryl, allyl, vinyl) but with the coupling partner generally containing sp and sp^2 carbon based compounds (alkynes, alkenes and arenes).

These sp and sp^2 carbon based compounds give rise to complications such as unwanted side-reactions. Various studies and development of novel catalytic systems (such as those involving π-carbon ligands eg. π-allyl groups) are now aimed at reducing by products resulting from these undesirable side-reactions such as β-Hydride elimination[7] (common in transition metal alkyl reactions) and these catalysts can become useful and versatile assets to all chemists, be it industrial or academic.[8/9]

Studies into the structure and mechanisms of organometallic complexes have been greatly advanced by the invention and or evolution of techniques such as NMR, laser Raman / FT-IR spectroscopy and more recently inelastic neutron spectroscopy[10/11] or diffraction[12] applied in conjunction with computational studies.

4.1.1. *Bis*-π-allyl Metal complexes (M = Ni, Pd)

In 1961 in the chemical journal *Angewandte Chemie* (German Language verison) Günther Wilke and his student Borislav Bogdanovič published the synthesis of *bis*(π-allyl) Nickel **1** (Figure 1). This had previously been reported by Bodanovič in his PhD thesis, but this is the earliest published account.

Mit diesem Ziel wurde wasserfreies Nickelbromid in Äther mit Allylmagnesiumchlorid umgesetzt. Bei −10 °C setzte augenblicklich eine Reaktion ein und man erhielt eine gelborange-farbige Lösung. Äther und Reaktionsprodukt wurden im Vakuum in eine auf −80 °C gekühlte Vorlage abgezogen. Bereits mit den ersten Äthermengen ging eine hellgelbe Verbindung über. Vom Kondensat wurde der Äther bei 200 mm Hg an einer Tieftemperaturkolonne (Kp 3 bis 5 °C) abdestilliert. Im Rückstand reicherte sich eine kristallisierte Verbindung an, die im Hochvakuum bei −80 °C von restlichem Äther befreit und dann bei tiefer Temperatur aus Pentan umkristallisiert wurde.

Figure 1. Extract from *Angewandte Chemie* 1961.[13]

Translated as "the goal of anhydrous Nickel Chloride reacting in Ether with Allylmagnesiumchloride has been implemented. At -10°C an immediate reaction to yield a yellow-orange coloured solution. Ether and the reaction product were removed under vacuum into to a cooled (-80°C) flask, with the first volumes of ether came a pale yellow compound. The residue was enriched to a crystalline compound under high vacuum at -80°C, removed from residual ether and recrystallized from pentane at this low temperature."[13]

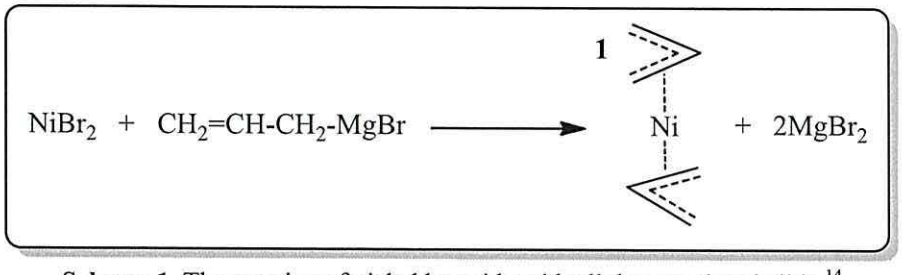

Scheme 1. The reaction of nickel bromide with allylmagnesium halide.[14]

They went on to say that the yellow-orange crystalline needles have the composition NiC_6H_{10} and melt at ≈ 1°C, that they ignite spontaneously in air, are attacked by water and are soluble in hydrocarbons. Analysed by mass spectrometry they reported the structure seen in Figure 2.

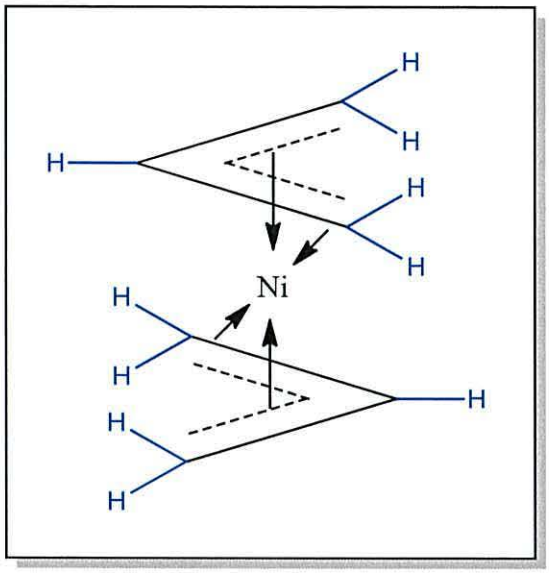

Figure 2. *bis*(π-allyl) Nickel as represented by Wilke and Bogdanovič in 1961.[13]

In 1963 in a paper by Wilke *et al* (including Bogdanovič) on the cyclo-oligomerization (or cyclic polymerization) of butadienes involving transition metal π-complexes, a scheme was proposed showing how *bis*(π-allyl) Nickel can be used to generate 1,5-hexadienes (Scheme 2).[15]

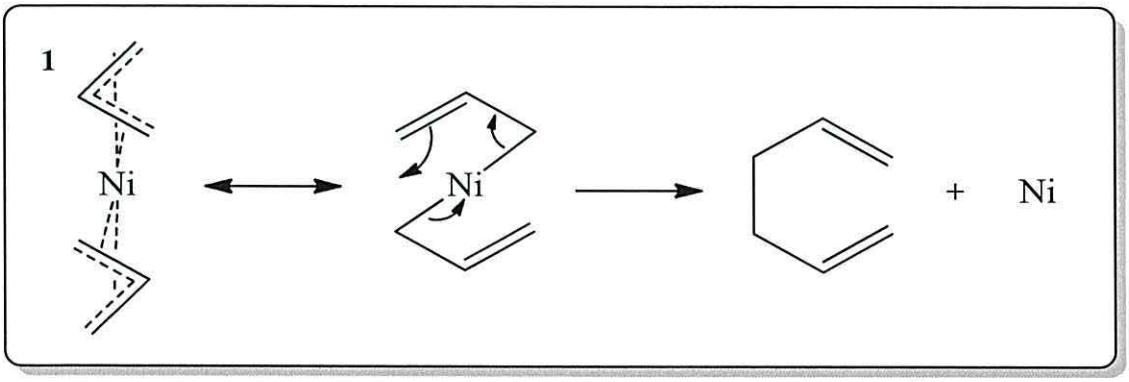

Scheme 2. Formation of 1,5-hexadienes from *bis*(π-allyl) Nickel.[15]

Also in 1963 was the first reported isolation of the analogous compound *bis*(π-allyl) Palladium **2** in a dissertation by Keim, which was prepared similarly to its Ni based analogoue.[16] This *bis*(π-allyl) Pd complex was also described in an extensive 1966 study by Wilke *et al* on transition metal allyl systems. As well as NiA_2 and PdA_2 (A = allyl or C_3H_5) also described were the syntheses of pure TM allyl compounds such as those shown in Table 1.

Table 1. Pure allyl compounds of the transition metals (in a tabular periodic table d-block representation).[14]

Group IIA	Group IVB	Group VB	Group VIB	Group VIIIB			Group IIB
MgA_2 Colourless							
	TiA? Brown	**VA_3** Brown	**CrA_3** Red	**FeA_3** Gold Orange	**CoA_3** Red Gold	**NiA_2** Light Yellow	**ZnA_2** Colourless
			$(CrA_2)_2$ Red Brown				
	ZrA_4 Red	**NbA_4** Green	**MoA_4** Green			**PdA_2** Bright Yellow	
			$(MoA_2)_2$ Dark Green				
		TaA_4 Green	**WA_4** Light Brown			**PtA_2** White	
	ThA_4 Light Yellow						

Included in the paper were investigations into the properties and reactions of these new compounds and also details of the structure and bonding. Significant emphasis however was put into the catalytic processes involved with Ni and Pd *bis*-π-allyl complexes, with Pd-$allyl_2$ being described as different in colour, significantly more stable as well as exhibiting different catalytic properties, specifically in relation to the cyclotrimerization of butadiene to cyclododecatriene (Scheme 3.), in comparison to Ni-$allyl_2$.[14]

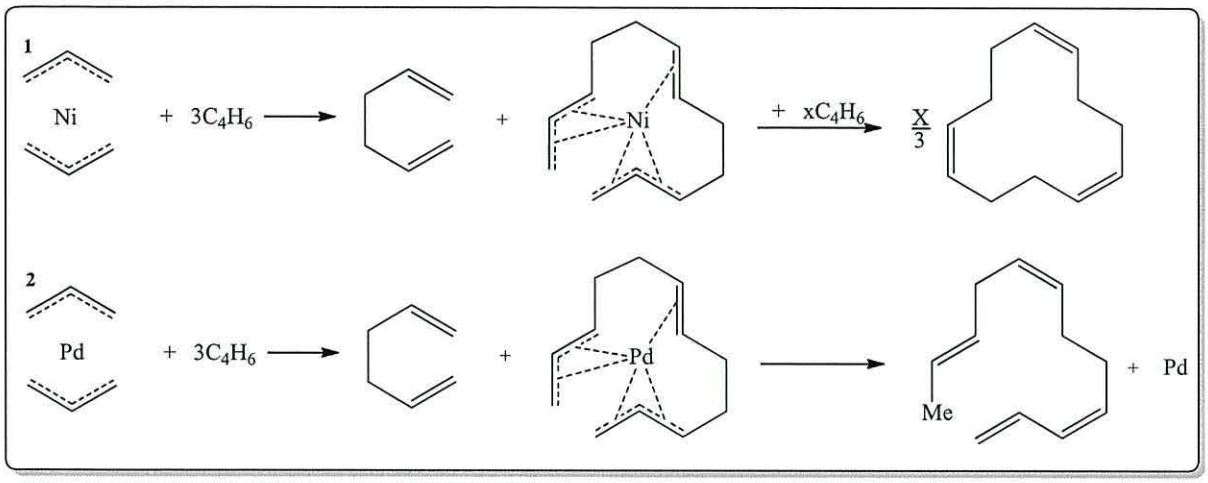

Scheme 3. The catalytic preparation of (Ni-allyl2 → cyclododecatriene) and (Pd-allyl2 → *n*-dodecatetraene).

The Ni-allyl$_2$ was found to be more active (and at lower temperatures) than the analogous Pd complex and was shown to catalytically produce cyclododecatriene where as the Pd-allyl$_2$ complex only produced *n*-dodecatetraene and at elevated temperatures resulted in the elimination of elemental palladium.

In 1967 Wilke, Bogdanovič and Bönnemann published a description of the *cis*- and *trans*- isomeric forms of *bis*(π-allyl)Ni using ^{1}H NMR and investigated the 180° rotation of the allyl groups to the σ-bond axis. The isomerism was described as temperature dependant with the sterically most stable (*cis*) arrangement being found at around 10°C.[17]

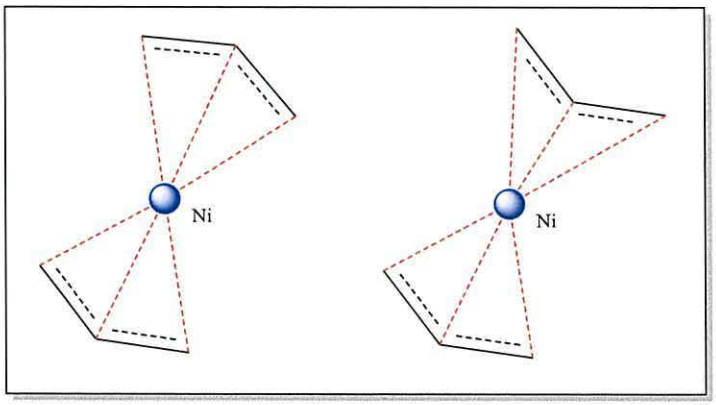

Figure 3. *Cis*- and *trans*- representations of *bis*(π-allyl) Nickel.[17]

Also in 1967 Becconsall and O'Brien published a similar paper investigating the "temperature dependence of the NMR spectrum of palladium bis-π-allyl".[18] They also found that the *cis* / *trans* arrangements exchange in solutions at varying temperatures but were unable to determine a mechanism for this process.

In 1970 O'Brien published a more detailed NMR study of π-allyl complexes in which they described the spectra of $Ni(C_3H_5)_2$ and $Pd(C_3H_5)_2$ to consist of two AM_2X_2 patterns (in unequal amounts) resulting from an equilibrium mixture of the two isomeric forms (*cis* and *trans*). Interestingly the structure of $Pt(C_3H_5)_2$ could not be described in terms of the symmetrical π-allyl ligands (as seen in Pd / Ni -$allyl_2$) but instead they proposed an asymmetric structure containing σ- and π- bonding (Figure 4.).[19]

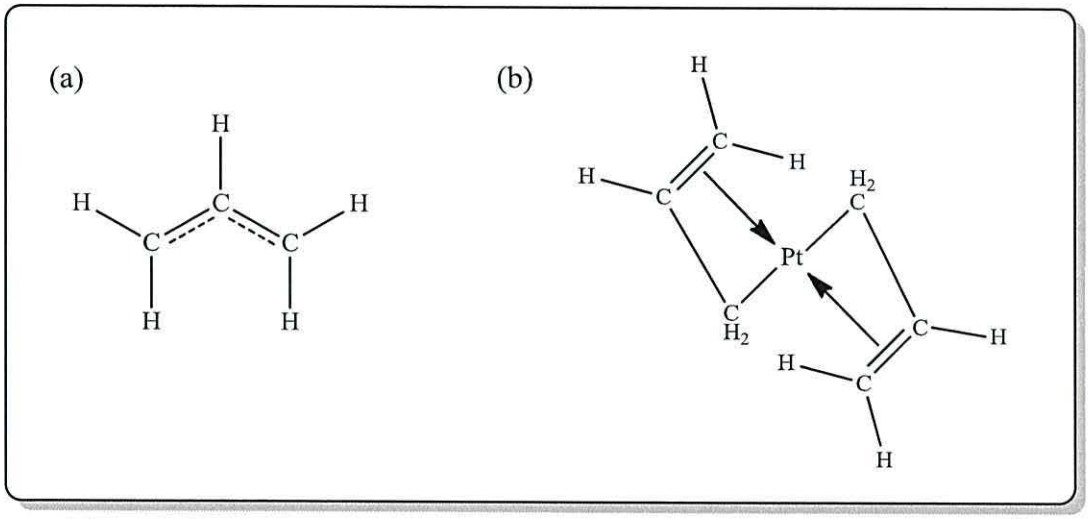

Figure 4. (a) Symmetrical π-allyl ligand. (b) Assymetrical σ- and π- bonded $Pt(C_3H_5)_2$.[19]

In a paper published in the *Journal of Organometallic Chemistry* in 1980 Wilke *et al* gave detailed NMR and IR / Raman studies into a series of $(\eta^3\text{-allyl})_2$ metal complexes.[20] Using IR / Raman spectroscopy they gave the vibrational frequencies for the different hapticities found in these complexes. Absorptions at ≈ 1600cm^1 were attributed to a η^1-allyl group and one at ≈ 1520cm^{-1} to a η^3-allyl group. They also considered an intramolecular fluxional process which had also been observed in complexes of Fe, Mo and W[21] (Figure 5.).

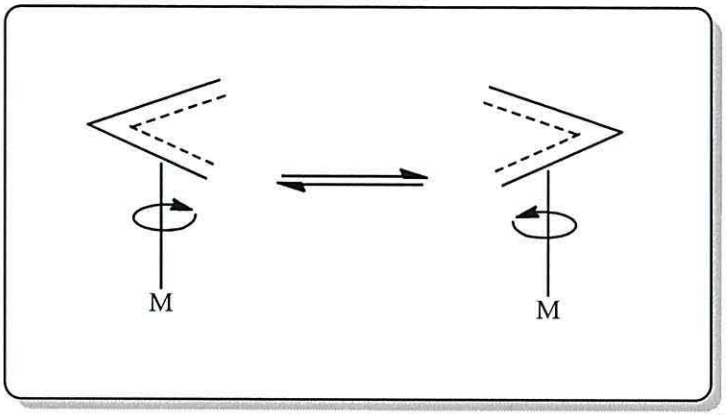

Figure 5. Rotation of the η^3-allyl group about the metal-allyl axis.[21]

However, in a paper published by Hoffmann *et al,* for the $(\eta^3C_3H_5)_2Ni$ complex qualitative molecular orbital calculations indicated that such a rotation about the metal-allyl axis is symmetry forbidden and therefore a high energy process.[22] They however go on to conclude that this dynamic process which interconvert's these isomers (ie. *cis* ←→ *trans*) becomes important only at elevated temperatures (which is in agreement with the temperature dependent NMR studies previously described) but state that "there is no evidence that this process is a simple rotation around the coordination axis".[22]

This allyl arrangement was again confirmed in a study by Wilke *et al* who also showed that the soluble $(\eta^3$-allyl$)_2$M complexes exist as a mixture of isomers (*cis / trans* and *anti / syn*). They also report on the increasing NMR chemical shifts of the order Pt < Ni < Pd.[20]

Recently synthesis of Pd(π-allyl)$_2$ has been achieved in a multi-step synthetic route starting from $PdCl_2$. Although the number of reaction steps is larger, the ease and efficiency in preparation of the Pd(π-allyl)$_2$ is greatly increased. $PdCl_2$ was shown to be converted into $PdCl_2(MeCN)_2$ by reflux in 100% acetonitrile followed by precipitation with petrol, as described in a 1984 paper by Michelin *et al.*[23] Generation of a *mono*-(π-allyl)-palladium(II)

chloride dimer complex **4** from $PdCl_2(MeCN)_2$ **3** was proposed by Hosokawa *et al* in 1999 and is shown in Scheme 4.[24]

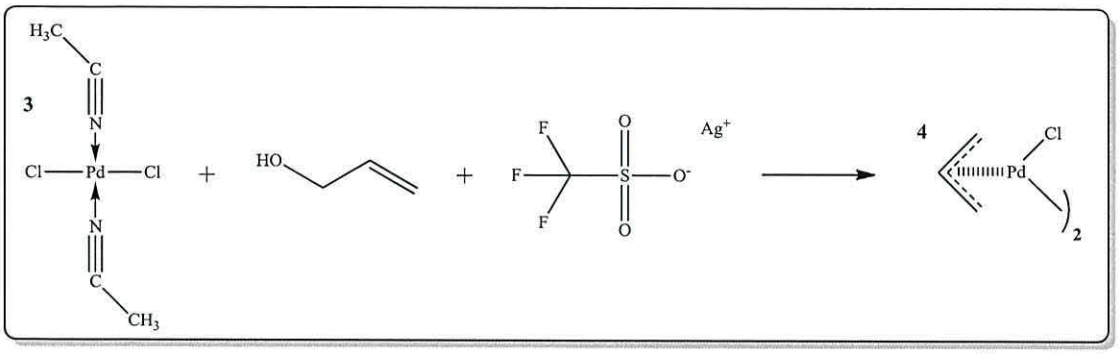

Scheme 4. Synthesis of a *mono*-(π-allyl)-palladium(II) chloride dimer complex.[24]

The final step in the synthesis of $Pd(\pi\text{-allyl})_2$ **2** was published in 2001 by Walther *et al* in the *European Journal of Inorganic Chemistry* and involved the reaction of dimer **4** with the Grignard reagent allylmagnesium chloride in THF at -30°C followed by extraction with pentane.[25] This method was referenced however to a 1963 patent by G. Wilke.[26]

Transition metal-catalysed cross-coupling reactions of organic halides are some of the most important carbon-carbon bond forming reactions known, between a variety of sp, sp^2 and sp^3 hybridized carbon atoms.[1] The use of $(\eta^3\text{-allyl})_2M$ (M = Pd, Ni) as catalysts in cross-coupling reactions give some of the best results, in terms of their yields and selectivities and also that they proceed without the presence of butadienes.

In a 2007 study by Kambe *et al* it was found that the presence of the two allyl ligands are essential to attain high product yields in the Nickel and Palladium catalysed cross-coupling of alkyl bromides (or tosylates) with Grignard reagents (Table 2.).[27]

Table 2. *Bis*-(η^3-allyl)metal catalysed cross-coupling reaction.[27]

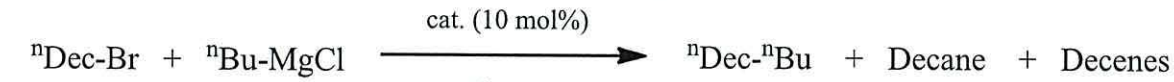

Catalyst	x	y	z
$PdCl_2$	3	54	26
$(PPh_3)_2PdCl_2$	2	1	1
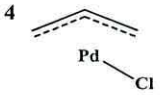	10	26	23
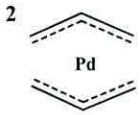	58	13	12
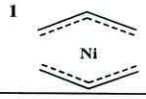	94	4	2

As well as discerning the importance of the two allyl ligands, the high yields and selectivities of the *bis*-allyl catalysts also showed that (as previously thought) the presence of an ethylene tether is not required (Figure 6).

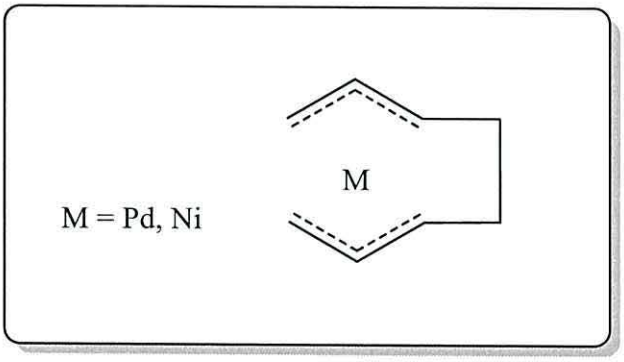

Figure 6. Tethered (CH_2-CH_2) *bis*-(allyl) metal complex.

It is well documented that transition metal alkyls are prone to β-hydride elimination reactions that produce undesirable products.[28] Methods to avoid this process include using a catalyst that delivers the desired compounds, the use of reagents that do not contain β-

hydrogen centres in the first place such as methyl and neopentyl's, or to use substrates that would produce strained alkene β-hydride elimination products such as metal complexes containing norbornyl ligands.[29]

More recent advances include "the use of ligands that never permit the formation of a metal-alkyl intermediate that has a fully vacant d-orbital" or ligands that produce a metal-alkyl intermediate that even with the correct electron count for β-hydride elimination can never attain the required geometry.[4] Despite the difficulties involved in finding and utilising such ligands, due to the nature of the metal co-ordinated sphere under catalytic conditions being uncontrollable and unpredictable, progress has been made in identifying said ligands.

It has also been reported that yields for alkyl-alkyl cross couplings involving Pd catalysts dropped by over 20% when NMP (*N*-methyl-2-pyrrolidone) was removed from the solvent,[30] with similar amide effects also being observed by Organ *et al.*[31]

4.1.2. Terpyridines (TPY's)

In 2006 Vicic *et al* reported a Ni-terpyridyl catalysed alkyl-alkyl cross-coupling reaction that ran without the use of amide additives in the solvent such as NMP as reported in previous systems (Scheme 5).[4]

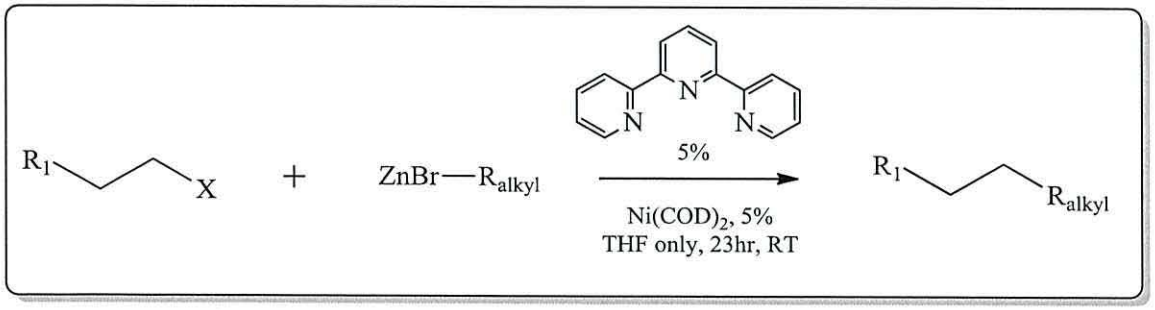

Scheme 5. Ni/terpyridine-catalyzed alkyl-alkyl cross-coupling reaction without amide additives.

Terpyridine (also known as tripyridyl, 2,6-bis(2-pyridyl)pyridine and abbreviated as TPY) was first synthesised in 1932 by Morgan and Burstall and was obtained from the residue left from the reaction of pyridine with iron(III) chloride during investigations into

other polypyridyl compounds (predominantly dipyridyls). They also described metal complexes derived from the co-ordination of terpyridine to platinum and ruthenium.[32/33/34] However the low yielding extraction of reaction residues was not a particularly efficient synthetic route to TPY and improvements to its synthesis (including substituted terpyridines) were published later.

In 1956 Case and Kasper reported on the significantly more efficient synthesis of TPY's with a general procedure shown in Scheme 6.[35]

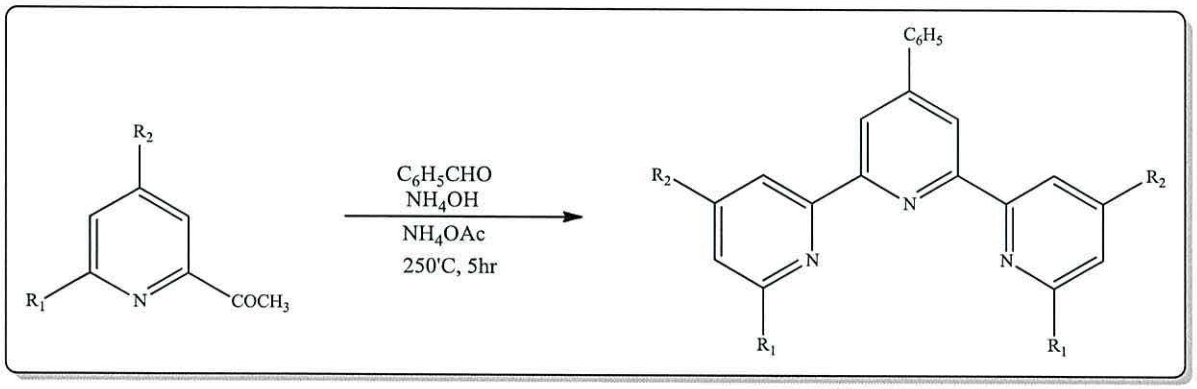

Scheme 6. Procedure for synthesis of TPY's.[35]

A similar three step reaction scheme was proposed by Kröhnke in 1976[36] (and later improved upon by Calzaferri and Spahni in 1984)[37] which gave TPY's with higher purities and dramatically improved yields. The TPY's were formed via a ring assembly reaction (now known as the Kröhnke condensation) and involve *N*-heteropyridinium salts and a subsequent ammonia condensation reaction with an enone (Scheme 7).

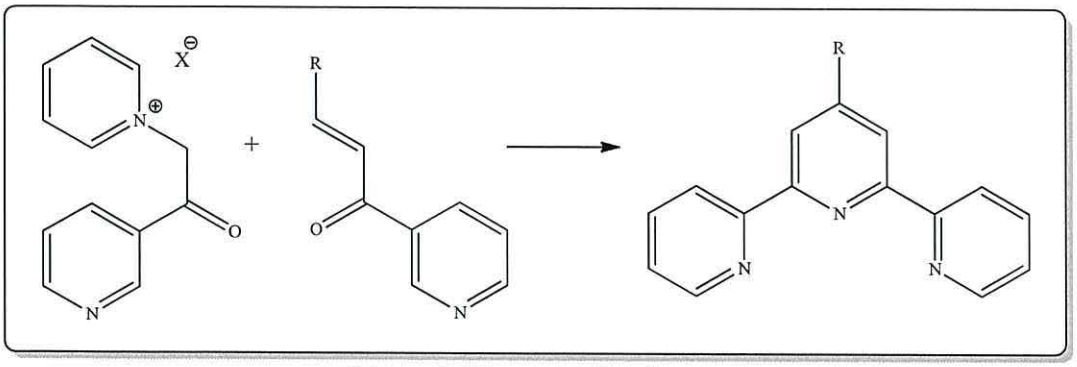

Scheme 7. Ring assembly of TPY's.

Other methodologies related to the synthesis of TPY's include the construction of 1,5-diketones and their subsequent ring closure (Scheme 8a. Lewis *et al* 1982)[38], an α-oxoketene dithioacetal procedure (Scheme 8b. Potts *et al* 1987)[39] and a similar route involving the condensation reaction of a (dimethylamino)enone with the enolate of 2-acetylpyridine (Scheme 8c. Jameson & Guise 1991)[40].

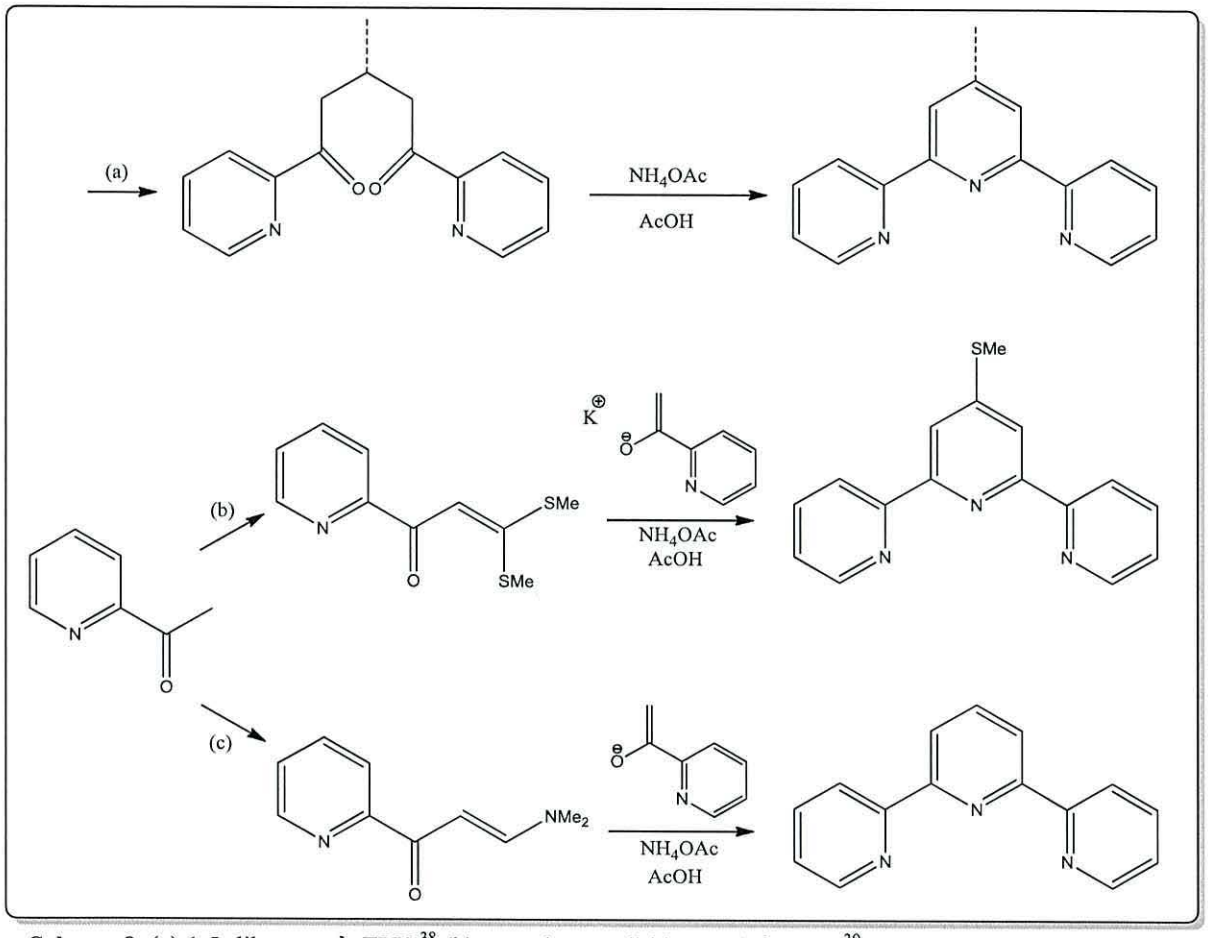

Scheme 8. (a) 1,5-diketone → TPY;[38] (b) α-oxoketene dithioacetal → TPY;[39] (c) (dimethylamino)enone → TPY.[40]

Due to the ability of the terpyridyl ligand system to stabilize complexes of a wide range of transition metal ions, much research went into the synthesis of substituted terpyridine derivatives. Their applications are not just limited to cross-coupling catalysis, but TPY's also exhibit special redox and photophysical properties that depend on the electronic influence of the substituents and have been used in photochemistry for the design of luminescent devices and as sensitisers for light-to-electricity conversion.[41/42]

The use of functionalised TPY's has also been applied to clinical and biochemical research including colorimetric metal determination,[43] DNA binding agents[44] and anti-tumor research.[45]

However the terpyridyl ligands affinity for forming complexes with nickel, paved the way for much research into the mechanism of nickel-mediated cross-coupling reactions by varying the Ni-terpyridyl's substituents. Vicic *et al* studied a variety of these ligand complexes (Figure 7) for their catalytic ability, with the most interesting results given in Table 3.[4]

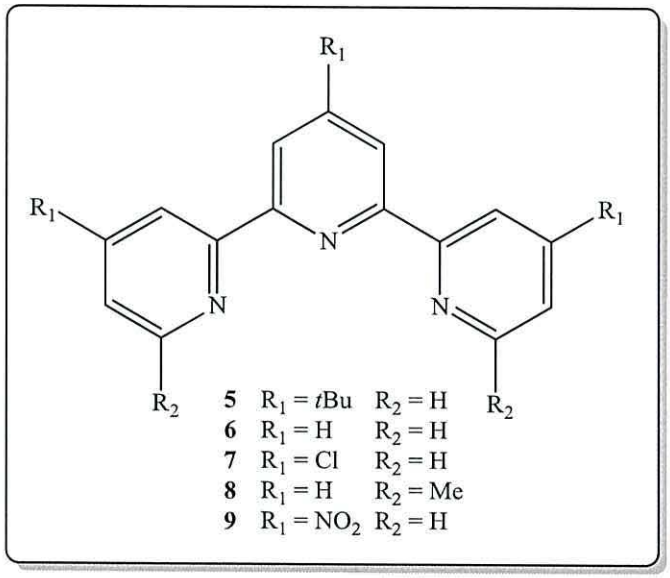

Figure 7. Ligands used in catalytic study.

Table 3. Ligands effects on yields of alkyl-alkyl cross-couplings (active catalyst used was $LNiI_2$).[4]

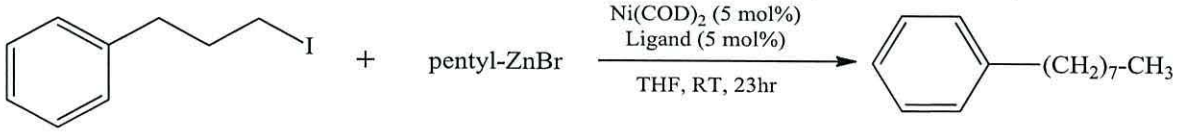

Entry	Ligand	% Yield
1	**5**	98
2	**6**	60
3	**7**	19
4	**8**	6
5	**9**	0

A range of cross-coupling yields were observed, TPY-*t*Bu gave the highest (Entry 1. 98%) and TPY-NO_2 giving no cross-coupling product at all (Entry 5. 0%).

4.1.3. Pd-NHC (NHC = *N*–Heterocyclic Carbene) PEPPSI Precatalysts

Palladium catalysed cross-coupling reactions are well documented powerful tools in carbon-carbon bond formations.[46] Coupling reactions with organometallic reagents were well studied, however alkyl-alkyl couplings were proven to be harder to achieve.

In the early 2000's Fu *et al* demonstrated how phosphine stabilised palladium compounds could act as effective catalysts for alkyl-alkyl cross-coupling reactions under Negishi and Suzuki conditions.[30/47] Problems encountered with such coupling reactions (specifically alkyl-halides with an alkyl-organometallic reagent) were the reluctance of saturated carbon-halogen bonds to undergo oxidative addition (OA – a key step in the catalytic cycle of alkyl-alkyl cross-coupling reactions) and also their tendencies to form unwanted β-hydride elimination products from these OA intermediates.

In 1968 Öfele described the metal co-ordination chemistry of *N*-heterocyclic carbenes (NHC's).[48] They were shown to form complexes with virtually all transition metals and also some main group elements (Be, S and I). Early attempts to apply NHC ligand stabilised Pd catalysts (Pd-NHC's) to alkyl-alkyl cross-coupling reactions gave disappointingly low yields.[49] However in a 2005 paper by Organ *et al* a Pd-NHC catalytic system was shown to achieve Negishi type cross-couplings at room temperature with a wide range of functional group compatibility (Scheme 9).[31]

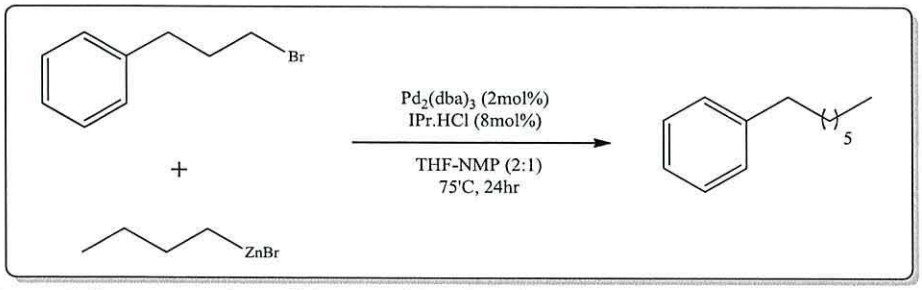

Scheme 9. Reagents and conditions used for the Pd-NHC catalysed cross-coupling reaction.

Due to the highly reactive / sensitive nature of active carbenes the Pd-NHC system was generated *in situ* using the protocol shown in Scheme 9. with structures for $Pd_2(dba)_3$ and IPr.HCl shown in Figure 8.

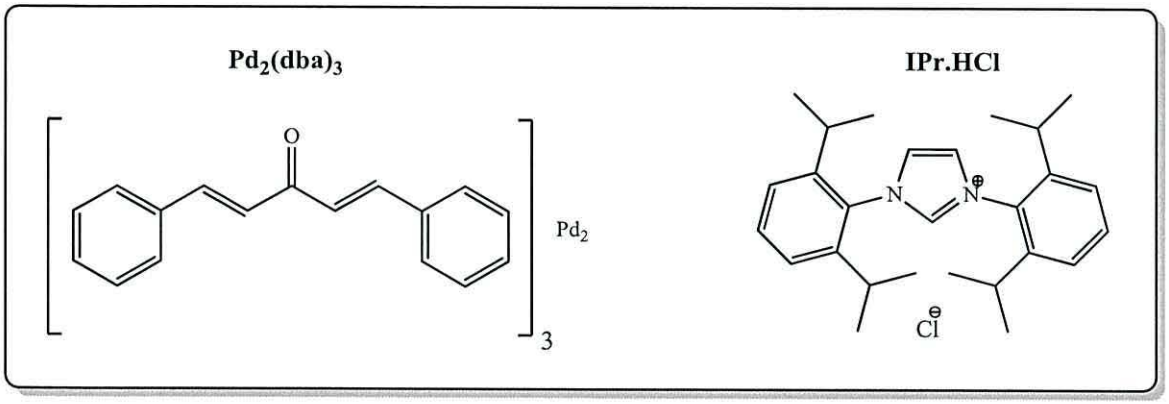

Figure 8. Structures of reagents from Scheme 9, for the *in situ* generation of Pd-NHC.

The necessity of handling NHC's in highly anhydrous conditions was easily overcome by the formation of an air / moisture stable Pd-NHC complex.[50] The proposed structure of the active catalyst was described as monoligated Pd-NHC complex with the synthesis and structure shown in Scheme 10.[51]

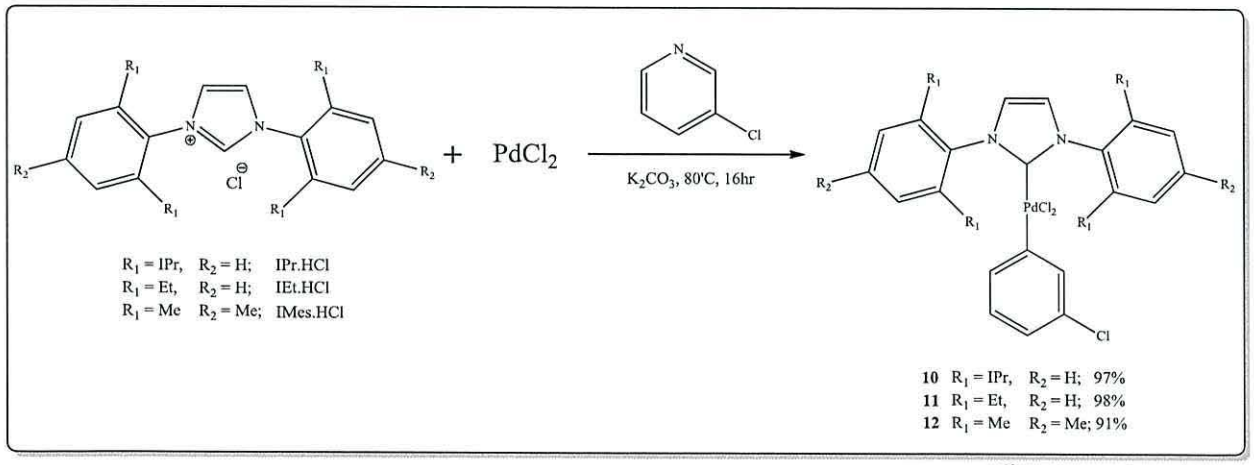

Scheme 10. Synthesis of NHC-$PdCl_2$-3-chloropyridine complexes **10 - 12**.[50]

These Pd-NHC's have become widely used in academia and industry and have been given the acronym PEPPSI (Pyridine-enhanced precatalyst preparation, stabilization and initiation)[52] with generally the best yields being achieved using the PEPPSI-IPr (IPr =

diisopropyl- phenylimidazolium) derivative. These precatalysts are easily synthesised, stable to air and moisture, exhibit high activity with good functional group tolerance and became the first compounds to surpass "related phosphine-ligated Negishi processes both in activity and use".[52]

4.1.4. Aims & Hypothesis

4.1.4.1. Synthesis and Neutron Characterisation of *bis*(π-allyl) Metal Compounds

Synthesis of the highly reactive and moisture / air sensitive *bis*-π-allyl Ni / Pd compounds (**1** & **2** Figure 9.) and their prerequisite intermediates, will be undertaken in order to acquire the multi-gram quantities (> 2 g) of the compounds needed to obtain neutron spectra with sufficient resolution.

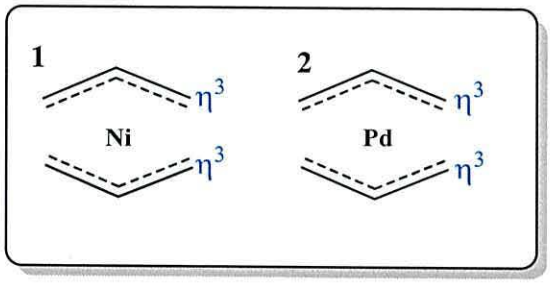

Figure 9. Structure of Ni **1** / Pd **2** *bis*-π-allyl compounds.

4.1.4.2. Synthesis and Neutron Spectroscopy of active Ni-Terpyridyl complexes ($LNiI_2$)

Terpyrdyl ligands **5** - **8** will be obtained commercially and converted to their "active catalyst" forms (**13** – **16** Figure 10.) by reaction with $Ni(COD)_2$ and I_2. INS spectra will be obtained for the TPY's and also their active Ni-Terpyridyl complexes. Although synthesis of these active catalyst complexes has been previously described[4] the reactions will be scaled up in order to again obtain the large quantities needed for neutron spectra with sufficient resolution.

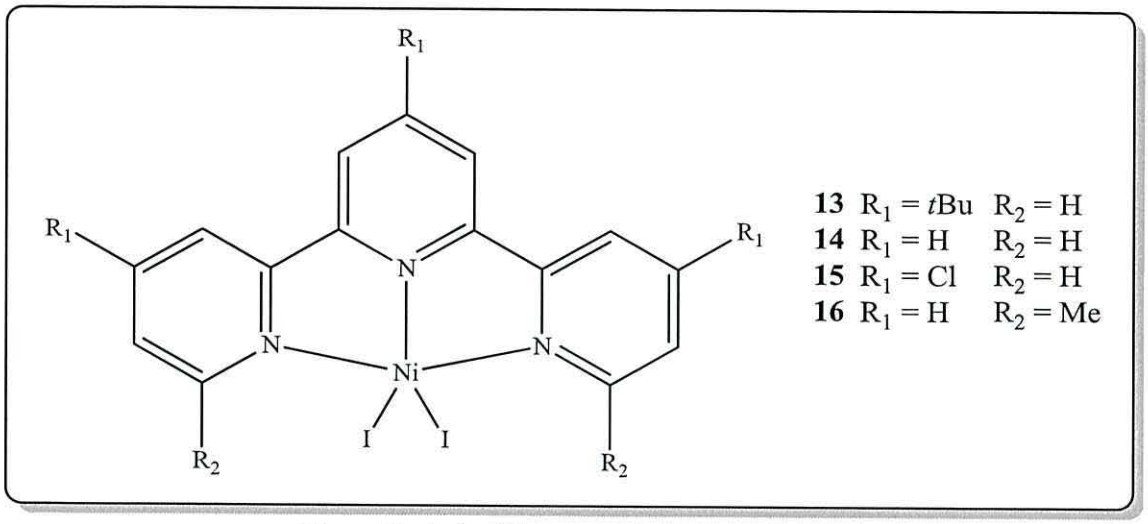

Figure 10. Active Ni-terpyridyl complexes ($LNiI_2$).

Although various homogenous cross-coupling catalytic studies have been performed on these 2 systems (π-allyl and TPY) it is common practice to generate the active catalysts *in situ.* With respect to the π-allyl systems it is due to their highly reactive nature and their sensitivity to moisture and air. Manipulation of relatively large (when compared to the *in situ* generated 10 mol% amounts used in catalytic testing) pure solid quantities of π-allyl complexes **1** & **2** will be performed in an argon filled glovebox at temperatures < -10°C as "Explosions are possible!".[25] Although the TPY series (**5** – **8**) and their active Ni complexes (**13** – **16**) are significantly more stable, synthesis of multi-gram quantities are complex and not cost effective.

Neutron spectroscopic data from these two different homogenous cross-coupling catalysts with be compared to previously obtained neutron spectral results on the active Palladium Precatalyst Pd-NHC PEPPSI (Pyridine-enhanced precatalyst preparation, stabilization and initiation) in its high yielding (PEPPSI-IPr **10**; IPr = diisopropylphenylimidazolium derivative) and low yielding (PEPPSI-IMes **12**; IMes = 1,3-bis(mesityl)-4,5-dihydroimidazolium) forms (see Figure 11).

Comparison of all INS spectra, specifically the vibrational signals from the low energy region (< 800 cm^{-1}), of high / low yielding forms (Figure 11.) of all catalysts is ongoing by project collaborators (Chass group, Queen Mary, University of London) and will then be combined with their theoretical computational research into low energy molecular vibrations being responsible for catalytic efficiency.

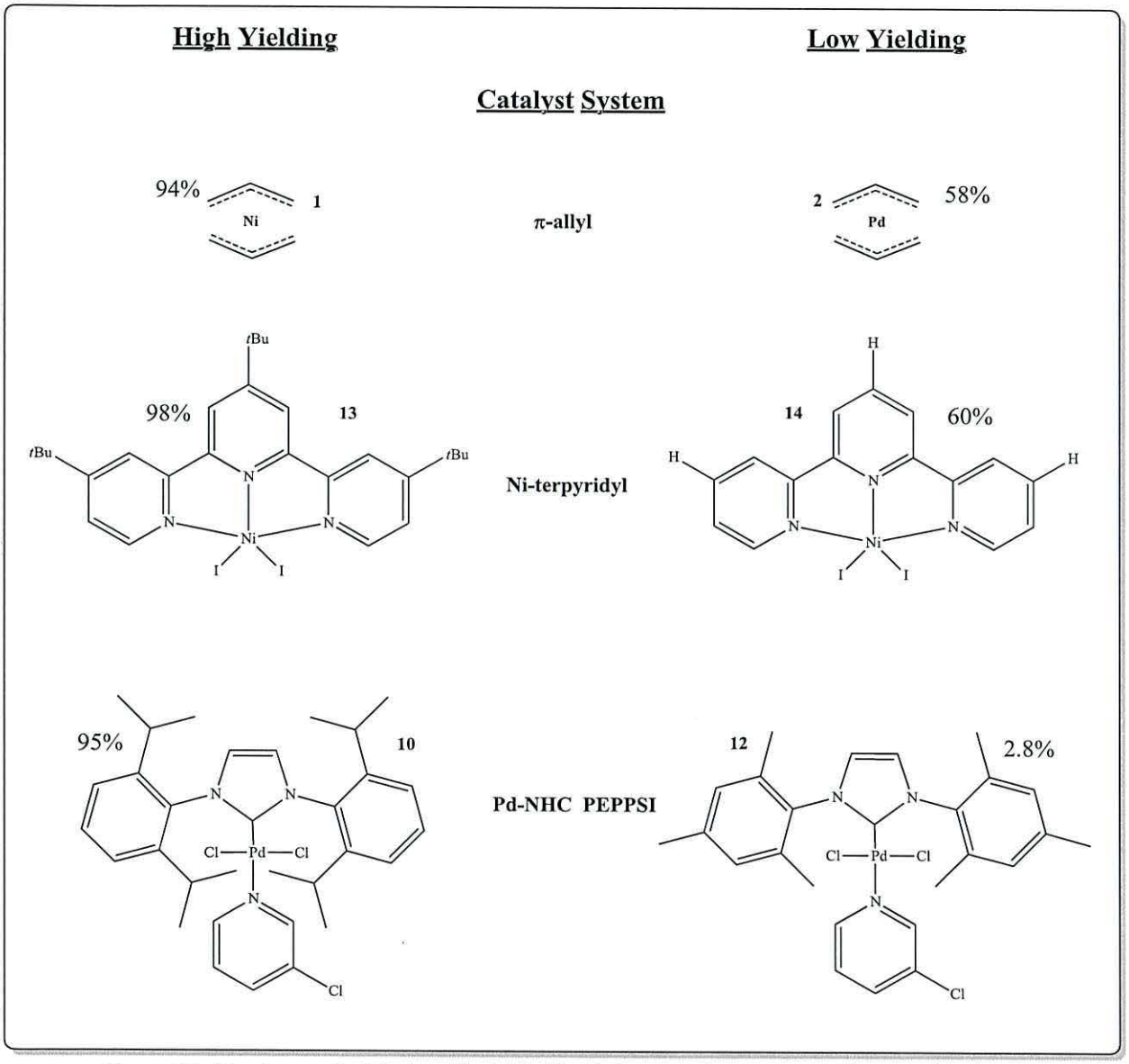

Figure 11. Structures of catalysts with yields (for their respective cross-coupling reactions).

4.2. Results and Discussion

4.2.1. Synthesis & Neutron Spectroscopy of Organometallic Catalysts and Ligands

Target compounds Ni(π-allyl)$_2$ **1** and Pd(π-allyl)$_2$ **2** have been shown to catalyse cross-coupling reactions (Figure 12.) with significant proficiency[1] (see Introduction).

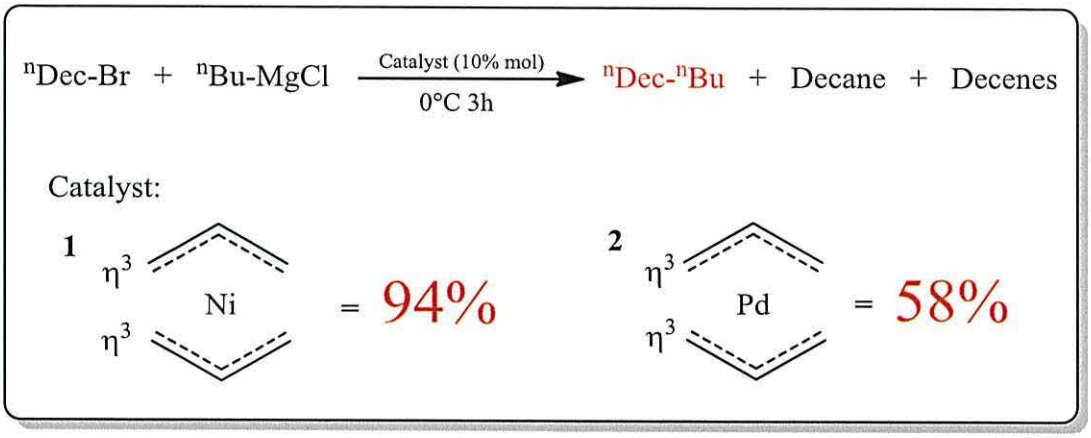

Figure 12. Catalytic proficiencies of target Metal(π-allyl)$_2$ compounds **1** & **2** (with product yields).

4.2.1.1. Bis(π-allyl) Palladium - Pd(π-allyl)$_2$ (Methodology 4a.)

First isolated in 1963 in a dissertation by W. Keim and then published in 1967 by Becconsall *et al*[53] the synthetic method proceeded via the formation of a *mono*-(π-allyl)-palladium(II) chloride dimer complex[24/23] **4** which can then undergo a Grignard reaction to form the final Pd(π-allyl)$_2$ compound **2** (Scheme 11.).

Preparation:

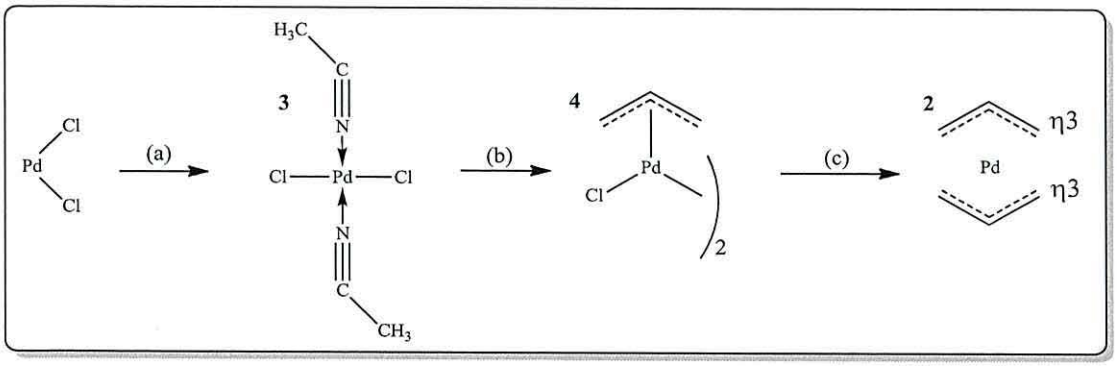

Scheme 11. (a) (i) CH_3CN / Reflux / 12 h; (ii) ppt Et_2O / 76%; (b) 1,2-dichloroethane / allyl alcohol / AgOTf / THF / 74%; (c) (i) CH_2=$CHCH_2MgCl$ / THF / -60°C; (ii) *n*-pentane / -50°C / 81%.

Synthesis towards the target compound $(\eta^3\text{-allyl})_2Pd$ **2** began from the readily available starting material $PdCl_2$. Step (a) involved the addition of anhydrous $PdCl_2$ to a large excess of CH_3CN and the orange/yellow dispersion was heated under reflux for 12 h, upon which there was a colour change from the yellow/orange dispersion to a translucent red/organge solution. After cooling, the product **3** (Figure 13.) was precipitated from Et_2O and collected by filtration in 76% yield.

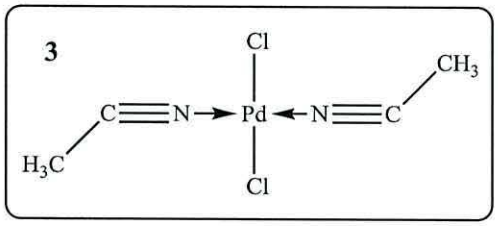

Figure 13. *Bis*(cyanomethyl) palladium(IV) chloride (**3**).

A higher yield could be achieved using anhydrous CH_3CN, also cooling using an ice bath and multiple filtration steps could lead to higher yields as the solution still remained a bright orange colour and contained visible amounts of solid product. However large quantities of **3** had been collected which was sufficient to perform multiple attempts at the subsequent reaction steps.

Step (b) in the synthesis of $(\eta^3\text{-allyl})_2Pd$ **2** was the formation of the *mono*-(π-allyl)-palladium(II) chloride dimer complex **4**.

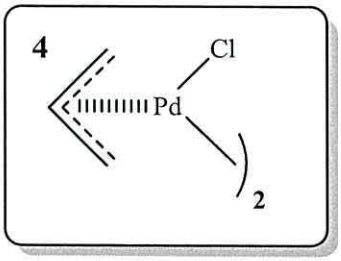

Figure 14. *mono*-(π-allyl)-palladium(II) chloride dimer complex **4**.

The compound **3** was dissolved in 1,2-dichloroethane under an atmosphere of argon, followed by addition of 10 equivalents of freshly distilled allyl alcohol and a slight excess of AgOTf (silver triflate) in THF. The mixture was stirred for 1 h at RT and subsequent filtration and purification via trituration in ether afforded the bright yellow crystal compound in a very reasonable yield of 74%. It is worth noting that early attempts at this reaction gave the product **4** in much lower yields. In these early attempts (in accordance with the literature)[24] the allyl alcohol was added to the mixture first and after the dispersion had fully dissolved into a translucent red solution the AgOtf in THF was added dropwise. This resulted in a black/grey suspension that if allowed to settle revealed a deep purple solution, work up of this suspension afforded **4** in relatively low yields (< 30%). However if the AgOTf solution was added to the mixture immediately after the allyl alcohol (before the dispersion had fully dissolved) it resulted in a light brown/beige suspension that if allowed to settle revealed the same deep purple solution. Work up of this light brown suspension afforded the product **4** in yields > 70% (more than double, highest 74% in 5 attempts). The formation of this palladium dimer complex **4** is from a comparatively recent method and although it requires more steps than the previous route[16] the final step in the formation of **2** becomes significantly easier, forming less Grignard salt by-products which makes extraction, isolation and purification of **2** more efficient.

The final step (c) was the Grignard reaction using allylmagnesium chloride in THF. The reaction was carried out under an atmosphere of argon and at a temperature of -60°C, achieved using a N_2(l) / acetone cooling bath. After the addition of the Grignard to the dimer **4**, the solvent was removed *in vacuo* at -30°C, after which the crude solid product was extracted with anhydrous pentane and transferred into another vesicle via a cannula fitted with a filter attachment to allow the transfer and filtration of the product under argon and at a

temperature of -50°C. It is extremely important to not open the system to the atmosphere as the increase in temperature (from -50°C) and the water vapour from the atmosphere (along with the atmospheric $O_{2(g)}$) will result in instantaneous decomposition.

The *n*-pentane was removed *in vacuo* at -50°C giving the product **2** as bright lemon yellow crystals in 81% yield.

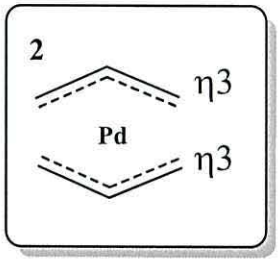

Figure 15. The η3-b*is*-(π-allyl) palladium complex **2**.

4.2.1.2. Bis(π-allyl) Nickel - Ni(π-allyl)$_2$ (Methodology 4b.)

First reported by Bodanovič in his PhD thesis and then published in 1961 by Bodanovič and Wilke[13] the synthetic route proceeded via the Grignard reaction of alkyl magnesium halides with nickel chloride. This Ni catalyst afforded high yields (up to 94%) of cross-coupling products.

Preparation:

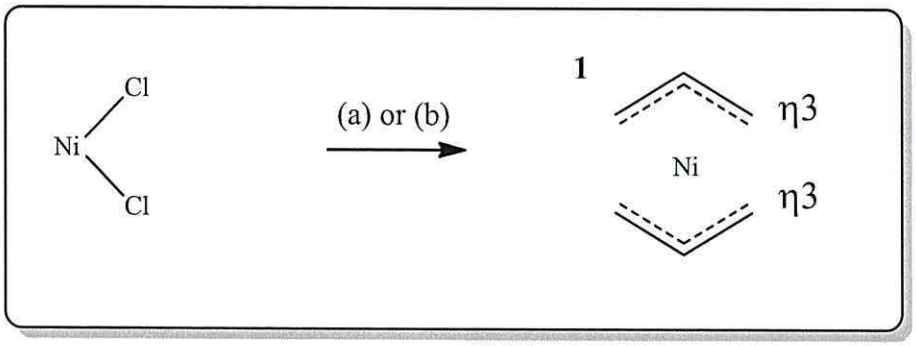

Scheme 12. (a) CH_2=$CHCH_2MgBr$ / Et_2O / -78°C; (b) CH_2=$CHCH_2MgCl$ / THF / -78°C;

In comparison to its palladium analogue **2**, this compound **1** is considerably more sensitive to moisture, temperature and atmospheric gases hence the multi-step synthetic method does not exist.

Initial attempts at the one-step synthesis of Ni(π-allyl)$_2$ **1** from $NiCl_2$ used the Grignard reagent Allyl MgBr (commercially available from Sigma Aldrich as a 1M solution in Et_2O) and therefore Et_2O was used as the reaction solvent (Scheme 12a.). $NiCl_2$ (2.08g, 16.05mmol) was slurried in anhydrous Et_2O and the mixture cooled to -25°C. Allyl MgBr (1M in Et_2O, 40ml, 40.00mmol) was added in 5ml portions over 2 hours and the reaction stirred for a further 3 hours where upon the vessel was left to stand overnight at -78°C. The mixture was filtered, washed with several portions of anhydrous Et_2O and the solvent removed *in vacuo*. However, the final product **1** proved difficult to separate from the reaction solvent Et_2O both having similar vapour pressures and all attempts at solvent removal (*in vacuo*) resulted in a mixture of product **1** and Et_2O, in the cold (liquid N_2) waste solvent finger-trap. Several variations in the methodology were performed in an attempt to obtain a sample of **1** completely free of Et_2O which would mask the compounds signals in the INS TOSCA spectra. The variations included changing reaction solvent volume, by-passing the -78°C overnight standing period and removal of the solvent at varying temperatures and pressures but all were to no avail.

All subsequent attempts involved the Grignard reagent Allyl MgCl (available as a 2M solution in THF from Sigma Aldrich, Scheme 12b.). A sample of Ni target compound **1** was obtained which produced an INS TOSCA spectrum albeit containing traces of THF. The signals corresponding to THF were removed by subtraction of an INS spectrum of pure THF run separately.

4.2.1.3. Spectroscopy of Pd(π-allyl)$_2$ & Ni(π-allyl)$_2$:

The final reaction step (c) in the preparation of Pd(π-allyl)$_2$ **2** and the complete one-step synthesis of Ni(π-allyl)$_2$ **1** were performed at the ISIS pulsed neutron and muon facility (RAL, UK) and the products loaded into the aluminium sample holder and sealed with indium wire. This was performed inside an argon filled glove bag which was kept at a temperature of ≈ -20°C using solid carbon dioxide. The reactions and products are extremely sensitive to increases in temperature and react violently and exothermically in air. The pure products were placed in the INS instrument TOSCA[54/55] almost immediately, to not allow any decomposition to occur. The INS spectra were measured at ≈ 20K, achieved using liquid helium.

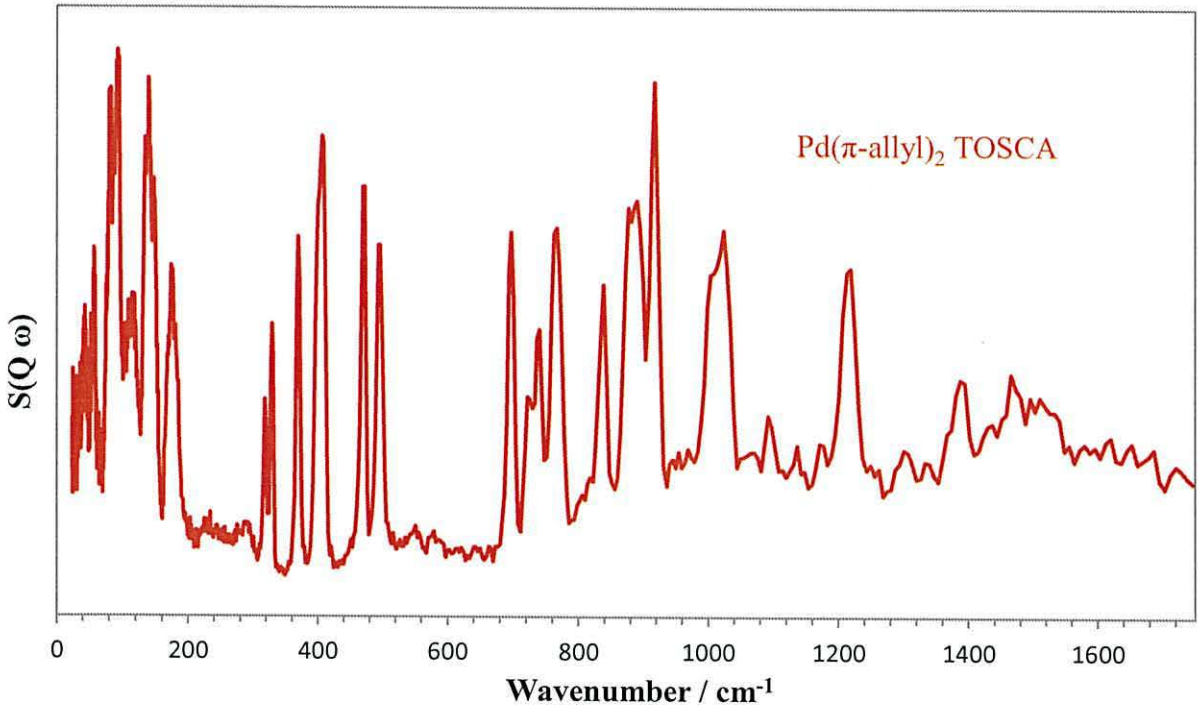

Figure 16. INS TOSCA spectrum of Pd(π-allyl)$_2$ **2** from 0 – 1750 cm^{-1} (for full spectra see appendix).

Figure 16. shows the INS vibrational spectrum for Pd(π-allyl)$_2$, measured on TOSCA, from 0 – 1750 cm^{-1} (fingerprint region). Measurements were taken up to 4000 cm^{-1} (with full spectra available in the appendix) although resolution is visibly reduced at energies above

1800 cm^{-1}, which is as expected for TOSCA (optimised for low energy vibrations). Sufficiently large quantities (> 2.5g) of the bright lemon yellow solid Pd(π-allyl)$_2$, completely void of impurities and residual solvent, resulted in an INS spectrum with clear and defined peaks showing good resolution.

Due to the increased sensitivity of the Ni(π-allyl)$_2$ compound (to air, moisture and changes in temperature) and also the previously mentioned issues with full removal of residual reaction solvent (Et_2O and then THF in the final preparations) the INS spectrum for the Ni analogue Ni(π-allyl)$_2$ **1** was not clear as due to signals from residual THF covering the regions of interest. Figure 17. shows the spectra for Ni(π-allyl)$_2$ (albeit containing traces of THF) and a separately run sample of pure THF (blue and black traces respectively).

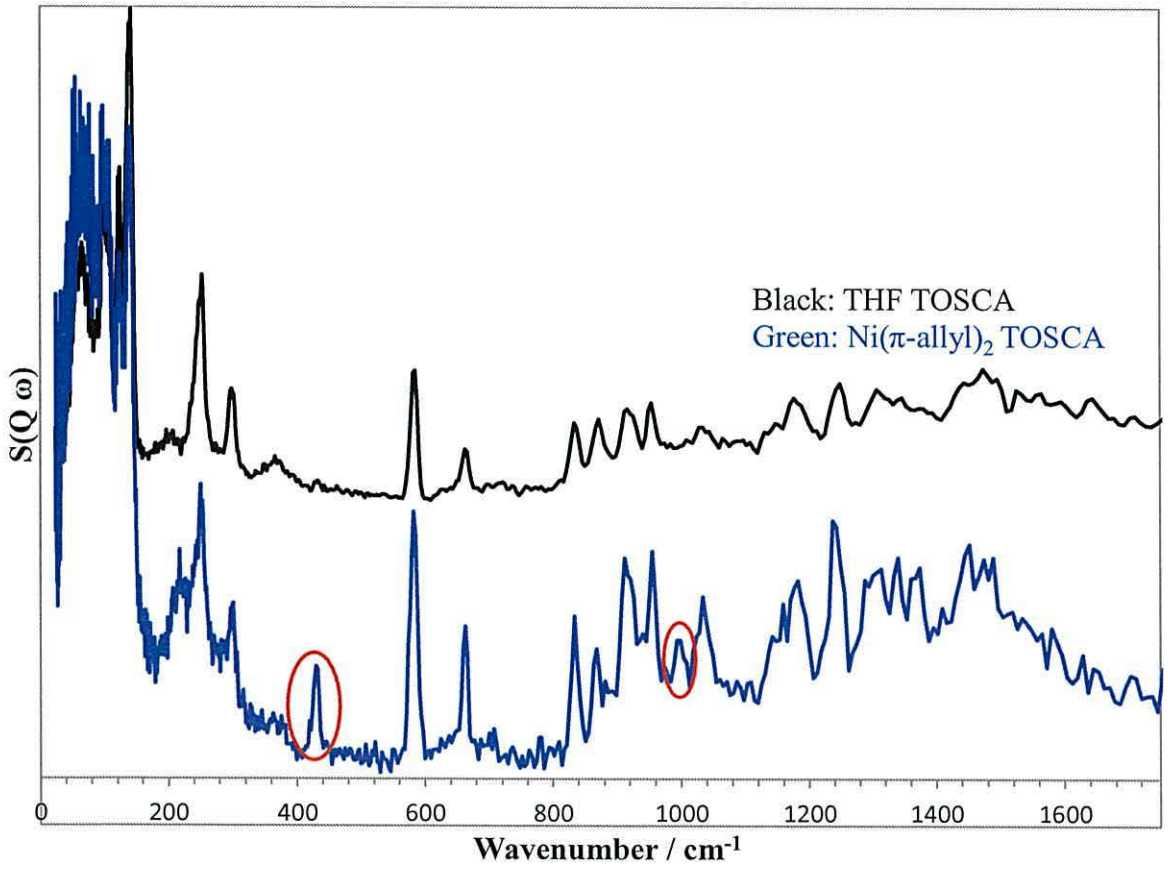

Figure 17. INS TOSCA spectra of Ni(π-allyl)$_2$ **1** (blue) and THF (black).

Figure 17. shows the Ni(π-allyl)$_2$ sample invariably contaminated with THF, although it is still possible to see vibrational signals resulting from the compound itself (at 430 and 994 cm^{-1} highlighted red in). Subtraction of the THF spectral data from the Ni(π-allyl)$_2$ sample results in an improved spectrum from which low energy vibrations can be observed (Figure 18.).

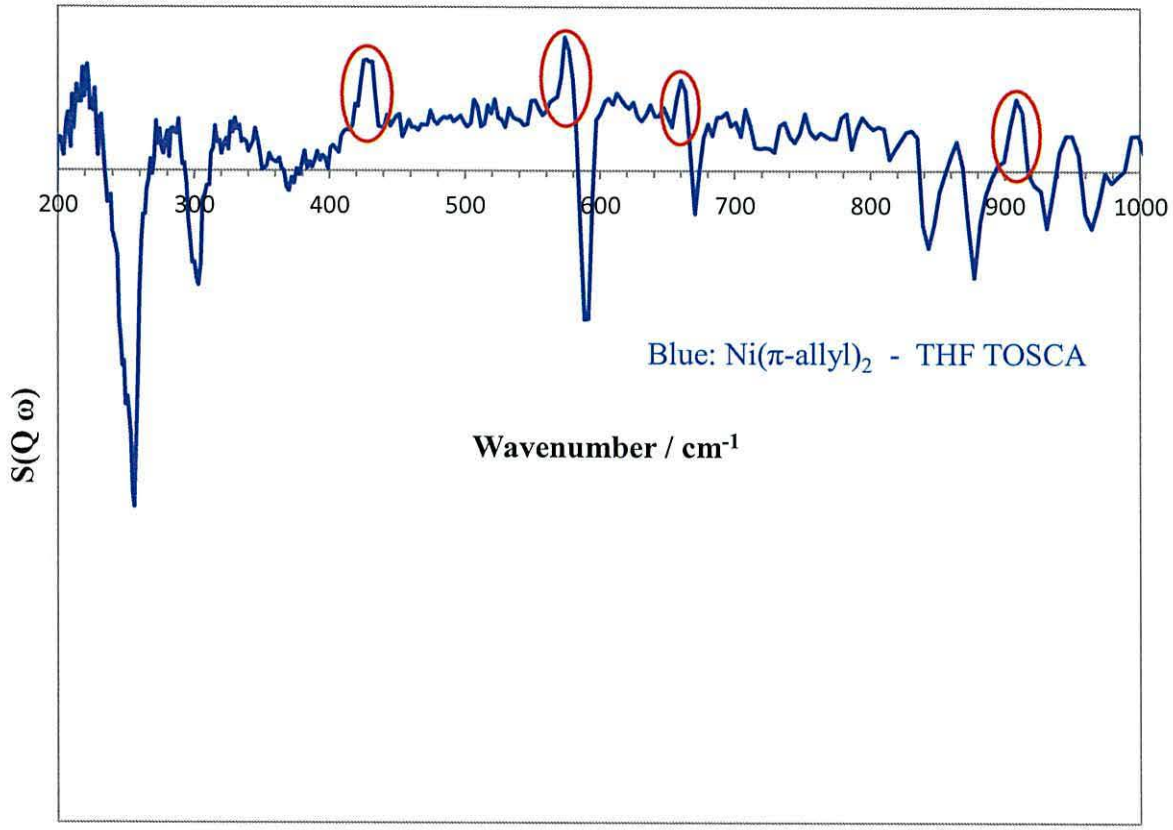

Figure 18. INS TOSCA spectrum of Ni(π-allyl)$_2$ **1** with THF subtraction.

Figure 18. (above) shows the INS TOSCA spectrum of **1** with the THF subtraction. Negative peaks correspond to the strong signals emanating from the THF, with peaks from **1** now also visible at 430, 574, 660 and 994 cm^{-1} (highlight red in Figure 18.).

4.2.2. Terpyridyl Ligand Complexes (Methodology 4c.)

The terpyridyl compounds **5** - **8** were commercially available and were subsequently transformed into the active Ni-terpyridyl complexes **13** - **16**. Solutions of **5** - **8** in anhydrous THF were combined with $Ni(COD)_2$ and I_2. The orange mixtures were stirred for 16 h at RT, filtered through a plug of celite® to remove the NiO_2 by-product and the solvent reduced to ≈ 1/3 volume *in vacuo*. The products were precipitated by the addition of dry ether and collected by filtration in high yields (**13** in 98% yield, **14** in 95% yield, **15** in 96% yield and **16** in 98% yield).

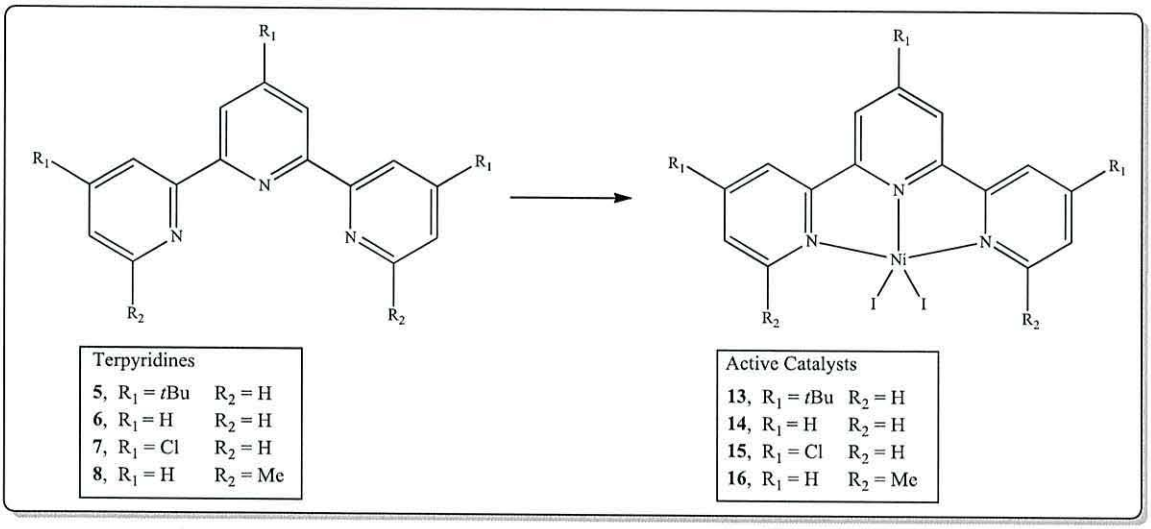

Figure 19. Terpyridines (**5** – **8**) and active Ni-terpyridyl complexes (**13** - **16**).

Spectroscopy:

The products were stable at room temperature and do not decompose in air, they were analysed by mass spectrometry.

Table 4. Mass spectrometry data (EPSRC Swansea - see appendix) – Electrospray ionisation (m/z: MS ESI)

Compound	Theoretical $[M\text{-}I]^+$	Observed $[M\text{-}I]^+$
13	586.1224	586.1220
14	417.9346	417.9337
15	521.80	521.80
16	446.0	446.0

Although INS is a non-destructive technique, the measurement times can be relatively long (up to 15+ h) and larger quantities of sample are required when compared to other commonly used techniques such as IR, MS and NMR. The more sample in contact with the neutron beam leads to reductions in experiment time and increases in resolution. The aluminium sample holders for the instrument TOSCA (Chapter 3 - Figure 8.) have an area of $\approx 3in^2$ and (although dependant on the sample density and also the number of hydrogen atoms in the molecule) $\approx$ 2.5g of sample is required for sufficient INS spectral resolution for samples run for $\approx$ 8 h. Terpyridines **5** & **6** were obtained from Sigma Aldrich which produced INS TOSCA spectra with good resolution and can be seen in Figure 20. (for full spectra see appendix).

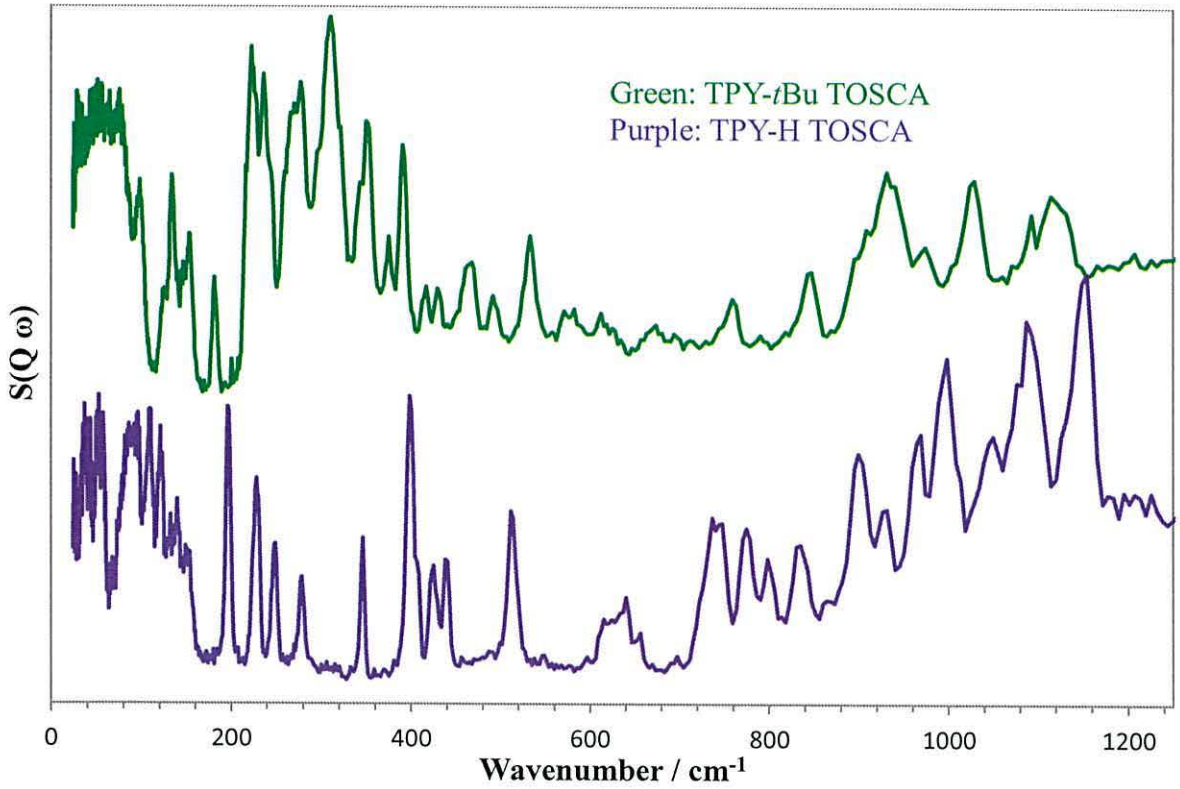

Figure 20. INS TOSCA spectra for **5** TPY-tBu (green) and **6** TPY-H (purple) from 0 – 1250 cm^{-1}.

Terpyridines **5** & **6** were then converted to the active catalysts **13** & **14** (general formula $LNiI_2$) in good yields (> 90%) providing > 2 g of sample which gave INS TOSCA spectra with good resolution.

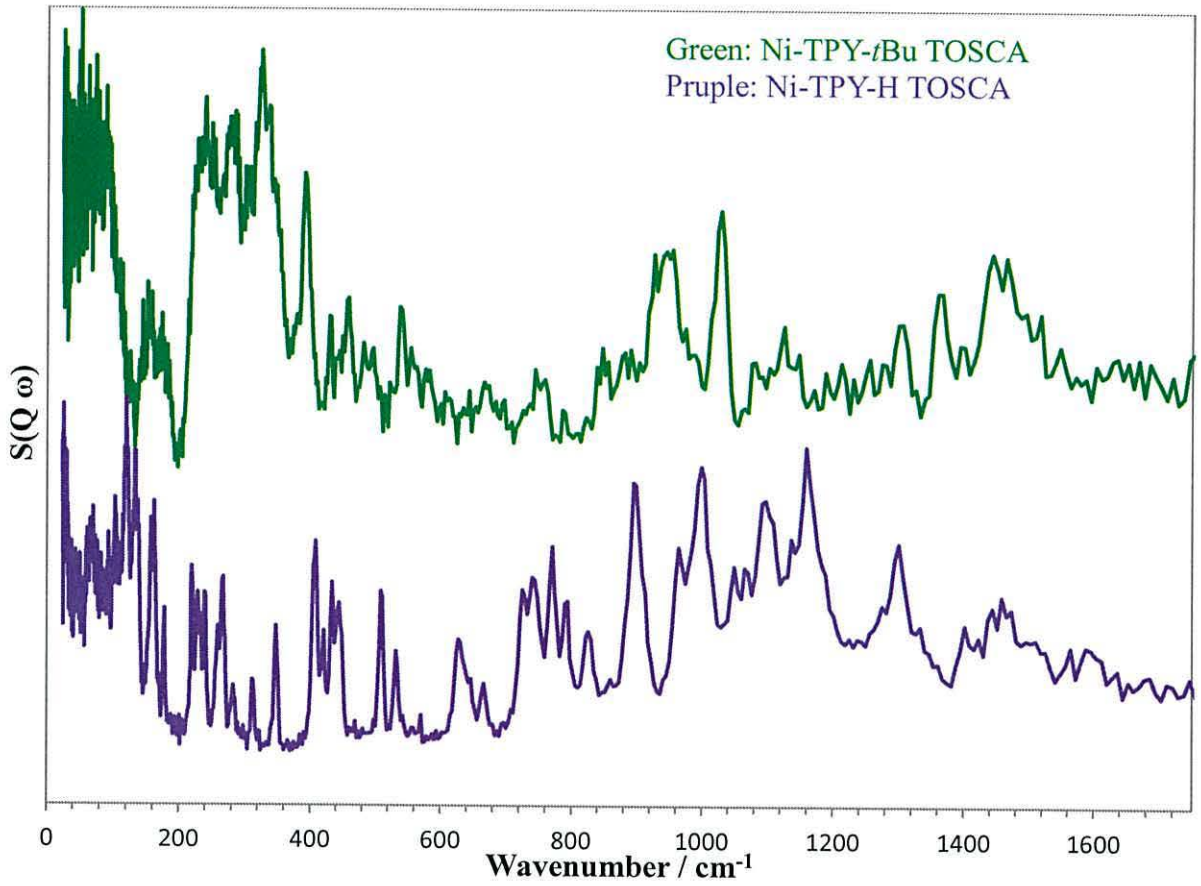

Figure 21. INS TOSCA spectra of active Ni-terpyridyl complexes **13** Ni-TPY-*t*Bu & **14** Ni-TPY-H.

Figure 21. shows INS TOSCA spectra for **13** (Ni-TPY-*t*Bu high yielding - 98%) & **14** (Ni-TPY-H lower yielding - 60%) from 0 – 1750 cm^{-1}, free from impurities and residual solvent (Et_2O). Resolution is sufficient for analysis of the low energy vibrations, and comparison with theoretical calculations of these modes, by the Chass group (see conclusion).

Starting material terpyrdines **7** (TPY-Cl) & **8** (TPY-Me_2) were only commercially available (HetCat) in small quantities and although conversion to the active Ni-terpyridyl complexes **15** (which gives a cross-coupling yield of 16%, see Figure 11.) & **16** (9% yield) was successfully confirmed by MS (see Table 4.) the < 1 g sample quantities did not lead to spectra with sufficient resolution for comparison of the low energy vibrational modes (even with experimental TOSCA running time increased to > 12 h).

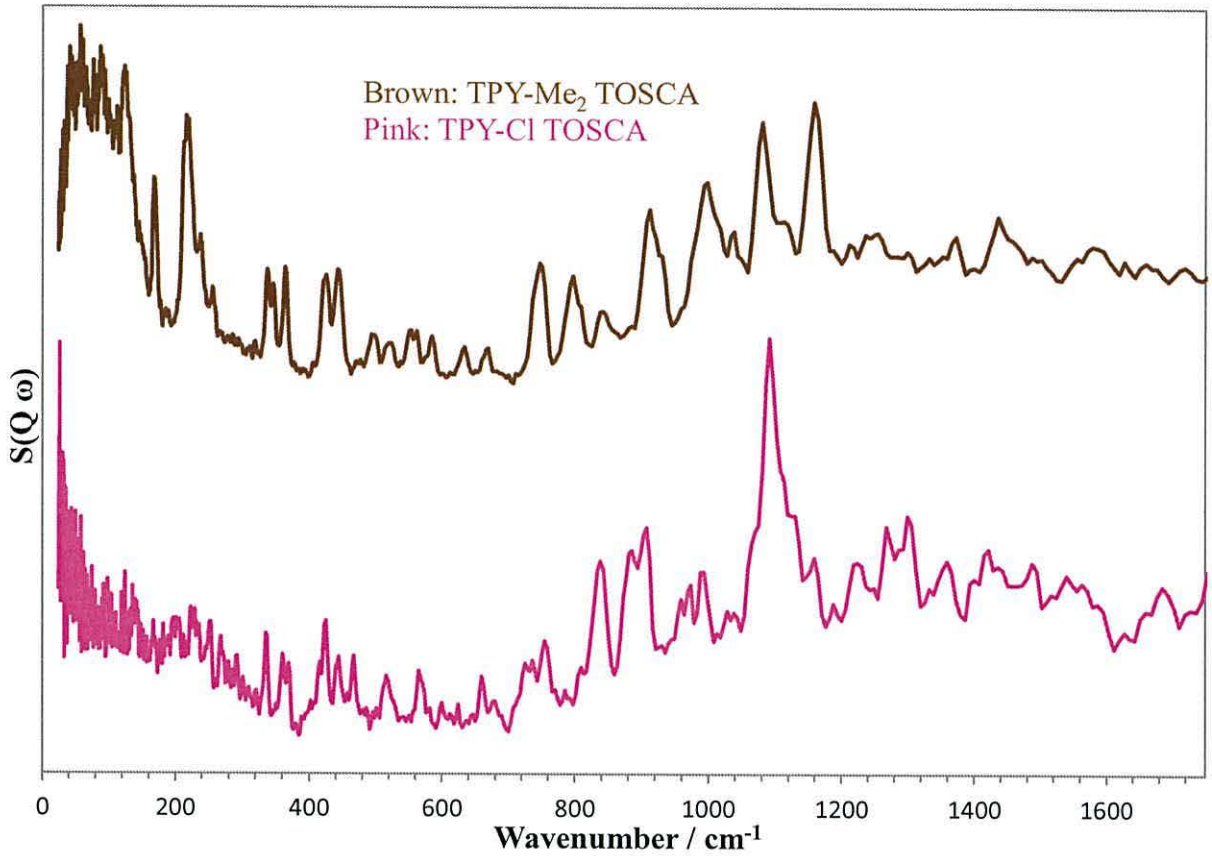

Figure 22. INS TOSCA spectra for terpyridine ligands **7** & **8**.

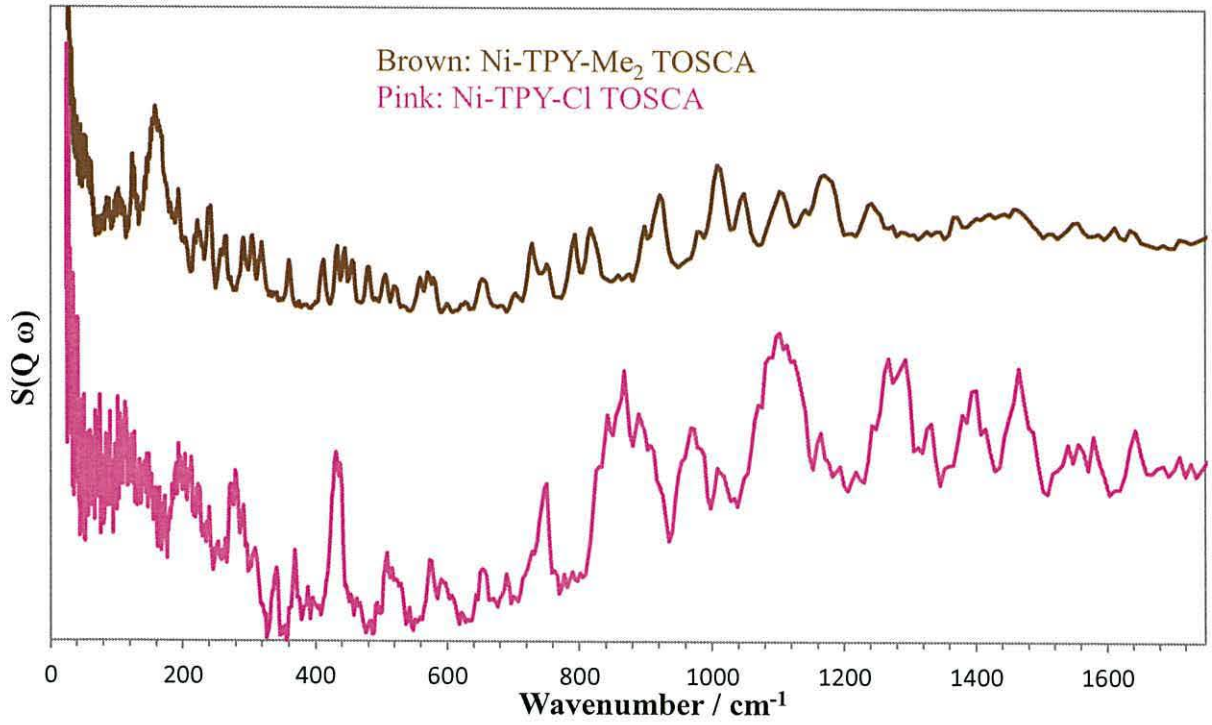

Figure 23. INS TOSCA spectra for Ni-terpyridyl complexes **15** & **16**.

It can be clearly seen in Figures 22. & 23. that the small sample quantity for the TPY-Cl analogues **7** & **15** (pink traces), produced spectral lines from which the signal to noise ratio is insufficient for any form of analysis, especially the comparison of low energy vibrations with the TPY-Me_2 analogues **8** & **16** (brown traces) which also exhibit insufficient signal to noise ratio, albeit to a lesser extent.

4.3. Conclusion

Successful conversion of the commercially available terpyridines **5** & **6** (TPY-*t*Bu and TPY-H) to the active catalyst Ni-terpyridyl complexes **13** & **14** (general formula $LNiI_2$) was successfully achieved in one step and their structures confirmed with MS (see Table 4.). The availability of large quantities of the starting material terpyridines lead to sufficient quantities of the complexes which produced INS spectra free from impurities / solvent and with good resolution. Expansion of the low energy vibrations resulted in clear peaks that can be combined with computational results from the Chass group into catalytic activity (see Figure 26.).

Disappointingly, only small quantities of starting material terpyridines **7** & **8** (TPY-Cl and TPY-Me_2) were available and although successful conversion to the active complexes **15** & **16** was achieved (and confirmed with MS, see Table 4.), the small sample amounts produced INS spectra with insufficient statistics (even with increased running times of > 12 h) leading to low resolution spectra. Low energy expansions of these spectra did not allow analysis of the vibrations relating to catalytic efficiency.

Successful synthesis of **2** ($Pd(\pi\text{-allyl})_2$) was achieved in three steps (Scheme 13a.), producing sufficient quantities needed for neutron spectroscopy (> 2.5 g) of the bright lemon yellow solid crystalline product, pure and free from residual traces of solvent, in high yields which are in agreement with those found in the literature.[24] An INS TOSCA spectrum for **2** was produced with excellent resolution and clear defined peaks which are also visible upon expansion of the low energy region (< 550 cm^{-1} Figure 25.).

The analogous nickel compound **1** (Ni(π-allyl)$_2$) was successfully synthesised in one step (Scheme 13b.), although the full removal of solvent (Et_2O and then THF in the latter preparations) was proven difficult due to compound **1** and solvent having similar vapour pressures. Any attempts to separate the compound from the solvent, at various temperatures and pressures, resulted in a bright yellow solid with a melting point of ≈ 0°C. This melting point was in agreement with the literature for **1**,[56] however (later confirmed with INS see Figure 17.) a mixture of **1** and THF also has a melting point of ≈ 0°C. It is still uncertain whether the literature preparation involves full removal of solvent, as their successful synthesis was only confirmed by two reported peaks in the IR spectrum (1520 and 1493 cm^{-1} but with ether also purportedly containing a peak at 1490 cm^{-1} in the IR spectrum).[57] Other instances in the literature for **1** are based upon catalytic testing with the small amounts required generated *in situ* from the Grignard reaction of $NiCl_2$ which therefore does not require any separation from the solvents.[1] Subtraction of THF INS data sets from data of **1** however, did result in a INS TOSCA spectrum from which analysis of the low energy vibrational peaks is possible (Figure 18.).

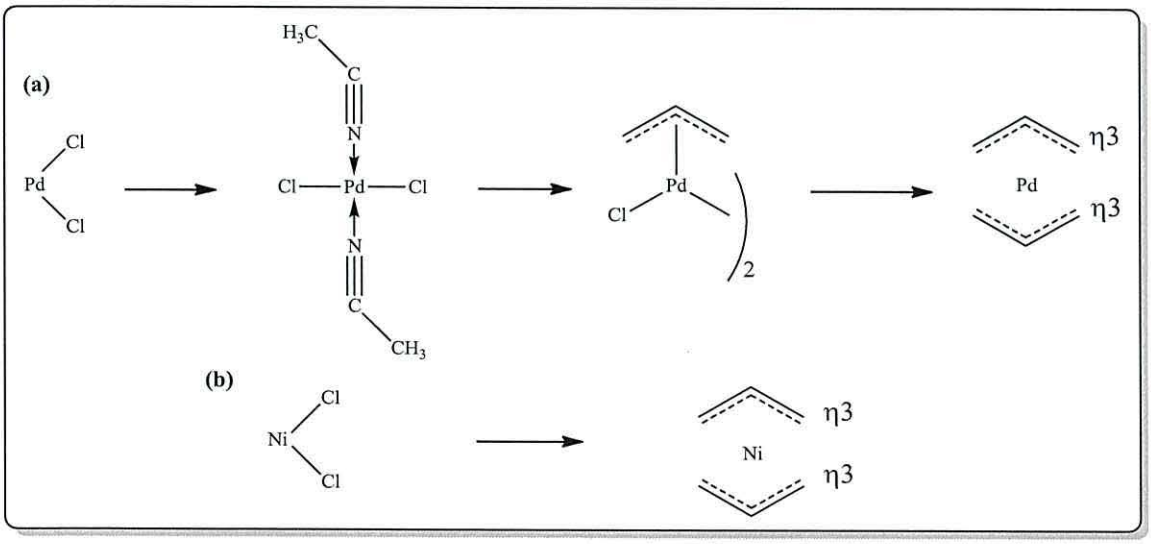

Scheme 13. Reaction pathways to (a) **2** Pd(π-allyl)$_2$.; (b) **1** Ni(π-allyl$_2$.

Computational calculations relating to molecular vibrations, specifically the changing hapticities of the allyl groups to the metal Pd centre, were performed by the Chass group (Chemistry, Queen Mary, University of London) and achieved by creating geometry optimised structures and calculating DFT frequencies (3N-6 vibrations) in Guassian09.[58]

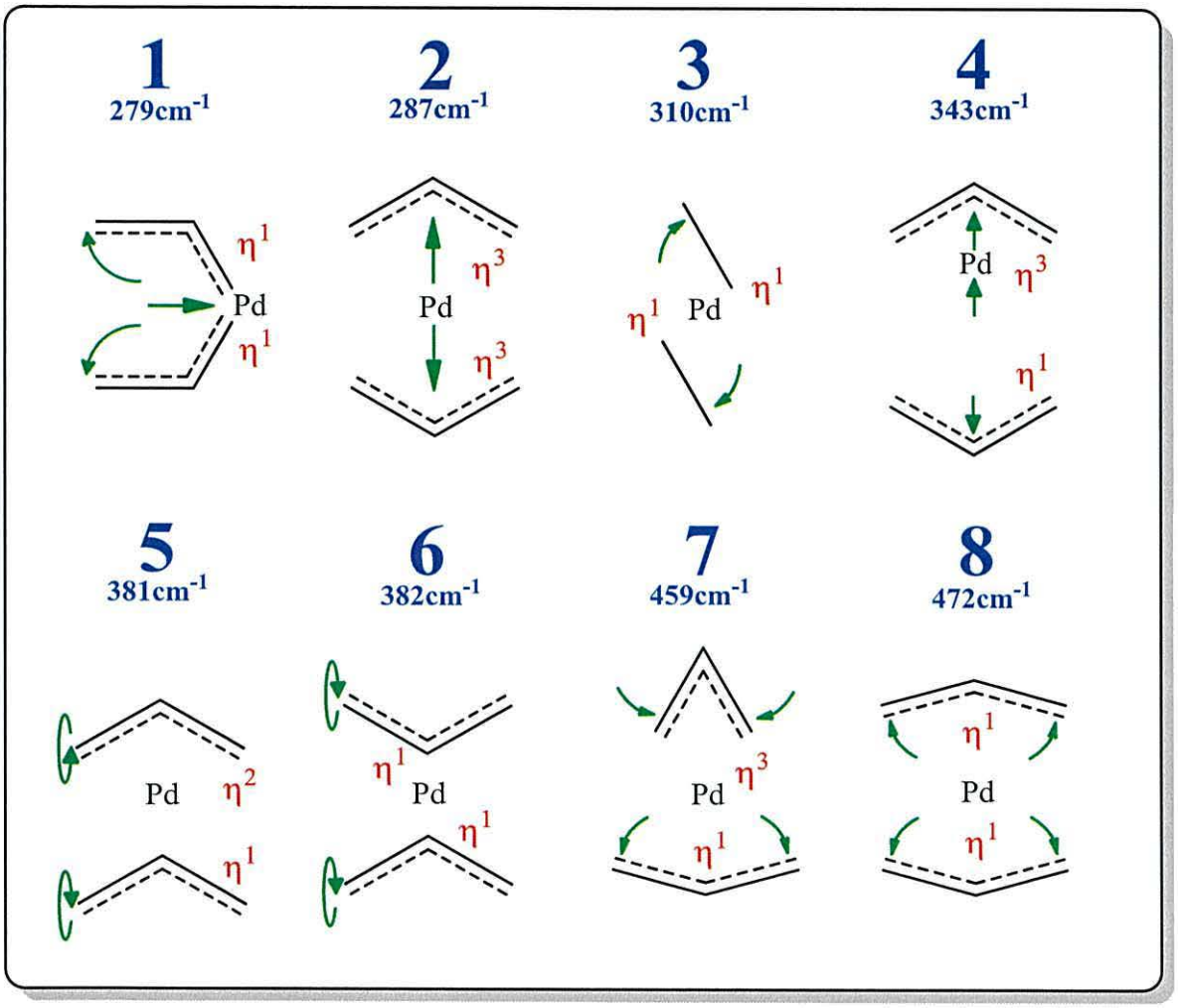

Figure 24. Vibrational modes and changing hapticities for Pd(π-allyl)$_2$ **2**.

The motions shown in Figure 24. correspond to the opening and closing of the catalysts active site, take place at low energies (between 250 – 500 cm^{-1}) and can be attributed to peaks seen in the INS TOSCA spectrum shown in Figure 16. and more clearly in the low energy expansion shown in Figure 25.

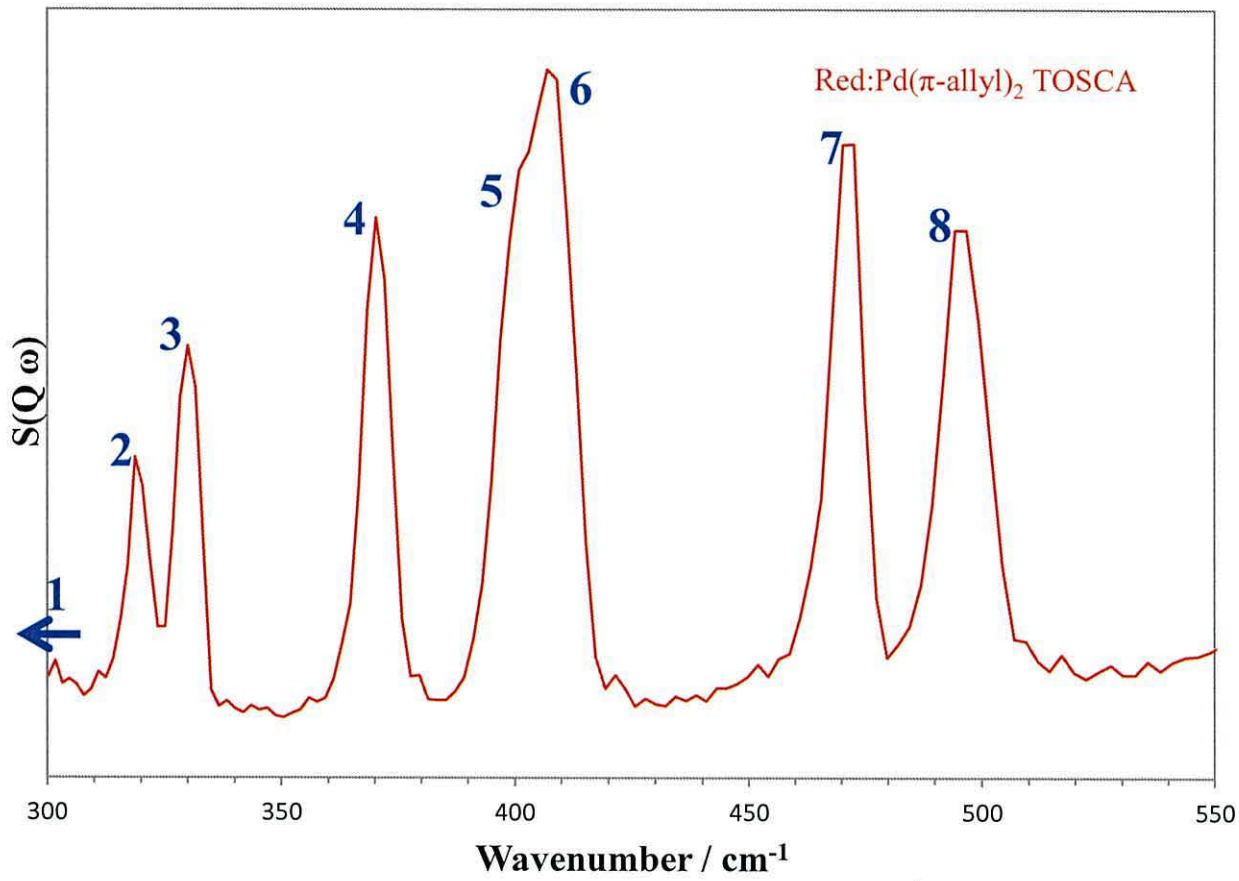

Figure 25. The INS TOSCA spectrum low energy expansion (300 – 550 cm^{-1}) of Pd(π-allyl)$_2$ **2**.

Figure 25. corresponds to peaks that particular vibrations have been attributed to using the theoretical data shown in Figure 24. Similar calculations have been performed for all catalytic systems (Metal-π-allyl$_2$'s, Ni-terpyridyls and the Pd-NHC PEPPSI's). Research is ongoing but preliminary results allude to catalysts that produce cross-coupling products with the highest yields exhibit these particular vibrations at blue-shifted frequencies (ie. peaks found at higher wavenumbers) and examples of this observation can be seen in Figure 26.

However, although 'blue-shifting' of peaks relating to the opening and closing of the catalysts active site (or motions corresponding to reductions in active site steric hindrance) is observed, it has still not been proven whether it is correlated or causative and therefore the nature of this potential phenomenon still unknown.

Figure 26. shows an example of the 'blue-shifted' peaks that correlate to molecule vibrations (in this particular case this refers to the wagging of the terpyridyl rings) hypothesised to be related to catalytic activity. This collaborative work with the Chass Group (Chemistry, Queen Mary, University of London) is on-going, with further analysis and conclusions currently underway.

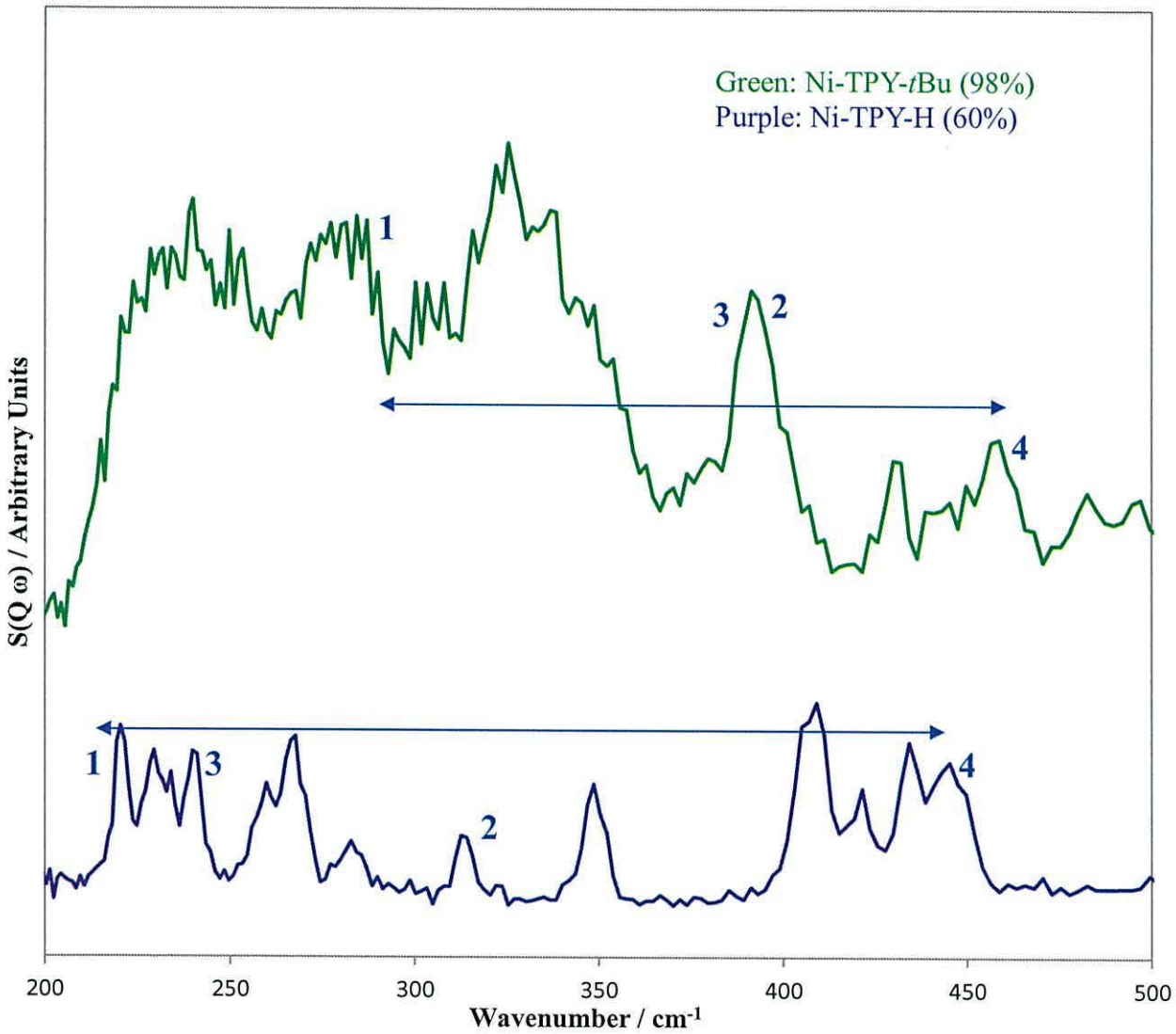

Figure 26. Example of 'blue-shifted' peaks between high / low yielding catalysts (low energy expansion of Ni-terpyridyl complexes **13** and **14**) INS TOSCA.

Table 5. Tabulation of shifted peaks for Ni-TPY-H & Ni-TPY-*t*Bu (shown in **Figure 26.**).

Peak No.	Ni-TPY-H (cm^{-1}) Lower Yielding	Ni-TPY-*t*Bu (cm^{-1}) Higher Yielding	Total Shift (cm^{-1})
1	220	285	+65
2	240	390	+150
3	315	380	+65
4	445	460	+15

Table 5. gives values for particular peaks and gives their relative shifts (in the positive direction or "blue-shifted" values).

Spectra have also been obtained for Pd-NHC-R (R = IMes and IPr) and with the data currently being analysed. The Pd-NHC-IPr PEPPSI catalyst spectrum can be seen in Figure 27. (below).

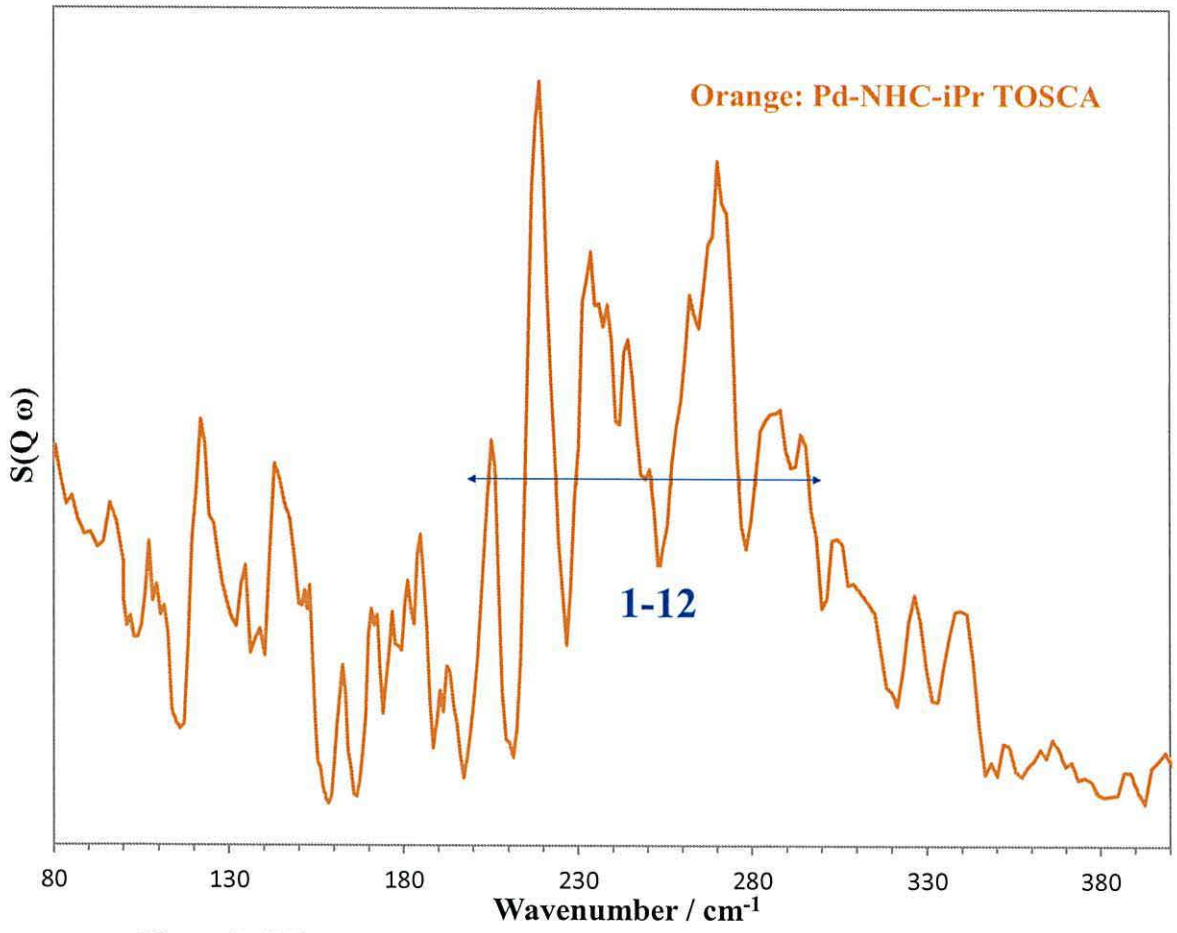

Figure 27. INS TOSCA spectrum for Pd-NHC-IPr **10** with labelled vibrational peaks.

4.4. Experimental

Materials: All chemicals and solvents were obtained from standard UK chemical suppliers (ie. Sigma Aldrich / Alfa Aesar). Dry solvents were obtained via distillation over sodium wire. All compounds were synthesized by variations of the literature.

Inelastic Neutron Scattering (INS) Spectroscopy: INS spectra were recorded with the spectrometers TOSCA[54/55] and MAPS[10/59] at ISIS. The operating principles of the two instruments are described in detail elsewhere.[60] Samples were loaded (in an argon filled glovebox containing < 0.1ppm of O_2 and H_2O) into aluminum cans, sealed with indium wire and put into a closed cycle cryostat, cooled to ~20 K (liquid helium) and the spectra recorded for 8-12 h.

Nuclear Magnetic Resonance (NMR): All spectra were obtained using Bruker Advance III Ultrashield 400 and 500 Plus NMR machines, particular frequencies for spectra are given, along with the type of deuterated solvent in which they were run.

Mass Spectrometry: All samples sent to the EPSRC national mass spectrometry service centre in Swansea.

Bis(cyanomethyl) palladium(IV) chloride 3[23]

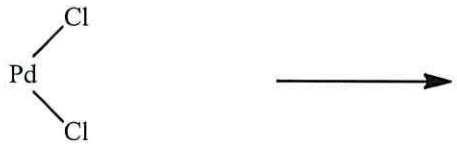

Chemical Formula: Cl_2Pd
Molecular Weight: 177.33

3

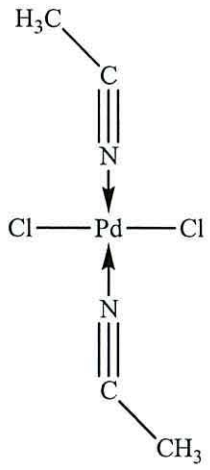

Chemical Formula: $C_4H_6Cl_2N_2Pd$
Molecular Weight: 259.43

Anhydrous $PdCl_2$ (5.00 g, 28.20 mmol) was added to an excess of acetonitrile. The orange/yellow dispersion was then heated under reflux for 12 h. Upon heating the $PdCl_2$ fully dissolved giving a translucent orange solution. After the 12 h reflux period the now red/orange solution was allowed to cool to RT. The red/brown/orange product **3** was precipitated from ether and collected by filtration (5.49 g, 21.33 mmol, 76% yield).

(π-allyl) palladium chloride dimer 4[24]

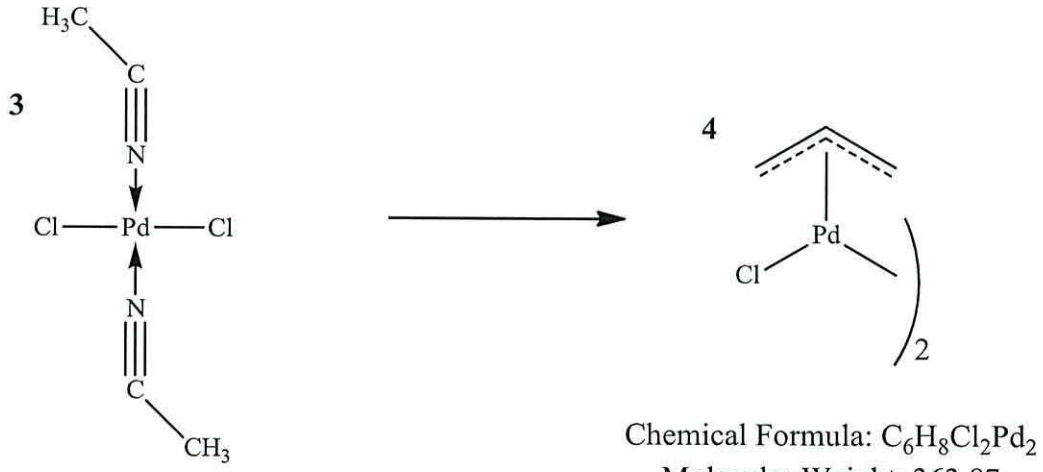

Chemical Formula: $C_4H_6Cl_2N_2Pd$
Molecular Weight: 259.43

Chemical Formula: $C_6H_8Cl_2Pd_2$
Molecular Weight: 363.87

In a 3-necked round-bottomed flask fitted with a pressure equalising dropping funnel, $PdCl_2(MeCN)_2$ **3** (2.30 g, 8.94 mmol) was dissolved in dry 1,2-dichloroethane (150 mL). The reaction was then carried out under an atmosphere of argon and approximately 10 equivalents of allyl alcohol (5.30 g, 90.0 mmol) was added. A very slight excess of AgOTf (2.57 g, 10.00 mmol) dissolved in dry THF (20 mL) was added instantaneously to the allyl alcohol, via the dropping funnel over a period of 5 mins. The mixture was stirred at RT for 1 h and then filtered through a mixture of $MgSO_4$: Silica (1 : 5) with a protective layer of sand. The solvent was removed *in vacuo* and ether was added to the purple crude product. It was triturated and the ether decanted. The crude solid product was then re-dissolved in 1,2-dichloroethane and re-filtered giving a bright yellow solution. Removal of the solvent *in vacuo* gave bright lemon yellow crystals which were further purified by precipitation from ether. The product **4** was dried under high vacuum (1.20 g, 3.30 mmol, 74% yield) and stored immediately at -20°C. The product was not stable to air, moisture or at room temperature.

Bis(π-allyl) palladium 2[61]

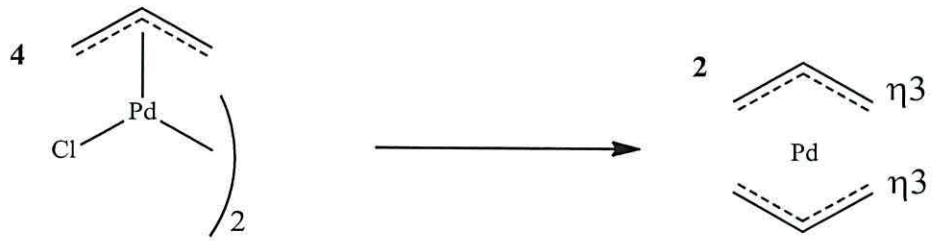

Chemical Formula: $C_6H_8Cl_2Pd_2$
Molecular Weight: 363.87

Chemical Formula: $C_6H_{10}Pd$
Molecular Weight: 188.56

Under an inert argon atmosphere, palladium dimer **4** (3.00 g, 8.25 mmol) was dissolved in dry THF (75 mL) and cooled to -60°C. To the clear yellow solution allylmagnesium chloride in THF (8.2 mL, 16.40 mmol) was added drop-wise and stirred. The mixture was allowed to warm very slowly to -30°C and the solvent removed *in vacuo* at this temperature. The crude solid product was washed with dry *n*-pentane (3 x 10 mL) at 10°C (decomposition at 20°C) under an inert argon atmosphere. The yellow *n*-pentane solution was extracted from the brown mixture via a cannula filter device into a separate flask pre-cooled to -50°C, all performed under argon. At this temperature (-50°C) the solvent was removed *in vacuo* giving the pure product **2** (2.5 g, 13.7 mmol, 81% yield). The product was very sensitive to air, moisture and changes in temperature. It was immediately placed into an argon filled environment and kept below -15°C using solid CO_2. It was then loaded into the necessary aluminium sample holder, sealed with indium wire and place inside the INS instrument TOSCA where it was cooled to ≈ 3 K using liquid helium. Care was taken to ensure the sample was not open to the atmosphere at any point.

Bis(π-allyl) nickel 1[62/56]

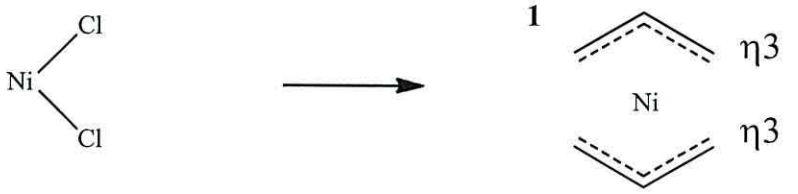

Chemical Formula: Cl_2Ni
Molecular Weight: 129.60

Chemical Formula: $C_6H_{10}Ni$
Molecular Weight: 140.84

(a) Allyl MgBr in Et_2O

Under an inert argon atmosphere anhydrous $NiCl_2$ (2.08 g, 16.05 mmol) was slurried with dry Et_2O (15 mL) and cooled to -25°C. Allyl MgBr (1.0 M in Et_2O, 40 mL, 40.00 mmol) was added in portions over 2 h and the reaction mixture stirred at -25°C for 3 h. The vessel was then left to stand at -78°C overnight under an inert argon atmosphere. The mixture was filtered via a cannula filter device into a pre-cooled (-30°C) vessel where it was washed with several portions of cold dry Et_2O (25 mL) in an inert argon atmosphere. The product **1** was removed from the solvent *in vauco* and isolated as a yellow solid with a m.p. = 0°C.[56]

(b) Allyl MgCl in THF

Under an inert argon atmosphere anhydrous $NiCl_2$ (4.41 g, 34.03 mmol) was slurried with dry THF (15 mL) and cooled to -25°C. Allyl MgCl (2.0 M in THF, 51.04 mL, 102.08 mmol) was added in portions over 2 h and the reaction mixture stirred at -25°C for 3 h. The vessel was then left to stand at -78°C overnight in an inert argon atmosphere. The mixture was filtered via a cannula filter device into a pre-cooled (-30°C) vessel where it was washed with several portions of cold dry THF (25 mL) in an inert argon atmosphere. The product **1** was removed from the solvent *in vauco* and isolated as a yellow solid with a m.p. = 0°C.[56]

CAUTION! Exothermic decomposition likely (explosions).

The product was extremely sensitive to air, moisture and changes in temperature. It was immediately place in an argon filled glovebox and constantly maintained at temperatures below -15°C. It was sealed into the necessary aluminium sample holder, sealed with indium wire and placed into the INS instrument TOSCA where it was immediately cooled to ≈ 3 K using liquid helium.

Nickel *tert*-butyl-terpyridyl halide complex 13[35]

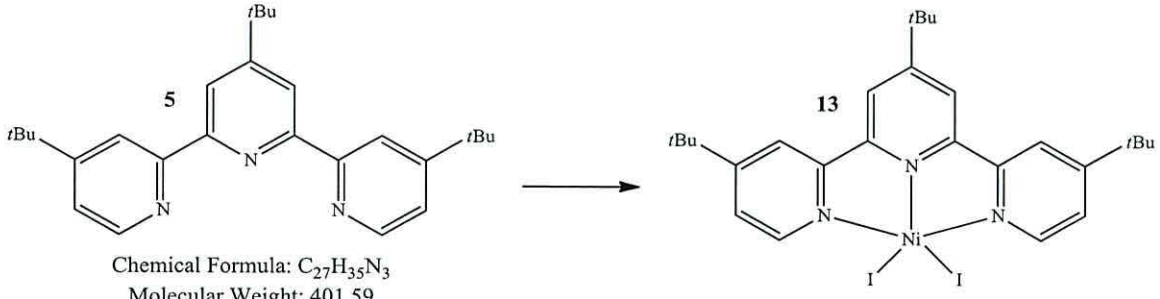

4,4',4''-tri-tert-butyl-2,2':6',2''-terpyridine **5** (1.37 g, 3.41 mmol) was dissolved in the minimum of dry THF in an inert atmosphere of argon. To the solution $Ni(COD)_2$ (0.92 g, 3.35 mmol) and I_2 (0.85 g, 3.36 mmol) was added and the mixture stirred at RT overnight. The orange/black mixture was then filtered through a plug of Celite® under a maintained flow of argon, where the black (NiO_2) was trapped on the Celite®. The organge solution was then reduced to ≈ 30% volume *in vacuo* and the product **13** precipitated by the addition of dry ether and collected via filtration (2.31 g, 3.23 mmol, 95% yield).

m/z: MS (ESI):

Theoretical Isotope Model: $[M\text{-}I]^+$ or $[C_{27}H_{35}N_3NiI]$ = 586.1224

Observed Data: $[M\text{-}I]^+$ or $[C_{27}H_{35}N_3NiI]$ = 586.1220

Nickel terpyridyl halide complex 14[4,63]

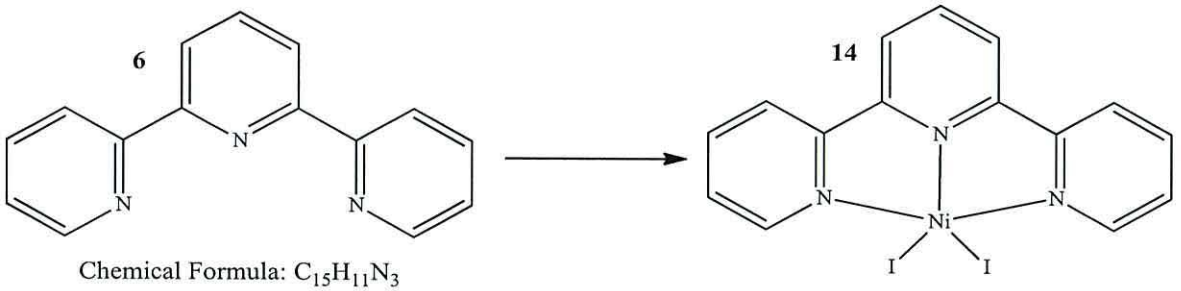

Chemical Formula: $C_{15}H_{11}N_3$
Molecular Weight: 233.27

Chemical Formula: $C_{15}H_{11}I_2N_3Ni$
Molecular Weight: 545.77

2,2':6',2''-terpyridine **6** (0.99 g, 4.23 mmol) was dissolved in the minimum of dry THF in an inert argon atmosphere. To the solution $Ni(COD)_2$ (1.14 g, 4.15 mmol) and I_2 (1.06 g, 4.16 mmol) was added. The orange/brown mixture was stirred at RT overnight. The mixture was filtered through a plug of Celite® under a maintained flow of argon. The solvent was reduced to ≈ 30% volume *in vacuo* and the product **14** was precipitated by the addition of dry ether and collected by filtration (2.27g, 4.16 mmol, 98% yield).

m/z: MS (ESI):

Theoretical Isotope Model: $[M\text{-}I]^+$ or $[C_{15}H_{11}N_3NiI]$ = 417.9346

Observed Data: $[M\text{-}I]^+$ or $[C_{15}H_{11}N_3NiI]$ = 417.9337

Nickel chloro-terpyridyl halide complex 15

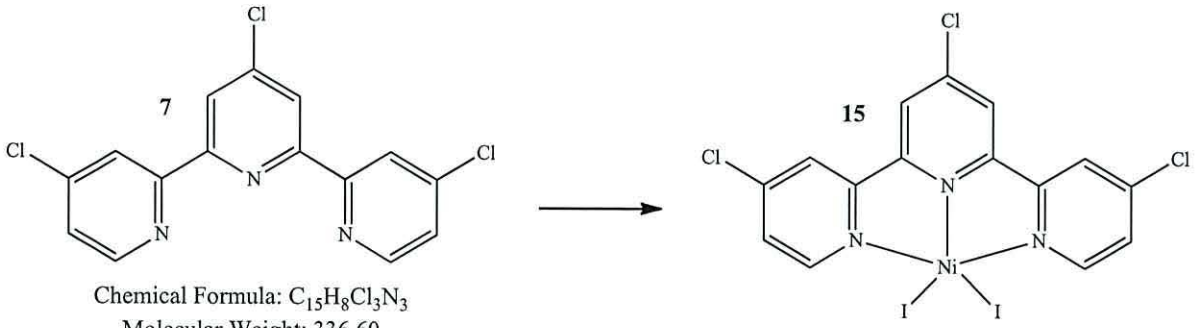

Chemical Formula: $C_{15}H_8Cl_3N_3$
Molecular Weight: 336.60

Chemical Formula: $C_{15}H_8Cl_3I_2N_3Ni$
Molecular Weight: 649.11

4,4',4''-trichloro-2,2':6',2''-terpyridine **7** (0.50 g, 1.49 mmol) was dissolved in the minimum of dry THF in an inert argon atmosphere. To the mixture $Ni(COD)_2$ (0.42 g, 1.53 mmol) and I_2 (0.38 g, 1.50 mmol) were added. The orange/brown mixture was stirred at RT overnight. The reaction mixture was filtered through a plug of celite® under a maintained flow of argon, to remove any black NiO_2 by-product. The solvent was removed *in vacuo* to ≈ 30% volume and the product **15** precipitated by the addition of dry ether and collected via filtration (0.93 g, 1.43 mmol, 96% yield).

m/z: MS (ESI):

Theoretical Isotope Model: $[M\text{-}I]^+$ or $[C_{15}H_8Cl_3N_3NiI]$ = 521.80

Observed Data: $[M\text{-}I]^+$ or $[C_{15}H_8Cl_3N_3NiI]$ = 521.80

Nickel dimethyl-terpyridyl halide complex 16

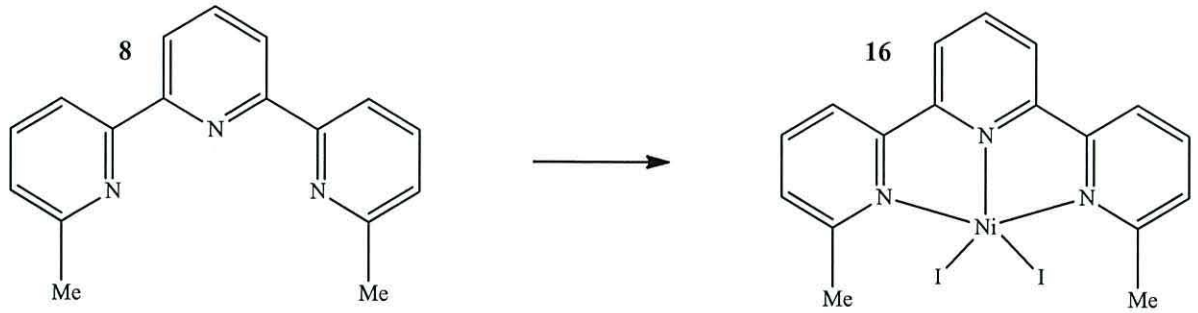

Chemical Formula: $C_{17}H_{15}N_3$
Molecular Weight: 261.32

Chemical Formula: $C_{17}H_{15}I_2N_3Ni$
Molecular Weight: 573.82

6,6"-dimethyl-2,2':6',2"-terpyridine **8** (0.95 g, 3.64 mmol) was dissolved in the minimum of dry THF in an inert argon atmosphere. To the mixture $Ni(COD)_2$ (1.00 g, 3.64 mmol) and I_2 (0.88 g, 3.47 mmol) were added and the orange/black reaction mixture was stirred at RT overnight. The mixture was then filtered through a plug of celite® under a maintained flow of argon. The solvent was removed *in vacuo* to ≈ 30% volume and the product **16** precipitated by the addition of dry ether and collected via filtration (1.93 g, 3.36 mmol, 98% yield).

m/z: MS (ESI):

Theoretical Isotope Model: $[M\text{-}I]^+$ or $[C_{17}H_{15}N_3NiI]$ = 446.0

Observed Data: $[M\text{-}I]^+$ or $[C_{17}H_{15}N_3NiI]$ = 446.0

4.5. References

1. J. Terao and N. Kambe, *Accounts of Chemical Research*, 2008, **41**, 1545–54.

2. R. Pearson, *Chemical Reviews*, 1985, **85**, 41–49.

3. F. Tappe, V. Trepohl, and M. Oestreich, *Synthesis*, 2010, **2010**, 3037–3062.

4. G. D. Jones, J. L. Martin, C. McFarland, O. R. Allen, R. E. Hall, A. D. Haley, R. J. Brandon, T. Konovalova, P. J. Desrochers, P. Pulay, and D. Vicic, *Journal of the American Chemical Society*, 2006, **128**, 13175–83.

5. S. Mecking, *Coordination Chemistry Reviews*, 2000, **203**, 325–351.

6. C. E. Tucker and J. G. De Vries, *Topics in Catalysis*, 2002, **19**, 111–118.

7. N. Koga, S. Obara, K. Morokuma, and K. Kitaura, *Journal of the American Chemical Society*, 1985, **107**, 7109–7116.

8. P. Binger, P. Wedemann, S. I. Kozhushkov, and A. De Meijere, *European Journal of Organic Chemistry*, 1998, 113–119.

9. U.S. Climate Change Technology Program, *INDUSTRIAL PROCESS EFFICIENCY Technology Options for the Near and Long Term*, 2005.

10. www.isis.stfc.ac.uk/instruments/maps, 20/2/13.

11. www.isis.stfc.ac.uk/instruments/tosca, 20/2/13.

12. www.isis.stfc.ac.uk/instruments/sandals, 25/2/13.

13. G. Wilke and B. Bogdanovič, *Angewandte Chemie*, 1961, **73**, 756.

14. G. Wilke, B. Bogdanovič, P. Hardt, P. Heimbach, W. Keim, and M. Kroner, *Angewandte Chemie*, 1966, **78**, 157–172.

15. W. Oberkirch, J. Schneider, J. Stedefeder, K. Tanaka, and G. Wilke, *Angewandte Chemie*, 1963, **75**, 10–20.

16. W. Keim, Dissertation - Technische Hochschule Aachen, 1963.

17. H. Bonneman, B. Bogdanovič, and G. Wilke, *Angewandte Chemie*, 1967, **79**, 817–818.

18. J. K. Becconsall and S. O'Brien, *Journal of Organometallic Chemistry*, 1967, **9**, 27–29.

19. S. O'Brien, *Journal of the Chemical Society A*, 1970, 9–13.

20. B. Henc, P. W. Jolly, R. Salz, G. Wilke, R. Benn, E. G. Hoffmann, G. Schroth, K. Seevogel, J. C. Sekutowski, C. Kruger, and R. Mynott, *Journal of Organometallic Chemistry*, 1980, **191**, 425–448.

21. J. W. Faller and D. A. Haitko, *Journal of Organometallic Chemistry*, 1978, **149**, 19–23.

22. N. Rosch and R. Hoffmann, *Inorganic Chemistry*, 1974, **13**, 2656–2666.

23. R. A. Michelin, G. Facchin, and P. Uguagliati, *Inorganic Chemistry*, 1984, **23**, 961–969.

24. T. Hosokawa, T. Tsuji, Y. Mizumoto, and S. I. Murahashi, *Journal of Organometallic Chemistry*, 1999, **574**, 99–101.

25. D. Walther, T. Döhler, N. Theyssen, and H. Görls, *European Journal of Inorganic Chemistry*, 2001, **2001**, 2049–2060.

26. G. Wilke, Belg., Patent, 631172, 1963.

27. J. Terao, Y. Naitoh, H. Kuniyasu, and N. Kambe, *Chemical Communications (Cambridge, England)*, 2007, 825–7.

28. P. L. Theofanis and W. A. Goddard, *Organometallics*, 2011, **30**, 4941–4948.

29. B. K. Bower and H. G. Tennent, *Journal of the American Chemical Society*, 1972, **94**, 2512–2514.

30. J. Zhou and G. C. Fu, *Journal of the American Chemical Society*, 2003, **125**, 12527–12530.

31. N. Hadei, E. A. B. Kantchev, C. J. O'Brien, and M. G. Organ, *Organic Letters*, 2005, **7**, 3805–7.

32. G. T. Morgan and F. H. Burstall, *Journal of the Chemical Society*, 1932, 20–30.

33. T. Morgan and H. Burstall, *Journal of the Chemical Society*, 1934, 1498–1500.

34. G. Morgan and F. H. Burstall, *Journal of the Chemical Society*, 1938, 1675–1678.

35. H. Case and J. Kasper, *Journal of the American Chemical Society*, 1956, **78**, 5842–5844.

36. F. Kröhnke, *Synthesis*, 1976, 1–24.

37. W. Spahni and G. Calzaferri, *Helvetica Chimica Acta*, 1984, **67**, 450–454.

38. E. C. Constable and J. Lewis, *Polyhedron*, 1982, **I**, 303–306.

39. K. T. Potts, D. A. Usifer, A. Guadalupe, and H. D. Abruna, *Journal of the American Chemical Society*, 1987, **109**, 3961–3967.

40. D. L. Jameson and L. E. Guise, *Tetrahedron Letters*, 1991, **32**, 1999–2002.

41. A. Harriman and R. Ziessel, *Coordination Chemistry Reviews*, 1998, **171**, 331–339.

42. M. Heller and U. S. Schubert, *European Journal of Organic Chemistry*, 2003, 947–961.

43. B. Zak, E. S. Baginski, E. Epstein, and L. M. Weiner, *Clinica Chimica Acta*, 1970, **29**, 77–82.

44. P. J. Carter, C. Cheng, H. H. Thorp, C. Hill, and N. Carolina, *Journal of the American Chemical Society*, 1998, **120**, 632–642.

45. L. Zhao, J. Sherchan, J. K. Park, Y. Jahng, B. Jeong, T. C. Jeong, C. Lee, and E. Lee, *Archives of Pharmacal Research*, 2006, **29**, 1091–1095.

46. E. Negishi, *Handbook of Organopalladium Chemistry for Organic Synthesis*, John Wiley & Sons, New York, 2002.

47. J. H. Kirchhoff, M. R. Netherton, I. D. Hills, and G. C. Fu, *Journal of the American Chemical Society*, 2002, **124**, 13662–3.

48. K. Öfele, *Journal of Organometallic Chemistry*, 1968, **12**, 42–43.

49. J. H. Kirchhoff, C. Dai, and G. C. Fu, *Angewandte Chemie (International ed. in English)*, 2002, **41**, 1945–1947.

50. C. J. O'Brien, E. A. B. Kantchev, C. Valente, N. Hadei, G. A. Chass, A. Lough, A. C. Hopkinson, and M. G. Organ, *Chemistry - A European Journal*, 2006, **12**, 4743–8.

51. C. J. O'Brien, E. A. B. Kantchev, G. A. Chass, N. Hadei, A. C. Hopkinson, M. G. Organ, D. H. Setiadi, T.-H. Tang, and D.-C. Fang, *Tetrahedron*, 2005, **61**, 9723–9735.

52. M. G. Organ, S. Avola, I. Dubovyk, N. Hadei, E. A. B. Kantchev, C. J. O'Brien, and C. Valente, *Chemistry - A European Journal*, 2006, **12**, 4749–55.

53. J. K. Becconsall, B. E. Job, and S. O'Brien, *Journal of the Chemical Society A*, 1967, 423–430.

54. F. P. Ricci, F. Sacchetti, M. Zoppi, S. F. Parker, C. J. Carlile, J. Tomkinson, R. J. Newport, and C. Andreani, *Physica B: Condensed Materials*, 1998, **241**, 154–156.

55. D. Colognesi, M. Celli, F. Cilloco, R. J. Newport, S. F. Parker, F. Sacchetti, J. Tomkinson, V. Rossi-Albertini, and M. Zoppi, *Applied Physics A: Materials Science and Processing*, 2002, **74**, 64–66.

56. S. O'Brian, M. Fishwick, and B. McDermitt, *Inorganic Syntheses*, 1972, **13**, 73–79.

57. B. Galabov, S. Ilieva, T. Dudev, H. V. Phan, and J. R. Durig, *Spectrochimica Acta Part A: Molecular Spectroscopy*, 1993, **49**, 2093–2103.

58. G. A. Chass, E. A. B. Kantchev, and D. C. Fang, *Chemical Communications (Cambridge, England)*, 2010, **46**, 2727–9.

59. S. F. Parker, D. Lennon, and P. W. Albers, *Applied Spectroscopy*, 2011, **65**, 1325–1341.

60. P. C. H. Mitchell, S. F. Parker, A. J. Ramirez-Cuesta, and J. Tomkinson, *Vibrational Spectroscopy with Neutrons, with Applications in Chemistry,Biology, Materials Science and Catalysis*, World Scientific, Singapore, 2005.

61. D. Wakther, T. Döhler, N. Theyssen, and H. Görls, *European Journal of Inorganic Chemistry*, 2001, 2049–2060.

62. E. J. Corey, L. S. Hegedus, and M. F. Semmelhack, *Journal of the American Chemical Society*, 1968, **90**, 2417–2418.

63. H. Case, *Journal of Organic Chemistry*, 1962, **27**, 640–641.